

2017

Synthesis of new classes of ionic liquids and their utilization in biological and pharmaceutical analysis

Omprakash Nacham
Iowa State University

Follow this and additional works at: <https://lib.dr.iastate.edu/etd>

 Part of the [Analytical Chemistry Commons](#)

Recommended Citation

Nacham, Omprakash, "Synthesis of new classes of ionic liquids and their utilization in biological and pharmaceutical analysis" (2017).
Graduate Theses and Dissertations. 15587.
<https://lib.dr.iastate.edu/etd/15587>

This Dissertation is brought to you for free and open access by the Iowa State University Capstones, Theses and Dissertations at Iowa State University Digital Repository. It has been accepted for inclusion in Graduate Theses and Dissertations by an authorized administrator of Iowa State University Digital Repository. For more information, please contact digirep@iastate.edu.

Synthesis of new classes of ionic liquids and their utilization in biological and pharmaceutical analysis

by

Omprakash Nacham

A dissertation submitted to the graduate faculty
in partial fulfillment of the requirements for the degree of

DOCTOR OF PHILOSOPHY

Major: Analytical Chemistry

Program of Study Committee:
Jared L. Anderson, Major Professor
Jacob W. Petrich
Robbyn K. Anand
Aaron Rossini
Reuben J. Peters

Iowa State University

Ames, Iowa

2017

Copyright © Omprakash Nacham, 2017. All rights reserved.

TABLE OF CONTENTS

	Page
ACKNOWLEDGEMENTS	vii
ABBREVIATIONS/SYMBOLS	viii
ABSTRACT	ix
CHAPTER 1 INTRODUCTION	
1.1 Fundamentals of ionic liquids (ILs) and strategies to control their physicochemical properties	1
1.2 A brief overview of magnetic ionic liquids (MILs)	5
1.3 Application of ILs diluents for analysis of impurities in pharmaceuticals using static headspace gas chromatography.....	7
1.4 A brief overview of interfacial and micellar properties of IL-based surfactants.....	10
1.5 A brief overview of the solid-phase microextraction technique (SPME).....	13
1.6 A brief overview of nucleic acid amplification techniques ...	15
1.7 Application of polymeric ionic liquid-based SPME for nucleic acid analysis	19
1.8 Organization of dissertation	22
References	24
CHAPTER 2 SYNTHETIC STRATEGIES FOR TAILORING THE PHYSICOCHEMICAL AND MAGNETIC PROPERTIES OF HYDROPHOBIC MAGNETIC IONIC LIQUIDS	
Abstract	27
2.1 Introduction	28
2.2 Experimental	30

2.3 Results and Discussion	42
2.4 Conclusion	50
Acknowledgements	51
References	51
CHAPTER 3 SYNTHESIS AND CHARACTERIZATION OF THE PHYSICOCHEMICAL AND MAGNETIC PROPERTIES FOR PERFLUOROALKYL ESTER AND Fe(III) CARBOXYLATE-BASED HYDROPHOBIC MAGNETIC IONIC LIQUIDS	
Abstract	54
3.1 Introduction	55
3.2 Experimental	57
3.3 Results and Discussion	66
3.4 Conclusion	74
Acknowledgements	75
References	75
CHAPTER 4 USE OF IONIC LIQUIDS AS HEADSPACE GAS CHROMATOGRAPHY DILUENTS FOR THE ANALYSIS OF RESIDUAL SOLVENTS IN PHARMACEUTICALS	
Abstract	77
4.1 Introduction	78
4.2 Experimental	81
4.3 Results and Discussion	83
4.4 Conclusion	95
Acknowledgements	96

References	96
CHAPTER 5 INTERFACIAL AND AGGREGATION BEHAVIOR OF DICATIONIC AND TRICATIONIC IONIC LIQUID-BASED SURFACTANTS IN AQUEOUS SOLUTION	
Abstract	99
5.1 Introduction	100
5.2 Experimental	103
5.3 Results and Discussion	109
5.4 Conclusion	129
Acknowledgements	130
References	131
CHAPTER 6 ANALYSIS OF BACTERIAL PLASMID DNA BY SOLID- PHASE MICROEXTRACTION	
Abstract	134
6.1 Introduction	135
6.2 Experimental	137
6.3 Results and Discussion	141
6.4 Conclusion	147
Acknowledgements	148
References	148

CHAPTER 7	EXTRACTION AND PURIFICATION OF DNA FROM COMPLEX BIOLOGICAL SAMPLE MATRICES USING SOLID-PHASE MICROEXTRACTION COUPLED WITH REAL-TIME PCR	
	Abstract	151
	7.1 Introduction	152
	7.2 Experimental	155
	7.3 Results and Discussion	158
	7.4 Conclusion	170
	Acknowledgements	171
	References	171
CHAPTER 8	RAPID AND SELECTIVE RNA ANALYSIS BY SOLID-PHASE MICROEXTRACTION	
	Abstract	174
	8.1 Introduction	175
	8.2 Experimental	178
	8.3 Results and Discussion	182
	8.4 Conclusion	191
	Acknowledgements	192
	References	192
CHAPTER 9	GENERAL CONCLUSIONS	194
APPENDIX A	SUPPLEMENTAL INFORMATION ACCOMPANYING CHAPTER 2	198
APPENDIX B	SUPPLEMENTAL INFORMATION ACCOMPANYING CHAPTER 3	222

APPENDIX C	SUPPLEMENTAL INFORMATION ACCOMPANYING CHAPTER 4	256
APPENDIX D	SUPPLEMENTAL INFORMATION ACCOMPANYING CHAPTER 5	259
APPENDIX E	SUPPLEMENTAL INFORMATION ACCOMPANYING CHAPTER 6	276
APPENDIX F	SUPPLEMENTAL INFORMATION ACCOMPANYING CHAPTER 7	281
APPENDIX G	SUPPLEMENTAL INFORMATION ACCOMPANYING CHAPTER 8	305

ACKNOWLEDGMENTS

I would like to thank my advisor, Dr. Jared Anderson, for his support, guidance, and giving me an opportunity to work in his research group. His constant enthusiasm toward research, perseverance for learning new things, and indispensable scientific intuition significantly influenced me to learn and grow during my PhD education.

I would like to acknowledge my committee members, Dr. Petrich, Dr. Peters, Dr. Anand, Dr. Rossini, and Dr. Ronning for their guidance and support in my research. I would like to thank my current group members: Kevin, He, Jiwoo, Stephen, Marcelino, Miranda, and Ashley for their collaboration and assistance. Additionally, I also extend my gratitude towards my previous lab mates: Cheng Zhang, Manishkumar, Tianhao, Tien, Honglian, Jeff, Ali, Rodney, Isaiah, Melissa, Pamela, and Will for their help and advice, and being good friends. I would like to thank my friends, colleagues, the department faculty and staff at Iowa State University and University of Toledo.

I would like to dedicate this PhD to my family and only because of their love and patience I completed this PhD.

Abbreviations/symbols

Entry	Abbreviation/symbol	Explanation
1	IL	Ionic liquids
2	MILs	Magnetic ionic liquids
3	LLE	Liquid liquid extraction
4	GC	Gas chromatography
5	SHS	Static headspace
6	SQUID	Superconducting quantum interference device
7	μ_B	Bohr magnetons
8	μ_{eff}	Effective magnetic moment
9	EMA	European medicines agency
10	DMSO	Dimethyl sulfoxide
11	NMP	N-methylpyrrolidone
12	API	Active pharmaceutical ingredient
13	LOD	Limited of detection
14	CMC	Critical micelle concentration
15	HPLC	High performance liquid chromatography
16	SPE	Soli-phase extraction
17	SPME	Solid-phase microextraction
18	NA	Nucleic acid
19	PCR	Polymerase chain reaction
20	dNTP	deoxynucleotide
21	qPCR	Quantitative real-time polymerase chain reaction
22	C _q	Quantification cycles
23	RT-qPCR	Reverse transcription quantitative polymerase chain reaction
24	mRNA	Messenger RNA
25	cDNA	Complementary DNA
26	dT	Deoxythymine
27	PIL	Polymeric ionic liquid
28	pDNA	Plasmid DNA
29	PA	Polyacrylate
31	SEM	Scanning electron microscopy
32	X_M	Molar magnetic susceptibility
33	N_{agg}	Aggregation number
34	C_{surf}	Surfactant concentration
35	γ_{CMC}	Surface tension at critical micelle concentration
36	Γ_{max}	Maximum surface adsorption
37	pA	Pico ampere
38	DLLME	Dispersive liquid-liquid microextraction

ABSTRACT

Ionic Liquids (ILs) are molten organic solvents comprised of unsymmetrical organic cations and inorganic/organic anions with melting points below 100 °C. The unique physicochemical properties of ILs including high thermal stabilities, negligible vapor pressures at room temperature, and tunable solubilities and viscosities have tremendously increased their applications in analytical chemistry.

The first part of research work presented in this dissertation focuses on different synthetic strategies that are employed to tailor the physicochemical properties as well as paramagnetic susceptibilities of magnetic ionic liquids (MILs). The developed synthetic methods yielded MILs with low aqueous solubilities (0.1% w/v) and high magnetic susceptibilities. The second part of dissertation describes the self-assembly properties of different classes of ILs in aqueous solutions. The last part of dissertation focuses on the applications of ILs and polymeric ionic liquids (PILs) for analysis of pharmaceuticals and nucleic acids, respectively.

MILs are a special class of ILs with paramagnetic component(s) in their molecular structure. In addition to favorable properties of ILs, MILs exhibit paramagnetic susceptibilities at room temperatures when suspended in aqueous solutions. As a result, their molecular motion can be readily controlled by exposure to an external magnetic field. Owing to their structural tunability as well as paramagnetic susceptibilities, MILs demonstrate a remarkable potential to address the challenges associated with liquid liquid extraction (LLE) techniques. Imidazolium-based cations with $[\text{FeCl}_4^-]$ / $[\text{FeCl}_3\text{Br}^-]$ anions represents the common class of MILs. The high aqueous solubility of iron (III)-based MILs represents a serious problem for their applicability in liquid liquid microextraction techniques. Three different classes of iron-based hydrophobic MILs including monocationic, dicationic, and tricationic MILs were prepared. The incorporation of long

hydrocarbon chains, benzyl groups, and perfluoroalkyl alkyl moieties as substituents within cation framework has significantly improved the hydrophobicity of resulting MILs. A series of dicationic imidazolium cations with weakly coordinating and relatively hydrophobic anions yielded MILs with low melting points and low aqueous solubilities. The paramagnetic susceptibility of MILs is controlled by varying the number of paramagnetic anions in the molecular structure. The developed MILs demonstrated structure-dependent extraction properties for analysis of DNA and polycyclic aromatic hydrocarbons (PAHs) from complex sample matrices.

ILs with long hydrocarbon chains and hydrophilic cations (e.g., imidazolium and pyridinium) exhibit self-assembly properties in aqueous solutions. Similar to conventional surfactants, IL-based surfactants demonstrate concentration dependent properties in aqueous solutions including bulk phase aggregation (micelle formation) and surface adsorption. The interfacial and micellar properties of three dicationic and two tricationic IL-based surfactants in aqueous solutions were examined using fluorescence spectroscopy, conductometry, and tensiometry techniques. In addition, the effects of inorganic and organic salts and organic solvent content on the aggregation properties of IL-based surfactants was investigated. The surface adsorption as well as micellar properties of tricationic IL-based surfactants was compared against the analogous trimeric quaternary ammonium-based surfactants.

The high thermal stability as well as relatively low vapor pressure at high temperatures are some interesting properties of ILs that represent them as new diluent systems in headspace gas chromatography (HS-GC) applications. Two ILs were examined as HS-GC diluents for analysis of residual solvents in pharmaceutical substances. To improve the analytical performance of the developed method, the HS-GC parameters were optimized including HS extraction time and HS incubation temperature. Owing to their favorable

physicochemical properties, IL-based HS-GC method yielded low detection limits (LODs), high sensitivities, and better sample throughput compared to conventional organic solvent-based HS-GC method.

Solid-phase microextraction (SPME) is a miniaturized and automated solvent-free sample preparation technique. In contrast to solid-phase extraction (SPE) and LLE methods, SPME streamlines the analytical workflow by combining sampling and sample preparation into a single step. This significantly reduces the overall analysis time. PILs represent as new class of sorbent coatings with tunable solvation properties and high thermal stabilities. The unique extraction properties of PILs were exploited for the purification of nucleic acids from complex sample matrices. Electrostatic and ion-exchange interactions between negatively charged phosphate backbone of nucleic acid and cationic framework of PIL sorbent coating are the main driving force for extraction of nucleic acids by PIL sorbent coatings. The developed PIL-based SPME method purified sufficient quantity and quality of DNA from bacterial cell lysate samples and subsequently used for downstream enzymatic amplification techniques including endpoint polymerase chain reaction (PCR) and quantitative real-time PCR.

Given the success of SPME toward DNA analysis, the applicability of the PIL-based SPME was also investigated for analysis of yeast RNA samples. The PIL-based sorbent coating featuring carboxylic acid groups within IL monomer and halide-based anions extracted the highest amount of mRNA from aqueous samples compared to analogous PIL sorbent coatings. Under similar experimental conditions, the PIL-based SPME method yielded higher quantities of mRNA for real-time reverse transcription quantitative PCR (RT-qPCR) compared to phenol/chloroform LLE method. The selectivity of PIL-based SPME method toward mRNA analysis was improved by modifying the surface composition of a commercial poly acrylate (PA) sorbent coating with oligo deoxythymine

(dT) that assist in specific capture of mRNA from total RNA samples. The developed oligo dT modified PA-based SPME method extracted low quantity of mRNA compared to commercial silica-based SPE kits. However, the modified PA-based SPME method isolated sufficient quantity and quality of mRNA for RT-qPCR assay with low analysis times and minimal experimental setup i.e., without the use of centrifugation apparatus, binding buffers and elution buffers which are essential for commercial SPE kits. These results demonstrate that SPME-based RNA sample preparation methods can address the limitations associated with existing RNA purification technologies and are particularly suitable for field sampling and point-of-care diagnostic applications.

CHAPTER 1

INTRODUCTION

1.1 Fundamentals of ILs and strategies to control their physicochemical properties

Ionic liquids (ILs) are class of molten organic salts, typically comprised of unsymmetrical organic cations and inorganic/organic anions with melting points at or below 100 °C.¹ Over the past few decades, the number of applications of ILs is tremendously increasing due to their unique physicochemical properties. ILs exhibit interesting properties including negligible vapor pressure at room temperatures, tunable viscosities, and high thermal stabilities. Owing to their ease in synthesis, a large number of ILs with different cations and anions have been prepared and exploited in a wide range of applications including catalysis,² chromatography,³ electrochemistry,⁴ as well as pharmaceutical⁵ and biological sample preparation.⁶

The physicochemical properties of ILs are largely determined by the chemical composition of the cation as well as the anion. Figure 1 represents the structures of cations and anions that are often used in the design of ILs. Depending on the requirements of an application, the properties of ILs can be easily modified using simple chemical reactions. For example, 1-alkyl-3-methylimidazolium-based ILs with halide anions possess good solubility in aqueous solutions and demonstrate excellent solvent properties for the dissolution of complex biomolecules.⁷ However, these ILs are not suitable for high temperature gas chromatography (GC) applications because of their low thermal stabilities. The replacement of halides with the bis[(trifluoromethyl)sulfonyl]imide ([NTf₂⁻]) anion via ion-exchange metathesis reaction provides ILs with high thermal stabilities and are consequently used as GC stationary phases.⁸ In addition, ILs can be custom designed through the incorporation of task specific functional groups within the cationic or anionic

portion of the IL. Metal chelators,⁹ chiral amino acids,¹⁰ and Lewis acids¹¹ are a few examples of task specific functional groups that are appended to ILs. Therefore, owing to their structural tunability and versatile nature, ILs are often described as designer solvents.

ILs with low melting points (< 25 °C), low viscosities, and high hydrophobicity are of

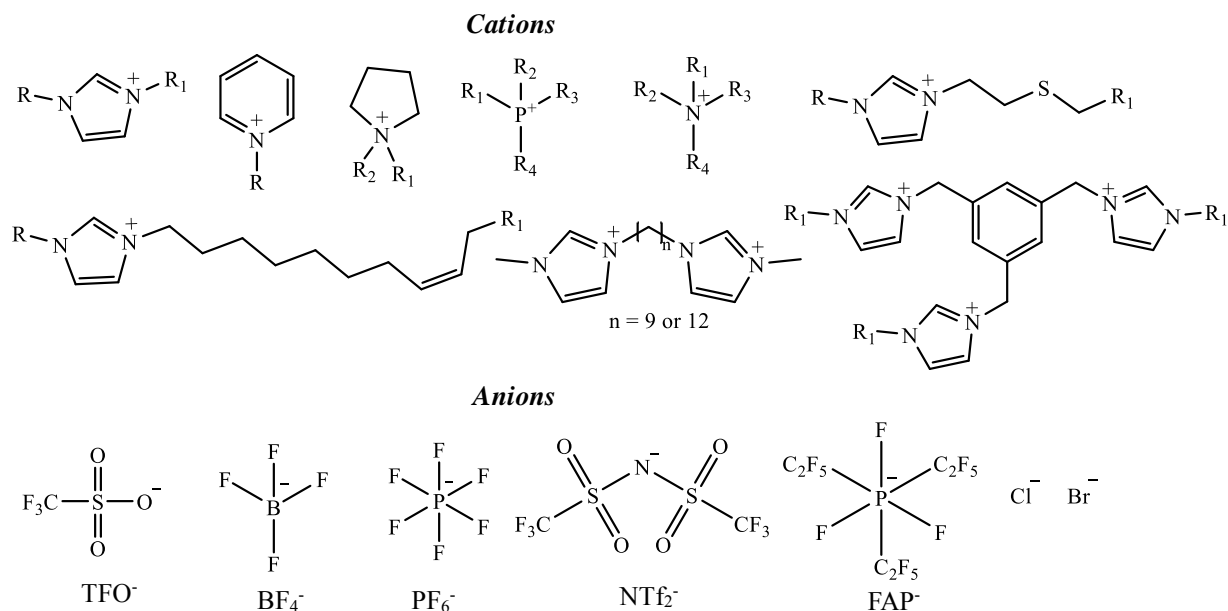


Figure 1. Chemical structures of cations and anions that are often used in the synthesis of ILs

significant interest to a variety of analytical applications including liquid-liquid extractions (LLEs). Important structural features such as charge delocalization, asymmetry of the cation, and size of cation and/or anion play a significant role in determining the melting point of resulting ILs. In general, ILs containing halide anions often exhibit high melting points. In such cases, the replacement of halide anions with charge delocalized and bulky organic anions such as trifluoromethanesulfonate ([TfO⁻]), [NTf₂⁻], and dicyanamide ([N(CN)₂⁻]) may provide low melting points.¹² Similarly, ILs comprised of asymmetrical cations tend to produce lower melting points than symmetrical cations. For example, 1-butyl-3-methylimidazolium salts melt at approximately 100 °C lower than analogous 1-butylpyridinium salts.¹³ Other approaches for reducing the melting point of monocationic ILs include functionalization of cation moieties with thioalkyl groups and lipophilic structural elements as observed in natural lipids.^{14,15} This class of ILs are called lipid-

inspired ILs, which exhibit great potential as stationary phases in multidimensional GC applications.¹⁶ In comparison to monocationic ILs, multi-cation (dicationic and tricationic) platforms provide more opportunities to control their physicochemical properties. Dicationic liquids are comprised of two cationic and two anionic moieties, with a spacer alkyl hydrocarbon chain separating the cationic headgroups. By varying the length of spacer alkyl chain as well as cation/anion combination, ILs with a wide range of physicochemical properties can be generated. Importantly, dicationic liquids comprised of longer spacer chains and asymmetrical cations (two different cations) provide lower melting points than symmetrical dicationic liquids and monocationic liquids.¹⁷ Alternatively, the mixing of dicationic imidazolium salts at a 1:1 ratio containing different anions produce ILs with low viscosity and low melting points when compared to their symmetrical counterparts. This class of ILs are called dicationic heteroanionic liquids.¹⁸

Viscosity is another important parameter of ILs that determines their usability as reaction solvents in organic synthesis as well as extraction solvents in microextractions. Due to the presence of long-range columbic forces and intermolecular hydrogen bonding (especially for ILs containing halide anions), ILs exhibit higher viscosities than analogous organic solvents at room temperature. Commonly, ILs containing halide anions possess high viscosity, making them less suitable for synthetic applications. In such cases, the substitution of halide-based anions with $[N(CN_2^-)]$ anions may provide ILs with low viscosity.¹⁹ This strategy was successfully exploited for the synthesis of several N-alkyl-N-methylpyrrolidinium and 1-alkyl-3-methylimidazolium salts. For example, the viscosity of 1-ethyl-3-methylimidazolium ($[EMIM]$) $[N(CN_2^-)]$ salt was as low as 21 centipoise (cP) at room temperature. Owing to their donor capabilities, dicyanamide ILs exhibited good solubility for Co(II) and Cu(II) salts at room temperature.¹⁹ Although dicyanamide salts possess low viscosity and good solvent properties, their high solubilities in aqueous

solutions have precluded their utilization in LLE studies. The most common and relatively low viscosity ILs that are often used in LLEs contain $[\text{NTf}_2^-]$, hexafluorophosphate ($[\text{PF}_6^-]$), and tris(perfluoroalkyl)trifluorophosphate ($[\text{FAP}^-]$) anions. The presence of perfluoroalkyl groups within their molecular structure significantly reduces their solubility in aqueous solution. In addition, the hydrophobicity of ILs can be improved by functionalizing the cation with long alkyl chains, benzyl moieties, and perfluoroalkyl groups.^{20,21} Unfortunately, these synthetic strategies potentially increase the overall viscosity of the resulting ILs and pose serious problems in the transfer and/or manipulation of extraction phase in LLE methods. Interestingly, trihexyltetradecyl phosphonium ($[\text{P}_{66614}^+]$) and a few other heavily alkylated quaternary ammonium cations that lack acidic hydrogen atoms when coupled with $[\text{NTf}_2^-]$ /halides, provide with low viscosity and high hydrophobicity compared to their 1-alkyl-3-methylimidazolium analogs.²²

The properties of high thermal stability and low vapor pressure have been exploited in the sample preparation of pharmaceuticals as well as the development of thermally-stable GC stationary phases. The investigation into thermal degradation products of ILs at high temperatures using mass spectrometry (MS) revealed that the chemical nature of the cation and/or anion plays a crucial role in thermal decomposition of ILs. Based on the chemical identity of decomposed products and chemical composition of cation and anion, two reaction mechanisms, namely, reverse Menshutkin and Hofmann elimination, primarily contribute to the decomposition of ILs at higher temperatures.²³ Generally, ILs comprised of weak nucleophilic anions such as $[\text{NTf}_2^-]$ and $[\text{TfO}^-]$ provide higher thermal stability than analogous halide salts. Interestingly, with the same anion composition, the thermal stabilities of multi-cation systems are significantly higher than monocationic systems.²⁴ For this reason, most of the commercial IL-based GC stationary phases are dicationic ILs with weak nucleophilic anions.²⁵ Owing to their favorable thermal properties, ILs demonstrate

remarkable diluent properties in the analysis of low volatility chemical impurities in pharmaceutical substances using headspace (HS) GC techniques.²⁶ Within these applications, [NTf₂⁻] salts are more commonly used relative to other weak nucleophilic anions.

The presence of water and synthetic impurities has a significant impact on the physicochemical properties of ILs. The most common chemical impurities encountered in the preparation of [NTf₂⁻] salts are the presence of halide salts, potentially contributing during the anion-exchange metathesis reaction between IL and LiNTf₂.²⁷ The presence of halide impurities in resulting ILs is often detected via titration with silver nitrate (AgNO₃). The ensuing silver halide salts precipitate in aqueous solutions because of their low solubility product. Commonly, halide impurities in [NTf₂⁻]-based ILs are minimized by washing several times with water. The presence of halide impurities in ILs results in lower thermal stability and alters the solvation properties of the resulting ILs. On the other hand, the presence of volatile impurities in ILs can be removed by conditioning at high temperatures under vacuum for several hours. This method of purification is an essential prerequisite for development of IL-based GC stationary phases and in the determination of trace level impurities in pharmaceutical substances.²⁸

1.2 A brief overview of magnetic ionic liquids

Magnetic ionic liquids (MILs) are a special class of ILs containing paramagnetic component(s) in their molecular structure. In addition to the core fundamental properties of ILs, MILs exhibit paramagnetic susceptibilities at room temperature. As a result, the molecular motion of MILs can be easily controlled using an external magnetic field. For the first time, Hayashi and co-workers examined the paramagnetic properties of 1-butyl-3-methylimidazolium tetrachloroferrate(III) ([BMIM⁺][FeCl₄⁻]) using superconducting quantum interference device (SQUID) magnetometry.²⁹ This remarkable work on [FeCl₄⁻]

salts provided a solid foundation for the development of different MILs with a range of transition and lanthanide metal-based anions including $[\text{MnCl}_4^{2-}]$, $[\text{CoCl}_4^{2-}]$, and $[\text{GdCl}_4^{1-}]$.²⁰ The interest in MILs is rapidly increasing within different areas of chemical sciences because of their particle-free magnetic properties, non-volatile nature, and interesting solvation properties. Importantly, the nanoparticle-free MILs are stable and not susceptible to agglomeration, a serious problem often encountered in particle-based magnetic materials.³⁰

Conventional methodologies of LLE involve differential partitioning of target analytes between the organic solvent-based extraction phase and aqueous phase. Although useful in many cases, LLE techniques are often confronted with some limitations. These methods are time-consuming, labor intensive, involve multiple sample transfer steps, require large volumes of toxic organic solvents, and lack capabilities for automation.³¹ As a result, conventional LLE-based sample preparation methods represent as serious bottleneck for high throughput sample analysis. The development of MILs as extraction solvents has the following advantages: (1) the structural tunability of MILs enables the incorporation of specific functional groups that can enhance the extraction performance of MILs; (2) because of their paramagnetic susceptibilities, MIL extraction solvents can be easily separated from the sample solution using an external magnetic field and provide opportunities for automation; (3) unlike conventional organic solvents, the chemical structure of MILs can be custom designed for task-specific analysis where the selectivity and sensitivity of the analytical method can be significantly improved. To accomplish these objectives, MILs should possess the following features: low melting points (i.e., liquids at room temperature), low aqueous solubilities, and minimal viscosities at ambient temperatures.

MILs comprising imidazolium cations and $[\text{FeCl}_4^-]$ / $[\text{FeCl}_3\text{Br}^-]$ anions are the most common class of MILs because of their ease in synthesis and low price of starting materials. However, this class of MILs exhibit high solubility in aqueous solutions due to the intrinsic hydrophilic properties of cations and anions. The hydrophobicity of iron-based MILs was successfully improved by employing several synthetic strategies, as described in section 1.1. As a result, three different classes of iron-based MILs with different cation structural motifs, namely, monocationic, dicationic, and tricationic MILs were prepared. Interestingly, tricationic imidazolium-based MILs comprising three $[\text{FeCl}_3\text{Br}^-]$ anions exhibited an μ_{eff} (effective magnetic moment) as high as 11.76 Bohr magnetons (μ_B), the highest ever reported for MILs. Figure 2 demonstrates the hydrophobicity and paramagnetic properties of ammonium-based MILs in aqueous solution using a 1 Tesla (T) Nd magnet. Owing to their high hydrophobicity and relatively low viscosities, ammonium, phosphonium and few dicationic imidazolium-based MILs have been used as extraction solvents for the preconcentration of nucleic acids and polyaromatic hydrocarbons from complex sample matrices.

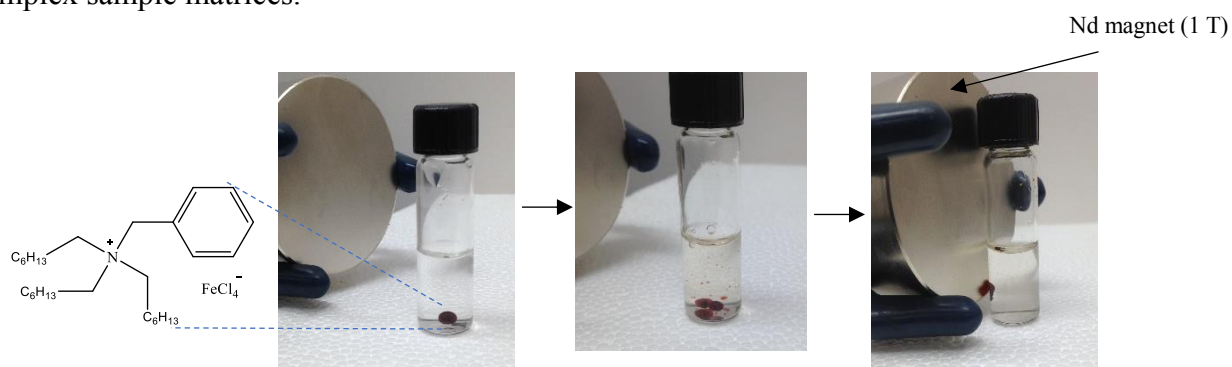


Figure 2. Hydrophobicity and paramagnetic susceptibility properties of benzyltrioctyl ammonium tetrachloroferrate MIL in aqueous solution

1.3 Application of ILs as diluents for analysis of impurities in pharmaceuticals using static headspace gas chromatography

The demand for high throughput, sensitive, and accurate analytical methods for the analysis of pharmaceutical impurities is high. Due to the stringent guidelines of various

regulatory agencies (e.g., FDA and European Medicines Agency (EMA)), the determination of trace level impurities in drug substances using robust and sensitive analytical methods is of significant interest to pharmaceutical companies. Static headspace (SHS) GC is one of the most common analytical techniques used for the analysis of volatile and semi-volatile impurities in drug products. In SHS-GC, the drug sample is either dissolved or impurities present in the sample are extracted into high boiling point organic solvents (commonly referred as diluents; e.g., dimethyl sulfoxide (DMSO) and N-methylpyrrolidone (NMP)). This step ensures that a co-crystallized impurity/residual solvent present in the drug sample is completely available for analysis. Subsequent to drug sample dissolution, the sample vial is incubated at high temperatures (less than the boiling point of a diluent) to volatilize the target analytes. Finally, a HS sampling unit injects only the volatile components of the sample vial into the gas chromatograph and prevents instrument contamination from non-volatile components of the drug sample.

The sensitivity of SHS-GC methods can be improved by optimizing the diluent solvent composition (mixing of diluents with different chemical and thermal properties) and/or by increasing the HS incubation time. These methods are time-consuming and increase the overall time required for method development and validation steps. Alternatively, the sensitivity of SHS-GC methods can be enhanced by increasing the HS incubation temperature since it promotes analyte partitioning into the sample vial HS.²⁶ However, employing this approach to organic solvent assisted HS-GC methods results in severe instrument contamination due to excessive diluent sampling as well as injection of non-volatile chemical components into the GC system. In these situations, ILs can be a potential alternative to organic solvent-based diluents because of their low volatility and high thermal stability at high incubation temperatures.

The application of ILs as SHS-GC diluents has the following advantages: (1) analyte vaporization will be significantly improved due to the negligible vapor pressure of ILs; while in case of organic diluents, the high vapor pressure of organic solvents reduces the partial pressure of analytes and results in lower amount of analytes in the HS of the sample vial; (2) because of their high thermal stability and low volatility, a high HS incubation temperature can be used; (3) due to the absence of background diluent peak, ILs enable faster gas chromatographic method development and validation; (4) the chemical structure of ILs can be customized to improve the solubility of drug samples. Figure 3 shows the schematic representation of analyte response in IL and organic solvent assisted SHS-GC techniques.

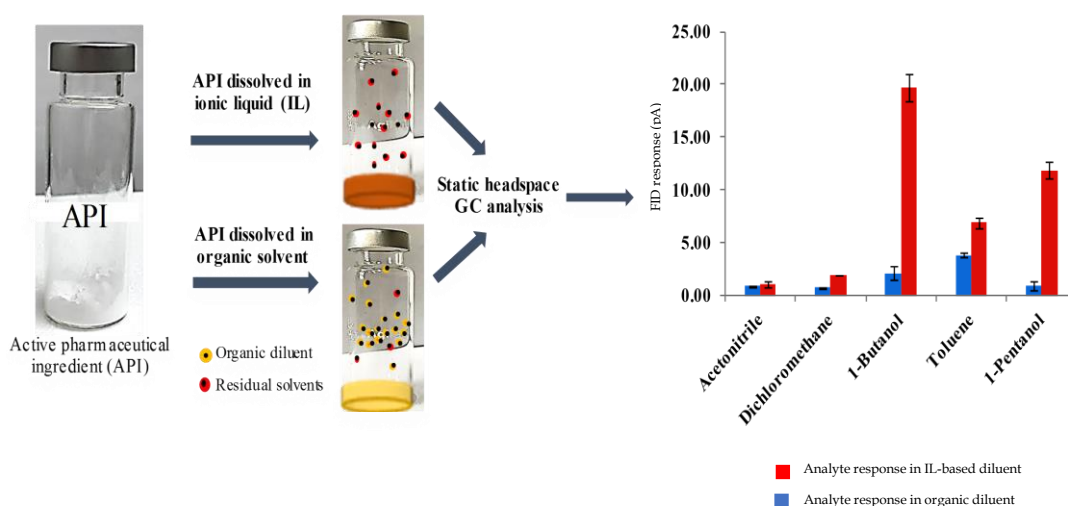


Figure 3. Headspace GC analysis of residual solvents in pharmaceuticals using ILs and organic solvents as diluents

Recently, our group and others have successfully developed an IL-based SHS-GC method for the analysis of volatile and semi-volatile genotoxic impurities and residual solvents in different active pharmaceutical ingredient (API) samples.^{26,32} The IL-based method yielded high sensitivities and superior limits of detection (LODs) when compared to conventional organic solvents as diluents.

1.4 A brief overview of interfacial and micellar properties of IL-based surfactants in aqueous solutions

Surfactants (surface active agents) are a class of self-assembling molecules that possess both hydrophilic (e.g., charged and/or polar functional groups) and lipophilic (e.g., long hydrocarbon chains and perfluoroalkyl groups) components within the same molecular structure. These compounds are broadly classified into three classes, namely, cationic (e.g., cetyltrimethylammonium bromide (CTAB)), anionic (e.g., sodium dodecyl sulfate (SDS)), and non-ionic (e.g., fatty alcohols and polyethylene glycols) surfactants. Depending on concentration, surfactants exhibit two distinct properties in aqueous solutions such as surface adsorption and micelle formation. At relatively low concentrations, surfactant molecules spontaneously adsorb onto the air/water interface and reduce the surface/interfacial tension of the aqueous solutions. At high concentrations subsequent to surface saturation, surfactants monomers tend to form aggregates in bulk solution. This process of aggregation is commonly called as micellization, and the concentration above which surfactant monomers begin to form micelles is termed the critical micelle concentration (CMC). Within these aggregates, surfactant monomers expose their hydrophilic headgroups towards the aqueous environment and lipophilic groups are oriented towards the interior of the aggregate. The CMC values of surfactants in aqueous solutions are directly related to the length of the hydrophobic chain. Conductometry, nuclear magnetic resonance (NMR) spectroscopy, tensiometry, and fluorescence spectroscopy are several common methods used to determine the interfacial and micellar properties of surfactants.³³

ILs comprised of long hydrocarbon chain substituents and hydrophilic cationic headgroups (e.g., imidazolium and pyridinium) have been demonstrated to be surface active and shown to aggregate in aqueous solutions, as observed in traditional quaternary

ammonium-based cationic surfactants (as shown in Figure 4).³⁴ Owing to their ease in synthesis and structural tunability, IL-based surfactants provide a multitude of opportunities to design and develop new chemical structures when compared to traditional surfactants.

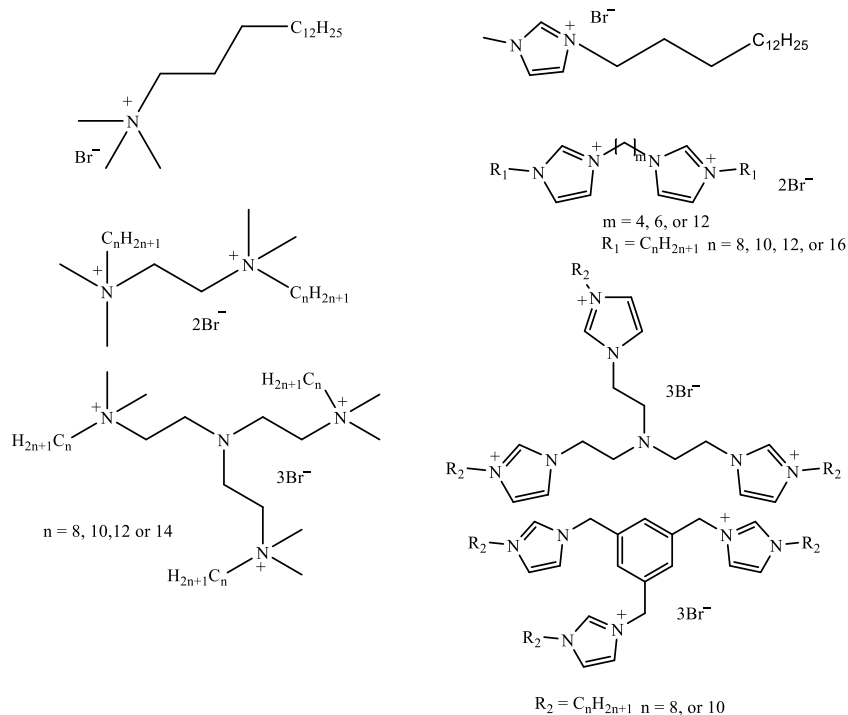


Figure 4. Chemical structures of conventional ammonium and IL-based surfactants

As a result, a large number of IL-based surfactants with different cationic structural motifs including monocationic, dicationic and tricationic surfactants can be prepared and exploited in a wide range of analytical applications. For the first time, Sirieix-Plenet et.al, determined the aggregation and interfacial properties of 1-decyl-3-methylimidazolium bromide in aqueous solutions using potentiometric and conductimetric techniques.³⁵ Similar to conventional cationic surfactants, the aggregation properties and CMC values of monocationic and dicationic imidazolium surfactants are highly dependent on the length of the hydrocarbon chain and shape of the surfactant molecule. For example, the IL-based surfactant 1-hexadecyl-3-methylimidazolium bromide ($C_{16}MIm-Br$) demonstrated micelle formation at much lower concentrations than analogous $C_6MIm-Br$ surfactant. Previously,

Anderson and co-workers reported the synthesis of a series of dicationic IL-based surfactants (shown in Figure 4) and examined their micellar properties using surface tensiometry. For dicationic IL-based surfactants with an identical linker chain connecting the two cationic headgroups, a decrease in CMC values are largely dependent on the length of free alkyl chain appended to the imidazolium cation.³⁶ For example, the C₁₂-Im-C₄-C₁₂-2Br dicationic surfactant presents a much lower CMC value than C₈-Im-C₄-C₈-2Br surfactants. Trigonal tricationic imidazolium salts (three imidazolium cation groups are linked to an organic core, as shown in Figure 1) represent as new class of ILs with interesting physicochemical properties.²⁴ Recently, our group and others have examined the micellar and surface adsorption properties of two classes of tricationic surfactants containing different cores using a variety of techniques including conductometry, fluorescence spectroscopy, and surface tensiometry. The CMC values of the studied tricationic surfactants presented a good correlation between the different measurement techniques. The obtained CMC values are much lower than conventional trimeric surfactants. In addition, the surfactant properties of tricationic surfactants were also investigated in the presence two different salts, where low CMC values were observed by increasing the salt concentration. The low CMC values in the presence of added salts could be attributed due to reduced charge repulsion between headgroups in the micelle.³⁷

The interest in the development of new IL-based surfactants is rapidly increasing due to their fascinating properties and remarkable potential in analytical methods and separations. IL-based micelle media has been successfully applied to preconcentrate the polycyclic aromatic hydrocarbons (PAHs) from contaminated sediment using micro-wave assisted extraction technique.³⁸ The developed method was rapid and yielded better results than conventional cationic surfactants. In addition, these compounds have been also used as additives in high performance liquid chromatography (HPLC) to mask the free silanol

effects of silica-based HPLC stationary phases.³⁹ Given their importance in different analytical applications, the determination of interfacial and micellar properties of IL-based surfactants is useful to design and develop new surfactant systems and extend their applicability in different chemical sciences.

1.5 A brief overview of the solid-phase microextraction technique

Despite the tremendous developments in analytical instrumentation, the necessity of sample preparation cannot be looked over. Sample preparation reduces sample matrix interference and improves the analytical performance of the method. LLE and solid-phase extraction (SPE) are common methods of sample preparation that are applied prior to routine chemical analysis. In SPE, a relatively large amount of sorbent phase is employed for the exhaustive extraction of target analytes from a sample matrix. Followed by extraction, target analytes are recovered from the sorbent bed using high volumes of organic solvents. The organic solvents are subsequently evaporated to low volumes to preconcentrate the target analytes. As a result, SPE methods are relatively time-consuming because of the separate extraction and preconcentration steps. In most cases, sorbent beds used in SPE procedures are not reusable and these methods are not capable of automation, representing serious problems in high throughput analytical laboratories.

Solid-phase microextraction (SPME) is a miniaturized and automated sample preparation technique developed by Pawliszyn and co-workers in the early 1990s.⁴⁰ In contrast to SPE, SPME is a non-exhaustive sample preparation technique where relatively low amounts of sorbent phase (< 1 mg) is employed for the isolation and preconcentration of target analytes. SPME consolidates sampling and preconcentration steps into a single step. As a result, the overall time required for the analysis is drastically reduced when compared to conventional SPE procedures. In SPME, a thin layer of sorbent coating is

immobilized onto the solid support and target analytes are adsorbed and/or partitioned to the sorbent coating. SPME has demonstrated promising potential for interfacing with a variety of analytical and bioanalytical techniques. Depending on the nature of the sample matrix and physicochemical properties of the target analytes, SPME can be operated in two different modes, namely, direct-immersion and headspace modes (as shown in Figure 5). In direct-immersion mode, the sorbent coating is directly exposed to sample solution and mostly target analytes with low volatilities are extracted using this mode. Subsequently, analytes will be recovered from sorbent coating using either a suitable solvent system or via thermal desorption conditions. In headspace mode, the sorbent coating is exposed to the headspace of the sample vial, where volatile analytes are extracted into the sorbent coating. The fiber is subsequently transferred to analytical instrumentation for desorption and analysis. In addition, this mode of SPME also facilitates the analysis of solid samples.

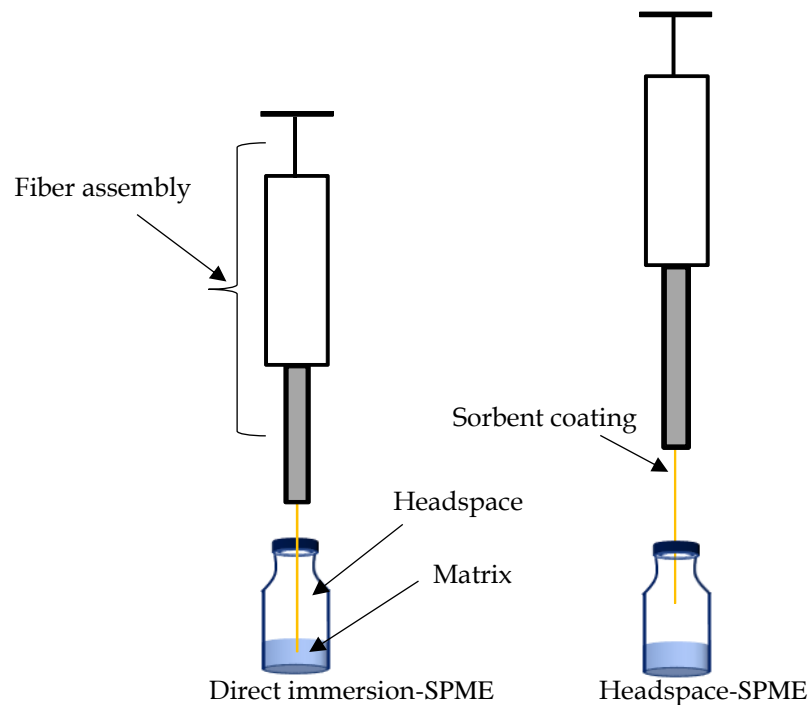


Figure 5. Schematic demonstration of different extraction modes of SPME for chemical analysis

1.6 A brief overview of nucleic acid amplification techniques

Nucleic acids (NAs) are important cellular biomolecules that are essential for the survival and development of every living organism. Since NAs play a crucial role in many biological processes, their analysis provides valuable information that holds a great importance in life sciences including functional genomics,⁴¹ food chemistry,⁴² clinical microbiology,⁴³ and pathology.⁴⁴ Within these applications, NA containing samples are often subjected to amplification techniques including polymerase chain reaction (PCR) to enhance the sensitivity and accuracy of the analysis. PCR is a simple and yet powerful diagnostic tool that enables amplification of a specific DNA fragment from a complex pool of DNA. It is an *in vitro* enzymatic DNA amplification technique that allows the detection of specific sequence and produce large amounts of DNA that can be used in downstream applications such as disease diagnostics, cloning, and gene sequencing studies. This technique was pioneered by Kary Mullis in the early 1990s. Each PCR assay requires a small amount of template DNA, primers (15 to 20 bases short DNA fragments with nucleotide sequence complementary to template DNA), deoxynucleotides (dNTPs), and a buffered aqueous solution containing DNA polymerase and co-factors (e.g., magnesium). The PCR reaction components are thoroughly mixed and placed in a thermal cycler, where the instrument performs a series of pre-programmed temperature cycles in a discrete and precise manner to yield the PCR products. Each thermal cycle contains three important steps, namely, denaturation, annealing, and extension. In the denaturation step, PCR samples are heated to a temperature (90-95 °C) above the melting point of two complementary DNA strands of target DNA. This allows the DNA strands to separate and make them available for the annealing step. During the annealing step, the reaction temperature is lowered so that the primers can selectively anneal to complementary regions of target DNA strands. Finally, at an optimal extension temperature, DNA polymerase

extends the primer sequence by incorporating dNTPs into the developing DNA strand in 5'→3' direction. Figure 6 depicts the schematic representation of a PCR-based NA amplification. Typically, forty thermal cycles are employed to obtain the maximum amount of PCR products. Commonly, PCR products are analyzed with the use of DNA intercalators (e.g., SYBR Safe and ethidium bromide; fluorescent dyes that preferentially bind to double stranded DNA molecules) and agarose gel electrophoresis. Since DNA quantification is performed at the end of PCR, this technique is commonly referred to as endpoint PCR. Endpoint PCR techniques are mostly used to detect the presence or absence of specific DNA fragments and when coupled with image densitometry techniques (software that helps in transforming the gel images to peaks that can be integrated), semi-quantitative information can be obtained.

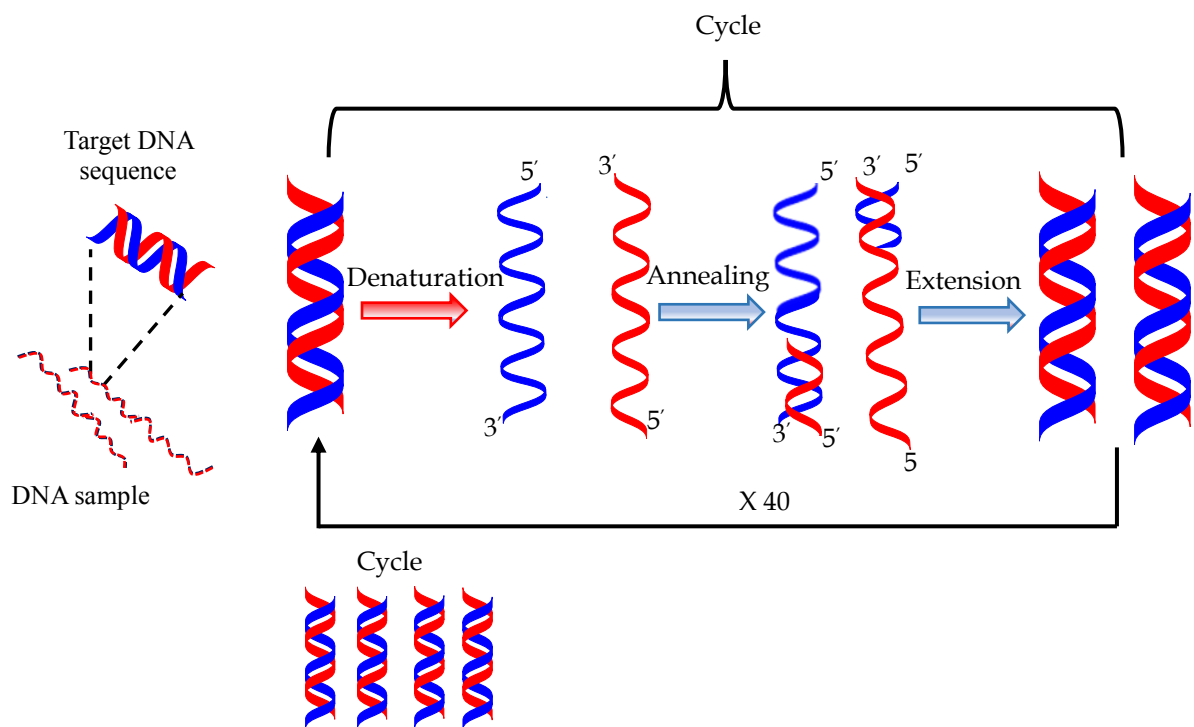


Figure 6. Schematic representation of the polymerase chain reaction (PCR) technique

Quantitative real-time PCR (qPCR) is an advanced version of the endpoint PCR technique, where DNA detection and quantification is performed in real-time using

sophisticated fluorescent technology. qPCR quantifies the initial amount of template DNA more accurately and precisely than end-point PCR by using non-specific DNA binding fluorophores (e.g., SYBR Green 1 and PicoGreen) or via sequence-specific DNA probes consisting of fluorescent reporter molecules. While being more sensitive than endpoint PCR techniques, qPCR eliminates the post-PCR processing steps and increases the throughput of DNA analysis. This technique was first introduced in 1992 by Higuchi and co-workers.⁴⁵ In a qPCR assay at the end of each cycle, the emitted fluorescence signal from the amplified DNA is collected. A fixed threshold fluorescence intensity will be set above the base line and the parameter, C_q (quantification cycles) measures the minimum number cycles required to reach the threshold fluorescence. For example, a sample with low C_q value represents that higher amount of template DNA that is initially present in the sample. Figure 7 shows a typical qPCR amplification plot for two different samples with varying initial template DNA concentrations. In a 100% efficient qPCR, amplified DNA doubles at the end of each cycle. In other words, a difference of one C_q value between two different samples indicates a two-fold difference in the amount of template DNA in each sample. For DNA quantification, the efficiency of qPCR should be in the range of 90 to 110%. The amplification efficiency can be calculated using Equation 1, where the slope is the slope of the linear regression in the calibration curve.

$$\text{Efficiency} = [10^{\left(\frac{-1}{\text{slope}}\right)} - 1] \times 100 \quad (1)$$

qPCR efficiency is highly dependent on the quality of input DNA. A careful optimization of reaction conditions is warranted prior to absolute quantification. Subsequent to qPCR amplification, reaction products are often subjected to melting point analysis to verify the amplification specificity and to detect the presence of non-specific amplification products and primer dimers, mostly responsible for false positive results.

Ribonucleic acid (RNA) plays a prominent role in regulating gene expression and encoding proteins that are required for the effective functioning of living organisms. Reverse transcription quantitative polymerase chain reaction (RT-qPCR) is the common method used in RNA quantification.⁴⁶ RT-qPCR consists of a multi-step protocol that combines the reverse transcription (RT) step with qPCR to provide a quantitative information on gene expression products including messenger RNA (mRNA). To accomplish mRNA quantification, the first step involves synthesis of a complementary DNA (cDNA) of mRNA using reverse transcriptase enzyme (RNA-dependent DNA polymerase). Reverse transcriptase synthesizes the cDNA either by using the primers that are complementary to target mRNA (gene-specific priming) or via oligo-dT (20 to 30-mer containing thymine nucleotides) primers that can selectively bind to the poly A tail of mRNA molecules.

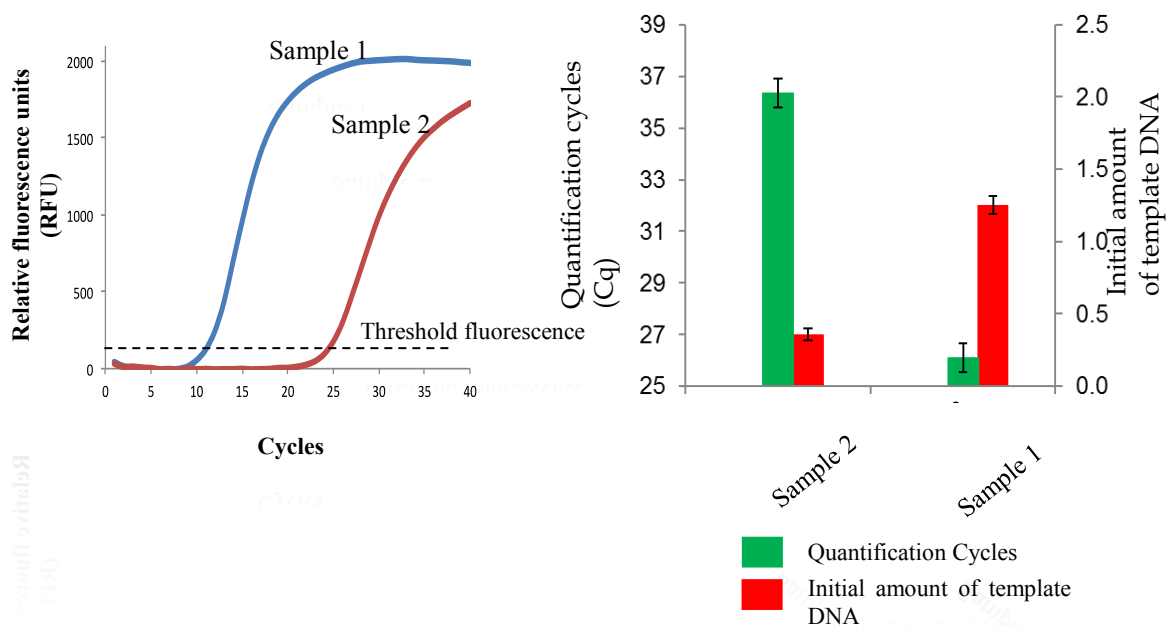


Figure 7. Schematic representation of qPCR amplification plots and data analysis

Using oligo-dT priming, a pool of cDNA is obtained representing a range of reverse transcription products rather than target cDNA. In most cases, the sensitivities and cDNA product yields of RT reaction using gene-specific primers are significantly higher than non-specific (random hexamers) and oligo-dT priming methods.⁴⁷ Followed by cDNA synthesis, RT products are subjected to qPCR amplification and melting point analysis to quantify the initial amount of mRNA and to determine the amplification specificity. Absolute and relative quantification methods commonly used for the determination of mRNA levels. The evaluation of RT efficiency, reproducibility, and the effects of cDNA quality on qPCR amplification are carefully investigated, since these parameters have a significant impact on RNA quantitation.

1.7 Application of polymeric ionic liquid-based SPME for NA analysis

Although PCR-based NA amplification techniques are robust and sensitive, the reliability and accuracy of the information obtained from these techniques rely on the purity and quantity of input NAs. The isolation and purification of NAs prior to PCR-based amplification techniques is an essential prerequisite. Phenol/chloroform-based LLE and silica-based SPE kits are commonly used to purify NAs from biological and/or environmental contaminants that often inhibit PCR amplification.³¹ LLE represents the least expensive and most widely adopted method to obtain high yields of purified NAs. However, they suffer from lengthy analysis times, require multiple sample transfer steps, demand large volumes of organic solvents and require high sample volumes, and are not particularly not suitable for point-of-care diagnostic applications. The advent of silica-based SPE technology has significantly reduced the use of toxic organic solvents and improved the throughput of the analysis. Yet, they are expensive, represent less scope for structural optimization, require high volumes of alcohols and chaotropic salts (PCR inhibitors), and are not particularly capable of automation.

SPME can be a potential alternative to the conventional NA purification technologies. SPME has demonstrated a promising potential in the preconcentration of drug metabolites⁴⁸ and proteins⁴⁹ from biological sample matrices. The selectivity and sensitivity of the SPME technique can be significantly enhanced by developing new types of sorbent coatings. Polymeric ionic liquids (PILs) are a new class of sorbent coatings with multiple solvation properties and high thermal stabilities. The central advantage of PIL-based sorbent coatings relies on the ability to engineer the chemical composition of sorbent phase with respect to target analytes and the sample matrix type. Recently, our group and others have demonstrated the applicability of PILs as extraction phases for the purification of bacterial plasmid DNA (pDNA).^{50,51} Figure 8 shows a schematic representation the PIL-based SPME method for NA analysis. The PIL-based SPME method was successfully coupled to endpoint and qPCR-based amplification techniques. Owing to electrostatic interactions and the ion-exchange mechanism between PIL sorbent phase and negatively charged phosphate backbone of DNA, the PIL sorbent coatings extracted higher amount of DNA than commercial polyacrylate (PA) fiber. The PIL sorbent phase containing polar functional groups such as carboxylic acid and hydroxy groups with halide anions, demonstrated superior capabilities in extraction when compared to other structural analogs. The DNA extraction capabilities of the developed method was also investigated in the presence of bacterial cell lysate samples. The developed PIL-based SPME method preconcentrated the DNA from crude cell lysates even at concentration as low as 1 pg mL⁻¹. The DNA extraction capabilities of PIL sorbent coating was also investigated in the presence of common PCR inhibitors including FeCl₃ and CaCl₂, where the developed method preconcentrated sufficient quantities of DNA that can be used in qPCR amplification.⁵⁰

Encouraged by these results, PIL-based SPME method was also investigated for RNA analysis. The PIL-based SPME method showed a remarkable potential in extracting tRNA from yeast cell lysate samples.

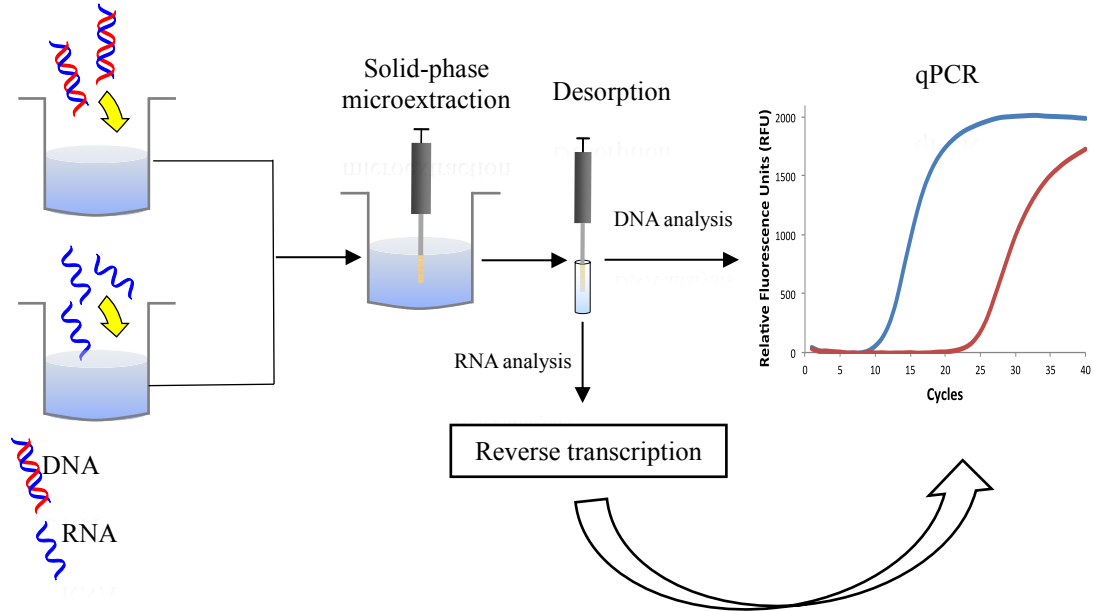


Figure 8. Schematic illustration of nucleic acid analysis using PIL-based SPME

In comparison to LLE, the developed PIL-based SPME method demonstrated superior performance in extracting tRNA from yeast cell lysate samples. Since the sensitivity of RNA analysis is highly dependent on the mRNA concentration, SPME devices that can selectively extract mRNA from tRNA samples were prepared using carbodiimide-based amide linker chemistry.⁵² The mRNA extraction performance of modified SPME devices were compared against the commercial silica-based mRNA isolation kit, where SPME devices have demonstrated low extraction efficiencies compared to SPE kits. Nevertheless, the total time and number of steps involved in mRNA isolation for SPME devices are considerably lower than the commercial SPE kit. These results demonstrate that PIL-based SPME can complement conventional NAs purification methodologies, and are potentially more useful in resource limited settings and are potentially suitable for point-of-care diagnostic applications.

1.8 Organization of the dissertation

Chapter 2 describes the challenges involved in the preparation of hydrophobic MILs and thereby describes different synthetic strategies to control their hydrophobicity and paramagnetic susceptibility properties. Three general classes of hydrophobic MILs, monocationic, dicationic, and tricationic were prepared and their melting points, thermal stabilities, and paramagnetic properties were evaluated. The developed hydrophobic MILs demonstrated sufficient hydrophobicity and magnetic susceptibilities when suspended in aqueous solutions and showed promising potential for LLEs and magnet-based separations.

Chapter 3 describes two new synthetic strategies for the preparation of hydrophobic MILs. In the first strategy, the hydrophobicity of MILs was enhanced by incorporation of perfluorobutyryl groups within the cationic portion of MILs. The developed MILs are insoluble in aqueous solutions at concentrations as low as 0.1% (w/v). Using the second strategy, Fe(III) carboxylate-based imidazolium MILs were prepared. Within this approach, the functionalization of imidazolium cations with carboxyl ligands enabled the chelation of paramagnetic Fe(III) metal centers. Unlike conventional paramagnetic anion-based MILs, the developed synthetic method provided the opportunity to incorporate task specific anions without sacrificing the paramagnetic properties of resulting MILs.

Chapter 4 describes the applicability of ILs as diluents for analysis of residual solvents in pharmaceutical substances using SHS-GC technique. The developed IL-based method yielded better sensitivities and superior detection limits when compared to traditional organic solvent diluents including NMP. The cost-analysis and potential advantages and disadvantages of the IL-based method with respect to conventional residual solvent analysis methods are discussed.

Chapter 5 describes the self-assembly properties of two different classes of IL-based surfactants in aqueous solutions. Surface adsorption and bulk phase aggregation properties

of selected IL-based surfactants were determined using tensiometry, conductometry, and fluorescence spectroscopy. For the first time, two new tricationic IL-based surfactants were prepared and their interfacial and micellar properties were determined and compared with the contemporary multi-cationic quaternary ammonium-based surfactants. In addition, the effects of organic solvents, inorganic and organic salts on the micellar properties of IL-based surfactants were investigated.

Chapter 6 describes the application of SPME technique using PIL as a sorbent coating for the analysis of bacterial pDNA samples using endpoint PCR technique. In comparison to the commercial PA sorbent coating, the PIL sorbent phase demonstrated superior performance in extracting pDNA from aqueous samples. The developed method was applied for the extraction of varying number of *E. coli* cells from aqueous samples. Followed by extraction, scanning electron microscopy (SEM) was performed to determine the adsorbed *E. coli* cells on the surface of PIL sorbent coating.

Chapter 7 describes the development of PIL-based SPME method for the analysis of DNA from complex biological sample matrices. The chemical composition of PIL sorbent coatings was optimized to enhance the DNA extraction performance. The developed method showed remarkable selectivity in isolating DNA in the presence of known PCR inhibitors. Furthermore, the feasibility of PIL-based SPME method was examined for its capability to isolate pDNA from bacterial cell lysate samples.

Chapter 8 describes the investigation of different SPME sorbent coatings including PILs and a commercial poly acrylate (PA) for isolation and purification of mRNA from different sample matrices. Under similar experimental conditions, the PIL-based SPME method provided high quantities of mRNA for RT-qPCR analysis compared to phenol/chloroform liquid extraction method.

The selectivity of SPME sorbent phase toward mRNA was enhanced by exploiting the oligo dT:mRNA hybridization approach. The modified SPME sorbent coatings enabled high mRNA extraction efficiencies from total RNA and yeast cell lysate samples.

Chapter 9 provides a summary of completed research projects.

References:

- (1) Hallett, J. P.; Welton, T. *Chem. Rev.* **2011**, *111*, 3508-3576
- (2) Zhang, Q.; Zhang, S.; Deng, Y. *Green Chem.* **2011**, *13*, 2619-2637
- (3) Xiaohua, X.; Liang, Z.; Xia, L.; Shengxiang, J. *Anal. Chim. Acta* **2004**, *519*, 207.
- (4) Wilkes, J. S.; Levisky, J. A.; Wilson, R. A.; Hussey, C. L. *Inorg Chem* **1982**, *21*, 1263-1264.
- (5) Liu, F.-h.; Jiang, Y. *J. Chromatogr. A* **2007**, *1167*, 116-119
- (6) Liu, R.; Liu, J.-f.; Yin, Y.-g.; Hu, X.-l.; Jiang, G.-b. *Anal. Bioanal. Chem.* **2009**, *393*, 871-883.
- (7) Swatloski, R. P.; Spear, S. K.; Holbrey, J. D.; Rogers, R. D. *J. Am. Chem. Soc.* **2002**, *124*, 4974-4975.
- (8) Armstrong, D. W.; He, L.; Liu, Y.-S. *Anal. Chem* **1999**, *71*, 3873-3876
- (9) Visser, A. E.; Swatloski, R. P.; Reichert, W. M.; Mayton, R.; Sheff, S.; Wierzbicki, A.; Davis Jr, J. H.; Rogers, R. D. *Chem. Commun.* **2001**, *1*, 135-136
- (10) Fukumoto, K.; Yoshizawa, M.; Ohno, H. *J. Am. Chem. Soc.* **2005**, *127*, 2398-2399
- (11) DeCastro, C.; Sauvage, E.; Valkenberg, M.; Hölderich, W. *J. Catal.* **2000**, *196*, 86-94
- (12) Tokuda, H.; Hayamizu, K.; Ishii, K.; Susan, M. A. B. H.; Watanabe, M. *J. Phys. Chem. B* **2005**, *109*, 6103-6110
- (13) Tokuda, H.; Hayamizu, K.; Ishii, K.; Susan, M. A. B. H.; Watanabe, M. *J. Phys. Chem. B* **2004**, *108*, 16593-16600
- (14) Mirjafari, A.; O'Brien, R. A.; West, K. N.; Davis, J. H. *Chem. Europ. J.* **2014**, *20*, 7576-7580
- (15) Murray, S. M.; O'Brien, R. A.; Mattson, K. M.; Ceccarelli, C.; Sykora, R. E.; West, K. N.; Davis, J. H. *Angew. Chem. Int. Ed.* **2010**, *122*, 2815-2818
- (16) Nan, H.; Zhang, C.; O'Brien, R. A.; Benchea, A.; Davis, J. H.; Anderson, J. L. *J. Chromatogr. A* **2017**, *1481*, 127-136

- (17) Payagala, T.; Huang, J.; Breitbach, Z. S.; Sharma, P. S.; Armstrong, D. W. *Chem. Mater.* **2007**, *19*, 5848-5850
- (18) Brown, P.; Butts, C. P.; Eastoe, J.; Hernández, E. P.; de Araujo Machado, F. L.; de Oliveira, R. J. *Chem. Commun.* **2013**, *49*, 2765-2767
- (19) MacFarlane, D. R.; Golding, J.; Forsyth, S.; Forsyth, M.; Deacon, G. B. *Chem. Commun.* **2001**, 1430-1431
- (20) Nacham, O.; Clark, K. D.; Yu, H.; Anderson, J. L. *Chem. Mater.* **2015**, *27*, 923-931
- (21) Nacham, O.; Clark, K. D.; Anderson, J. L. *RSC Adv.* **2016**, *6*, 11109-11117
- (22) Tsunashima, K.; Sugiya, M. *Electrochemistry* **2007**, *75*, 734-736
- (23) Maton, C.; De Vos, N.; Stevens, C. V. *Chem. Soc. Rev.* **2013**, *42*, 5963-5977
- (24) Sharma, P. S.; Payagala, T.; Wanigasekara, E.; Wijeratne, A. B.; Huang, J.; Armstrong, D. W. *Chem. Mater.* **2008**, *20*, 4182-4184
- (25) Poole, C. F.; Lenca, N. *J. Chromatogr. A* **2014**, *1357*, 87-109
- (26) Ho, T. D.; Yehl, P. M.; Chetwyn, N. P.; Wang, J.; Anderson, J. L.; Zhong, Q. *J. Chromatogr. A* **2014**, *1361*, 217-228
- (27) Seddon, K. R.; Stark, A.; Torres, M.-J. *Pure Appl. Chem.* **2000**, *72*, 2275-2287
- (28) Laus, G.; Andre, M.; Bentivoglio, G.; Schottenberger, H. *J. Chromatogr. A* **2009**, *1216*, 6020-6023
- (29) Hayashi, S.; Hamaguchi, H.-o. *Chem. Lett.* **2004**, *33*, 1590-1591
- (30) Brown, P.; Bushmelev, A.; Butts, C. P.; Eloi, J.-C.; Grillo, I.; Baker, P. J.; Schmidt, A. M.; Eastoe, J. *Langmuir* **2013**, *29*, 3246-3251
- (31) Clark, K. D.; Nacham, O.; Yu, H.; Li, T.; Yamsek, M. M.; Ronning, D. R.; Anderson, J. L. *Anal. Chem.* **2015**, *87*, 1552-1559.
- (32) Nacham, O.; Ho, T. D.; Anderson, J. L.; Webster, G. K. *J. Pharma. Biomed. Anal.*, DOI: 10.1016/j.jpba.2017.05.033
- (33) Menger, F. M.; Mbadugha, B. N. A. *J. Am. Chem. Soc.* **2001**, *123*, 875-885
- (34) Pino, V.; Germán-Hernández, M.; Martín-Pérez, A.; Anderson, J. L. *Separ. Sci. Technol.* **2012**, *47*, 264-276
- (35) Sirieix-Plénet, J.; Gaillon, L.; Letellier, P. *Talanta* **2004**, *63*, 979-986
- (36) Baltazar, Q. Q.; Chandawalla, J.; Sawyer, K.; Anderson, J. L. *Colloids and Surfaces A: Physicochemical and Engineering Aspects* **2007**, *302*, 150-156
- (37) Nacham, O.; Martín-Pérez, A.; Steyer, D. J.; Trujillo-Rodríguez, M. J.; Anderson, J. L.; Pino, V.; Afonso, A. M. *Colloids Surf., A* **2015**, *469*, 224-234

- (38) Pino, V.; Anderson, J. L.; Ayala, J. H.; González, V.; Afonso, A. M. *J. Chromatogr. A* **2008**, *1182*, 145-152
- (39) Marszałł, M. P.; Kaliszan, R. *Crit. Rev. Anal. Chem.* **2007**, *37*, 127.
- (40) Arthur, C. L.; Pawliszyn, J. *Anal. Chem.* **1990**, *62*, 2145-2148
- (41) Morozova, O.; Marra, M. A. *Genomics* **2008**, *92*, 255-264
- (42) Meyer, R. *Food Control* **1999**, *10*, 391-399
- (43) Clarridge, J. E. *Clin. Microbiol. Rev.* **2004**, *17*, 840-862
- (44) Siebolts, U.; Varnholt, H.; Drebber, U.; Dienes, H.-P.; Wickenhauser, C.; Odenthal, M. *J. Clin. Pathol.* **2009**, *62*, 84-88
- (45) Heid, C. A.; Stevens, J.; Livak, K. J.; Williams, P. M. *Genome Res.* **1996**, *6*, 986-994
- (46) Wong, M. L.; Medrano, J. F. *Biotechniques* **2005**, *39*, 75-77
- (47) Bustin, S. *J. Mol. Endocrinol.* **2002**, *29*, 23-39
- (48) Kataoka, H.; Lord, H. L.; Yamamoto, S.; Narimatsu, S.; Pawliszyn, J. *J. Microcolumn Sep.* **2000**, *12*, 493
- (49) Du, F.; Alam, M. N.; Pawliszyn, J. *Anal. Chim. Acta* **2014**, *845*, 45.
- (50) Nacham, O.; Clark, K. D.; Anderson, J. L. *Anal. Chem.* **2016**, *88*, 7813-7820
- (51) Wang, X.; Xing, L.; Shu, Y.; Chen, X.; Wang, J. *Anal. Chim. Acta* **2014**, *837*, 64-69
- (52) Wang, C.; Yan, Q.; Liu, H.-B.; Zhou, X.-H.; Xiao, S.-J. *Langmuir* **2011**, *27*, 12058-12068

CHAPTER 2**SYNTHETIC STRATEGIES FOR TAILORING THE PHYSICOCHEMICAL AND MAGNETIC PROPERTIES OF HYDROPHOBIC MAGNETIC IONIC LIQUIDS**

Reprinted with permission from *Chemistry of Materials* **2015**, 27, 923-931

Copyright © 2015, American Chemical Society

Omprakash Nacham, Kevin D. Clark, Honglian Yu, and Jared L. Anderson

Abstract

Magnetic ionic liquids (MILs) are a subclass of ionic liquids (ILs) containing paramagnetic components and are readily manipulated by an external magnetic field. Due to their hydrophilic nature, very few applications of MILs in aqueous systems have been reported. In this study, three general classes of hydrophobic MILs including monocationic, symmetrical/unsymmetrical dicationic, and symmetrical/unsymmetrical tricationic MILs were synthesized and characterized. By tuning the structure of the MIL, various physicochemical properties including water solubility, magnetic susceptibility, and melting point were regulated. MILs synthesized with the benzimidazolium cation were shown to exhibit lower water solubility (0.1% (w/v)) when compared to those containing imidazolium cations (0.25% (w/v)). By incorporating asymmetry into the cationic component of the MIL, the melting point of dicationic MILs was lowered while the effective magnetic moment (μ_{eff}) and hydrophobicity remained unchanged. Tricationic MILs paired with three $[\text{FeCl}_3\text{Br}^-]$ anions exhibited an μ_{eff} as high as 11.76 Bohr magnetons (μ_{B}), the highest ever reported for MILs. The synthetic strategies employed in this study facilitate the generation of hydrophobic MILs that show great promise for liquid-liquid extraction and catalytic studies where the MIL can be easily removed or in microfluidic applications where the MIL microdroplet can be manipulated by an external field.

2.1 Introduction

Ionic liquids (ILs) are molten organic salts composed of organic cations and inorganic/organic anions with low melting points (≤ 100 °C). These solvents have garnered much attention due to their low vapor pressure at ambient temperatures, high thermal stability, wide electrochemical window, and multiple solvation capabilities.¹ Furthermore, the physicochemical properties of ILs can be modulated through careful design of the cation/anion pair.² By incorporating high-spin transition metals into the IL structure, an intriguing subclass of ILs called magnetic ionic liquids (MILs) has been generated.³⁻⁶ In addition to the unique and tunable properties of conventional ILs, MILs exhibit susceptibility to external magnetic fields.⁷ Owing to their paramagnetic nature, MILs have been exploited in a wide range of applications including reusable catalysts in synthesis,^{8,9} electro-active species in electrochemistry,¹⁰ magnetic hydraulics in engineering,¹¹ and materials for gas absorption.¹² The excellent thermal stability of some MILs has been exploited when used as stationary phases in multidimensional gas chromatography.¹³

The 1-butyl-3-methylimidazolium tetrachloroferrate(III) ($[\text{BMIM}^+][\text{FeCl}_4^-]$) MIL represents the earliest example of magnetoactive ILs and was prepared by mixing equimolar amounts of the halide salt and neutral metal halide complex.^{3,4} The popular imidazolium cation has since appeared in MIL structures paired with lanthanide-containing anions synthesized by metathesis reaction.¹⁴ Using a similar approach, dysprosium(III)-based MILs with enhanced magnetic susceptibilities and, in some cases, luminescent properties have been prepared.¹⁵ An investigation of the $[\text{BMIM}^+][\text{FeCl}_4^-]$ MIL showed that phase separation of the MIL from aqueous solutions (greater than 20% (v/v) MIL) was possible upon application of a strong magnetic field (1 T).¹⁶ The study demonstrated the ease with which MILs can be manipulated by a magnetic field and has been noted as an important advantage when compared to traditional solvents, particularly in separation

processes.¹⁷ Traditional liquid-liquid extraction relies on the partitioning of analytes between two immiscible phases followed by a recovery step (e.g., centrifugation or evaporation) in which the extraction phase is isolated for purification or analysis. Employing MILs as extraction solvents has the potential to rapidly recover the MIL extraction phase by simply applying an external magnetic field. Unfortunately, the high phase ratio required for recovery of the imidazolium-based MILs precludes their use in aqueous microextraction systems. This is likely a consequence of the intrinsic hydrophilic nature associated with imidazolium-based MILs.

Similar to conventional ILs, the water miscibility of MILs can be controlled by inclusion of nonpolar moieties into the MIL structure. Typical non-coordinating, hydrophobic anions such as the bis[(trifluoromethyl)sulfonyl]imide ($[\text{NTf}_2^-]$) anion cannot be used in the design of monocationic MILs due to lack of paramagnetic properties, thus confining structural modifications to the cationic portion. The heavily alkylated trihexyl(tetradecyl)phosphonium ($[\text{P}_{6,6,6,14}^+]$) cation has been paired with $[\text{MnCl}_4^{2-}]$, $[\text{CoCl}_4^{2-}]$, and $[\text{GdCl}_6^{3-}]$ anions to form MILs that are relatively hydrophobic when compared to their imidazolium counterparts.¹⁸ Although aqueous solutions containing less than 1% (v/v) of the $[\text{P}_{6,6,6,14}^+][\text{FeCl}_4^-]$ MIL have reportedly achieved phase separation upon application of an external magnetic field,¹⁹ the production of stable and inexpensive functionalized phosphonium-based cations is not easy or straightforward. An alternate route for tuning the physicochemical properties of MILs involves a dicationic platform incorporating both paramagnetic and hydrophobic anions produced through the mixing of homoanion precursors.²⁰

In an effort to further understand the interplay of hydrophobicity and magnetic susceptibility in MILs, eleven (11) novel hydrophobic MILs were synthesized in this study.

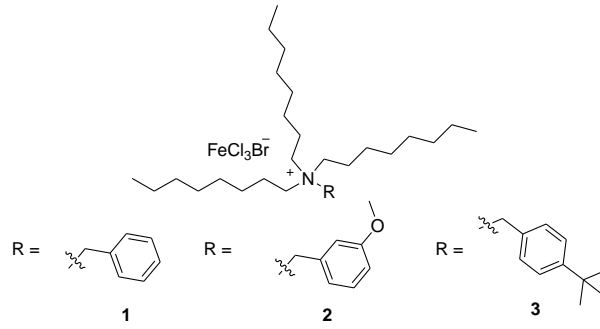
Figure 1 groups the MILs into the following three classes: monocationic ammonium-based

MILs (**1-3**), symmetrical/unsymmetrical dicationic MILs with heteroanions (**4a**, **4b**, **6-8**), and symmetrical/unsymmetrical tricationic MILs (**10-12**). Each synthetic route undertaken offers a unique approach towards incorporating hydrophobicity and magnetic susceptibility to the MIL structure. By designing MILs with multiple paramagnetic iron(III) centers, high effective magnetic moments (μ_{eff}) were achieved. The tricationic MIL **12** exhibited an μ_{eff} of 11.76 Bohr magnetons (μ_{B}), which is, to our knowledge, the highest μ_{eff} reported for a MIL. Moreover, the low water solubility values observed for the MILs in this study (less than 0.25% (w/v)) are ideal for employing these compounds in magnet-based aqueous biphasic systems. The thermal properties of each MIL were evaluated using thermal gravimetric analysis (TGA) and differential scanning calorimetry (DSC).

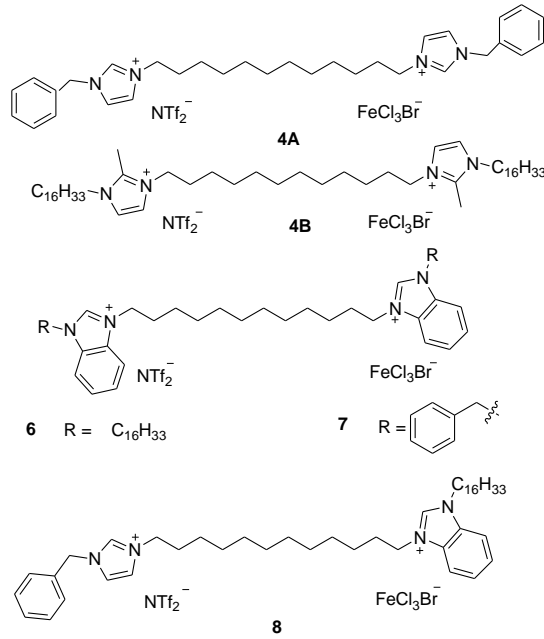
2.2 Experimental

2.2.1 Materials and Measurements. Imidazole (99%), 2-methylimidazole (99%), benzimidazole (98%), trioctylamine (97%), benzyl bromide (98%), 3-methoxybenzene (98%), 4-(*tert*-butyl)benzene (97%), octanethiol ($\geq 98.5\%$), 2,2-dimethoxy-2-phenylacetophenone (99%), lithium bis(trifluoromethyl)sulfonylimide and 1,12-dibromododecane (98%) were purchased from Acros Organics (NJ, USA). Acetonitrile, chloroform, dichloromethane, methanol, and diethyl ether were purchased from Fisher Scientific (Fair Lawn, NJ, USA). Deuterated chloroform and dimethylsulfoxide were obtained from Cambridge Isotope Laboratories (Andover, MA, USA). The NMR solvents were used as received without additional drying. Iron(III) chloride hexahydrate ($\text{FeCl}_3 \cdot 6\text{H}_2\text{O}$) (97%), 1-bromohexadecane (99%), 1-bromododecane (99%), 1,3,5-tris(bromomethyl)benzene (97%), dimethylsulfoxide were purchased from Sigma-Aldrich (St. Louis, MO, USA). All reagents were used as received without any further purification.

Monocationic Hydrophobic Magnetic Ionic Liquids



Dicationic Hydrophobic Magnetic Ionic Liquids



Tricationic Hydrophobic Magnetic Ionic Liquids

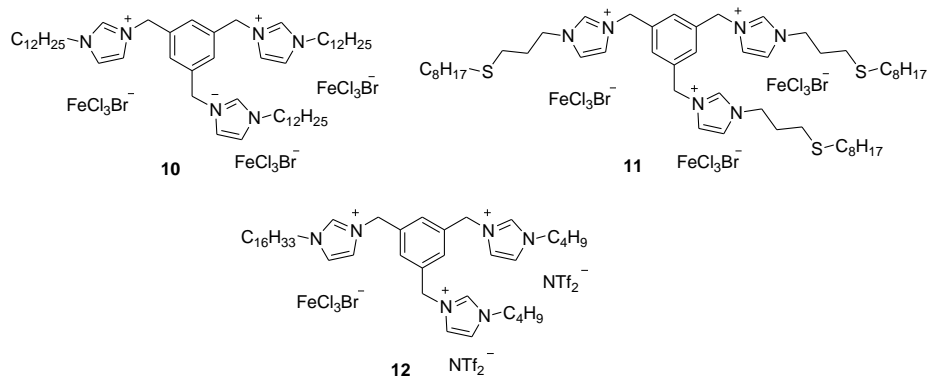


Figure 1. Chemical structures of the three general classes of hydrophobic magnetic ionic liquids synthesized in this study

^1H NMR and ^{13}C NMR spectra were recorded using a Varian 400 MHz nuclear magnetic resonance spectrometer. Chemical shifts reported in this manuscript are relative to tetramethylsilane. Mass spectra were obtained using an Esquire-LC-MS/MS from

Bruker Daltonics. Thermogravimetric analyses were performed using a TA Instruments TGA Q600 thermogravimetric analyzer. All samples were loaded in platinum pans and heated at a rate of 5 °C min⁻¹ under nitrogen flow (50 mL min⁻¹). Differential scanning calorimetry (DSC) traces were obtained using a Diamond DSC from Perkin-Elmer. Magnetic susceptibility measurements were determined using a Magnetic Susceptibility Balance (MSB) from Johnson Matthey. The MSB was calibrated with CuSO₄·5H₂O and validated using the previously reported data for the [P_{6,6,6,14}⁺][FeCl₄⁻] MIL.¹⁹ Visible absorption spectra were obtained using a Thermo Scientific Evolution 300 UV-Vis Spectrophotometer. Absorption spectra of MILs were collected using acetonitrile as the solvent.

2.2.2 General Procedure for the Synthesis of Monocationic Hydrophobic MILs. As shown in Scheme 1, the synthesis of MILs **1-3** involved the reaction of trioctylamine (1 mmol) with bromomethyl substituents (R-CH₂Br; R= benzene, methoxybenzene, and *tert*-butylbenzene; 1.1 mmol) in chloroform (25 mL) for 72 h under reflux conditions. The solvent was evaporated under reduced pressure followed by washing the crude compound with hexanes (4 x 25 mL) under sonication to remove the unreacted starting materials. The bromide salt was then dried under vacuum at 60 °C for 12 h. Characterization of compounds **1a-3a** was performed using ¹H NMR, ¹³C NMR, and ESI-MS. After confirming the purity of the intermediates, compounds **1a-3a** were reacted with equimolar amounts of FeCl₃·6H₂O in methanol at room temperature under nitrogen atmosphere for 4 h. After evaporation of solvent, the crude MIL was washed with an excess of deionized water to remove unreacted FeCl₃ from the final product. The MILs **1-3** were then dried under vacuum at 80 °C for 48 h and characterized using visible spectrophotometry and elemental analysis. All spectra are provided in the supplemental information in Appendix A.

Characterization of 1a. Yield 92%. $^1\text{H-NMR}$ (400 MHz; CDCl_3); δ/ppm : 0.86 (t, $J_{H-H} = 6.35$ Hz, 9H); 1.25 (m, 30H); 1.75 (m, 6H); 3.29 (t, $J_{H-H} = 8.06$ Hz, 6H); 4.92 (s, 2H); 7.42 (m, 3H); 7.53 (m, 2H). $^{13}\text{C-NMR}$ (400 MHz; CDCl_3); δ/ppm : 14.31; 22.81; 22.97; 26.61; 29.28; 31.84; 59.08; 63.51; 127.68; 129.60; 130.97; 132.76.

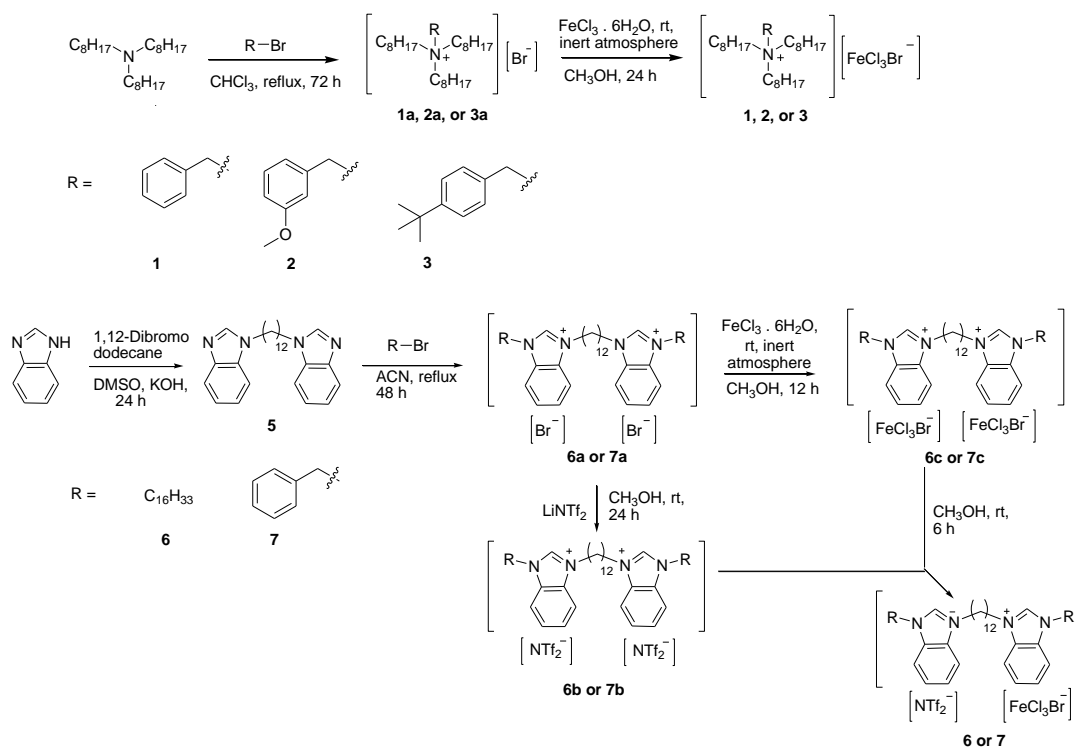
Characterization of MIL 1. Yield 91%. A dark reddish-brown viscous liquid. Characteristic bands for $[\text{FeCl}_3\text{Br}^-]$ anion were observed at 534, 619, and 688 nm using visible spectroscopy. Elemental Anal. Calcd (%) for $\text{C}_{31}\text{H}_{58}\text{BrCl}_3\text{FeN}$ (686.91): C, 54.21; H, 8.51; N, 2.04; Found: C, 53.67; H, 8.06; N, 1.56.

Characterization of 2a. Yield 93%. $^1\text{H-NMR}$ (400 MHz; CDCl_3); δ/ppm : 0.89 (t, $J_{H-H} = 6.35$ Hz, 9H); 1.25 (m, 30H); 1.75 (m, 6H); 3.33 (t, $J_{H-H} = 8.42$ Hz, 6H); 3.86 (s, 3H); 4.89 (s, 2H); 7.22 (m, 3H); 7.35 (m, 1H). $^{13}\text{C-NMR}$ (400 MHz; CDCl_3); δ/ppm : 14.41; 22.90; 23.08; 26.72; 29.41; 31.93; 56.05; 59.28; 63.62; 116.71; 118.41; 124.61; 129.05; 130.62; 160.61.

Characterization of MIL 2. Yield 91%. A dark reddish-brown viscous liquid. Visible spectroscopy showed characteristic bands for the $[\text{FeCl}_3\text{Br}^-]$ at 534, 619, and 688 nm. Elemental Anal. Calcd (%) for $\text{C}_{32}\text{H}_{60}\text{BrCl}_3\text{FeNO}$ (716.93): C, 53.61; H, 8.44; N, 1.95; Found: C, 54.41; H, 7.64; N, 1.31.

Characterization of 3a. Yield 89%. $^1\text{H-NMR}$ (400 MHz; CDCl_3); δ/ppm : 0.88 (t, $J_{H-H} = 6.23$ Hz, 9H); 1.32 (m, 39H); 1.75 (m, 6H); 3.30 (t, $J_{H-H} = 8.06$ Hz, 6H); 4.82 (s, 2H); 7.44 (m, 4H). $^{13}\text{C-NMR}$ (400 MHz; CDCl_3); δ/ppm : 14.32; 22.81; 22.94; 26.62; 29.30; 29.36; 31.36; 31.87; 58.86; 63.12; 124.33; 126.61; 132.38; 154.50.

Characterization of MIL 3. Yield 95%. A dark reddish-brown viscous liquid. Characteristic bands for $[\text{FeCl}_3\text{Br}^-]$ anion were observed at 534, 619, and 688 nm using visible spectroscopy. Elemental Anal. Calcd (%) for $\text{C}_{35}\text{H}_{66}\text{BrCl}_3\text{FeN}$ (743.01): C, 56.58; H, 8.95; N, 1.89; Found: C, 57.38; H, 8.35; N, 1.62.



Scheme 1. Synthesis of monocationic and dicationic hydrophobic magnetic ionic liquids

Synthesis of Compound 5. Compound **5** was synthesized as shown in scheme 1. Benzimidazole (2.00 g, 17.0 mmol) and potassium hydroxide (2.01 g, 35.0 mmol) were dissolved in dimethylsulfoxide (30 mL) and stirred for 6 h at room temperature. Then, 1,12-dibromododecane (2.80 g, 8.53 mmol) was added and continuously stirred for 24 h. Water (30 mL) was added to the reaction mixture and the contents subsequently transferred to a separatory funnel. The reaction mixture was then extracted with chloroform (4 x 40 mL). The organic phases were washed several times with water until the aqueous phase was a neutral pH. The organic phases were then collected and dried over anhydrous sodium sulfate. After evaporation of the solvent, compound **5** was dried at 70 °C under reduced pressure for 12 h.²¹ Yield 80-83%. ¹H-NMR (400 MHz; DMSO);

δ /ppm: 1.14 (m, 16H); 1.75 (m, 4H); 4.21 (t, $J_{H-H} = 6.84$ Hz, 4H); 7.18 (m, 2H); 7.23 (m, 2H); 7.58(m, 2H); 7.65 (m, 2H); 8.22 (s, 2H). ^{13}C -NMR (400 MHz; DMSO); δ /ppm: 26.07; 28.47; 28.83; 29.35; 44.04; 110.41; 110.41; 119.38; 119.45; 121.32; 122.19; 133.75; 143.46; 144.04.

2.2.3 General Procedure for the Synthesis of Benzimidazolium Containing Dicationic Heteroanion-based MILs. The synthesis of MILs **6** and **7** is shown in Scheme 1. To a stirred solution of compound **5** (1.24 mmol) in acetonitrile (15 mL), hexadecyl/benzyl bromide (2.60 mmol) was added and stirred at reflux for 48 h. The solvent was evaporated under reduced pressure and the crude compound **6a/7a** was washed with an excess of diethyl ether (4 x 20 mL) using sonication. The dicationic bromide salt (**6a/7a**) was then dried at 80 °C under reduced pressure for 6 h to remove the residual solvent from the product. Compounds **6b** and **7b** were prepared by reacting **6a/7a** (1 mmol) with lithium bis[(trifluoromethyl)sulfonyl]imide (2.2 mmol) in methanol at room temperature for 24 h. After solvent evaporation, the crude compounds were washed with an excess of water and the halide impurities monitored by adding silver nitrate to the aqueous phase. Compounds **6c** and **7c** were obtained by reacting **6b/7b** (1 mmol) with $\text{FeCl}_3 \cdot 6\text{H}_2\text{O}$ (1.2 mmol) in methanol at room temperature under nitrogen atmosphere for 12 h. The solvent was evaporated and the compounds were washed with water (4 x 10 mL) under sonication to remove unreacted iron chloride. Compounds **6c/7c** were dried under vacuum at 80 °C for 16 h to remove residual water. Finally, heteroanion-based MILs (**6** and **7**) were synthesized by mixing **6c** or **7c** (1 mmol) with **6b** or **7b** (1 mmol), respectively, in methanol for 6 h at room temperature.²⁰

Characterization of 6a. Yield 91%. $^1\text{H-NMR}$ (400 MHz; CDCl_3); δ/ppm : 0.82 (t, $J_{\text{H-H}} = 6.32$ Hz, 6H); 1.18 (m, 68H); 2.01 (m, 8H); 4.60 (m, 8H); 7.74 (m, 8H); 11.33 (s, 2H). $^{13}\text{C-NMR}$ (400 MHz; CDCl_3); δ/ppm : 14.17; 22.71; 26.41; 29.68; 29.70; 31.94; 47.71; 113.13; 113.32; 127.20; 131.29; 131.30; 142.51. ESI-MS: $m/2z$ (+): 426.7.

Characterization of 6b. Yield 87%. $^1\text{H-NMR}$ (400 MHz; CDCl_3); δ/ppm : 0.87 (t, $J_{\text{H-H}} = 6\text{H}$); 1.25 (m, 68H); 1.98 (m, 8H); 4.48 (m, 8H); 7.74 (m, 8H); 9.42 (s, 2H). $^{13}\text{C NMR}$ (400 MHz; CDCl_3); $\delta/(\text{ppm})$: 14.40, 22.96; 26.39; 26.69; 29.07; 29.74, 29.95; 32.19; 48.05; 113.33; 113.60; 127.68; 127.76; 131.61; 141.09. ESI-MS: $m/2z$ (+): 426.7; m/z (-): 279.1.

Characterization of MIL 6. Yield 91%. The presence of the paramagnetic anion, $[\text{FeCl}_3\text{Br}^-]$, was confirmed using visible spectroscopy. Elemental Anal. Calcd (%) for $\text{C}_{60}\text{H}_{100}\text{BrCl}_3\text{F}_6\text{FeN}_5\text{O}_4\text{S}_2$ (1375.7): C, 52.38; H, 7.33; N, 5.09; Found: C, 53.28; H, 7.30; N, 5.06.

Characterization of 7a. Yield 92%. $^1\text{H-NMR}$ (400 MHz; DMSO); δ/ppm : 1.21 (m, 16H); 1.92 (m, 4H); 4.52 (t, $J_{\text{H-H}} = 7.14$ Hz, 4H); 5.80 (s, 4H); 7.39 (m, 6H); 7.52 (m, 4H); 7.66 (m, 4H); 7.97 (m, 2H); 8.11 (m, 2H); 10.10 (s, 2H). $^{13}\text{C-NMR}$ (400 MHz; DMSO); δ/ppm : 25.82; 28.45; 28.49; 28.94; 46.84; 49.83; 113.90; 126.64; 128.23; 128.96; 131.29; 134.12; 142.38. ESI-MS: $m/2z$ (+): 292.4.

Characterization of 7b. Yield 90%. $^1\text{H-NMR}$ (400 MHz; CDCl_3); δ/ppm : 1.24 (m, 16H); 1.99 (m, 4H); 4.48 (t, $J_{\text{H-H}} = 7.32$ Hz, 4H); 5.63 (s, 4H); 7.36 (m, 10H); 7.59 (m, 2H); 7.62 (m, 4H); 7.76 (m, 2H); 9.44 (s, 2H). $^{13}\text{C-NMR}$ (400 MHz; CDCl_3); δ/ppm : 26.29; 28.67; 29.01; 29.26; 48.01; 51.56; 113.41; 113.92; 118.33; 121.52; 121.67; 128.22; 129.57; 132.38; 140.90. ESI-MS: $m/2z$ (+): 292.4; m/z (-): 279.1.

Characterization of MIL 7. Yield 88%. A dark brown viscous liquid. Characteristic bands for the $[\text{FeCl}_3\text{Br}^-]$ anion were observed at 534, 619, 688 nm using visible spectroscopy. Elemental Anal. Calcd (%) for $\text{C}_{42}\text{H}_{48}\text{BrCl}_3\text{F}_6\text{FeN}_5\text{O}_4\text{S}_2$ (1107.09): C, 45.57; H, 4.37; N, 6.33; Found: C, 45.93; H, 4.14; N, 6.35.

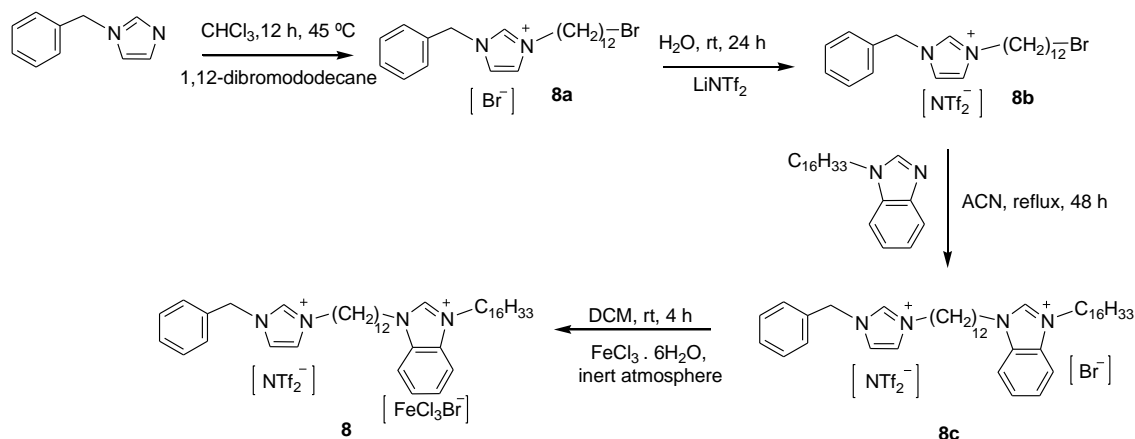
Synthesis of MIL 8. As shown in Scheme 2, compound **8** was synthesized using a reported procedure from the literature with some modifications.²² Briefly, a solution of 1,12-dibromododecane (8.20 g, 25.0 mmol in 30 mL of chloroform) was added dropwise using a syringe to a stirred solution of *N*-benzylimidazole (1.00 g, 6.32 mmol) in chloroform (40 mL) for 2 h. The reaction mixture was allowed to stir for 12 h under reflux. The crude compound, **8a**, was obtained by evaporating the solvent under reduced pressure and washed with excess of hexanes and ethyl acetate (1:1; 3 x 30 mL) under sonication to remove the unreacted starting materials. Compound **8a** was dried in vacuum at 70 °C for 16 h to remove the residual solvents. Compound **8b** was obtained by anion-exchange of **8a** with LiNTf_2 in water at room temperature for 24 h. After drying, compound **8b** (0.30 g, 0.43 mmol) was reacted with previously synthesized 1-hexadecylbenzimidazole²³ (0.153 g, 0.450 mmol) in acetonitrile under reflux for 48 h. The resulting crude compound **8c** was washed with an excess of diethyl ether under sonication and dried under reduced pressure at 70 °C for 24 h. Finally, **8c** (1 mmol) was reacted with $\text{FeCl}_3 \cdot 6\text{H}_2\text{O}$ (1.1 mmol) in dichloromethane at room temperature for 6 h to yield crude compound **8**. After evaporation of the solvent, compound **8** was washed several times with water to remove the unreacted iron chloride and dried under vacuum for 4 h at 70 °C.

Characterization of 8b. Yield 65%. $^1\text{H-NMR}$ (400 MHz; DMSO); δ/ppm : 1.23 (m, 16H); 1.78 (m, 4H); 3.52 (t, $J_{\text{H-H}} = 6.59$ Hz, 2H); 4.16 (t, $J_{\text{H-H}} = 6.96$ Hz, 2H); 5.41 (s, 2H); 7.41 (m, 5H); 7.81 (m, 2H); 9.29 (s, 1H).

^{13}C -NMR (400 MHz; DMSO); δ/ppm : 26.17; 28.19; 28.79; 28.99; 29.49; 29.49; 29.55; 29.90; 32.89; 35.95; 49.64; 52.63; 123.28; 123.49; 128.87; 129.69; 136.79. ESI-MS: m/z (+): 407.3;

Characterization of 8c. Yield 82%. ^1H -NMR (400 MHz; DMSO); δ/ppm : 0.84 (t, $J_{\text{H-H}} = 6.59$ Hz, 3H); 1.21 (m, 42H); 1.76 (m, 2H); 1.89 (m, 4H); 4.15 (t, $J_{\text{H-H}} = 6.96$ Hz, 2H); 4.48 (t, $J_{\text{H-H}} = 6.59$ Hz, 4H); 5.41 (s, 2H); 7.40 (m, 5H); 7.70 (m, 2H); 7.82 (m, 3H); 8.11 (m, 2H); 9.29 (s, 1H); 9.80 (s, 1H). ^{13}C -NMR (400 MHz; DMSO); δ/ppm : 13.98; 22.13; 25.58; 25.72; 25.82; 28.43; 29.06; 29.31; 31.32; 46.69; 48.89; 51.98; 113.74; 122.61; 122.80; 126.57; 128.21; 129.01; 131.10; 134.48; 136.10; 142.04. ESI-MS: m/z (+): 334.7;

Characterization of MIL 8. Yield 91%. A dark brown viscous liquid. Characteristic bands for the $[\text{FeCl}_3\text{Br}^-]$ anion were observed at 534, 619, and 688 nm using visible spectroscopy. Elemental Anal. Calcd (%) for $\text{C}_{47}\text{H}_{72}\text{BrCl}_3\text{F}_6\text{FeN}_5\text{O}_4\text{S}_2$ (1191.33): C, 47.38; H, 6.09; N, 5.88; Found: C, 47.85; H, 6.17; N, 6.07.



Scheme 2. Synthesis of dicationic heterocation-based hydrophobic magnetic ionic liquids

Synthesis of Compound 9. Compound **9** was synthesized according to a previously reported procedure.²¹ A detailed synthetic procedure is available in the Supporting Information Yield 70-75%. ^1H -NMR (400 MHz; CDCl_3); δ/ppm : 5.08 (s, 6H); 6.84 (m, 6H); 7.12 (s, 3H); 7.52 (s, 3H). ^{13}C -NMR (400 MHz; CDCl_3); δ/ppm : 50.37; 119.40; 125.77; 130.45; 137.61; 138.65.

Synthesis of Compound 10. As shown in Scheme 3, compound **10a** was synthesized from compound **9** by following a procedure from the literature.²¹ Compound **10** was prepared by mixing compound **10a** (1 mmol) with $\text{FeCl}_3 \cdot 6\text{H}_2\text{O}$ (3.1 mmol) in methanol under nitrogen atmosphere at room temperature for 4 h. After evaporation of solvent, compound **10** was washed with water (4 x 10 mL) and dried under vacuum at 60 °C for 12 h.²⁰

Characterization of 10a. Yield 87%. $^1\text{H-NMR}$ (400 MHz; CDCl_3); δ/ppm : 0.88 (t, $J_{\text{H-H}} = 6.59$ Hz, 9H); 1.26 (m, 54H); 1.89 (m, 6H); 4.22 (t, $J_{\text{H-H}} = 7.32$ Hz, 6H); 5.55 (s, 6H); 7.08 (s, 3H); 8.62 (m, 6H); 10.41 (s, 3H). $^{13}\text{C-NMR}$ (400 MHz; CDCl_3); δ/ppm : 14.36; 22.91; 26.51; 29.19; 29.55; 29.59; 29.81; 32.12; 50.45; 52.21; 121.46; 124.62; 132.12; 135.77; 136.58.

Characterization of MIL 10. Yield 94%. A dark brown viscous liquid. The $[\text{FeCl}_3\text{Br}^-]$ anion was characterized using visible spectroscopy showing characteristic bands at 534, 619, and 688 nm. Elemental Anal. Calcd (%) for $\text{C}_{54}\text{H}_{90}\text{Br}_3\text{Cl}_9\text{Fe}_3\text{N}_6$ (1549.66): C, 41.85; H, 5.85; N, 5.42; Found: C, 41.65; H, 6.22; N, 5.82;

Synthesis of MIL 11. For the synthesis of MIL **11**, shown in Scheme 3, allylbromide (0.590 g, 4.89 mmol) was added to a stirred solution of compound **9** (0.50 g, 1.6 mmol) in acetonitrile (15 mL) at 40-50 °C and stirred for 48 h. After evaporating the solvent *in vacuo*, the residue was washed with hexanes (3 x 15 mL) and dried under vacuum at 60 °C for 6 h to yield compound **11a**. A mixture of **11a** (0.30 g, 0.44 mmol), 1-octanethiol (0.579 g, 3.96 mmol) and 2,2-dimethoxy-2-phenylacetophenone (0.169 g, 0.659 mmol) in 10 mL of methanol/dichloromethane (1:1) was then transferred to a quartz tube and stirred until homogeneity. The contents were then exposed to UV radiation (254 nm) for 16 h. The solvent was evaporated and the crude compound washed with hexanes (4 x 30 mL) under sonication. Removal of residual solvents under vacuum yielded compound **11b**.²⁴ Finally,

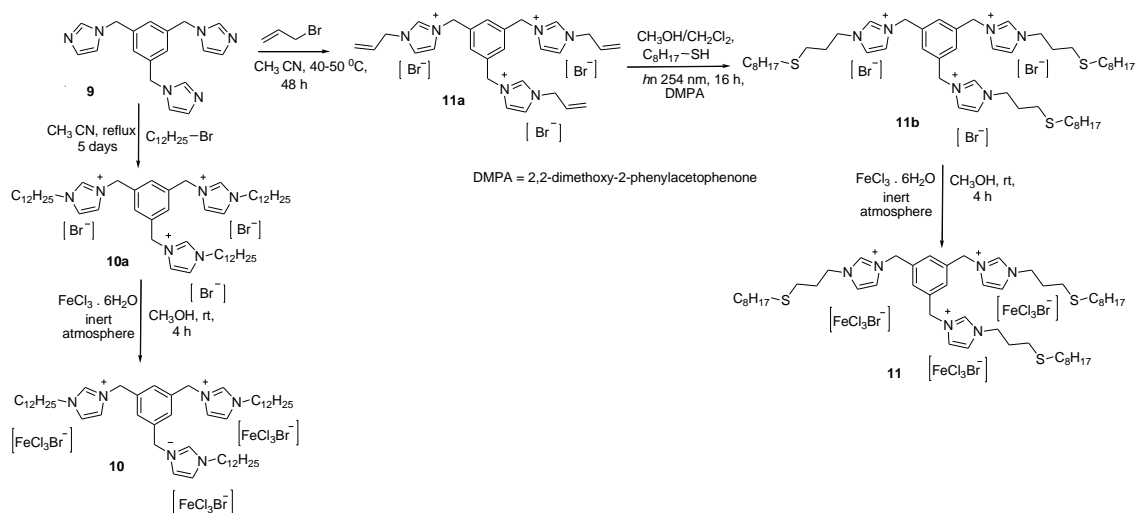
11b (1 mmol) was mixed with $\text{FeCl}_3 \cdot 6\text{H}_2\text{O}$ (3.10 mmol) in methanol at room temperature under nitrogen atmosphere for 4 h to form compound **11**. Methanol was evaporated and MIL **11** was washed with deionized water and dried at 70 °C for 12 h.²⁰

Characterization of 11a. Yield 91%; $^1\text{H-NMR}$ (400 MHz; CDCl_3); δ/ppm : 4.89 (d, $J_{H-H} = 6.59$ Hz, 6H); 5.45 (m, 3H); 5.48 (d, $J_{H-H} = 4.76$ Hz, 3H); 5.58 (s, 6H); 5.99 (m, 3H); 7.16 (s, 3H); 8.46 (s, 3H); 8.52 (s, 3H); 10.34 (s, 3H). $^{13}\text{C-NMR}$ (400 MHz; CDCl_3); δ/ppm : 52.28; 52.50; 121.42; 123.23; 124.58; 129.68; 131.91; 135.71; 136.74.

Characterization of 11b. Yield 85%. $^1\text{H-NMR}$ (400 MHz; CDCl_3); δ/ppm : 0.88 (t, $J_{H-H} = 6.23$ Hz, 9H); 1.27 (m, 35H); 1.55 (m, 6H); 2.21 (m, 6H); 2.49 (t, $J_{H-H} = 7.32$ Hz, 6H); 2.55 (t, $J_{H-H} = 6.59$ Hz, 6H); 4.39 (t, $J_{H-H} = 6.96$ Hz, 6H); 5.56 (s, 6H); 7.17 (s, 3H); 8.58 (m, 6H); 10.42 (s, 3H); $^{13}\text{C-NMR}$ (400 MHz; CDCl_3); δ/ppm : 14.67; 23.20; 28.82; 29.43; 29.74; 30.03; 32.35; 32.71; 49.18; 52.66; 122.25; 124.88; 132.53; 136.02; 137.15.

Characterization of MIL 11. Yield 91%. A dark brown viscous liquid. Characteristic bands for the $[\text{FeCl}_3\text{Br}^-]$ anion were observed at 534, 619, and 688 nm using visible spectroscopy. Elemental Anal. Calcd (%) for $\text{C}_{51}\text{H}_{87}\text{Br}_3\text{Cl}_9\text{Fe}_3\text{N}_6\text{S}_3$ (1606.8): C, 38.12; H, 5.46; N, 5.23; Found: C, 39.10; H, 5.62; N, 5.44.

Synthesis of MIL 12. The synthesis of MIL **12** is shown in Scheme 4. Compound **9** (0.60 g, 1.9 mmol) was dissolved in acetonitrile (50 mL) and added dropwise to a solution of bromobutane (0.517 g, 3.78 mmol) in acetonitrile (20 mL). The reaction mixture was stirred under reflux for 72 h. After evaporation of solvent, the crude compound was washed with diethyl ether (3 x 30 mL) under sonication for 30 min.²⁵ Compound **12a** (1 mmol) was then dissolved in water and allowed to react with LiNTf_2 (2.20 mmol) at room temperature for 24 h. **12b** was then filtered and washed several times with water and monitored for the presence of halide impurities by adding silver nitrate. Compound **12b** (0.4 g, 0.4 mmol) was reacted with bromohexadecane (0.126 g, 0.413 mmol) in acetonitrile under reflux for



Scheme 3. Synthesis of symmetrical tricationic alkylated and thiaalkylated-based hydrophobic magnetic ionic liquids

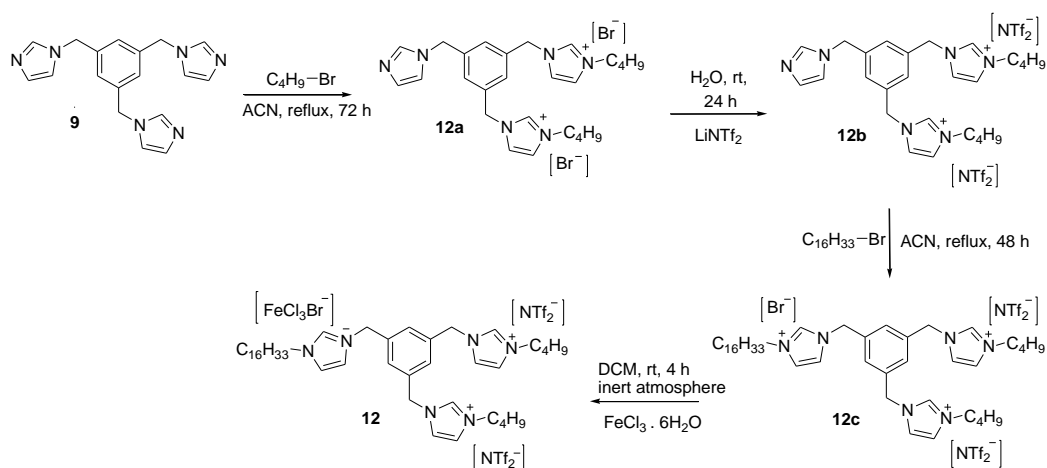
in vacuo, the residue was washed several times with hexanes (4 x 10 mL) and dried at 70 °C for 12 h. Finally, MIL **12** was synthesized by reacting **12c** (0.30 g, 0.23 mmol) with $\text{FeCl}_3 \cdot 6\text{H}_2\text{O}$ (0.062 g, 0.25 mmol) in dichloromethane at room temperature for 4 h under nitrogen atmosphere. The solvent was evaporated and MIL **12** was washed with water (10 mL) under sonication to remove unreacted iron chloride.²⁰

Characterization of 12a. Yield 78%. $^1\text{H-NMR}$ (400 MHz; DMSO); δ/ppm : 0.91 (t, $J_{\text{H-H}} = 6.59$ Hz, 6H); 1.26 (m, 4H); 1.79 (m, 4H); 4.20 (m, 4H); 5.20 (m, 2H); 5.44 (m, 4H); 6.92 (s, 1H); 7.32 (m, 3H); 7.75 (m, 6H); 9.42 (m, 2H); $^{13}\text{C-NMR}$ (400 MHz; DMSO); δ/ppm : 14.01; 19.51; 31.96; 49.41; 52.09; 123.27; 123.51; 128.35; 129.36; 136.80; 136.93; 139.77; 140.08.

Characterization of 12b. Yield 91%. $^1\text{H-NMR}$ (400 MHz; DMSO); δ/ppm : 0.91 (t, $J_{\text{H-H}} = 6.59$ Hz, 6H); 1.23 (m, 4H); 1.77 (m, 4H); 4.17 (m, 4H); 5.22 (m, 2H); 5.41 (m, 4H); 7.00 (s, 1H); 7.25 (m, 3H); 7.42 (m, 1H); 7.84 (m, 5H); 9.25 (s, 2H); $^{13}\text{C-NMR}$ (400 MHz; DMSO); δ/ppm : 13.35; 18.87; 31.35; 48.79; 49.50; 51.51; 122.60; 122.65; 122.92; 126.65; 127.65; 136.18; 136.26;

Characterization of 12c. Yield 85%. $^1\text{H-NMR}$ (400 MHz; DMSO); δ/ppm : 0.91 (t, $J_{\text{H-H}} = 6.59$ Hz, 9H); 1.23 (m, 28H); 1.78 (m, 6H); 4.18 (t, $J_{\text{H-H}} = 7.32$ Hz, 6H); 5.43 (s, 6H); 7.46 (s, 3H); 7.76 (s, 3H); 7.85 (s, 3H); 9.33 (s, 3H). $^{13}\text{C-NMR}$ (400 MHz; DMSO); δ/ppm : 13.34; 18.86; 22.14; 29.09; 31.33; 48.78; 51.41; 122.58; 122.82; 128.66; 136.26.

Characterization of MIL 12. Yield 90%. A dark brown viscous liquid. The $[\text{FeCl}_3\text{Br}^-]$ anion was characterized using visible spectroscopy showing absorption bands at 534, 619, and 688 nm. Elemental Anal. Calcd (%) for $\text{C}_6\text{H}_6\text{BrCl}_3\text{F}_{12}\text{FeN}_8\text{O}_8\text{S}_4$ (1457.15): C, 37.83; H, 4.76; N, 7.67; Found: C, 37.33; H, 4.37; N, 7.39.



Scheme 4. Synthesis of unsymmetrical tricationic heterocation-based hydrophobic MILs

2.3 Results and discussion

2.3.1 Preparation of Monocationic Ammonium-based Hydrophobic MILs. The general strategy used to prepare MILs in this study is based on the synthesis of bromide salt precursors and their subsequent reaction with $\text{FeCl}_3 \cdot 6\text{H}_2\text{O}$. Coordination of bromide to the iron(III) center produces the $[\text{FeCl}_3\text{Br}^-]$ anion, which imparts paramagnetic properties to the resulting MIL.

Imidazolium-based MILs are an extensively studied class of compounds due to relatively low reagent costs and ease of functionalization. Initial attempts were made to enhance the hydrophobicity of MILs by incorporating long hydrocarbon chains and/or

bulky aromatic moieties to the imidazolium cation, as shown in Table S1. However, entries **1-4**^{20,23} were soluble in water below 5% (w/v) and were room temperature solids with higher melting points. In addition to van der Waals and π - π interactions, it has been suggested that the presence of the acidic proton on the 2-position of the imidazolium ring favors hydrogen bonding with the MIL anion and discourages the formation of lower melting point MILs.¹⁸ Therefore, the strategy employed in this study involved the design of monocationic MILs that lack acidic protons and could be readily functionalized.

Quaternary ammonium cations are commonly exploited in IL structures due to their ease of customization and control over physicochemical properties.^{26,27} To improve the hydrophobic character of the resulting MIL, trioctylamine was chosen and quaternized with alkyl halides. The reaction of trioctylamine and butyl/decyl bromide resulted in low yields of the bromide salt (<20%) with most of the starting materials left unreacted, even after 7 days (based on ¹H NMR spectroscopy). In contrast, the same reaction conditions with benzyl bromide produced higher yields (>90%) and proceeded to completion within 72 h, as shown in Scheme 1. This may be due to resonance stabilization of the carbocation by the aromatic moiety. It was also possible to incorporate functionalized benzyl substituents including 3-methoxybenzyl and 4-*tert*-butylbenzyl into the quaternary ammonium structure, demonstrating the ability to generate unique substitutions within the monocationic MIL framework.

The solubility of the ammonium-based MILs in water and hexane is shown in Table 1. Independent of the substituent functional groups imparted by the quaternization reaction, MILs **1-3** were immiscible with water at compositions as low as 0.1% (w/v) MIL. The hydrophobic properties of the monocationic MILs are thus ideal for applications such as aqueous liquid-liquid microextractions, where extremely low phase ratios of extraction solvent are employed.

2.3.2 Structural Tuning of Symmetrical/Unsymmetrical Dicationic Hydrophobic

MILs. Dicationic ILs provide more opportunities for control of physical and chemical properties compared to conventional monocationic ILs. The dicationic IL platform is especially relevant and useful for MILs, which require at least a paramagnetic anion to provide sufficient magnetic susceptibility. Previous work by Brown *et al.* prompted an investigation in this study to pair one cation in a dicationic system with the $[\text{NTf}_2^-]$ anion and produce functionalized hydrophobic MILs based on imidazolium cations.²⁰ In general, the synthesis of symmetrical imidazolium-based dicationic MILs was performed in three steps. Firstly, a dicationic bromide salt was synthesized with alkyl/aromatic substituents on the cation. A dodecyl linkage chain between the imidazolium-based cations was employed to increase the conformational degrees

Table 1. Physicochemical and magnetic properties of hydrophobic MILs synthesized in this study.

MIL	MW (g/mol)	Melting point (°C)	μ_{eff}^a (μ_B)	Thermal stability ^b (°C)	Solubility in hexanes	Solubility in water
1	686.9	-53.2 (T_g)	5.26	258	I	I ^c
2	716.9	<-65	5.60	203	I	I ^c
3	743.01	-50.7 (T_g)	5.68	222	I	I ^c
4A	1035.0	-32.6 (T_g)	5.40	310	I	I ^d
4B	1303.6	<25	5.37	294	I	I ^d
6c	1338.9	<25	7.58	299	I	I ^d
6	1375.7	-0.6	5.69	314	I	I ^c
7	1107.1	-6.7 (T_g)	5.45	311	I	I ^c
8	1191.3	-16.7	5.30	312	I	I ^c
10	1549.6	<-65	11.25	312	I	I ^d
11	1606.8	<-65	11.76	225	I	I ^d
12	1457.1	5.0	5.10	276	I	I ^c

T_g = glass transition temperature; ^a μ_{eff} = effective magnetic moment measured at 295 K; ^b Thermal gravimetric analysis (TGA) = temperature at which 5% wt loss of MIL is observed; I = insoluble; ^c Insoluble at 0.1% (w/v); ^d Insoluble at 0.25% (w/v).

of freedom, thus improving the likelihood of forming low-melting MILs. Two homoanion precursors were then synthesized from the dibromide salt, either by anion-exchange to incorporate hydrophobic $[\text{NTf}_2^-]$ anions or reaction with $\text{FeCl}_3 \cdot 6\text{H}_2\text{O}$ to generate paramagnetic $[\text{FeCl}_3\text{Br}^-]$ anions. Finally, mixing equimolar quantities of the $[\text{NTf}_2^-]$ and $[\text{FeCl}_3\text{Br}^-]$ salts produced dicationic MILs with heteroanions.

When functionalized with benzyl substituents, the imidazolium-based dicationic MIL **4A**^{20,28} exhibited water solubility below 0.25% (w/v), as shown in Table 1. Blocking the acidic C-2 proton of the hexadecyl functionalized imidazolium dication with a methyl group (**4B**)^{20,23,28} resulted in similar water solubility to **4A**. The hydrophobicity of this class of MILs was significantly improved by replacing the imidazolium cation with the benzimidazolium cation. MILs **6** and **7** were synthesized according to Scheme 1. Improved hydrophobic character was observed for **6** and **7**, which were insoluble in water at 0.1% (w/v) MIL.

Another important structural feature that has profound implications on the physicochemical properties of ILs is the presence of asymmetry in the molecule.²⁹ Dicationic ILs are uniquely amenable to unsymmetrical archetypes since it is possible to independently functionalize the cationic moieties.^{29,30} Drawing on the improved hydrophobicity obtained for dicationic MILs **6** and **7**, a MIL that tethers benzimidazolium and imidazolium cations was produced. Scheme 2 illustrates the synthesis of the heterocationic MIL **8**. Initially, reaction of 1,12-dibromododecane with benzylimidazole in a 1:1 mole ratio resulted in formation of 20% (based on ^1H NMR) of the dibromide salt. However, increasing the mole ratio of 1,12-dibromododecane to 4.5:1 significantly reduced the formation of the dibromide salt to $\leq 5\%$, based on ^1H NMR. The metathesis reaction of compound **8a** with 1.2 molar equivalent of LiNTf_2 formed a precipitate (**8b**) while the dicationic $[\text{Br}^-]/[\text{NTf}_2^-]$ analogue remained in the aqueous phase.³⁰ After the incorporation

of the hydrophobic anion, compound **8b** was reacted with previously synthesized hexadecylbenzimidazole to generate the unsymmetrical dicationic $\text{Br}^-/\text{NTf}_2^-$ salt **8c**. Finally, hydrophobic MIL **8** was synthesized by reacting compound **8c** with $\text{FeCl}_3 \cdot 6\text{H}_2\text{O}$. Similar to MILs **1-3**, **6**, and **7**, the heterocationic MIL **8** was insoluble in water down to 0.1% (w/v) MIL.

2.3.3 Synthesis of Symmetrical Alkylated/Thiaalkylated and Unsymmetrical Tricationic Hydrophobic MILs. The synthesis of symmetrical tricationic hydrophobic MILs **10** and **11** is shown in Scheme 3. With the aim of minimizing water solubility of the resulting MILs, a relatively hydrophobic benzene core functionalized with three imidazole moieties (**9**) was selected from the literature as a precursor and prepared accordingly.²¹ Compound **9** was then alkylated by reaction with 1-bromododecane for 5 days in acetonitrile to generate compound **10a**. Subsequent mixing with $\text{FeCl}_3 \cdot 6\text{H}_2\text{O}$ produced hydrophobic MIL **10**. From Scheme 3, it is clear that synthesis of the tribromide salt **10a** was the most time-consuming step. In an effort to reduce the time required for the generation of a MIL with similar magnetic susceptibility and hydrophobicity to MIL **10**, thiol-ene click chemistry was employed. The thiol-based approach has been shown to provide a convenient route for modification of the cationic portion of monocationic ILs,²⁴ but has been unexplored in tricationic IL systems. Using a similar synthetic route, the tricationic hydrophobic MIL **11** was synthesized as shown in Scheme 3.

For synthesis of MIL **11**, intermediate **9** was reacted with allylbromide for 48 h in acetonitrile to produce compound **11a**. In comparison to the sluggish formation of the bromide salt **10a**, compound **11a** was more rapidly generated, possibly due to the resonance stabilization of allylic carbocation. Compound **11b** was prepared by reacting **11a** with octanethiol in a methanol/dichloromethane (1:1) solvent mixture in the presence of UV irradiation for 16 h. Exclusive formation of anti-Markovnikov oriented products as

previously noted by Davis *et al*²⁴ was confirmed by ¹H NMR. Excess amounts of unreacted starting materials were easily removed by washing the crude compound with hexanes. Thus, the total reaction time required for the generation of the thiaalkyl-based tribromide salt (**11b**) was significantly less in comparison with **10a**. Finally, the hydrophobic MIL **11** was prepared by reacting **11b** with FeCl₃·6H₂O. From Table 1, MILs **10** and **11** were shown to be insoluble in aqueous solution down to 0.25% (w/v) MIL.

In an effort to improve the hydrophobic character of the tricationic MILs, hydrophobic [NTf₂⁻] anions were incorporated into the molecular structure, as shown in MIL **12**. Previous studies indicated that when intermediate **9** was reacted with alkyl halides such as 1-bromooctane, subsequent anion-exchange with [NTf₂⁻] led to the formation of room temperature solids ($T_m = 51.1$ °C).²⁵ Formation of MILs with lower melting points involved reacting intermediate **9** with 1-bromobutane to yield the dibromide salt (**12a**), as shown in Scheme 4. Hydrophobic [NTf₂⁻] anions were then incorporated by metathesis reaction of **12a**. Generation of the unsymmetrical tricationic IL was accomplished by reacting **12b** with 1-bromohexadecane to produce compound **12c**. Finally, MIL **12** was generated by reacting compound **12c** with FeCl₃·6H₂O in dichloromethane for 4 h. As shown in Table 1, MIL **12** exhibited improved hydrophobicity in comparison to MILs **10** and **11**.

2.3.4 Thermal Properties of Hydrophobic MILs. The phase transition behavior and thermal stability of the eleven hydrophobic MILs were studied using DSC and TGA and the results compiled in Table 1. Monocationic MILs **1** and **3** exhibited glass transition temperatures (T_g) of -53.2 °C and -50.7 °C, respectively. A melting point (T_m) for MIL **2** could not be detected above -65 °C. These values were much lower in comparison with ammonium-based MILs possessing only linear alkyl substituents.³¹ Previous reports dictate that the total number of carbon atoms and asymmetry of the cation structure govern the T_m of quaternary ammonium salts.²⁷ Hence, the relatively low T_g of MILs **1** and **3** may be

explained by the asymmetry resulting from incorporation of aromatic moieties within the cation structure. Interestingly, while MIL **1** was thermally stable up to 258 °C, similar weight loss (5%) was observed at lower temperatures for the methoxy (**2**) and *t*-butyl (**3**) functionalized monocationic MILs.

Symmetrical dicationic MILs with heteroanions (**4A**, **4B**, **6**, and **7**) exhibited higher phase transition temperatures than the monocationic MILs but were nonetheless liquids at room temperature. Despite similar cation substituents, MIL **7** exhibited a higher T_g than **4A** which may be attributed to enhanced π - π interactions as a consequence of the benzimidazolium cation. The dicationic MILs exhibited no more than 5% weight loss below temperatures ranging from 294 °C to 312 °C. No significant enhancement in thermal stability was observed for the dicationic MILs containing $[\text{NTf}_2^-]/[\text{FeCl}_3\text{Br}^-]$ heteroanions compared to those containing $2[\text{FeCl}_3\text{Br}^-]$ homoanions.

The effect of dissimilar cationic moieties on the melting point of dicationic MILs is shown in Figure S1. Unsymmetrical replacement of the hexadecylbenzimidazolium cation with the benzylimidazolium cation lowered the T_m from -0.6 °C to -16.7 °C (MILs **6** and **8**, respectively), an outcome that may be attributed to diminished π - π interactions as well as removal of the dication symmetry component.²⁹ Analogous to conventional dicationic ILs, endothermic peaks in DSC traces were quite broad with observable shouldering. This may be due to the highly flexible nature of the MIL cations, which allows different conformations and multiple step phase transitions.²⁵

Phase transitions were not observed above -65 °C for the heavily alkylated/thiaalkylated symmetrical tricationic MILs **10** and **11**. Both compounds **10** and **11** are room temperature liquids in contrast to their corresponding bromide salts. This is most certainly a function of incorporating the weaker coordinating $[\text{FeCl}_3\text{Br}^-]$ anion.

The thermal decomposition temperatures varied significantly between the alkylated (**10**) and thiaalkylated (**11**) hydrophobic tricationic MILs. Possessing a more thermally labile C–S bond,³² MIL **11** exhibited 5% weight loss at 225 °C compared to 312 °C and 275 °C for MIL **10** and **12**, respectively.

2.3.5 Magnetic properties of hydrophobic MILs. The paramagnetic properties of MILs provide a unique advantage over conventional ILs by permitting control over substrate motion through the application of an external magnetic field. MILs containing high-spin d⁵ iron(III) centers are well characterized owing to the abundance and low cost of iron materials and have repeatedly been shown to exhibit paramagnetism at ambient temperatures.^{3,7,20,31} Table 1 shows the effective magnetic moments for all eleven MILs, determined using an Evans magnetic susceptibility balance.³³ The general expression for molar magnetic susceptibility using the Evans balance is shown in Equation 1:

$$X_M = \frac{C_{bal}LM(R-R_o)}{10^9m} \quad (\text{Equation 1})$$

where X_M represents the molar magnetic susceptibility, C_{bal} is the balance calibration constant, L corresponds to the length of the sample in the tube, M is the molecular weight of the compound being measured, R is the instrument reading for the sample in the tube, R_o is the instrument reading for the empty sample tube, and m is the mass of sample introduced into the Evan's balance. From X_M , it is possible to calculate μ_{eff} according to Equation 2:

$$\mu_{\text{eff}} = 2.83\sqrt{X_M T} \quad (\text{Equation 2})$$

where T is the absolute temperature. The μ_{eff} for ammonium-based monocationic MILs ranged from 5.26 to 5.68 μ_B and were comparable to those determined for heteroanionic MILs possessing a single $[\text{FeCl}_3\text{Br}^-]$ anion (**4A**, **4B**, **6**, **7**, **8**, and **12**). A video showing the magnetic manipulation of MIL **1** in aqueous solution is available in the ESI†. In an effort to increase the magnetic susceptibility of MILs, multiple paramagnetic iron(III) centers were incorporated into the MIL structure. For example, dicationic MIL **6c** was designed to

possess two paramagnetic iron(III) centers providing an increase in μ_{eff} to nearly $7.6 \mu_{\text{B}}$. Further enhancement of magnetic susceptibility was observed in tricationic MILs **10** and **11**, which exhibited $\mu_{\text{eff}} = 11.25 \mu_{\text{B}}$ and $11.76 \mu_{\text{B}}$, respectively. The iron(III)-based MILs represent an inexpensive and readily available alternative to MILs based on lanthanides, such as Dy(III) ($\mu_{\text{eff}} = 10.6 \mu_{\text{B}}$).¹⁵ Moreover, the higher response of MILs **10** and **11** toward magnetic fields enables the use of smaller magnets with lower field strength for their manipulation in solution, which may prove useful in miniaturized magnet-based systems.³⁴

2.4 Conclusions

In this study, three general classes of hydrophobic MILs were successfully synthesized and characterized. Within each class, unique synthetic approaches were exploited to control the magnetic and physicochemical properties of MILs. The incorporation of benzyl substituents within the MIL structure of monocationic quaternary ammonium-based hydrophobic MILs produced lower melting point compounds compared to linear alkyl substituents. The hydrophobicity of dicationic MILs was enhanced by replacing imidazolium cations with benzimidazolium cations, resulting in MILs that are insoluble in water down to 0.1% (w/v). Moreover, the inclusion of asymmetry within the cationic portion of dicationic MILs lowered the melting point without sacrificing hydrophobicity or magnetic susceptibility. Additionally, increasing the number of paramagnetic iron(III) centers in the MIL structure resulted in higher μ_{eff} values. Throughout the preparation of tricationic MILs, a common intermediate was chosen and modified to alter the hydrophobicity and magnetic properties of resulting MILs. Tricationic MILs containing three $[\text{FeCl}_3\text{Br}^-]$ anions exhibited μ_{eff} values as high as $11.76 \mu_{\text{B}}$, representing the highest known value reported for MILs. The synthesis of iron(III)-based tricationic hydrophobic MILs possessing large μ_{eff} is an inexpensive alternative to MILs based on lanthanides.

Acknowledgments

The authors acknowledge funding from Agilent Technologies and the Chemical Measurement and Imaging Program at the National Science Foundation (Grant number CHE-1413199). K. D. C. thanks the University of Toledo College of Graduate Studies for a graduate fellowship. Omar Badawi is thanked for his assistance during the synthesis of the MILs.

Supporting information

NMR spectra, absorbance spectrum of $[\text{FeCl}_3\text{Br}^-]$, synthesis of compound **9**, Table S1, Figure S1 are provided in Appendix A.

References

- (1) Hallett, J. P.; Welton, T. *Chem. Rev.* **2011**, *111*, 3508-3576.
- (2) H. Davis, J. J. *Chem. Lett.* **2004**, *33*, 1072-1077.
- (3) Hayashi, S.; Hamaguchi, H.-o. *Chem. Lett.* **2004**, *33*, 1590-1591.
- (4) Sitze, M. S.; Schreiter, E. R.; Patterson, E. V.; Freeman, R. G. *Inorg. Chem.* **2001**, *40*, 2298-2304.
- (5) Santos, E.; Albo, J.; Irabien, A. *RSC Adv.* **2014**, *4*, 40008-40018.
- (6) Yoshida, Y.; Saito, G. *Phys. Chem. Chem. Phys.* **2010**, *12*, 1675-1684.
- (7) Yoshida, Y.; Saito, G. *J. Mater. Chem.* **2006**, *16*, 1254-1262.
- (8) Wang, G.; Yu, N.; Peng, L.; Tan, R.; Zhao, H.; Yin, D.; Qiu, H.; Fu, Z.; Yin, D. *Catal. Lett.* **2008**, *123*, 252-258.
- (9) Dobbelin, M.; Jovanovski, V.; Llarena, I.; Claros Marfil, L. J.; Cabanero, G.; Rodriguez, J.; Mecerreyes, D. *Polym. Chem.* **2011**, *2*, 1275-1278.
- (10) Branco, A.; Branco, L. C.; Pina, F. *Chem. Commun.* **2011**, *47*, 2300-2302.
- (11) Scovazzo, P.; Portugal, C. A. M.; Rosatella, A. A.; Afonso, C. A. M.; Crespo, J. G. *J. Colloid Interface Sci.* **2014**, *428*, 16-23.
- (12) Santos, E.; Albo, J.; Daniel, C. I.; Portugal, C. A. M.; Crespo, J. G.; Irabien, A. *J. Membr. Sci.* **2013**, *430*, 56-61.
- (13) Hantao, L. W.; Najafi, A.; Zhang, C.; Augusto, F.; Anderson, J. L. *Anal. Chem.* **2014**, *86*, 3717-3721.

- (14) Nockemann, P.; Thijs, B.; Postelmans, N.; Van Hecke, K.; Van Meervelt, L.; Binnemans, K. *J. Am. Chem. Soc.* **2006**, *128*, 13658-13659.
- (15) Mallick, B.; Balke, B.; Felser, C.; Mudring, A.-V. *Angew. Chem. Int. Ed.* **2008**, *47*, 7635-7638.
- (16) Lee, S. H.; Ha, S. H.; Ha, S.-S.; Jin, H.-B.; You, C.-Y.; Koo, Y.-M. *J. Appl. Phys.* **2007**, *101*, 09J102-3.
- (17) Wang, J.; Yao, H.; Nie, Y.; Bai, L.; Zhang, X.; Li, J. *Ind. Eng. Chem. Res.* **2012**, *51*, 3776-3782.
- (18) Del Sesto, R. E.; McCleskey, T. M.; Burrell, A. K.; Baker, G. A.; Thompson, J. D.; Scott, B. L.; Wilkes, J. S.; Williams, P. *Chem. Commun.* **2008**, 447-449.
- (19) Deng, N.; Li, M.; Zhao, L.; Lu, C.; de Rooy, S. L.; Warner, I. M. *J. Hazard. Mater.* **2011**, *192*, 1350-1357.
- (20) Brown, P.; Butts, C. P.; Eastoe, J.; Padron Hernandez, E.; Machado, F. L. d. A.; de Oliveira, R. J. *Chem. Commun.* **2013**, *49*, 2765-2767.
- (21) Planellas, M.; Pleixats, R.; Shafir, A. *Adv. Synth. Catal.* **2012**, *354*, 651-662.
- (22) Lee, B. S.; Chi, Y. S.; Lee, J. K.; Choi, I. S.; Song, C. E.; Namgoong, S. K.; Lee, S.-g. *J. Am. Chem. Soc.* **2003**, *126*, 480-481.
- (23) Baltazar, Q. Q.; Chandawalla, J.; Sawyer, K.; Anderson, J. L. *Colloids Surf., A* **2007**, *302*, 150-156.
- (24) Mirjafari, A.; O'Brien, R. A.; West, K. N.; Davis, J. H. *Chem. Eur. J.* **2014**, *20*, 7576-7580.
- (25) D'Anna, F.; Nimal Gunaratne, H. Q.; Lazzara, G.; Noto, R.; Rizzo, C.; Seddon, K. R. *Org. Biomol. Chem.* **2013**, *11*, 5836-5846.
- (26) Eike, D. M.; Brennecke, J. F.; Maginn, E. J. *Green Chem.* **2003**, *5*, 323-328.
- (27) Gordon, J. E.; Rao, G. N. S. *J. Am. Chem. Soc.* **1978**, *100*, 7445-7454.
- (28) Anderson, J. L.; Ding, R.; Ellern, A.; Armstrong, D. W. *J. Am. Chem. Soc.* **2004**, *127*, 593-604.
- (29) Payagala, T.; Huang, J.; Breitbach, Z. S.; Sharma, P. S.; Armstrong, D. W. *Chem. Mater.* **2007**, *19*, 5848-5850.
- (30) Chang, J.-C.; Ho, W.-Y.; Sun, I. W.; Tung, Y.-L.; Tsui, M.-C.; Wu, T.-Y.; Liang, S.-S. *Tetrahedron* **2010**, *66*, 6150-6155.

- (31) Brown, P.; Bushmelev, A.; Butts, C. P.; Cheng, J.; Eastoe, J.; Grillo, I.; Heenan, R. K.; Schmidt, A. M. *Angew. Chem. Int. Ed.* **2012**, *51*, 2414-2416.
- (32) Kerr, J. A., Bond Dissociation Energies by Kinetic Methods. *Chem. Rev.* **1966**, *66*, 465-500.
- (33) Evans, D. *J. Phys. E: Sci. Instrum.* **1974**, *7*, 247.
- (34) A. M. Gijs, M. *Microfluid. Nanofluid.* **2004**, *1*, 22-40.

CHAPTER 3

SYNTHESIS AND CHARACTERIZATION OF THE PHYSICO-CHEMICAL AND MAGNETIC PROPERTIES FOR PERFLUOROALKYL ESTER AND Fe(III) CARBOXYLATE-BASED HYDROPHOBIC MAGNETIC IONIC LIQUIDS

Reproduced from *RSC Advances* 2016, 6, 11109-11117 with permission from the Royal Society of Chemistry

Omprakash Nacham, Kevin D. Clark, and Jared L. Anderson

Abstract

Magnetic ionic liquids (MILs) are a new class of ionic liquids (ILs) that incorporate a paramagnetic component in their chemical structure. Although imidazolium-based MILs can be synthesized using inexpensive and relatively straightforward procedures, these compounds often are water soluble which limits their usefulness in aqueous applications. In this study, two classes of hydrophobic MILs, including perfluorobutyryl ester-based and Fe(III) carboxylate-based MILs, were synthesized and characterized. Functionalization of the cation with fluorinated substituents yielded MILs that were insoluble in aqueous solution at concentrations as low as 0.1% (w/v). In contrast to conventional MILs that rely on paramagnetic anions, Fe(III) carboxylate-based MILs were prepared featuring carboxylate ligands in the cationic moiety capable of chelating a paramagnetic Fe(III) center. The hydrophobic character of the Fe(III) carboxylate-based MILs was subsequently controlled by incorporating the bis[(trifluoromethyl)sulfonyl]imide ($[\text{NTf}_2^-]$) anion, resulting in MILs that were insoluble in aqueous solutions at 0.1% (w/v). This synthetic strategy has the potential to impart dual functionality to MILs by providing the flexibility to incorporate a task specific anion without sacrificing paramagnetic properties. The molar magnetic susceptibilities (χ_m) and effective magnetic moments (μ_{eff}) of the studied MILs were determined using superconducting quantum interference device (SQUID) magnetometry. Consistent with the Curie-Weiss law, a linear relationship between

temperature and inverse magnetic susceptibility (χ_m^{-1}) was observed for the hydrophobic MILs. The μ_{eff} values of the MILs examined in this study ranged from 3.56 to 8.06 Bohr magnetons (μ_B).

3.1 Introduction

Ionic liquids (ILs) are a class of non-molecular solvents with low melting points (≤ 100 °C) and are typically comprised of unsymmetrical organic cations and symmetrical/unsymmetrical inorganic/organic anions. ILs possess a number of intriguing physicochemical properties including negligible vapor pressure at ambient temperatures, high thermal stabilities, wide electrochemical windows, and unique solvation capabilities.¹ By choosing different combinations of cations and anions, the properties of ILs can be readily modified. Magnetic ionic liquids (MILs) are a subclass of ILs and are produced by incorporating a high spin metal complex in either the cationic or anionic component.²⁻⁴ MILs can be designed to contain most if not all of the desirable features of conventional ILs, but also exhibit a paramagnetic property. As a result, their motion can be easily manipulated in the presence of an external magnetic field. MILs have been featured in a wide range of applications including solvents for DNA extraction,⁵ CO₂ absorption media,⁶ switchable electrochromic materials,⁷ and magnetic stimuli responsive surfactants.⁸

Although transition metal-based ILs were reported decades ago, the magnetic properties of these materials were initially overlooked.⁹⁻¹¹ However, Hayashi *et al.* reported in 2004 the synthesis of the 1-butyl-3-methylimidazolium tetrachloroferrate(III) [BMIM⁺][FeCl₄⁻] MIL and demonstrated this compound's paramagnetic behavior in an external magnetic field.² Subsequently, a variety of MILs have been prepared using imidazolium cations and transition metal or lanthanide-based anions.¹²⁻¹⁴ By incorporating different metal complexes into the anion, it is possible to modify the physicochemical and magnetic properties of imidazolium-based MILs. However, the hydrophilic nature of the

imidazolium cation has limited the application of MILs in aqueous systems. Lee *et al.* have studied the phase separation behavior of the [BMIM⁺][FeCl₄⁻] MIL in aqueous solution. At concentrations lower than 20% (v/v) MIL, no observable phase separation occurred upon the application of a 1 T external magnetic field.¹⁵ To address this challenge, heavily alkylated phosphonium and ammonium cations have been shown to increase the hydrophobic character of MILs.^{16,17} Nonetheless, the synthesis and structural modification of imidazolium-based MILs is often preferred due to their lower cost and lower complexity when compared to MILs with functionalized phosphonium or ammonium cations.

Present strategies for enhancing the hydrophobic nature of MILs include modifying the structure of the cation (e.g., increasing the alkyl chain length of substituent groups) or by mixing equimolar quantities of weakly coordinating anions, such as bis[(trifluoromethyl)sulfonyl]imide ([NTf₂⁻]).^{17,18} In these approaches, the choice of anion is often fixed because the paramagnetic properties of the MIL are governed by the anionic component. As a result, the MIL cation represents the primary basis for structural customization, greatly limiting the tunability of hydrophobic MILs. However, this can be overcome through the preparation of either magnetoactive cations or through the synthesis of ILs that are capable of chelating paramagnetic metals, thereby providing flexibility in tuning the anion of the resulting MIL. Very recently, the synthesis and magnetic properties of ferrocenium-based MILs possessing [NTf₂⁻] and hexafluorophosphate [PF₆⁻] anions were reported.^{3,19} By incorporating a magnetoactive cation in the MIL structure, greater flexibility in the choice of anion was achieved. Unfortunately, the instability of ferrocenium complexes in air as well as the multiple step synthesis involved in preparing these compounds presents substantial challenges.

In this study, two different classes of hydrophobic MILs were synthesized, as shown in Figure 1. Within each class, unique synthetic strategies were exploited to enhance the

hydrophobic nature and impart paramagnetic properties to the resulting MIL. The first class features hydrophobic imidazolium-based MILs with fluorinated substituents as the side chain of the cation. In the second class, imidazolium-based cations capable of chelating the paramagnetic iron(III) center were prepared. In this case, carboxylate groups appended to the imidazolium cation act as ligands for the paramagnetic center, thereby providing the flexibility to incorporate the $[\text{NTf}_2]^-$ anion into the MIL structure. The thermal properties of all MILs were investigated using differential scanning calorimetry (DSC) and thermal gravimetric analysis (TGA). Within the first class, the melting point of IL intermediates were found to be significantly reduced through esterification with perfluorobutyryl chloride. The paramagnetic properties of the synthesized MILs were examined using superconducting quantum interference device (SQUID) magnetometry and the effective magnetic moment (μ_{eff}) values of the MILs synthesized in this study were between 3.56–8.03 Bohr magnetons (μ_{B}).

3.2 Materials and Measurements

Benzimidazole (98%), benzylbromide (98%), 1,12-dibromododecane (98%), and perfluorobutyryl chloride (98%) were purchased from Acros Organics (Morris Plains, NJ, USA). 6-bromohexanol (97%), benzylimidazole (99%), 2-bromoethanol (95%), 1-bromohexadecane (99%), thionyl chloride (99.5%), iron (III) chloride ($\text{FeCl}_3 \cdot 6\text{H}_2\text{O}$) (97%), and dimethylsulfoxide (DMSO) were purchased from Sigma-Aldrich (St. Louis, MO, USA). Acetonitrile, chloroform, acetone, methanol, hexanes, and ethyl acetate were obtained from Fisher Scientific (Fair Lawn, NJ, USA). Lithium bis(trifluoromethyl)sulfonylimide (98%) was purchased from Synquest Labs (Alachua, FL, USA). All solvents and reagents were used as received without any additional purification. Deuterated chloroform, methanol, and DMSO were obtained from Cambridge Isotope Laboratories (Andover, MA, USA) and were used as received without any further drying.

NMR spectra (^1H , ^{13}C , and ^{19}F) were recorded using either a Varian 400 MHz or Bruker 500 MHz nuclear magnetic resonance spectrometer. Solvents peaks were used as reference values for reporting the chemical shifts. Mass spectra were obtained using an Esquire-LC-MS/MS from Bruker Daltonics. A Perkin Elmer PYRIS Diamond Differential Scanning Calorimeter was used to evaluate the phase transition behavior of MILs and selected intermediates. Thermal decomposition temperatures of the MILs were probed using a Netzsch STA449 F1 thermogravimetric analyzer under nitrogen gas flow of 60 mL min^{-1} at a thermal rate of $20\text{ }^\circ\text{C min}^{-1}$. The evolved gases from the thermogravimetric analyzer were examined using Netzsch QMS 403 D Aeolos mass spectrometer. Magnetic susceptibility measurements were determined using a magnetic susceptibility balance (MSB) from Johnson Matthey. The MSB was calibrated using $\text{CuSO}_4\cdot 5\text{H}_2\text{O}$. Prior to MIL measurements, the instrument was validated using the previously reported data for the $[\text{P}_{6,6,6,14}^+][\text{FeCl}_4^-]$ MIL. Visible absorption spectra of MILs were recorded in acetonitrile using a Thermo Scientific Evolution 300 UV-vis spectrophotometer. IR spectra of MILs were obtained using a Frontier FT-IR spectrometer from Perkin Elmer. The spectra were collected by dissolving a small amount of MIL in chloroform followed by evaporation to a thin film on the sample platform.

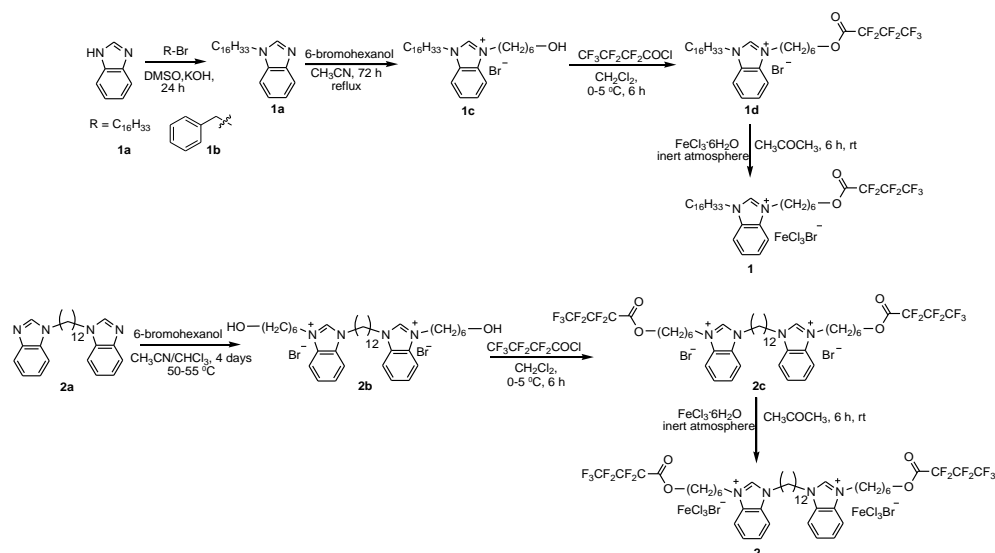
3.2.1 Preparation of Monocationic and Dicationic Perfluorobutyryl Ester-based Hydrophobic MILs

MIL **1** was synthesized as shown in Scheme 1. Benzimidazole (1 mmol) and potassium hydroxide (5 mmol) were dissolved in DMSO (30 mL) at room temperature and stirred for 12 h. A desired amount of alkyl/aryl bromide was added to the reaction mixture and stirred at $30\text{-}35\text{ }^\circ\text{C}$ for 12 h. Water (35 mL) was added to the reaction mixture and the contents transferred to a separatory funnel. Compound **1a/1b** was extracted from the reaction mixture using chloroform (3 x 35 mL). The organic phases were washed several times with

excess water until a neutral pH was observed. The combined organic phases were dried over sodium sulfate for 20 min and filtered using vacuum filtration. After evaporation of the chloroform, compound **1a/1b** was dried at 75 °C for 3 h under reduced pressure. Compound **1a** (1 mmol) and 6-bromohexanol (1.5 mmol) were dissolved in acetonitrile (30 mL) and stirred for 72 h under reflux conditions. The solvent was evaporated under reduced pressure. Crude compound **1c** was washed with hexanes (3 x 30 mL) and dried at 60 °C under reduced pressure for 5 h. Compound **1d** was synthesized by reacting **1c** (1 mmol) with perfluorobutyryl chloride (2.1 mmol) in dichloromethane at 0-5 °C for 6 h. Following solvent evaporation, the crude compound was washed with ethyl acetate and dried at 60 °C for 4 h under vacuum to remove residual solvents and excess perfluorobutyryl chloride. Finally, MIL **1** was prepared by reacting **1d** (1 mmol) with FeCl₃·6H₂O (1.3 mmol) in acetone (10 mL) at room temperature under a nitrogen atmosphere for 6 h. After solvent evaporation, compound **1** was dissolved in dichloromethane and washed several times with water to remove unreacted FeCl₃. The solvent was evaporated and MIL **1** was dried at 60 °C for 5 h under vacuum.

MIL **2** was prepared using a previously reported procedure from the literature with some modifications,¹⁷ as shown in Scheme 1. Compound **2b** was prepared by reacting previously synthesized compound **2a** (1 mmol) with 6-bromohexanol (2.4 mmol) in acetonitrile/chloroform 9:1 ratio (40 mL) at 50-55 °C for 4 days. The reaction mixture was partially evaporated and acetone was added to precipitate compound **2b**. The precipitate was then washed with chloroform (10 mL) followed by diethylether (30 mL). Compound **2b** was dried under reduced pressure for 5 h at 60 °C to remove residual solvents. Compound **2c** was synthesized by reacting **2b** (1 mmol) with perfluorobutyryl chloride (3 mmol) in dichloromethane at 0-5 °C for 5 h. Following solvent evaporation, compound **2c** was washed with ethyl acetate and dried at 70 °C for 6 h under reduced pressure. MIL **2**

was prepared by reacting **2c** (1 mmol) with $\text{FeCl}_3 \cdot 6\text{H}_2\text{O}$ (1.3 mmol) in acetone at room temperature under a nitrogen atmosphere for 6 h. Followed by solvent evaporation the compound was dissolved in chloroform (10 mL) and washed with water (3 x 10 mL) to remove the unreacted FeCl_3 . Chloroform was evaporated under reduced pressure and MIL **2** was dried at 60°C for 5 h under vacuum.



Scheme 1. Synthesis of monocationic and dicationic perfluorobutyryl ester-based hydrophobic magnetic ionic liquids

NMR Analysis of 1a. A dark brown solid. Yield 87%. ^1H NMR (400 MHz, $\text{DMSO}-d_6$) δ (ppm) 8.20 (s, 1H), 7.63 (d, $J = 7.8$ Hz, 1H), 7.55 (d, $J = 7.9$ Hz, 1H), 7.19 (dt, $J = 20.0, 7.3$ Hz, 2H), 4.20 (t, $J = 7.0$ Hz, 2H), 1.75 (p, $J = 7.0$ Hz, 2H), 1.19 (d, $J = 10.5$ Hz, 26H), 0.82 (t, $J = 6.5$ Hz, 3H). ^{13}C NMR (100 MHz, $\text{DMSO}-d_6$) δ (ppm) 144.72, 143.46, 143.18, 133.76, 123.03, 122.09, 121.18, 120.33, 120.08, 119.25, 118.75, 110.92, 109.93, 109.61, 44.05, 30.36, 29.66, 29.40, 29.09, 28.97, 28.79, 28.54, 26.14, 22.14. 13.30. ESI-MS: m/z (+) 342.3.

NMR Analysis of 1b. A white solid. Yield 91%. ^1H NMR (400 MHz, Chloroform-*d*) δ (ppm) 7.85 (s, 1H), 7.76 – 7.71 (m, 1H), 7.27 – 7.12 (m, 6H), 7.08 (dd, $J = 7.2, 2.5$ Hz, 2H), 5.25 (s, 2H). ^{13}C NMR (100 MHz, Chloroform-*d*) δ (ppm) 143.02, 135.27, 133.73, 128.82, 128.05, 126.86, 122.85, 122.04, 120.05, 109.81, 48.64. ESI-MS: m/z (+) 209.4.

NMR Analysis of 1c. A dark brown solid. Yield 75%. ^1H NMR (400 MHz, Chloroform-*d*) δ (ppm) 11.44 (s, 1H), 7.80 – 7.63 (m, 4H), 4.64 (m, 4H), 3.65 (t, $J = 5.8$ Hz, 2H), 2.09 (m, 4H), 1.68 – 1.11 (m, 32H), 0.87 (t, $J = 6.6$ Hz, 3H). ^{13}C NMR (100 MHz, Chloroform-*d*) δ (ppm) 143.44, 131.79, 131.73, 127.58, 127.55, 113.61, 113.54, 62.55, 48.33, 47.91, 32.38, 32.35, 30.16, 30.11, 30.06, 29.98, 29.87, 29.82, 29.54, 29.33, 27.08, 26.28, 25.33, 23.16, 14.61.

NMR Analysis of 1d. A light brown viscous liquid. Yield 90%. ^1H NMR (400 MHz, Chloroform-*d*) δ (ppm) 10.54 (s, 1H), 7.75 – 7.65 (m, 4H), 4.52 (dt, $J = 18.4, 7.6$ Hz, 4H), 4.36 (t, $J = 6.4$ Hz, 2H), 2.01 (m, 4H), 1.74 (m, 2H), 1.50 – 1.19 (m, 30H), 0.87 (t, $J = 6.6$ Hz, 3H). ^{13}C NMR (100 MHz, Chloroform-*d*) δ (ppm) 142.78, 131.41, 127.33, 113.20, 113.02, 68.39, 47.87, 47.51, 32.07, 29.81, 29.77, 29.71, 29.62, 29.51, 29.49, 29.47, 29.20, 29.09, 27.89, 26.63, 25.99, 25.07, 22.85, 14.28. ^{19}F NMR (376 MHz, Chloroform-*d*) δ (ppm) -81.28 (dt, $J = 24.6, 8.7$ Hz, 3F), -119.76 (dq, $J = 107.6, 9.0$ Hz, 2F), -127.56 (d, $J = 21.4$ Hz, 2F).

Visible Spectrum of MIL 1. A dark brown viscous liquid. Yield 83%. Characteristic bands for the $[\text{FeCl}_3\text{Br}^-]$ anion were observed at 534, 619, and 688 nm. Elem. Anal. Calcd (%) for $\text{C}_{33}\text{H}_{50}\text{BrCl}_3\text{F}_7\text{FeN}_2\text{O}_2 \cdot 1.0\text{H}_2\text{O}$: C, 44.05; H, 5.82; N, 3.11. Found: C, 43.91; H, 5.82; N, 3.04;

NMR Analysis of 2b. White powder. Yield 74%. ^1H NMR (500 MHz, Methanol-*d*₄) δ 9.65 (s, 2H), 8.01 (dp, $J = 7.6, 4.3$ Hz, 4H), 7.73 (dt, $J = 6.3, 3.6$ Hz, 4H), 4.55 (q, $J = 7.0$ Hz, 8H), 3.54 (t, $J = 6.3$ Hz, 4H), 2.10 – 1.97 (m, 8H), 1.54 (s, 4H), 1.49 – 1.36 (m, 16H),

1.29 (s, 8H). ^{13}C NMR (125 MHz, Methanol- d_4) δ 142.13, 132.46, 127.76, 114.11, 62.10, 48.94, 48.77, 48.54, 48.02, 47.93, 32.77, 30.12, 30.06, 29.72, 29.68, 27.06, 26.78, 25.87.

NMR Analysis of 2c. A light brown viscous liquid. Yield 87%. ^1H NMR (400 MHz, Chloroform- d) δ (ppm) 10.54 (s, 2H), 7.75 – 7.65 (m, 8H), 4.52 (dt, $J = 18.4, 7.6$ Hz, 8H), 4.36 (t, $J = 6.4$ Hz, 4H), 2.01 (m, 8H), 1.74 (m, 4H), 1.50 – 1.19 (m, 24H). ^{13}C NMR (100 MHz, Chloroform- d) δ (ppm) 142.78, 131.41, 127.33, 113.20, 113.02, 68.39, 47.87, 47.51, 32.07, 29.81, 29.77, 29.71, 29.62, 29.51, 29.49, 29.47, 29.20, 29.09, 27.89, 26.63, 25.99, 25.07, 22.85, 14.28. ^{19}F NMR (376 MHz, Chloroform- d) δ -78.57 (dt, $J = 31.4, 8.8$ Hz, 6F), -116.71 (dq, $J = 206.7, 8.7$ Hz, 4F), -124.65 (d, $J = 43.0$ Hz, 4F).

Visible Spectrum of MIL 2. A brown viscous liquid. The $[\text{FeCl}_3\text{Br}^-]$ anion of MIL 2 showed the characteristic bands at 534, 619, and 688 nm which were similar to the previously reported compounds.^{16, 17} Elem. Anal. Calcd (%) for $\text{C}_{46}\text{H}_{58}\text{Br}_2\text{Cl}_6\text{F}_{14}\text{Fe}_2\text{N}_4\text{O}_4 \cdot 6.0\text{H}_2\text{O}$: C, 34.76; H, 4.44; N, 3.53; Found: C, 34.95; H, 4.09; N, 3.80.

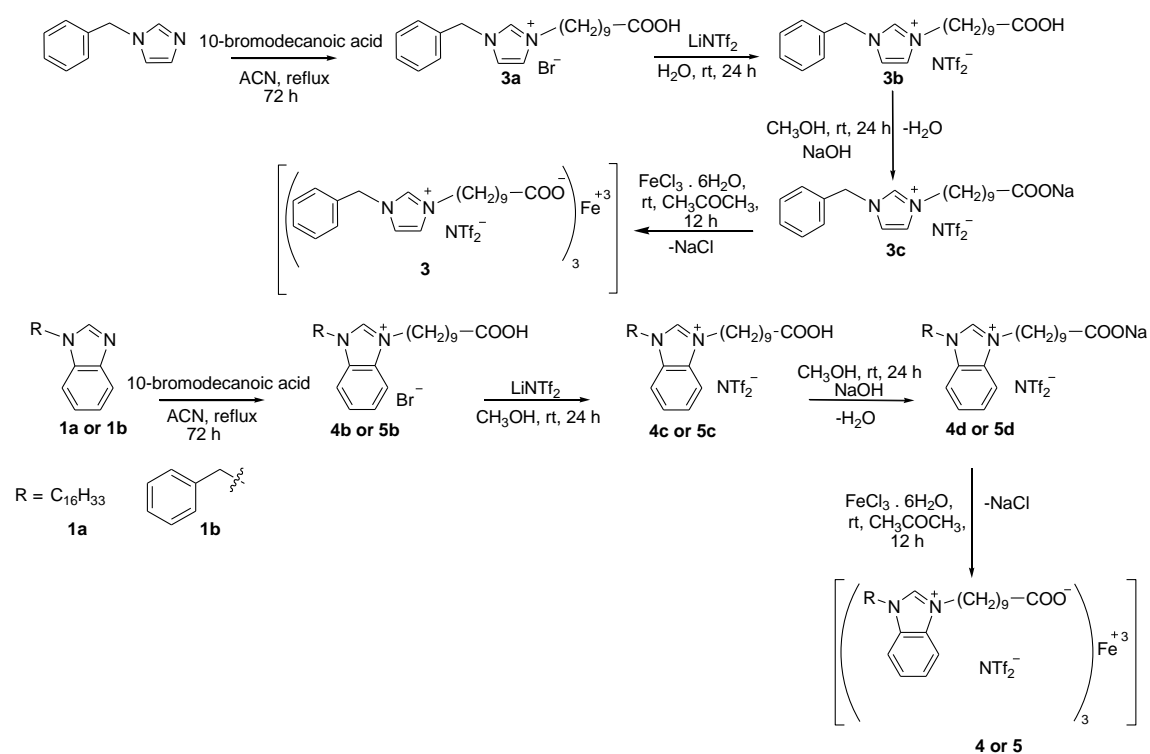
3.2.2 General Procedure for the Synthesis of Fe(III) Carboxylate-based Hydrophobic MILs

MIL 3 was synthesized as shown in Scheme 2. Benzylimidazole (1 mmol) was reacted with an excess of 10-bromodecanoic acid (2.1 mmol) in acetonitrile (35 mL) for 72 h under reflux conditions. The solvent was evaporated under reduced pressure followed by washing of the crude product with ethyl acetate (4 x 35 mL) under sonication to remove excess 10-bromodecanoic acid. The bromide salt **3a** was then dried at 60 °C for 2 h under reduced pressure to remove residual solvents. Compound **3b** was synthesized by reacting **3a** (1 mmol) with lithium bis[(trifluoromethyl)sulfonyl]imide (1.5 mmol) in water at room temperature for 12 h. After solvent evaporation, compound **3b** was washed with an excess of water and the bromide impurities were monitored by adding silver nitrate to the aqueous phase. Compound **3b** was then dried at 65 °C under reduced pressure for 12 h to remove

residual water. Compound **3c** was prepared by reacting **3b** (1 mmol) with sodium hydroxide (1.8 mmol) in methanol at room temperature for 24 h. The solvent was evaporated under reduced pressure and compound **3c** was washed with dichloromethane. After solvent evaporation, compound **3c** was dried under vacuum at 60 °C for 4 h to remove residual solvents. Compound **3** was synthesized by reacting **3c** (3 mmol) with FeCl₃•6H₂O (1.3 mmol) in acetone (10 mL) at room temperature for 12 h. The ensuing precipitate was separated using vacuum filtration and the filtrate evaporated under reduced pressure to yield compound **3**. Compound **3** was washed with water to remove any excess FeCl₃ and dried under reduced pressure to remove residual water.

MILs **4** and **5** were synthesized as shown in Scheme 2. Compound **4b/5b** was prepared by reacting previously prepared **1a/1b** with excess of 10-bromodecanoic acid in acetonitrile (40 mL) for 72 h under reflux conditions. Followed by solvent evaporation, the crude compound was washed with ethyl acetate to remove the unreacted 10-bromodecanoic acid. Compound **4b/5b** was dried at 60 °C under vacuum for 2 h to remove residual solvents. Compound **4c/5c** was prepared by reacting lithium bis[(trifluoromethyl)sulfonyl]imide (1.5 mmol) with **4b/5b** (1 mmol) in methanol at room temperature for 12 h. The solvent was evaporated under reduced pressure and the crude compound washed several times with water to remove excess lithium bis[(trifluoromethyl)sulfonyl]imide. Compound **4c/5c** was dried at 65 °C under vacuum for 5 h to evaporate residual water. Compound **4d/5d** was prepared by reacting **4c/5c** (1 mmol) with sodium hydroxide (1.8 mmol) in methanol at room temperature for 24 h. Following solvent evaporation, the crude product was washed with dichloromethane. Compound **4d/5d** was dried at 60 °C under vacuum for 4 h to remove the residual solvent from the product.

Finally, compound **4/5** was synthesized by reacting **4d/5d** (3 mmol) with $\text{FeCl}_3 \cdot 6\text{H}_2\text{O}$ (1.3 mmol) in acetone (10 mL) at room temperature for 12 h. The reaction mixture was filtered using vacuum filtration to separate the precipitate; the filtrate was then evaporated under reduced pressure to yield crude compound **4/5**.



Scheme 2. Synthesis of Fe(III) carboxylate-based hydrophobic magnetic ionic

The final product was washed with excess water to remove unreacted FeCl_3 and dried under vacuum at $60\text{ }^\circ\text{C}$ for 6 h to remove residual solvent.

NMR Analysis of 3a. A light brown solid. Yield 83%. ^1H NMR (400 MHz, $\text{DMSO-}d_6$) δ (ppm) 11.99 (s, 1H), 9.38 (t, $J = 1.6$ Hz, 1H), 7.84 (p, $J = 1.9$ Hz, 2H), 7.46 – 7.34 (m, 5H), 5.44 (s, 2H), 4.17 (t, $J = 7.2$ Hz, 2H), 2.18 (t, $J = 7.3$ Hz, 2H), 1.78 (p, $J = 7.3$ Hz, 2H), 1.52 – 1.42 (m, 2H), 1.31 – 1.15 (m, 10H). ^{13}C NMR (100 MHz, $\text{DMSO-}d_6$) δ (ppm) 174.50, 136.12, 134.94, 129.01, 128.75, 128.24, 122.81, 122.59, 51.93, 48.97, 33.68, 29.25, 28.70, 28.64, 28.53, 28.29, 25.49, 24.50.

NMR Analysis of 3b. A dark brown viscous liquid. Yield 92%. ^1H NMR (400 MHz, $\text{DMSO-}d_6$) δ (ppm) 11.99 (s, 1H), 9.29 (d, $J = 1.7$ Hz, 1H), 7.81 (d, $J = 1.6$ Hz, 2H), 7.47 – 7.35 (m, 5H), 5.41 (s, 2H), 4.16 (t, $J = 7.2$ Hz, 2H), 2.18 (t, $J = 7.3$ Hz, 2H), 1.78 (p, $J = 7.2$ Hz, 2H), 1.46 (q, $J = 7.1$ Hz, 2H), 1.23 (q, $J = 8.7, 7.4$ Hz, 10H). ^{13}C NMR (100 MHz, $\text{DMSO-}d_6$) δ (ppm) 174.50, 136.12, 134.89, 129.01, 128.76, 128.20, 122.81, 122.61, 121.07, 117.87, 51.99, 48.98, 33.67, 29.24, 28.69, 28.63, 28.53, 28.28, 25.49, 24.49.

FT-IR Characterization of MIL 3. A dark reddish brown viscous liquid. IR spectra of metal carboxylates are usually characterized in the range of 1650-1510 cm^{-1} . MIL 3 showed two distinctive bands at 1596 and 1443 cm^{-1} which are similar to the previously reported iron carboxylate compounds.²⁰ Elem. Anal. Calcd (%) for $\text{C}_{66}\text{H}_{84}\text{F}_{18}\text{FeN}_9\text{O}_{18}\text{S}_6 \cdot 2.0\text{H}_2\text{O}$: C, 41.34; H, 4.63; N, 6.57; Found C, 41.37; H, 4.22; N, 6.16;

NMR Analysis of 4b. A dark brown solid. Yield 83%. ^1H NMR (400 MHz, $\text{DMSO-}d_6$) δ (ppm) 11.98 (s, 1H), 9.82 (s, 1H), 8.10 (dd, $J = 6.4, 3.1$ Hz, 2H), 7.69 (dd, $J = 6.3, 3.1$ Hz, 2H), 4.48 (t, $J = 7.1$ Hz, 4H), 2.16 (t, $J = 7.3$ Hz, 2H), 1.90 (t, $J = 7.1$ Hz, 4H), 1.52 – 1.10 (m, 38H), 0.85 (t, $J = 6.6$ Hz, 3H). ^{13}C NMR (100 MHz, $\text{DMSO-}d_6$) δ (ppm) 198.91, 174.46, 142.06, 131.11, 126.57, 113.75, 46.69, 33.66, 31.33, 29.08, 29.05, 28.92, 28.87, 28.75, 28.67, 28.54, 28.47, 28.44, 28.41, 25.74, 24.49, 22.14, 14.02.

NMR Analysis of 4c. A dark brown liquid. Yield 93%. ^1H NMR (400 MHz, $\text{DMSO-}d_6$) δ (ppm) 11.98 (s, 1H), 9.80 (s, 1H), 8.14 – 8.05 (m, 2H), 7.69 (dt, $J = 6.3, 3.6$ Hz, 2H), 4.48 (t, $J = 7.1$ Hz, 4H), 2.16 (t, $J = 7.3$ Hz, 2H), 1.90 (t, $J = 7.0$ Hz, 4H), 1.45 (t, $J = 6.8$ Hz, 2H), 1.28 (t, $J = 5.1$ Hz, 36H), 0.89 – 0.79 (m, 3H). ^{13}C NMR (100 MHz, $\text{DMSO-}d_6$) δ (ppm) 198.91, 174.46, 142.06, 131.11, 126.57, 113.75, 117.14, 46.69, 33.66, 31.33, 29.08, 29.05, 28.92, 28.87, 28.75, 28.67, 28.54, 28.47, 28.44, 28.41, 25.74, 24.49, 22.14, 14.02.

FT-IR Characterization of MIL 4. A dark brown viscous liquid. IR spectrum of MIL 4 showed two characteristics bands at 1596 and 1443 cm^{-1} . Elem. Anal. Calcd (%) for $\text{C}_{105}\text{H}_{168}\text{F}_{18}\text{FeN}_9\text{O}_{18}\text{S}_6 \cdot 6.0\text{H}_2\text{O}$: C, 49.60; H, 7.14; N, 4.96; Found: C, 49.29; H, 6.30; N, 5.15.

NMR Analysis of 5b. A light brown solid. Yield 86%. ^1H NMR (400 MHz, $\text{DMSO-}d_6$) δ (ppm) 11.99 (s, 1H), 9.98 (s, 1H), 8.14 – 8.09 (m, 1H), 7.97 (dd, $J = 7.3, 2.1$ Hz, 1H), 7.71 – 7.61 (m, 2H), 7.54 – 7.49 (m, 2H), 7.45 – 7.34 (m, 3H), 5.77 (s, 2H), 4.51 (t, $J = 7.2$ Hz, 2H), 2.18 (t, $J = 7.3$ Hz, 2H), 1.92 (p, $J = 7.3$ Hz, 2H), 1.46 (p, $J = 7.0$ Hz, 2H), 1.35 – 1.19 (m, 10H). ^{13}C NMR (100 MHz, $\text{DMSO-}d_6$) δ (ppm) 174.50, 142.38, 134.10, 131.30, 130.84, 128.89, 128.72, 128.21, 126.71, 126.66, 113.93, 49.87, 46.93, 33.72, 29.17, 28.82, 28.36, 28.06, 25.78, 24.43.

NMR Analysis of 5c. ^1H NMR (400 MHz, $\text{DMSO-}d_6$) δ (ppm) 11.99 (s, 1H), 9.99 (s, 1H), 8.14 – 8.09 (m, 1H), 7.97 (dd, $J = 7.3, 1.9$ Hz, 1H), 7.71 – 7.61 (m, 2H), 7.53 – 7.48 (m, 2H), 7.44 – 7.33 (m, 3H), 5.77 (s, 2H), 4.51 (t, $J = 7.2$ Hz, 2H), 2.18 (t, $J = 7.4$ Hz, 2H), 1.92 (p, $J = 7.1$ Hz, 2H), 1.45 (q, $J = 7.2$ Hz, 2H), 1.38 – 1.16 (m, 10H). ^{13}C NMR (100 MHz, $\text{DMSO-}d_6$) δ (ppm) 198.95, 177.63, 142.79, 134.21, 131.34, 130.88, 129.00, 128.73, 128.26, 126.71, 126.67, 121.12, 117.92, 113.90, 49.88, 46.83, 38.46, 29.38, 28.96, 28.85, 28.41, 26.46, 25.78.

FT-IR Characterization of MIL 5. A dark brown viscous liquid. IR spectrum of compound 5 showed the characteristic bands at 1593 and 1443 cm^{-1} . Elem. Anal. Calcd (%) for $\text{C}_{78}\text{H}_{90}\text{F}_{18}\text{FeN}_9\text{O}_{18}\text{S}_6 \cdot 3.0\text{H}_2\text{O}$: C, 44.91; H, 4.64; N, 6.04; Found: C, 44.44; H, 4.33; N, 5.98.

3.3 Results and Discussion

3.3.1 Structural Tuning and Optimization of Reaction Conditions for Synthesis of Perfluorobutyryl Ester-based MILs

In liquid-liquid extraction (LLE) approaches, a water immiscible extraction solvent is often employed to isolate analytes of interest from the aqueous phase. Subsequently, recovery of the extraction phase is often achieved via a time consuming and laborious centrifugation process prior to sample analysis. MILs possess a significant advantage over conventional extraction solvents in the ease with which they can be manipulated by external magnetic fields. Using a MIL-based LLE technique, the paramagnetic properties of MILs can be exploited to enable rapid recovery of the analyte-enriched MIL extraction phase. However, previous studies have revealed that imidazolium-based MILs are soluble in aqueous solution at compositions less than 20% (v/v) MIL. As a result of their solubility, they can no longer be manipulated using an external magnetic field. Therefore, disadvantages associated with imidazolium-based MILs can be addressed by tuning the structure of the MIL to impart sufficient hydrophobic nature to the resulting compound.

In order to improve the hydrophobicity of the resulting MILs, a relatively hydrophobic benzimidazole core as well as alkyl and perfluoroalkyl groups were selected and utilized for the synthesis of MILs (**1-2**), as shown in Scheme 1. The initial strategy employed for the synthesis of MIL **1** involved the preparation of a bromo-substituted perfluoroalkyl ester followed by reaction with hexadecylbenzimidazole to generate the bromide salt. Following this approach, 2-bromoethanol was reacted with perfluorobutyryl chloride to produce a bromo-substituted perfluorobutyryl ester. Unfortunately, when this compound was reacted with **1a**, low product yields (< 21%) were observed with most of the hexadecylbenzimidazole remaining unreacted (based on ¹H NMR). This may be attributed to the strong inductive effect from the perfluoroalkyl ester functional group. In order to

overcome this challenge, a bromide salt with terminal hydroxyl groups on the benzimidazolium cation was prepared prior to the esterification reaction. Firstly, a 2:1 mole ratio of 2-bromoethanol was reacted with compound **1a**. The resulting bromide salt was then esterified with perfluorobutyryl chloride in an effort to incorporate fluorinated substituents, but the esterification reaction did not progress to completion (< 45% based on ^1H NMR). However, substantially improved product formation (90.1%) was observed under similar reaction conditions when **1c** was reacted with perfluorobutyryl chloride. The bromide salt was subsequently reacted with $\text{FeCl}_3 \cdot 6\text{H}_2\text{O}$ to generate the paramagnetic iron(III) center in MIL **1**. In order to remove unreacted FeCl_3 , the final product was dissolved in dichloromethane and washed several times with water. When the same conditions were applied for reaction of **1c** with longer perfluoroacid chlorides (e.g. hexyl and octyl), the final products were isolated as room temperature solids.

The general synthetic strategy utilized for the preparation of MIL **2** is described in Scheme 1. In an attempt to reduce the melting point of the MIL products, a precursor comprised of two benzimidazole moieties separated by a dodecyl linkage chain (**2a**) was prepared. Initially, **2a** was reacted with 6-bromohexanol in neat chloroform for 7 days under reflux. However, the desired dibromide salt was not formed using these conditions. When a mixture of acetonitrile/chloroform (9:1) was employed as the reaction solvent, **2b** was generated with 74% yield. The hydroxyl groups of the dibromide salt were subsequently reacted with excess perfluorobutyryl chloride to form compound **2c**. Finally, the perfluorobutyryl-ester based dibromide salt was reacted with $\text{FeCl}_3 \cdot 6\text{H}_2\text{O}$ to incorporate the paramagnetic anion $[\text{FeCl}_3\text{Br}^-]$ in the resulting MIL **2**.

The solubilities of perfluorobutyryl ester-based monocationic and dicationic MILs in water and hexanes are shown in Table 1. Due to the presence of fluorinated substituents as well benzimidazole moieties, MILs **1-2** were found to be immiscible in aqueous solutions

at compositions as low as 0.1% (w/v) of MIL and were found to be miscible with hexane. Perfluoroalkyl ester-based hydrophobic MILs may be useful candidates for liquid-liquid microextractions, where low volumes of extraction solvent are often employed.

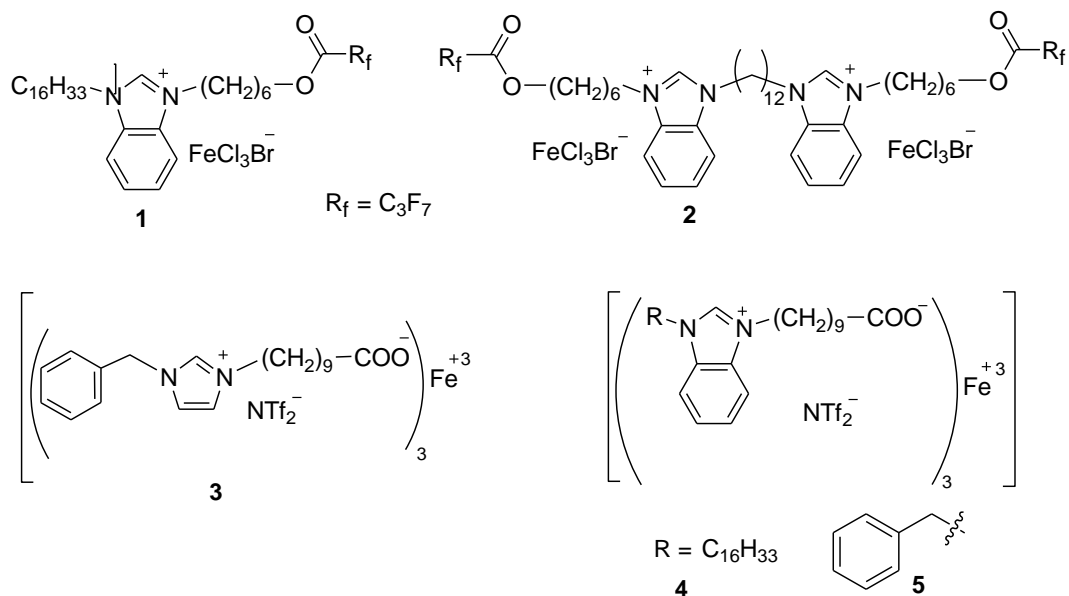


Figure 1. Chemical structures of perfluorobutyryl ester (1-2) and Fe(III) carboxylate-based hydrophobic magnetic ionic liquids (3-5).

3.3.2 Preparation of Fe(III) Carboxylate-based Hydrophobic MILs

The most common approach employed in the preparation of MILs involves the pairing of a functionalized cation with a paramagnetic anion. While it is possible to impart hydrophobic character to the MIL by incorporating long alkyl chains/perfluoroalkyl or benzyl groups in the cationic component, the anion must remain unchanged in order to maintain the paramagnetic susceptibility of the compound. This paradigm severely limits the opportunity to include functional or task-specific anions other than those that impart paramagnetic properties to the MIL. To overcome this challenge and expand the variety of anions that can be incorporated into the MIL structure, the synthesis of imidazolium-based cations capable of chelating a paramagnetic iron(III) center was explored.

The general synthetic strategy employed for the preparation of Fe(III) carboxylate-based hydrophobic MILs is described in Scheme 2. With the aim of incorporating carboxylate functional groups into the imidazolium cation, a n-bromo-substituted alkyl carboxylic acid was reacted with an alkyl or aromatic substituted imidazole/benzimidazole. Initial attempts to react 5-bromovaleric acid with benzylimidazole resulted in low product yields (<30% based on ^1H NMR) with most of the starting material remaining unreacted. In contrast, similar reaction conditions with 10-bromodecanoic acid resulted in substantially improved product formation (83-86%). Following preparation of the bromide salt, the carboxyl group was deprotonated with sodium hydroxide. Initially, **3a** was reacted with sodium hydroxide in methanol, but the deprotonation reaction did not progress to completion (based on ^1H NMR). However, similar reaction conditions with **3b** resulted in complete formation of the desired sodium carboxylate. After dissolving the deprotonated compound in acetone, $\text{FeCl}_3 \cdot 6\text{H}_2\text{O}$ was added to the reaction mixture. A white precipitate was observed during the reaction that corresponded to the formation of NaCl and was separated from the product by filtration. The final product was washed several times with water to remove unreacted FeCl_3 . Compound **3** exhibited a water solubility below 0.25% (w/v). In order to improve upon the hydrophobic character of **3**, the imidazolium cation was replaced with the benzimidazolium cation to produce MILs **4** and **5**, as shown in Scheme 2. Significant enhancement in the hydrophobicity for **4** and **5** was observed, and these compounds were found to be insoluble in water at 0.1% (w/v) of MIL.

3.3.3 Thermal Properties of Perfluoroalkyl Ester-based and Fe(III) Carboxylate-based Hydrophobic MILs

The thermal properties of the five hydrophobic MILs prepared in this study were investigated using DSC and TGA. As shown in Table 1, the only MIL to exhibit a melting point (T_m) above $-45\text{ }^\circ\text{C}$ was the monocationic perfluoroalkyl ester-based MIL **1**. Although

phase transitions were not observed for MILs **2–5** under the temperatures studied, these compounds existed as room temperature liquids. Interestingly, the dicationic MIL **2** was found to be a viscous liquid despite having a component of symmetry. Further investigation of the intermediates used to generate MIL **2** revealed that the perfluoroalkyl ester group had a profound influence on the melting point of the salt. While **2b** was isolated as a room temperature solid with a melting point of 119 °C, esterification with perfluorobutyryl chloride generated compound **2c** with no detectable phase transition above –45 °C. This may be explained by the higher propensity of **2b** to participate in hydrogen bonding when compared to the ester-functionalized compound **2c**. Thermal stabilities for the perfluoroalkyl ester-based MILs **1** and **2** were found to be 254 °C and 225 °C, respectively.

Hydrophobic MILs derived from carboxylate-functionalized imidazolium and benzimidazolium cations (MILs **3–5**) did not exhibit phase transitions above –45 °C. This behavior is likely due to the incorporation of the non-coordinating [NTf₂⁻] anion in the MIL structure. Compared to the perfluoroalkyl ester-based MILs, compounds **3–5** possessed enhanced thermal stabilities as high as 314 °C in the case of MIL **3**. TGA coupled with mass spectrometry (TGA-MS) enabled the analysis of volatile components released from the MILs during temperature ramping. When heated beyond 250 °C, a prominent peak at *m/z* 44 was observed for all three Fe(III) carboxylate-based MILs corresponding to the release of CO₂. These results indicate that the decomposition of MILs **3–5** initially proceeds through a decarboxylation pathway.

3.3.4 Magnetic Properties of Hydrophobic MILs

The ability to precisely control the motion of MILs by application of a magnetic field represents a significant advantage for these compounds over conventional ILs. Due to the presence of unpaired electrons in the valence orbitals of metal ions, MILs align their spins in response to an external magnetic field and exhibit a net magnetization. When the

magnetic field is removed, thermal motion causes the spins to orient themselves randomly resulting in the loss of net magnetization. The Curie-Weiss law describes the inverse relation between the magnetic susceptibility and the temperature of paramagnetic materials. Imidazolium-based MILs comprised of high-spin d^5 Fe(III) centers have been well studied as a result of their relative ease of preparation and the low cost of iron materials.^{4, 14} Table 1 shows μ_{eff} values at 295 K for the five hydrophobic MILs prepared in this study. The μ_{eff} values of the perfluorobutyryl ester-based MILs containing the $[\text{FeCl}_3\text{Br}^-]$ anion (**1-2**) were determined according to previously reported procedures using an Evans magnetic susceptibility balance^{17, 21} and SQUID magnetometer.¹⁸

Table 1. Physicochemical and magnetic properties of hydrophobic MILs and intermediates synthesized in this study

Entry	MW (g/mol)	Melting point (°C)	μ_{eff} (μ_{B})	Thermal stability ^c (°C)	Solubility in hexanes	Solubility in water
1	881.85	-18	5.36 ^a	254	S	I ^d
2	1480.21	<-45	8.03 ^b	225	S	I ^d
2b	764.73	119	-----		I	I ^e
2c	691.81	<-45	-----		I	I ^d
3	1881.46	<-45	3.56 ^b	314	I	I ^e
4	2437.96	<-45	4.16 ^b	311	I	I ^d
5	2037.96	<-45	4.71 ^b	309	I	I ^d

^a μ_{eff} = effective magnetic moment measured at 295 K using magnetic susceptibility balance; ^b μ_{eff} = effective magnetic moment measured at 295 K using SQUID; ^c Thermal gravimetric analysis (TGA) = temperature at which 5% wt loss of MIL is observed; I = insoluble; ^e Insoluble at 0.1% (w/v); ^d Insoluble at 0.25% (w/v); S = soluble.

The μ_{eff} values of the monocationic and dicationic perfluorobutyryl ester-based MILs were 5.36 and 8.03 μ_{B} , respectively, and found to be in good agreement with previously reported high-spin d^5 Fe(III)-based MILs.^{17, 18} Figures 2a and b show the temperature dependence of molar magnetic susceptibilities (χ_{m}) and the reciprocal magnetic susceptibilities (χ_{m}^{-1}) for the dicationic MIL **2** as a representative example of $[\text{FeCl}_3\text{Br}^-]$ -based MILs. The linear

relationship between χ_m^{-1} and temperature for MIL **2** indicates that this compound follows the Curie-Weiss law. The paramagnetic properties of MIL solvents often depend on the incorporation of a magnetoactive anion into the MIL structure. However, the synthesis of Fe(III) carboxylate-based MILs provides an alternative method for generating MILs in which the choice of anion is greatly expanded. The μ_{eff} values of the Fe(III) carboxylate-based hydrophobic MILs ranged from 3.56 to 4.71 μ_B at 295 K, which is in line with previously reported Fe(III) complexes possessing carboxylate ligands.^{22, 23}

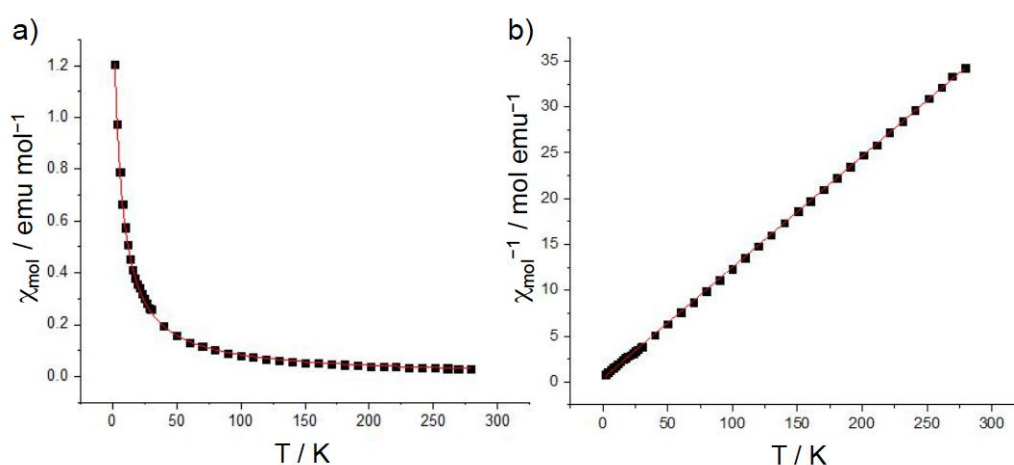


Figure 2. Temperature dependence of the (a) molar magnetic susceptibility and the (b) reciprocal molar susceptibility for MIL **2** using a field of 20,000 Oe.

Figures 3a and b show the temperature dependence of χ_m and χ_m^{-1} for the Fe(III) carboxylate-based MIL **4** (for MILs **3** and **5**, see the Supporting Information). A linear relationship between χ_m^{-1} and temperature was observed from room temperature down to approximately 50 K, providing evidence of paramagnetic behavior for MIL **4**. Although the μ_{eff} values are considerably less than those observed for MILs containing high spin Fe(III) centers (e.g., tetrahaloferrates(III)), the Fe(III) carboxylate-based MILs can nonetheless be readily manipulated by application of an external magnetic field.

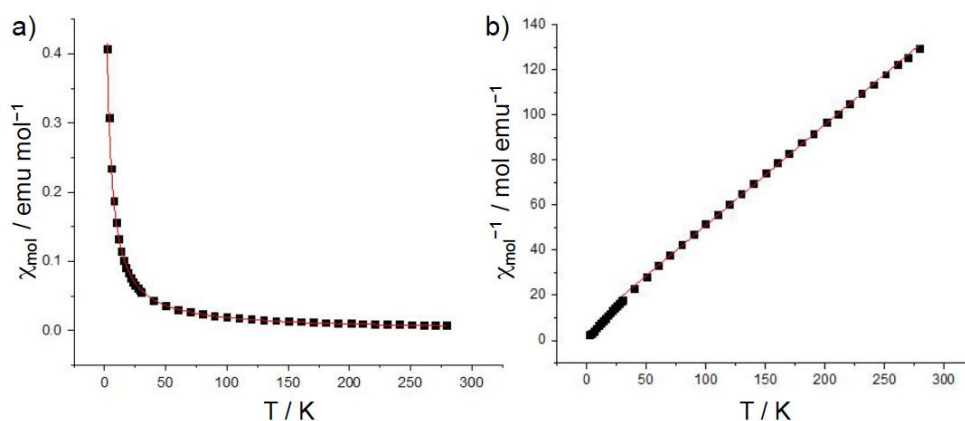


Figure 3. Temperature dependence of the (a) molar magnetic susceptibility and the (b) reciprocal molar susceptibility for MIL **4** using a field of 20,000 Oe.

3.4 Conclusions

In this study, two classes of hydrophobic MILs were successfully synthesized and characterized. Within each class, unique synthetic strategies were employed to control the hydrophobicity, melting point, and magnetic susceptibility of the resulting MILs. In the first class, imidazolium cations were functionalized with fluorinated substituents in an effort to improve the hydrophobic character of the MIL. Both mono and dicationic perfluoroalkyl ester-based MILs were insoluble in aqueous solution at concentrations as low as 0.1% (w/v) MIL. Interestingly, reaction of the intermediates bearing hydroxyl groups with perfluorobutyryl chloride significantly lowered the melting points of the esterified products. Within the second class, the structure of the imidazolium cation was designed to possess carboxylate ligands as chelators for a paramagnetic iron(III) center. This novel approach generated MILs with a paramagnetic component in the cationic moiety, thereby allowing incorporation of $[\text{NTf}_2^-]$ anions into the MIL structure without sacrificing paramagnetic properties. The magnetic properties of the MILs were investigated using SQUID magnetometry. The highest μ_{eff} ($8.03 \mu_{\text{B}}$, 295 K) was obtained for the dicationic MIL possessing two $[\text{FeCl}_3\text{Br}^-]$ anions, while the Fe(III) carboxylate-based MILs exhibited μ_{eff} values ranging from 3.56 to $4.71 \mu_{\text{B}}$ at 295 K. Despite the lower μ_{eff} values,

the Fe(III) carboxylate-based MILs are readily manipulated by application of an external magnetic field. The hydrophobic MILs synthesized in this study may be intriguing candidates for extraction solvents in liquid-liquid microextraction techniques or in catalytic applications wherein the MIL can be easily isolated using a magnetic field, circumventing the need for time-consuming centrifugation steps.

Acknowledgments

The authors acknowledge funding from Chemical Measurement and Imaging Program at the National Science Foundation (Grant number CHE-1413199). Assistance from Dr. Yaroslav Mudryk is greatly appreciated during magnetic susceptibility measurements using the SQUID magnetometer. The authors thank the Iowa State University Chemical Instrumentation Facility and staff member Steve Veysey for training and assistance pertaining to Netzsch TGA and MS instruments.

Supporting information

NMR spectra, absorbance spectra, IR spectra, Figure S1-S7 are available in supplemental information in Appendix B.

References

1. J. P. Hallett and T. Welton, *Chem. Rev.*, 2011, **111**, 3508-3576.
2. S. Hayashi and H.-o. Hamaguchi, *Chem. Lett.*, 2004, **33**, 1590-1591.
3. T. Inagaki and T. Mochida, *Chem. Lett.*, 2010, **39**, 572-573.
4. E. Santos, J. Albo and A. Irabien, *RSC Adv.*, 2014, **4**, 40008-40018.
5. K. D. Clark, O. Nacham, H. Yu, T. Li, M. M. Yamsek, D. R. Ronning and J. L. Anderson, *Anal. Chem.*, 2015, **87**, 1552-1559.
6. E. Santos, J. Albo, C. I. Daniel, C. A. M. Portugal, J. G. Crespo and A. Irabien, *J. Membr. Sci.*, 2013, **430**, 56-61.
7. A. Branco, L. C. Branco and F. Pina, *Chem. Commun.*, 2011, **47**, 2300-2302.

8. P. Brown, T. A. Hatton and J. Eastoe, *Curr. Opin. Colloid Interface Sci.*, 2015, **20**, 140-150
9. M. Lipsztajn and R. A. Osteryoung, *Inorg. Chem.*, 1985, **24**, 716-719.
10. S. A. Bolkan and J. T. Yoke, *J. Chem. Eng. Data.*, 1986, **31**, 194-197.
11. M. S. Sitze, E. R. Schreiter, E. V. Patterson and R. G. Freeman, *Inorg. Chem.*, 2001, **40**, 2298-2304.
12. B. Mallick, B. Balke, C. Felser and A.-V. Mudring, *Angew. Chem. Int. Ed.*, 2008, **47**, 7635-7638.
13. P. Nockemann, B. Thijs, N. Postelmans, K. Van Hecke, L. Van Meervelt and K. Binnemans, *J. Am. Chem. Soc.*, 2006, **128**, 13658-13659.
14. Y. Yoshida and G. Saito, *J. Mater. Chem.*, 2006, **16**, 1254-1262.
15. S. H. Lee, S. H. Ha, S.-S. Ha, H.-B. Jin, C.-Y. You and Y.-M. Koo, *J. Appl. Phys.*, 2007, **101**, 09J102-103.
16. R. E. Del Sesto, T. M. McCleskey, A. K. Burrell, G. A. Baker, J. D. Thompson, B. L. Scott, J. S. Wilkes and P. Williams, *Chem. Commun.*, 2008, 447-449.
17. O. Nacham, K. D. Clark, H. Yu and J. L. Anderson, *Chem. Mater.*, 2015, **27**, 923-931.
18. P. Brown, C. P. Butts, J. Eastoe, E. Padron Hernandez, F. L. d. A. Machado and R. J. de Oliveira, *Chem. Commun.*, 2013, **49**, 2765-2767.
19. Y. Funasako, T. Inagaki, T. Mochida, T. Sakurai, H. Ohta, K. Furukawa and T. Nakamura, *Dalton Trans.*, 2013, **42**, 8317-8327.
20. L. M. Bronstein, X. Huang, J. Retrum, A. Schmucker, M. Pink, B. D. Stein and B. Dragnea, *Chem. Mater.*, 2007, **19**, 3624-3632.
21. D. Evans, *J. Phys. E: Sci. Instrum.*, 1974, **7**, 247.
22. J. Catterick, P. Thornton and B. W. Fitzsimmons, *Dalton Trans.*, 1977, 1420-1425.
23. A. K. Boudalis, C. P. Raptopoulou, A. Terzis and S. P. Perlepes, *Polyhedron*, 2004, **23**, 1271-1277.

CHAPTER 4

USE OF IONIC LIQUIDS AS HEADSPACE GAS CHROMATOGRAPHY
DILUENTS FOR THE ANALYSIS OF RESIDUAL SOLVENTS IN
PHARMACEUTICALS

Reprinted with permission from *Journal of Pharmaceutical and Biomedical Analysis*

2017, DOI: 10.1016/j.jpba.2017.05.033

Copyright © 2017, Elsevier

Omprakash Nacham, Tien D. Ho, Jared L. Anderson, and Gregory K. Webster

Abstract

In this study, two ionic liquids (ILs), 1-butyl-3-methylimidazolium bis[(trifluoromethyl)sulfonyl]imide ([BMIM][NTf₂]) and trihexyltetradecylphosphonium bis[(trifluoromethyl)sulfonyl]imide ([P₆₆₆₁₄][NTf₂]) were examined as contemporary diluents for residual solvent analysis using static headspace gas chromatography (SHS-GC) coupled with flame ionization detection (FID). ILs are a class of non-molecular solvents featuring negligible vapor pressure and high thermal stabilities. Owing to these favorable properties, ILs have potential to enable superior sensitivity and reduced interference, compared to conventional organic diluents, at high headspace incubation temperatures. By employing the [BMIM][NTf₂] IL as a diluent, a 25-fold improvement in limit of detection (LOD) was observed with respect to traditional HS-GC diluents, such as N-methylpyrrolidone (NMP). The established IL-based method demonstrated LODs ranging from 5.8 parts-per-million (ppm) to 20 ppm of residual solvents in drug substances. The optimization of headspace extraction conditions was performed prior to method validation. An incubation temperature of 140 °C and a 15 min incubation time provided the best sensitivity for the analysis. Under optimized experimental conditions, the mass of residual solvents partitioned in the headspace was higher when using [BMIM][NTf₂] than NMP as

a diluent. The analytical performance was demonstrated by determining the repeatability, accuracy, and linearity of the method. Linear ranges of up to two orders of magnitude were obtained for class 3 solvents. Excellent analyte recoveries were obtained in the presence of three different active pharmaceutical ingredients. Owing to its robustness, high throughput, and superior sensitivity, the HS-GC IL-based method can be used as an alternative to existing residual solvent methods.

4.1 Introduction

Manufacturers in the pharmaceutical industry are required to detect and quantify volatile organic solvents (“residual solvents”) present during API (active pharmaceutical ingredient) manufacturing or in the preparation of drug products. The levels of these impurities in pharmaceutical products need to be regulated due to their potential toxicity toward humans [1, 2]. The International Council for Harmonisation of Technical Requirements for Pharmaceuticals for Human Use (ICH) has issued stringent limits for the levels of residual solvents in pharmaceutical products. Based on ICH guideline Q3C, depending on the level of hazard to humans and environment, residual solvents are classified by risk assessment or their potential toxicity. Class 1 solvents are known human carcinogens or they have strongly suspected carcinogens and/or environmental hazards. Their use is minimized or maintained at levels as low as 2 parts-per-million (ppm) in drug products. Class 2 are non-genotoxic impurities, but with a level of toxicity that must be limited in drug products. Class 3 residual solvents tend to be limited by quality-based requirements in drug substances, excipients, and drug products. Table 1 lists the allowable limits of these solvents used in this study and ranges from 290 to 5000 ppm [3].

Traditional techniques used for monitoring volatile impurities, such as loss on drying (LOD), typically rely upon subjecting the sample to high temperatures and assessing the weight loss to determine the amount of organic content (and moisture) in the sample. The

high sample size requirements, effects of humidity, inability to quantify the solvate form or trapped residual solvent within the sample matrix, and non-specific nature of the technique, has limited its applications [4, 5]. Other techniques, including infrared spectroscopy and nuclear magnetic resonance spectroscopy, relieved some of the problems associated with the earlier techniques, but are still affected by sample matrix interferences and poor limits of detection (LOD), especially for most toxic solvents [4]. In order to address the issues associated with the traditional techniques, gas chromatography (GC) has been employed for the analysis of residual solvents in drug substances and pharmaceutical products. When compared to traditional techniques, GC methods are able to selectively identify and quantify target analytes from complex sample matrices with greater sensitivity using a broad range of detectors [1, 4, 6].

Sampling techniques in GC include direction injection (DI), headspace (HS) extraction, and solid phase microextraction (SPME). Among these techniques, HS-GC has been the widely used technique in pharmaceutical industries for the analysis of residual solvents in drug substances [7]. In HS-GC, the API is either dissolved or the residual solvent is extracted into high boiling point organic solvents, such as dimethylsulfoxide (DMSO) or N-methylpyrrolidone (NMP) to ensure that the solvate form present in the sample matrix is available for analysis. Subsequently, the HS sample vial is incubated at temperatures below the boiling point of dissolving solvent (diluent) to volatilize the target analytes out of the sample matrix. As a result, the HS unit samples only the volatile components within the sample vial, which minimizes potential instrument contamination from non-volatile components present in the sample matrix [8].

A number of studies have provided valuable insight for optimizing the method sensitivity of volatile analytes when employing HS-GC in conjunction with organic diluents [2, 9, 10]. Otero *et.al.* claimed that combining two different diluents, such as water

and dimethylformamide, resulted in enhanced sensitivity and recovery of the target analytes when compared to a single diluent system [9]. Other modifications such as addition of salts (e.g., NaCl, NaHSO₄) to diluents or sample matrix enhances the analyte partitioning into gas phase. However, these methods are mostly limited to aqueous samples since many of the inorganic salts exhibit poor solubilities in organic diluents [11, 12]. On the other hand, it was reported that increasing the incubation temperature can also enhance the sensitivity of the volatile compounds since it promotes the partitioning of analytes into the HS of the sample vial [13]. However, employing this approach using conventional organic diluents can lead to major instrument contamination due to excessive diluent sampling and the introduction of less-volatile matrix components that are not of interest into the system. In addition, by incubating the sample vial at high temperatures, a substantial amount of pressure may build-up and can compromise the integrity of the sample vial, resulting in safety issues [14].

Ionic liquids (ILs) are a class of non-molecular solvents composed entirely of ions and possess melting points at or below 100 °C. This class of compounds are commonly comprised of organic cations with inorganic or organic anions [15]. By judicious selection of structural components, the physicochemical properties of the resulting IL can be easily tailored and optimized for the desired analytical application [16]. ILs possess a variety of physicochemical properties such as tunable viscosity, negligible vapor pressure, unique solvation properties, and high thermal stability [17]. Recently, ILs have been applied as diluents towards the analysis of high boiling point genotoxic impurities in pharmaceuticals [18]. This IL-based method yielded superior LODs with reduced chromatographic background interference when compared to conventional organic diluents, such as DMSO. Previously, Laus and co-workers successfully applied the 1-butyl-3-methylimidazolium dimethyl phosphate ([BMIM][DMP]) in HS-GC for the analysis of high boiling point

solvents (e.g., DMSO, NMP, and tetralin) in pharmaceutical excipients, such as carboxymethylcellulose and magnesium stearate. Due to favorable physicochemical properties of ILs, low LODs were achieved [19]. Owing to their negligible vapor pressure and high thermal stability, the use of ILs as diluents in HS-GC enables operation at higher HS incubation temperatures compared to traditional organic solvents. This can have profound influence on the sensitivity and throughput of the method.

To the best of our knowledge, this study constitutes the first report on the investigation of two ILs, 1-butyl-3-methylimidazolium bis[(trifluoromethyl)sulfonyl]imide ([BMIM][NTf₂]) and trihexyltetradecylphosphonium bis[(trifluoromethyl)sulfonyl]imide ([P₆₆₆₁₄][NTf₂]), as diluents for the analysis of residual solvents commonly used in manufacturing of the drug substances. HS-GC coupled with flame ionization detection (FID) was employed for the analysis. Table 1 lists the chemical structures of the diluents and APIs examined in this study. By using [BMIM][NTf₂] as a diluent, the effects of HS extraction parameters on the response of residual solvents were thoroughly investigated. Method validation was performed subsequent to optimization of HS extraction parameters using [BMIM][NTf₂]. The analytical performance of the [BMIM][NTf₂] diluent was examined and compared to a conventional diluent, namely, NMP. Finally, the cost of analysis and feasibility of IL-based HS-GC methods for routine and non-routine analyses were evaluated.

4.2 Experimental

4.2.1 Chemicals and equipment

The residual solvents tested in this study (Table 1) were obtained from Sigma-Aldrich (St. Louis, MO, USA). Indomethacin was purchased from TCI (Tokyo, Japan). Quinidine anhydrous was obtained from Sigma-Aldrich. 1-butyl-3-methylimidazolium bis[(trifluoromethyl)sulfonyl]imide was obtained from EMD Millipore (Billerica, MA,

USA) and IOLITEC (Tuscaloosa, AL, USA). Trihexyltetradecylphosphonium bis[(trifluoromethyl)sulfonyl] imide was obtained from Strem Chemicals (Newburyport, MA, USA) and IOLITEC. N-methylpyrrolidone was received from Sigma-Aldrich. Headspace vials (20 mL) and magnetic seals with septa were obtained from Restek (Bellefonte, PA, USA). The gas tight syringe (250 μ L) was obtained from SGE Analytical Science (Austin, TX, USA).

4.2.2 Sample preparation

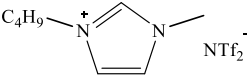
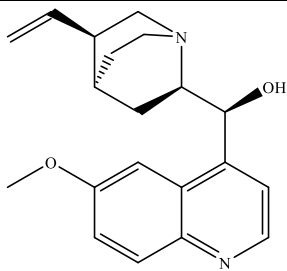
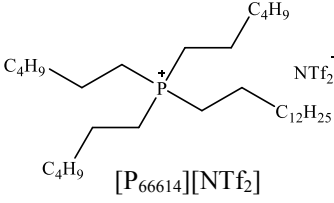
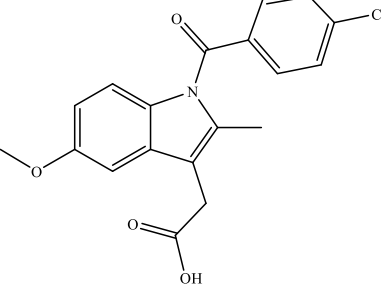
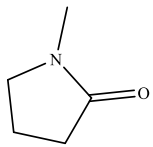
A combined stock solution of residual solvents (class 2 and class 3) with desired concentrations was prepared using 10 mL of either NMP or [BMIM][NTf₂]. Thereafter, working standards were prepared by spiking the desired volume of combined stock solution into standard volumetric flask and diluted with the diluent. For sample solution preparation, 500 mg of the desired drug substances was dissolved in 10 mL of desired diluent and subsequently diluted with the desired working standard to reach the final sample concentration of 25 mg mL⁻¹ of drug substance and recovery studies were performed on these samples.

4.2.3 Instrumentation and Chromatographic conditions

Residual solvents employed in this study (Table 1) were separated on a DB-5 capillary column (30 m x 0.32 mm I.D x 1 μ m film thickness, Agilent, CA, USA) coupled to DB-624 capillary column (30 m x 0.32 mm I.D x 1.8 μ m film thickness, Agilent, CA, USA) in a Thermo Scientific TRACE 1310 GC-FID with TRIPLUS RSH auto sampler (MA, USA). The HS incubator of the HS auto sampler was operated at 80 °C for experiments performed using NMP as a diluent. The HS incubator temperature was varied from 80 °C to 140 °C to investigate the IL diluent properties and examined the response of residual solvents.

The HS injector temperature was maintained at 5 °C above the incubator temperature. For the IL-based method, an optimum incubation time of 15 min was chosen for validation and recovery experiments. For separation, the GC inlet was maintained at 150 °C with a 1:50 split ratio. Helium was used as carrier gas at a constant flow of 2.3 mL min⁻¹. The FID was operated at 250 °C with helium as make-up gas at 29 mL min⁻¹. The hydrogen and air flows were maintained at 40 mL min⁻¹ and 450 mL min⁻¹, respectively. The column temperature used for residual solvents was as follows: initial temperature was 50 °C (16 min hold) followed by a ramp 25 °C/min to 250 °C (4 min hold).

Table 1. ICH limits of residual solvents and chemical structures of diluents and active pharmaceutical ingredients employed in this study

Residual solvent	ICH limit (ppm)	ICH class	Diluent	Active pharmaceutical ingredient
Methanol	3000	3	 [BMIM][NTf ₂]	 Quinidine
Ethanol	5000	3		
Acetone	5000	2		
2-Propanol	5000	3		
Acetonitrile	410	2		
Dichloromethane	600	2	 [P ₆₆₆₁₄][NTf ₂]	 Indomethacin
<i>tert</i> -Butylmethyl ether	5000	3		
1-Propanol	5000	3		
n-Hexane	290	2		
Methyl ethyl ketone	5000	3		
Ethyl acetate	5000	3	 NMP	
Tetrahydrofuran	720	2		
2-Methyl-1-Propanol	5000	3		
Isopropyl acetate	5000	3		
1-Butanol	5000	3		
n-Heptane	5000	3		
Toluene	890	2		
1-Pentanol	5000	3		

4.3 Results and discussion

4.3.1 Evaluation of background contributions of diluents using HS-GC/FID

In HS techniques, the choice of the diluent system plays an important role in contributing to the sensitivity of the method. Often at high HS incubation temperatures,

impurities present in the diluent potentially co-elute with target analytes and present serious problems in quantitation. The quality of ILs play a significant role in chromatographic applications. Owing to their process related impurities, ILs are often purified either by conditioning at high temperatures or using column chromatography [20, 21]. Therefore, it is essential to evaluate the chromatographic interferences of the diluent prior to its application. In this study, two ILs, [BMIM][NTf₂] and [P₆₆₆₁₄][NTf₂], were examined as diluents for the analysis of residual solvents in pharmaceutical drug substances. Under the studied experimental conditions, the chromatographic background contributions of [BMIM][NTf₂] were heavily dependent on the IL manufacturer. Figure S1 (Supporting Information) shows the background profiles of neat [BMIM][NTf₂] obtained from two different manufacturers, IOLITEC and EMD Millipore. It appears that the [BMIM][NTf₂] obtained from IOLITEC requires additional purification before its application for residual solvents analysis. The conditioning of ILs at high temperatures under reduced pressure resulted in the removal of volatile impurities from the IL [18, 19]. Figure 1A represents the chromatographic background intensities of [BMIM][NTf₂] (IOLITEC), subsequent to conditioning at 150 °C under reduced pressure (≤ 30 mmHg) for 12 h. Because of its relatively lower cost versus the material received from EMD Millipore and reduced chromatographic interferences, [BMIM][NTf₂] (IOLITEC) was utilized for all subsequent experiments. In contrast to [BMIM][NTf₂], [P₆₆₆₁₄][NTf₂] exhibited relatively higher background noise and only showed a slight reduction in noise levels subsequent to conditioning, as shown in Figure 1B. Therefore, a thorough investigation on diluent properties of this IL was not pursued.

Often in HS extractions, sample solutions are subjected to elevated temperatures to increase the volatility of the target analytes. However, conventional diluents such as NMP and DMSO often provide significant background peaks, which may lead to possible

contamination of the instrument and carry-over issues. As shown in Figure 1A, the high thermal stability and negligible vapor pressure of [BMIM][NTf₂] provided low chromatographic background noise with no diluent peak when compared to NMP (Figure 1C). Potentially, these favorable properties of ILs enable operation at higher HS temperatures compared to traditional diluents.

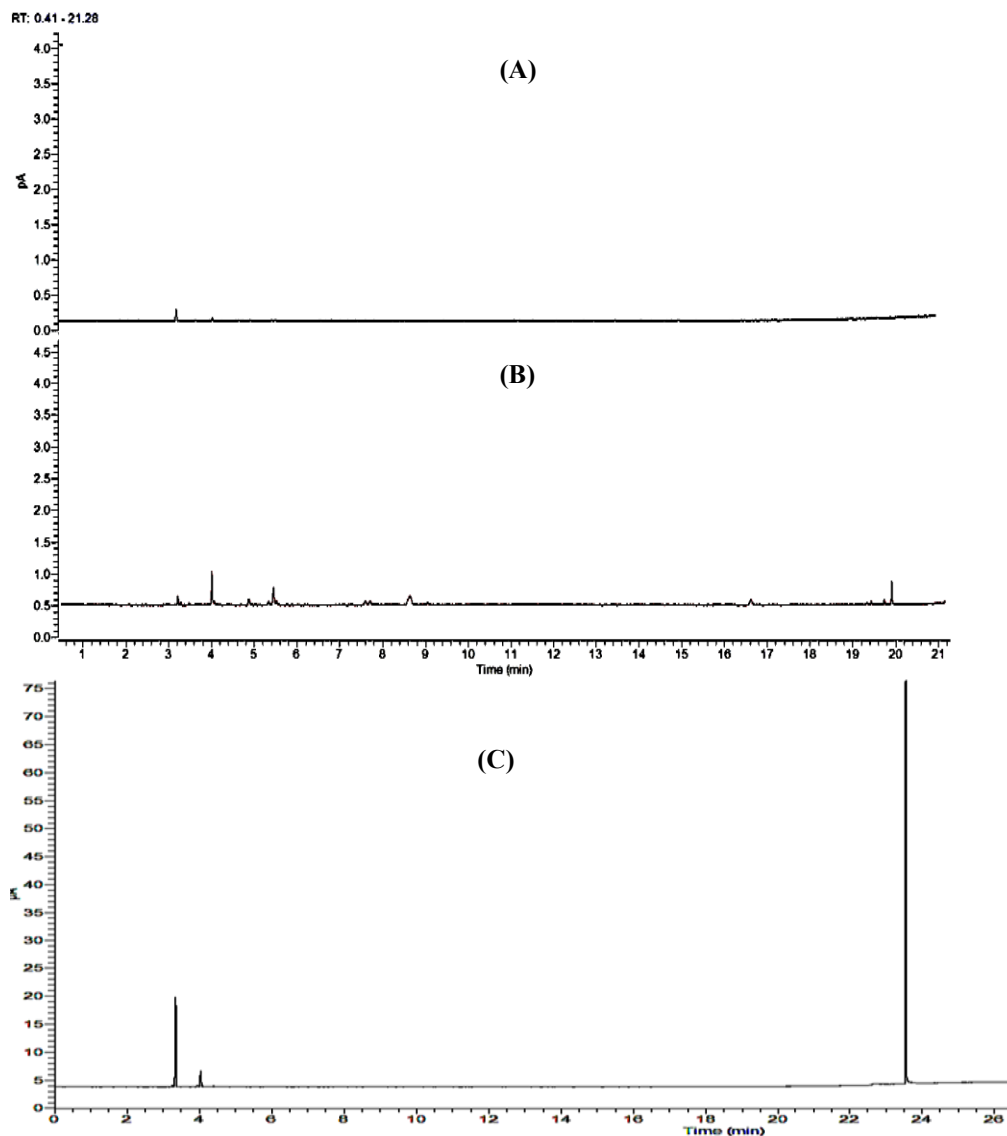


Figure 1. Evaluation of chromatographic background contributions of diluents subsequent to conditioning (A) neat IOLITEC-based [BMIM][NTf₂] (B) IOLITEC-based [P₆₆₆₁₄][NTf₂] and (c) NMP. Diluent volume: 1 mL; headspace incubator temperature: 140 °C for 45 min.

As a result, this promotes the partitioning of less volatile analytes into the HS and increases the overall sensitivity of the method. In addition, due to the absence of the diluent peak in the chromatogram, the GC separation conditions can be further optimized to reduce method run times.

4.3.2 Effect of [BMIM][NTf₂] on the response of residual solvents

A representative profile of the residual solvent profile is illustrated in Figure 2 using [BMIM][NTf₂]. Aside from the background components, the profile is independent of the HS solvent used. Owing to their distinct physicochemical properties, the partitioning behavior of residual solvents in ILs may be significantly different from conventional organic diluents. A side-by-side comparison of the peak areas using [BMIM][NTf₂] and NMP is shown in Figure 3. The signal intensities of most of the residual solvents were significantly higher in [BMIM][NTf₂] than NMP. Specifically, 1-butanol and 1-pentanol gained an approximate 10-fold enhancement in response (Figure 3A), while a similar trend was also observed for other alkyl alcohols and alkanes (Figure 3B). The increase in signal intensities may be due to the negligible vapor pressure and unique solvation properties of [BMIM][NTf₂], which can promote the volatilization and partitioning of residual solvents into the sample vial HS. In contrast, using NMP as a diluent can contribute significant partial pressure to the HS in the vial, due to its relatively high vapor pressure under conditions of the measurement. In turn, the partial pressure of the analytes in the HS will be drastically reduced, leading to poor signal intensities. These results are also in good agreement with a previous study, where the quantification of high boiling solvents used in API manufacturing was determined using 1-butyl-3-methylimidazolium tetrafluoroborate ([BMIM][BF₄]) as the diluent [6].

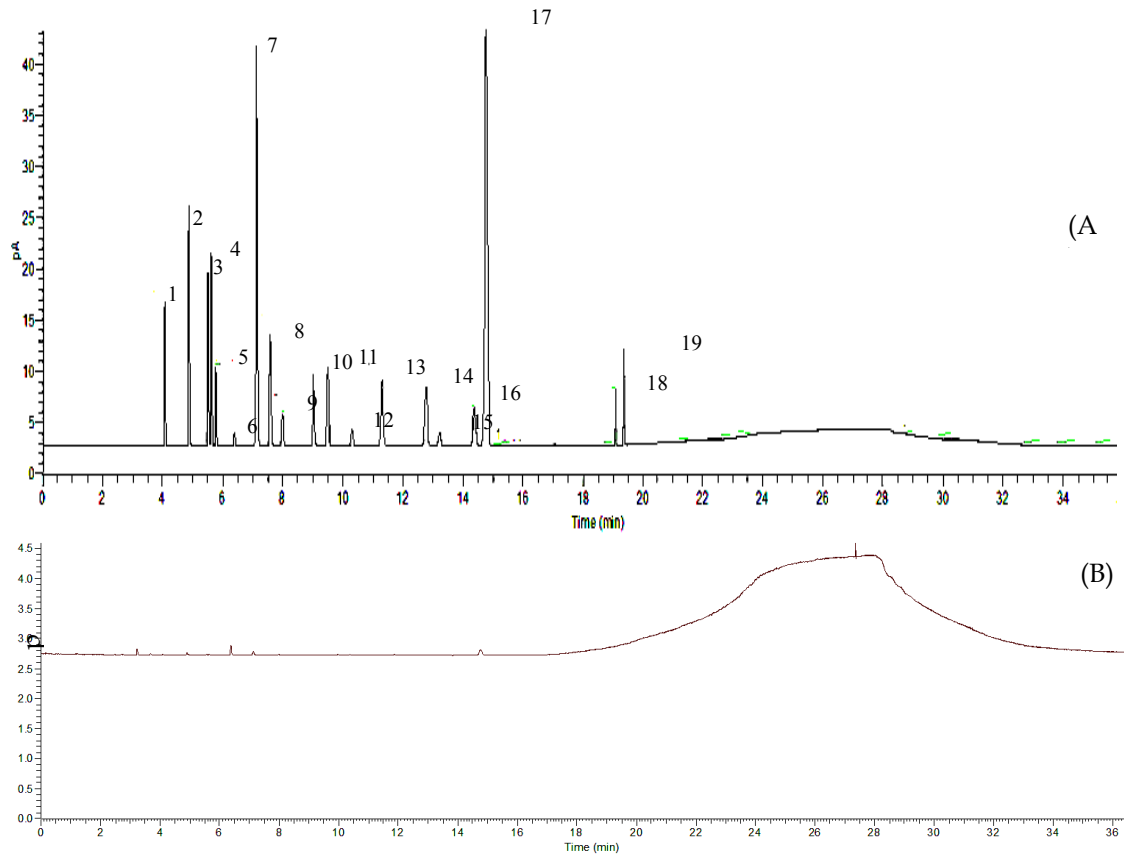


Figure 2A. Response of residual solvents in [BMIM][NTf₂] subsequent to conditioning. Spiking concentration: 60% ICH limit; sample volume: 1 mL; headspace incubator temperature: 80 °C for 45 min. (1) methanol; (2) ethanol; (3) acetone; (4) 2-propanol; (5) acetonitrile (6) dichloromethane; (7) *tert*-butylmethyl ether; (8) 1-propanol; (9) n-hexane; (10) methyl ethyl ketone; (11) ethyl acetate; (12) tetrahydrofuran; (13) 2-methyl-1-propanol; (14) isopropyl acetate; (15) methyl tetrahydrofuran ; (16) 1-butanol; (17) n-heptane; (18) toluene; (19) 1-pentanol. **Figure 2B.** Background contribution from [BMIM][NTf₂] IL.

4.3.3 Optimization of HS extraction parameters using [BMIM][NTf₂]

Unlike conventional diluents, the low chromatographic background contributions and negligible volatility of [BMIM][NTf₂] enables operation at high incubation temperatures without contaminating the instrument. The effects of incubation temperature on the response of residual solvents was examined by spiking 30% of the ICH limit for each residual solvent in 1 mL [BMIM][NTf₂]. The incubation temperature was varied from 80 °C to 140 °C for 10 min. Due to the limited thermostat capacity of the incubator (40 °C to 150 °C), temperatures beyond 140 °C were not examined.

The gastight syringe temperature was operated at 5 °C above the incubator temperature to prevent condensation of the analytes during GC injection. Preliminary experiments using Thermo Scientific-based gastight syringe resulted in poor reproducibility and low peak areas at high syringe temperatures (Figure S2 in supporting information). However, a significant improvement in reproducibility was observed by replacing this syringe with a SGE high temperature rated gastight syringe. In addition, the mass of residual solvents extracted from the HS was also increased. For example, the RSD value for 1-pentanol was drastically reduced from 34% to 6%, while at the same time a 3-fold enhancement in signal intensity was observed when using the SGE syringe. As shown in Figure 4, by increasing the incubation temperature from 80 °C to 140 °C, the peak areas of many residual solvents increased. For example, as shown in Figure 4A, 1-pentanol demonstrated approximately 8-fold enhancement in response. Similarly, other alkyl alcohols, including 1-butanol, ethanol, 1-propanol, and 2-propanol exhibited approximately 5-fold increase in peak areas when the incubation temperature was increased (Figure 4B). However, no significant enhancement in signal intensity was observed for n-hexane, n-heptane, and *tert*-butylmethyl ether when increasing the temperature beyond 100 °C, suggesting these analytes have reached their HS equilibrium concentration. Nonetheless, in an effort to increase the HS concentration for more number of residual solvents, an incubation temperature of 140 °C was chosen for subsequent experiments. The incubation time is another important parameter which affects the HS equilibrium concentration of the analytes.

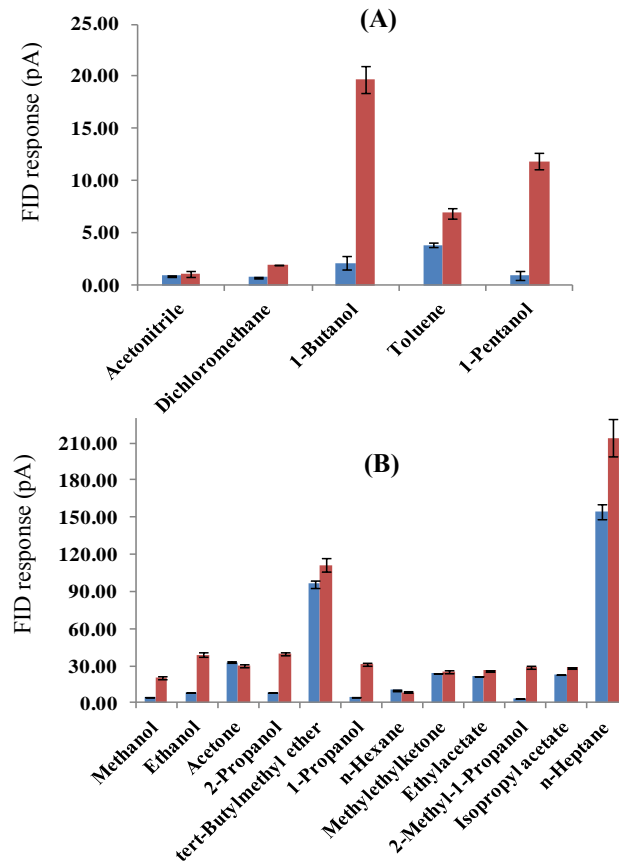


Figure 3. Comparison of response of the residual solvent in (■) NMP and (■) [BMIM][NTf₂]. All experiments were performed in triplicate (n = 3). Residual solvents concentration: 60% ICH limit (relative to API); incubator temperature: 80 °C; incubation time: 45 min; Sample volume: 1 mL.

The optimization of the incubation time may result in enhancing the sensitivity as well as throughput of the overall method. In this study, the effects of incubation time with respect to the response of the residual solvents were evaluated by varying the incubation time from 5 to 45 min at 140 °C (optimized incubation temperature). As illustrated in Figure 5A, 1,4-dioxane, acetonitrile, toluene, and dichloromethane yielded no significant increase in peak areas following a 5 min incubation. On the other hand, the peak intensities of the remaining residual solvents were significantly increased when changing the incubation time from 5 to 15 min. No significant improvement in peak areas was observed beyond 15 min; suggesting that most of the analytes reached their HS equilibrium concentration within 15 min. Overall, a HS incubator temperature of 140 °C and an incubation time of 15 min provided the best response for most analytes, and these optimized conditions were selected for method validation experiments.

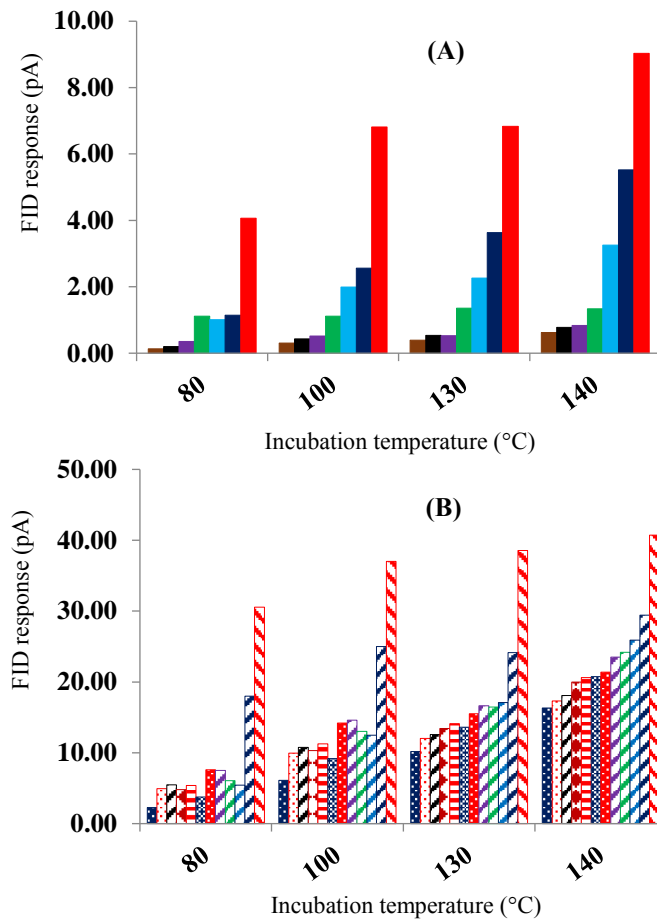


Figure 4. Incubation temperature effects on response of the residual solvent in [BMIM][NTf₂]. Residual solvents concentration: 30% ICH limit (relative to API); incubation time: 10 min; Sample volume: 1 mL. (■) methanol; (■) toluene; (■) tetrahydrofuran; (■) n-hexane; (■) dichloromethane; (■) acetonitrile; (■) 1,4-dioxane; (■) n-heptane; (■) *tert*-butyl methyl ether; (■) 2-methyl-1-propanol; (■) 1-propanol; (■) 2-propanol; (■) isopropyl acetate; (■) ethanol; (■) 1-butanol; (■) methyl ethyl ketone; (■) acetone; (■) ethyl acetate; (■) 1-pentanol.

4.3.4 Analytical performance of [BMIM][NTf₂] and method validation

The analytical performance of [BMIM][NTf₂] was evaluated by generating calibration curves for each of the residual solvents studied (Table 2). Linear ranges up to two orders of magnitude (representing 1.2%-120% of their ICH limit) were obtained for most of the studied residual solvents, except for dichloromethane, n-hexane, acetonitrile, tetrahydrofuran, and toluene. The linear correlation coefficients (R) were no less than 0.996 for most analytes, apart from n-heptane and *tert*-butyl methyl ether. The precision of the IL-based method was also evaluated at 6% and 30% of the ICH limits (n = 4). Because of

their high toxicity and low tolerance limits, only PQL of class 2 was chosen to evaluate the precision of IL-based method at low concentrations. The resulting RSD values were no more than 8% for all the residual solvents investigated at both spiking concentrations.

Table 2. Analytical figures of merit for [BMIM][NTf₂] in the analysis of residual solvents

Residual solvent	Linear range ^{a,b} ($\mu\text{g g}^{-1}$)	Linear range (% ICH limit)	Slope _b	R ^b	%RSD ^{b,c}	%RSD ^{b,d}	LOD ^{b,e} ($\mu\text{g g}^{-1}$)	LOD ^f ($\mu\text{g g}^{-1}$)
Methanol	36-3600	1.2-120	27	0.999	6	2	12	300
Ethanol	60-6000	1.2-120	64	0.997	5	1	20	500
Acetone	60-6000	1.2-120	59	0.999	5	1	20	500
2-Propanol	60-6000	1.2-120	75	0.999	5	1	20	500
Acetonitrile	24.6-492	6-120	3	0.998	7	1	8.2	41
Dichloromethane	36-720	6-120	2	0.996	7	8	20	60
Toluene	53.4-1068	6-120	19	0.999	3	1	17.8	89
2-Methyl-1-Propanol	60-6000	1.2-120	89	0.999	7	1	20	500
Isopropyl acetate	60-6000	1.2-120	70	0.999	6	1	20	500
1-Butanol	60-6000	1.2-120	72	0.999	8	1	20	500
n-Heptane	60-6000	1.2-120	85	0.991	8	1	20	500
1-Pentanol	60-6000	1.2-120	59	0.999	3	1	20	500
<i>tert</i> -Butyl methyl ether	60-6000	1.2-120	83	0.991	8	1	20	500
1-Propanol	60-6000	1.2-120	80	0.999	5	1	20	500
Methyl ethyl ketone	60-6000	1.2-120	67	0.999	3	1	20	500
Ethyl acetate	60-6000	1.2-120	57	0.999	5	2	20	500
n-Hexane	17.4-348	6-120	29	0.999	7	3	5.8	29
Tetrahydrofuran	43.2-864	6-120	10	0.999	3	4	14.4	72

^aResidual solvents spiked at the desired concentration assuming 25 mg of drug substance in 1 mL [BMIM][NTf₂]; ^b data obtained by using [BMIM][NTf₂] as diluent with an incubation temperature of 140 °C for 15 min; ^c data obtained by performing repeated experiments at 6% ICH limit of residual solvents (n = 4); ^ddata obtained by performing repeated experiments at 30% ICH limit of residual solvents (n = 4); ^eLOD obtained by using [BMIM][NTf₂] as diluent; ^fLOD obtained by using NMP as diluent; ^g data obtained by using NMP as diluent with an incubation temperature of 80 °C for 45 min.

The slopes of the calibration curves were determined for all analytes in order to evaluate their sensitivities using [BMIM][NTf₂] as diluent (Table 2). When comparing the analyte-to-analyte sensitivities, the highest values were obtained for 2-methyl-1-propanol and n-heptane, while the lowest values were observed for acetonitrile and dichloromethane. Additionally, 1-propanol, 2-propanol, and 1-butanol, exhibited better sensitivities compared to methanol and ethanol. With only a difference in one unit of methylene substituent, an approximate 3-fold reduction in sensitivity was observed for n-hexane, in

comparison to n-heptane. This is to be expected with flame ionization detection. The analytical performance of the NMP method was determined at HS incubation temperature of 80 °C for 45 min. The possibility of instrument contamination and safety issues due to high vapor pressure of NMP has precluded us to investigate its diluent properties at high incubation temperatures. The LOD for the [BMIM][NTf₂]-based method was evaluated by decreasing the concentration of residual solvents until a 3:1 signal-to-noise was achieved. As listed in Table 2, the LOD values of the IL-based method were superior to the NMP-based method. For example, a 25-fold enhancement was observed in the case of the alkyl alcohols and esters in the data set when using [BMIM][NTf₂] as the diluent. Similarly, a 5-fold improvement was observed with acetonitrile, n-hexane, and tetrahydrofuran. Overall, the IL-based method demonstrated superior detection limits with excellent precision and sensitivities for all residual solvents when compared to NMP as a diluent.

4.3.5 Real sample analysis using [BMIM][NTf₂]

Residual solvent studies in representative API compounds were executed using 1 mL of [BMIM][NTf₂] and 25 mg of API. The solubility of these APIs in [BMIM][NTf₂] largely depended on the incubation temperature and chemical nature of the API. At the investigated concentrations, Quinidine and Indomethacin were not completely soluble in [BMIM][NTf₂] at room temperature. However, increasing the temperature to 80 °C resulted in complete miscibility of these APIs. At the investigated incubation temperatures, all APIs studied were found to be completely miscible in 1 mL [BMIM][NTf₂]. The chromatographic background contributions of each API in the IL were evaluated and any unknown peaks eluting at the retention time of residual solvents were

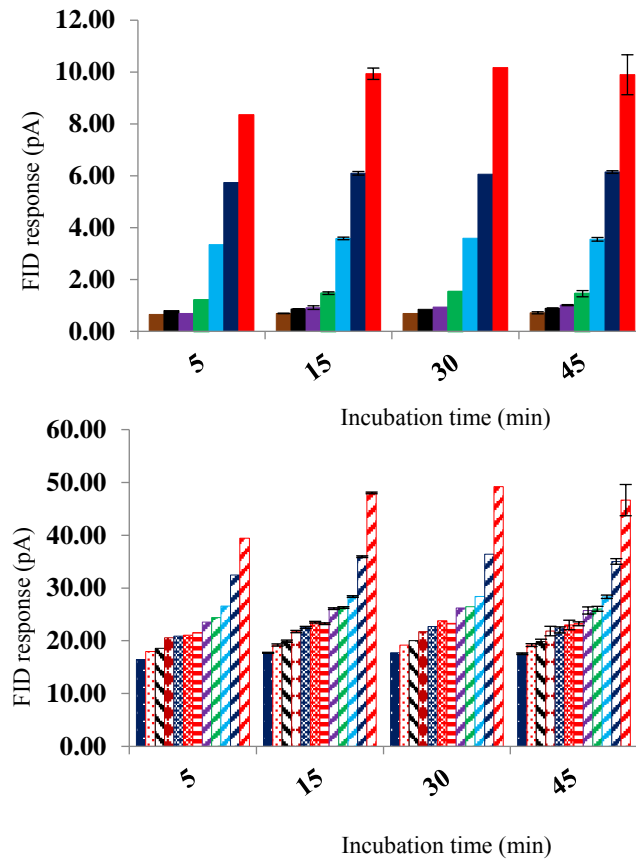


Figure 5. Incubation time effects on response of the residual solvent in [BMIM][NTf₂]. Residual solvents concentration: 30% ICH limit (relative to API); incubation temperature: 140 °C; sample volume: 1 mL. Experiments at 15 min and 45 min incubation time were performed in triplicate (n = 3). (■) methanol; (■) toluene; (■) tetrahydrofuran; (■) n-hexane; (■) dichloromethane; (■) acetonitrile; (■) 1,4-dioxane; (■) n-heptane; (■) *tert*-butyl methyl ether; (■) 2-methyl-1-propanol; (■) 1-propanol; (■) 2-propanol; (■) isopropyl acetate; (■) ethanol; (■) 1-butanol; (■) methyl ethyl ketone; (■) acetone; (■) ethyl acetate; (■) 1-pentanol.

determined prior to recovery analysis. Three spiking concentrations, 6%, 60%, and 120% of the ICH limit of residual solvents (relative to API substance), were chosen for the analysis (Table 3). At these spiking concentrations, recoveries ranging from 94 to 108% were observed in the presence of Indomethacin and Quinidine; demonstrating minimal matrix effects from these two APIs. In addition, the technique yielded excellent recoveries with proprietary compounds not reported here.

Table 3. Recovery of residual solvents in the presence of different APIs using [BMIM][NTf₂]

Residual solvent	Indomethacin ^b			Quinidine ^b		
	Spiking concentration (%ICH limit)			Spiking concentration (%ICH limit)		
	6 ^a	60	120	6 ^a	60	120
Methanol	103%	99%	94%	89%	90%	89%
Ethanol	108%	100%	102%	101%	92%	90%
Acetone	107%	98%	104%	100%	96%	99%
2-Propanol	107%	99%	101%	101%	94%	94%
Acetonitrile	101%	97%	101%	92%	100%	97%
Dichloromethane	99%	101%	100%	90%	100%	103%
<i>tert</i> -Butylmethyl ether	100%	97%	104%	120%	100%	107%
1-Propanol	105%	100%	100%	100%	93%	90%
n-Hexane	108%	98%	106%	91%	69%	120%
Methyl ethyl ketone	104%	100%	105%	100%	97%	98%
Ethyl acetate	106%	100%	105%	100%	98%	100%
Tetrahydrofuran	105%	99%	104%	96%	99%	100%
2-Methyl-1-Propanol	104%	103%	103%	98%	96%	93%
Isopropyl acetate	105%	100%	105%	99%	98%	100%
1-Butanol	103%	113%	101%	98%	94%	90%
n-Heptane	107%	97%	105%	91%	102%	115%
Toluene	104%	101%	107%	106%	99%	100%
1-Pentanol	101%	116%	101%	97%	94%	90%

^aData obtained by performing repeated experiments at 6% ICH limit of residual solvents (n = 3); ^bdata obtained by using 1 ml [BMIM][NTf₂] containing 25 mg of API. Incubation temperature: 140 °C; incubation time: 15 min.

4.3.6 Cost differences in using ILs for HS-GC

The primary non-analytical challenges to using ILs in regulated laboratories are the cost and availability. For availability, ILs can be purchased or produced in-house. While ionic liquids can be easily produced in most laboratories, for Good Manufacturing Practices (GMP) it is generally accepted that commercial availability is the preferred way to source. While more expensive than in-house production, commercially available ILs allow the solvents to be readily assessable by regulatory agencies and contract laboratories. Regardless of the source, the IL used must have any volatile components isolated before use. The non-volatile solvent of choice in most pharmaceutical industries is high boiling point organic solvents such as NMP and DMSO, which were purchased (at the time of this study) at an approximate price of \$0.15 per gram. The ILs used in this study were sourced

at a much higher cost of approximately \$2.25, or fifteen times higher in price. However, the use of ILs has shown to significantly increase sensitivity of the HS-GC method and has shown the potential to shorten the chromatographic run. Yet, because their use in the method does not significantly shorten analyst time, routine use of ILs is likely not cost justified. However, for the analysis of individual impurities of significant toxicity that cannot be determined using traditional HS solvents, the use of ILs are warranted.

4.4 Conclusions

The demand for high throughput and sensitive methods for the analysis of pharmaceutical impurities is rapidly increasing. Holistically speaking, the primary advantage to using ILs as a diluent in HS-GC (compared to organic diluents) is the overall enhancement in analyte detection sensitivity. ILs can also provide the unique solvation power needed to dissolve drug substances that cannot be dissolved by traditional organic solvents. Conversely, the main disadvantage of IL-based diluents lies in the high cost of these compounds, which may limit them from being used for routine analyses in a commercial setting. This study demonstrates the feasible determination of residual solvents in pharmaceuticals with [BMIM][NTf₂] as a diluent, by employing HS-GC coupled with FID. The [BMIM][NTf₂]-based method yielded higher sensitivities, required low amounts of sample, and superior throughput when compared to conventional residual solvent methods. Due to their negligible vapor pressure and high thermal stability, at high incubation temperature, [BMIM][NTf₂] produced no solvent peaks and reduced noise levels in comparison to organic diluents such as NMP. This provided the opportunity to increase the HS incubation temperature to enhance the sensitivity of the method.

Due to their relatively higher cost of production, ILs are recommended for niche or non-routine uses in the pharmaceutical industry. Their application can be focused toward challenging analytical methods where traditional HS solvents fail to achieve the needed

sensitivity or selectivity for semi-volatile analytes. In particular, exploiting ILs as diluents for the trace-level quantification of highly toxic/potent impurities (i.e. GTIs, carcinogens, etc..) is beneficial, since method sensitivity can be achieved without the need for complicated mass spectrometric detection techniques. ILs can also be useful in the analysis of high boiling point residual solvents, such as DMSO and dimethylformamide (DMF) in drug substances. Traditionally, these analytes are not easily determined by HS-GC using conventional organic diluents, due to their similar boiling points and vapor pressures to the diluent. Exploiting the high thermal stability and vapor-free characteristics of ILs can enable the quantification of high-boiling residual solvents, without significant chromatographic background contributions. Lastly, ILs are highly convenient for analyzing drug substances and/or products possessing poor solubility in organic diluents, as these ionic diluents can be finely tuned to provide suitable solvation capabilities. Employing the appropriate IL for dissolution will minimize the need for additional sample preparation/manipulation and enable better analytical accuracy/recovery.

Acknowledgements

Omprakash Nacham is a graduate student at Iowa State University and a 2016 summer intern at AbbVie. Jared L. Anderson is a professor at Iowa State University. Tien D. Ho and Gregory K. Webster are employees of AbbVie.

Supplemental information

Figure S1 and Figure S2 are provided in Appendix C.

References

- [1] Y. Liu, C.-Q. Hu, Establishment of a knowledge base for identification of residual solvents in pharmaceuticals, *Anal. Chim. Acta* 575 (2006) 246.
- [2] K. Urakami, A. Higashi, K. Umemoto, M. Godo, Matrix media selection for the determination of residual solvents in pharmaceuticals by static headspace gas chromatography, *J. Chromatogr. A* 1057 (2004) 203.

- [3] Harmonised Tripartite Guideline on Impurities: Residual Solvents (Q3C), International Conference on Harmonisation of Technical Requirements for Registrations of Pharmaceuticals for Human Use (ICH), Geneva, 1997.
- [4] C. B'Hymer, Residual Solvent Testing: A Review of Gas-Chromatographic and Alternative Techniques, *Pharm. Res.* 20 (2003) 337.
- [5] C.C. Camarasu, M. Mezei-Szűts, G.B. Varga, Residual solvents determination in pharmaceutical products by GC-HS and GC-MS-SPME, *J. Pharm. Biomed. Anal.* 18 (1998) 623.
- [6] F.-h. Liu, Y. Jiang, Room temperature ionic liquid as matrix medium for the determination of residual solvents in pharmaceuticals by static headspace gas chromatography, *J. Chromatogr. A* 1167 (2007) 116.
- [7] J.L. Pérez Pavón, M. del Nogal Sánchez, M.E. Fernández Laespada, C. García Pinto, B. Moreno Cordero, Analysis of class 1 residual solvents in pharmaceuticals using headspace-programmed temperature vaporization-fast gas chromatography-mass spectrometry, *J. Chromatogr. A* 1141 (2007) 123.
- [8] N.H. Snow, G.C. Slack, Head-space analysis in modern gas chromatography, *TrAC Trends in Analytical Chemistry* 21 (2002) 608.
- [9] R. Otero, G. Carrera, J.F. Dulsat, J.L. Fábregas, J. Claramunt, Static headspace gas chromatographic method for quantitative determination of residual solvents in pharmaceutical substances according to European Pharmacopeia requirements, *J. Chromatogr. A* 1057 (2004) 19.
- [10] N. Kumar, J.G. Gow, Residual solvent analysis by headspace gas chromatography, *J. Chromatogr. A* 667 (1994) 235.
- [11] M. Ortega-Heras, M.L. González-SanJosé, S. Beltrán, Aroma composition of wine studied by different extraction methods, *Anal. Chim. Acta* 458 (2002) 85-93.
- [12] J.A. Cruwys, R.M. Dinsdale, F.R. Hawkes, D.L. Hawkes, Development of a static headspace gas chromatographic procedure for the routine analysis of volatile fatty acids in wastewaters, *J. Chromatogr. A* 945 (2002) 195-209.
- [13] C. Cheng, S. Liu, B.J. Mueller, Z. Yan, A generic static headspace gas chromatography method for determination of residual solvents in drug substance, *J. Chromatogr. A* 1217 (2010) 6413.
- [14] J.P. Hallett, T. Welton, Room-temperature ionic liquids: solvents for synthesis and catalysis. 2, *Chem. Rev.* 111 (2011) 3508.
- [15] B. Kolb, L.S. Ettre, *Static headspace-gas chromatography: theory and practice*. John Wiley & Sons, 2006, pp 51-62
- [16] T.D. Ho, C. Zhang, L.W. Hantao, J.L. Anderson, Ionic liquids in analytical chemistry: fundamentals, advances, and perspectives, *Anal. Chem.* 86 (2013) 262.

- [17] S. Pandey, Analytical applications of room-temperature ionic liquids: A review of recent efforts, *Anal. Chim. Acta* 556 (2006) 38.
- [18] T.D. Ho, P.M. Yehl, N.P. Chetwyn, J. Wang, J.L. Anderson, Q. Zhong, Determination of trace level genotoxic impurities in small molecule drug substances using conventional headspace gas chromatography with contemporary ionic liquid diluents and electron capture detection, *J. Chromatogr. A* 1361 (2014) 217.
- [19] G. Laus, M. Andre, G. Bentivoglio, H. Schottenberger, Ionic liquids as superior solvents for headspace gas chromatography of residual solvents with very low vapor pressure, relevant for pharmaceutical final dosage forms, *J. Chromatogr. A* 1216 (2009) 6020.
- [20] P. Nockemann, K. Binnemans, K. Driesen, Purification of imidazolium ionic liquids for spectroscopic applications, *Chem. Phys. Lett.* 415 (2005) 131-136.
- [21] R.J. Soukup-Hein, M.M. Warnke, D.W. Armstrong, Ionic liquids in analytical chemistry, *Annu. Rev. Anal. Chem.* 2 (2009) 145-168.

CHAPTER 5

INTERFACIAL AND AGGREGATION BEHAVIOR OF DICATIONIC AND TRICATIONIC IONIC LIQUID-BASED SURFACTANTS IN AQUEOUS SOLUTION

Reprinted with permission from *Colloids and Surfaces A: Physicochemical and Engineering Aspects* **2015**, 469, 224-234

Copyright © 2015, Elsevier

Omprakash Nacham, Armide Martín-Pérez, Daniel J. Steyer, María J. Trujillo-Rodríguez, Jared L. Anderson, Verónica Pino, Ana M. Afonso

Abstract

The interfacial and aggregation behavior of three dicationic and two tricationic ionic liquid-based (IL) surfactants in aqueous solutions have been carried out. The studied dicationic IL-based surfactants were 1,12-di(3-butyylimidazolium)dodecane bromide ((C₄Im)₂C₁₂-2Br), 1,12-di(3-decyylimidazolium)dodecane bromide ((C₁₀Im)₂C₁₂-2Br), and 1,12-di(3-hexadecylimidazolium)dodecane bromide ((C₁₆Im)₂C₁₂-2Br). Two classes of trigonal tricationic surfactants containing triethylamine (Am) and 1,3,5-trimethylbenzene (Bn) cores were synthesized for first time and characterized, specifically, 3,3',3''-octyl-1,1',1''-(2-ethylamino) imidazolium bromide ((C₈Im)₃Am-3Br), and 3,3',3''-octyl-1,1',1''-(1,3,5)tris(methylene) benzene imidazolium bromide ((C₈Im)₃Bn-3Br). The critical micelle concentration (CMC) values and other aggregation parameters, including adsorption efficiency (pC₂₀), surface tension at the CMC (γ_{cmc}), degree of dissociation (α), and the degree of counterion binding in the micelle (β) were obtained using a variety of techniques including surface tension, conductivity and fluorescence measurements. For the first time, the aggregation numbers (N_{agg}) were also obtained for this group of surfactants. A study into the influence of acetonitrile on the stability and aggregation behavior of dicationic and tricationic IL-based surfactants was also undertaken. The CMC values of the

dicationic surfactants clearly decrease as a function of the side chain, when the same linker is maintained. The CMC values of the tricationic surfactants were lower than analogous linear trimeric surfactants. For the novel tricationic surfactants, the effect of sodium salts (C_6H_5COONa , $NaBr$, and NaI) on the surface activity was also investigated. It was also observed that the surface activity parameters (pC_{20} and CMC/C_{20}) of tricationic surfactants increased significantly in the presence of added electrolytes.

5.1 Introduction

Ionic liquids (ILs) are class of organic molten salts having low melting points (<100 °C), negligible vapor pressure, and high thermal stability. The physicochemical properties of ILs can be tailored for specific applications by structural modification of either the cation or anion [1]. Merrigan *et al.* reported the synthesis of imidazolium-based fluorosurfactants and examined the surface activity of these compounds in the solubilization of fluoroalkanes in conventional ILs [2]. Anderson *et al.* studied the aggregation phenomena of traditional surfactants in ILs using surface tension measurements [3]. It was observed that the surface tension values of ILs were decreased due to solvophobic interactions between the IL and traditional surfactants. It was also reported for first time that the solvation properties of micellar IL solutions were modified due to the formation of traditional surfactant micelles in ILs [3].

The first reports on the study of amphiphilic association structures of monocationic imidazolium-based IL-surfactants in aqueous solutions was in 2004 [4,5]. The aggregation or micelle formation ability of ILs in aqueous solutions is due to the intrinsic amphiphilic nature of ILs [4-7]. Blesic *et al.* studied the self-aggregation behavior of the 1-alkyl-3-methyl imidazolium C_nMIm^+ family of cations with various alkyl chain lengths and counter ions [8]. It was observed that ILs possessing octyl and higher alkyl chain analogues exhibited self-aggregation, whereas lower alkyl chain length analogues did not show

significant reduction in surface tension. Baltazar *et al.* performed an extensive study on the surface activity of monocationic and dicationic imidazolium based IL-surfactants in aqueous solution by surface tensiometry measurements [9]. It was shown that the critical micelle concentration (CMC) values of monocationic IL-based surfactants depended on the length of alkyl chain substituent attached to the head group. Freire *et al.* also examined the effect of cation/anion, temperature, and water content on the surface activity of monocationic ILs containing the imidazolium head group [10]. Recently, Bhargava *et al.* performed molecular dynamic simulation studies on dicationic IL-based surfactants in aqueous solutions [11]. In their theoretical studies, it was observed that the hydrophobic tails of ILs were organized in a manner such that they possess minimum interaction with water molecules and anions of the IL. It was also observed that in comparison with anions, the cationic head groups of the ILs possessed weaker hydrogen bonding interaction with water molecules. Ao *et al.* investigated the effect of spacer length on the surface activity of Gemini IL-based surfactants [12]. It was observed that spacer groups containing lower number of carbon atoms possessed higher surface activity.

The surface activity of IL-based surfactants can be influenced by their molecular structure [13,14] and the presence of added electrolytes [15,16]. Recently, Jiao *et al.* studied the effect of organic and inorganic salts on the aggregation of 1-butyl-3-methyl imidazolium dodecylsulfate in aqueous solutions [15]. It was observed that the CMC values of the surfactants decreased with the increase in concentration of electrolyte. From their study, it was also observed that hydrophobicity and hydration ability of added electrolytes were crucial in promoting aggregation.

Trigonal tricationic ILs are new class of ILs comprised of three cationic moieties appended to a central core with various combinations of anions. Recently, Planellas *et al.* studied palladium nanoparticle catalyzed Suzuki cross-coupling reactions, wherein the

stabilization of nanoparticles was improved by the application of tris-imidazolium based tricationic ILs [17]. The number of applications of tricationic imidazolium-based ILs within the literature is very small in comparison with monocationic and dicationic imidazolium-based ILs. Therefore, studying the self-assembly behavior of tricationic imidazolium-based ILs in aqueous solutions will provide significant fundamental understanding of these compounds which may extend their applications into different areas, including extraction solvents in aqueous biphasic systems (ABS), ion-pairing reagents in liquid chromatography, and as catalysts in organic synthesis.

In this study, the behavior of a group of dicationic IL-based surfactants is presented in an effort to increase the fundamental knowledge of these surfactant systems. In addition, this is the first study to examine the interfacial and aggregation properties of trigonal tricationic imidazolium-based ILs. The synthetic preparation of a novel group of tricationic IL-based surfactants and the overall characterization of their aggregation behavior is presented. The two classes of trigonal tricationic imidazolium-based ILs are comprised of two different cores, namely, triethylamine (Am) and 1,3,5-trimethylbenzene (Bn) and were synthesized for first time in this study. CMC values and surface activity parameters including adsorption efficiency (pC_{20}), CMC/C_{20} , and surface tension at the CMC (γ_{cmc}), micelle degree of dissociation (α), degree of counterion binding to the micelle (β), and the aggregation number (N_{agg}) were obtained using a number of techniques including conductivity, fluorescence, and surface tensiometry. The influence of the acetonitrile content was also addressed for the dicationic and tricationic IL-based surfactant micelles.

In order to understand the effect of electrolytes on the aggregation of the novel tricationic surfactants in aqueous solutions, one organic and two inorganic salts were examined. Furthermore, the adsorption and aggregation phenomenon of tricationic IL-based surfactants was compared with traditional quaternary ammonium-based cationic surfactants.

5.2 Experimental

5.2.1. Reagents

The dicationic IL-based surfactants used in this study were 1,12-di(3-butylimidazolium)dodecane bromide $((C_4Im)_2C_{12}-2Br)$, 1,12-di(3-decylimidazolium)dodecane bromide $((C_{10}Im)_2C_{12}-2Br)$, and 1,12-di(3-hexadecylimidazolium)dodecane bromide $((C_{16}Im)_2C_{12}-2Br)$. These dicationic IL-based surfactants were synthesized and fully characterized according to the procedures described by Baltazar *et al.* [9].

The new tricationic IL-based surfactants prepared were 3,3',3''-octyl-1,1',1''-(2-ethylamino) imidazolium bromide $((C_8Im)_3Am-3Br)$, and 3,3',3''-octyl-1,1',1''-(1,3,5)tris(methylene) benzene imidazolium bromide $((C_8Im)_3Bn-3Br)$.

The structures of all surfactants utilized in this work are shown in Figure S1 of the supplemental information in Appendix D.

The reagents used for the synthesis of the dicationic and tricationic IL-based surfactants were: 1-bromobutane, 1-bromooctane, 1-bromodecane, 1-bromohexadecane, 1,12-dibromododecane, imidazole, toluene, anhydrous dimethylsulfoxide (DMSO), tris(2-chloroethyl) amine hydrochloride, sodium iodide, sodium bromide, and sodium benzoate, which were supplied by Sigma-Aldrich (St. Louis, MO, USA). Isopropanol, methanol, dichloromethane, chloroform, sodium hydroxide, potassium hydroxide, ethyl acetate, acetonitrile, 1,3,5-tris(bromomethyl)benzene, and diethyl ether were purchased from Fisher

Scientific (Fair Lawn, NJ, USA). Deuterated chloroform was purchased from Cambridge Isotope Laboratories (Andover, MA, USA). Ultrapure water with a conductivity value of $18.2 \text{ M}\Omega \cdot \text{cm}^{-1}$ and a total organic carbon content of $4 \text{ mg} \cdot \text{L}^{-1}$, was obtained from Milli-Q water purification system with A-10 gradient (Millipore, Bedford, MA, USA).

For conductivity measurements, a standard solution of potassium chloride (specific conductance of $1.41 \text{ mS} \cdot \text{cm}^{-1}$) from Merck (Darmstadt, Germany) was utilized.

For fluorescence measurements, pyrene and benzophenone-3 (<97.0%), were both supplied by Sigma-Aldrich.

5.3 Synthesis of tricationic IL-based surfactants

Tricationic IL-based surfactants were synthesized as shown in Figure 1, using a slightly modified procedure of Planellas and co-workers [17].

5.3.1. Synthesis of 3,3',3''-octyl-1,1',1''-(1,3,5)tris (methylene) benzene imidazolium bromide ((C₈Im)₃Bn-3Br)

Imidazole (1.00 g, 14.68 mmol) and potassium hydroxide (3.49 g, 62.3 mmol) were dissolved in 40 mL of dimethylsulfoxide and the solution stirred for 6 h at room temperature. The compound 1,3,5-tris(bromomethyl)benzene (1.58 g, 4.45 mmol) was added and stirred for 24 h at room temperature. Water (40 mL) was then added to the reaction mixture and the contents transferred to a separatory funnel and the mixture extracted using chloroform ($4 \times 40 \text{ mL}$). The organic phases were collected, washed several times with water, and then dried over anhydrous sodium sulfate and filtered. The solvent was partially evaporated under reduced pressure followed by the addition of excess diethyl ether. Upon addition of excess diethyl ether, a white powder was precipitated, filtered, and washed with diethyl ether. Compound **1A** was recrystallized using a dichloromethane-diethyl ether solvent mixture and dried at $60 \text{ }^\circ\text{C}$ for 12 h. The yield was 75%. Compound **1A** was characterized using ^1H NMR, ^{13}C NMR, and ESI-MS. All spectra are provided in

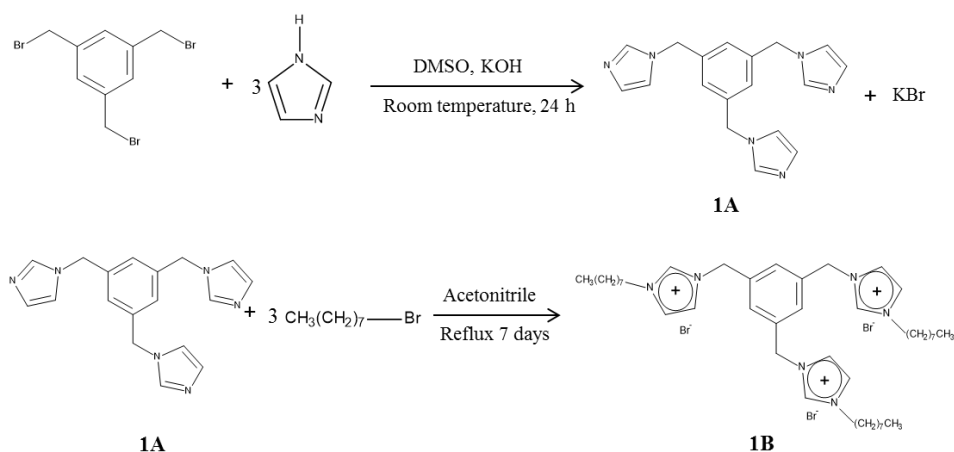
the supplemental information (Figures S2 and S3) in Appendix D. A stirred solution of **1A** (1 g, 3.14 mmol) and the appropriate 1-bromoalkane (4.09 mmol) in acetonitrile (40 mL) was heated under reflux for 7 days. After cooling the reaction flask to room temperature, the solvent was partially evaporated under reduced pressure. Upon addition of excess diethyl ether, a yellow precipitate was observed. The solid was filtered and washed several times with diethyl ether to afford a light yellow colored product (**1B**). The compound was recrystallized using a dichloromethane-diethyl ether solvent mixture followed by removal of residual solvent under reduced pressure and dried at 70 °C for 24 h. The yield was 85%. The final product was characterized using ¹H NMR, ¹³C NMR, ESI-MS, and elemental analysis. All spectra and elemental analysis data are provided in the supplemental information (Figures S4 and S5) in Appendix D.

5.3.2. Synthesis of 3,3',3''-octyl-1,1',1''-(2-ethyl amino)imidazolium bromide ((C₈Im)₃Am-3Br)

Imidazole (1.5 g, 22 mmol) and potassium hydroxide (3.74 g, 67 mmol) were dissolved in dimethylsulfoxide (30 mL) and stirred for 5 h at room temperature. The compound tris (2-chloroethyl)amine hydrochloride (1.61 g, 6.67 mmol) was added and the solution continually stirred for 48 h at 30-40 °C. After evaporating the solvent under reduced pressure, the crude product was washed with anhydrous chloroform to precipitate potassium chloride. The mixture was filtered and chloroform evaporated under reduced pressure to yield a light yellow colored compound **2A**. This compound was dried at 70 °C under reduced pressure for 6 h. The yield was 70 %. The final product was characterized using ¹H NMR, ¹³C NMR, and ESI-MS. All spectra are provided in supplemental information (Figures S6 and S7) in Appendix D. A stirred solution of **2A** and the appropriate 1-bromoalkane (6 mmol) in acetonitrile (45 mL) was heated under reflux for 5 days. After evaporation of the solvent under reduced pressure, the crude product was

washed several times with hexane and ethyl acetate to remove excess starting material. The compound **2B** was filtered and dried at 70 °C under reduced pressure for 24 h to remove residual solvent. The yield was 80%. The final product was characterized using ^1H NMR, ^{13}C NMR, ESI-MS, and elemental analysis. All spectra and elemental analysis data are provided in supplemental information (Figures S8 and S9) in Appendix D.

Synthesis of $(\text{C}_8\text{Im})_3\text{Bn-3Br}$



Synthesis of $(\text{C}_8\text{Im})_3\text{Am-3Br}$

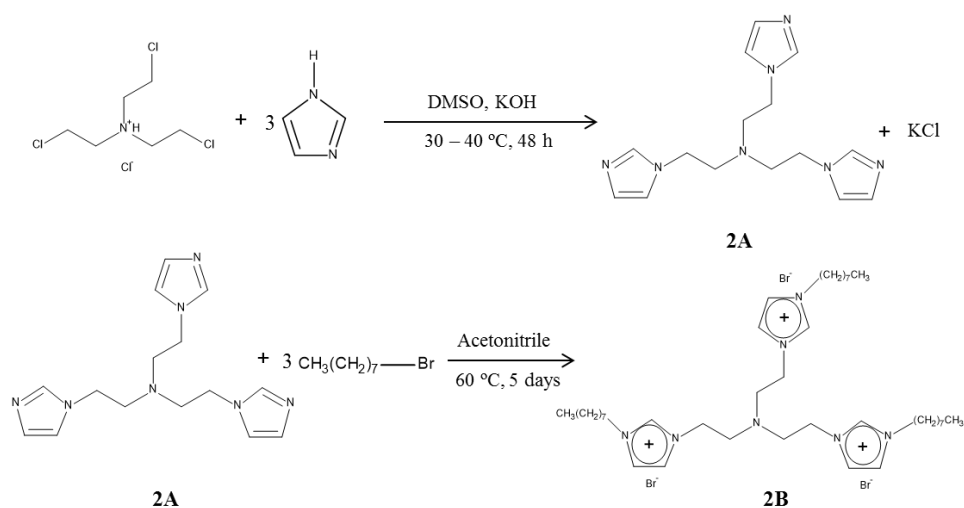


Figure 1. Synthesis of trigonal tricationic IL-based surfactants

5.4 Instrumentation and equipment

Surface tension measurements were performed using a Fisher Scientific Model 20 Du Nouy surface tensiometer equipped with a platinum-iridium ring having a mean circumference of 6.00 cm.

A CM35 Crison conductimeter ($\pm 0.02 \mu\text{S}\cdot\text{cm}^{-1}$ precision) equipped with a temperature sensor ($\pm 0.2 \text{ }^\circ\text{C}$ precision) was used for conductivity measurements and supplied by Crison Instruments (Alella, Barcelona, Spain). The conductimeter was calibrated by using a standard solution of potassium chloride. All measurements were carried out at $25 \pm 1 \text{ }^\circ\text{C}$ by the use of a IKA HB 10 digital thermostatic bath ($\pm 1 \text{ }^\circ\text{C}$ precision) acquired to IKA Instruments Werke GmbH & Co. KG (Staufen, Germany). The solutions were measured in 15 mL Pyrex® tubes supplied by SciLabware Limited (Cambell Road, Stoke on Trent, UK).

Fluorescence measurements were carried out using a Cary Eclipse Varian spectrofluorimeter (Mulgrave, Victoria, Australia) and employed a quartz cell.

5.5 Procedures

5.5.1 Surface tension measurements

Surface tension measurements were performed by immersing the platinum-iridium ring in aqueous solutions of tricationic IL-based surfactant solutions prepared by dissolving required amounts of the surfactants in deionized water. After each measurement, the ring was washed with deionized water and subjected to high temperature flame to remove residual surfactant. Surfactant solutions were kept at room temperature ($20 \pm 1 \text{ }^\circ\text{C}$) for at least 1 h before performing the surface tension measurements. All glassware used in the preparation of surfactant solutions was cleaned with chromic acid, rinsed with deionized water, and dried at room temperature.

5.5.2 Conductivity measurements

Conductivity studies were carried out with dicationic and tricationic IL-based surfactant solutions prepared by dissolving required amounts of surfactant in deionized water. For the study of the acetonitrile effect in the micellization, aqueous solutions of the surfactants were dissolved in acetonitrile (between 0 and 15 %v/v, of acetonitrile) to prepare the three component systems (IL-based surfactant, water and acetonitrile).

All measurements were made immersing the conductivity cell, previously calibrated, in 10 mL of surfactant solution immersed in the thermostatic bath at 25 ± 1 °C. Conductivities values ($\text{mS}\cdot\text{cm}^{-1}$ or $\mu\text{S}\cdot\text{cm}^{-1}$) were obtained by duplicate. Proper mixing and equilibration of solutions were ensured before the measurements.

5.5.3 Fluorescence measurements

For the determination of the CMCs values, pyrene was added (using a constant concentration of $8 \cdot 10^{-7} \text{ mol}\cdot\text{L}^{-1}$) as the fluorescence probe in all of the measured IL-based surfactant solutions. Emission spectra were registered in the range of 350 to 450 nm, with an excitation wavelength (λ_{ex}) of 335 nm, and 2.5 nm as excitation and emission slit widths. The ratio of band intensities of pyrene I_1/I_3 , obtained at λ_{em} of 375 and 385 nm, respectively, was selected for the measurements.

For the determination of the N_{agg} values, benzophenone-3 was used as a quencher to inhibit pyrene fluorescence. In optimum conditions, IL-based surfactant solutions with a constant concentration (at least two times above their respective CMC values) were mixed with pyrene ($1.6 \cdot 10^{-6} \text{ mol}\cdot\text{L}^{-1}$) as the fluorescence probe and different concentrations of benzophenone-3 (between 10^{-6} and $10^{-4} \text{ mol}\cdot\text{L}^{-1}$). Emission spectra were registered in the range of 350 to 450 nm, with λ_{ex} of 335 nm, and 2.5 nm as excitation and emission slit widths. An emission wavelength of 375 nm was selected for estimation of N_{agg} values.

5.6 Results and discussion

The interfacial and micellar behavior of the novel tricationic IL-based surfactants reported in this work have been characterized for first time using conductivity, fluorescence, and surface tensiometry measurements.

The micellization behavior of the selected group of dicationic IL-based surfactants has been studied before using surface tensiometry [9], but not yet by fluorescence or conductivity measurements; therefore, this characterization has been undertaken and the results presented in this work.

5.6.1 Synthesis of novel tricationic IL-based surfactants

In this study, two classes of trigonal tricationic IL-based surfactants containing different cores based on triethylamine (Am) and 1,3,5-trimethylbenzene (Bn) were synthesized (Figure S1, Figure 1). In each analogous series, the free hydrocarbon chain length employed was octyl, which was directly appended to the imidazolium head group.

The aqueous solubility of a surfactant also depends on the counter-ion and valency of the counter-ion. Recently, Yoshimura *et al.* reported star-shaped trimeric quaternary ammonium surfactants with bromide counter-ions [18]. In their study, it was shown that trimeric surfactants with bromide counter-ions were more soluble than iodide counter-ions due to the difference in the size and hydrophobicity of the counter-ion [18]. Based on the solubility behavior of trimeric quaternary ammonium surfactants, tricationic IL-based surfactants in the present study were prepared with bromide counter ions in an effort to maximize surfactant solubility.

Both tricationic IL-based surfactants were synthesized in two steps (Figure 1). In the first step, imidazole was reacted with the core molecule using potassium hydroxide as a base. The addition of a base facilitated nucleophilic substitution on the core [19]. In the second step, excess alkyl halide was reacted with the intermediate synthesized in the first

step. Initial attempts to synthesize tricationic surfactants containing longer alkyl chains (e.g., hexadecyl) resulted in poor solubility of the surfactants in aqueous solutions. Since the surface activity of surfactants in aqueous solutions is very sensitive to impurities present in the surfactant, re-crystallization of the final products was performed using a dichloromethane-diethyl ether solvent system (1:5). All reports of characterization of the tricationic IL-based surfactants are included in Figures S4, S5, S8, and S9 of the supplemental information in Appendix D.

5.6.2 Determination of micellization parameters by conductivity measurements

5.6.2.1 Determination of CMC

The determination of the CMC values was carried out according to section 2.4.2, and so the specific conductivity (κ) was measured at different surfactant concentrations. It was observed that the value of κ increased almost linearly with the increase in the surfactant concentration. At a certain concentration value, there is a change in the slope of such trend, due to the beginning of surfactant aggregation to form micelles. Depending on the surfactant, the change in the slopes was abrupt, whereas in other cases was not that significant. The concentration corresponding to the break-point of the two slopes indicates the CMC value. Below and above CMC, the relationships between κ and the IL-based surfactant concentration were linear with correlation coefficients (R values) between 0.992 and 0.999 for all surfactants studied, as it can be observed in Table S1 of the supplemental information in Appendix D.

Below the CMC (premicellar region), the increase of κ with the surfactant concentration is due to the increasing amount of free ions in solution. Above the CMC (postmicellar region), the increase of κ with the concentration is more gradual for two reasons, as stated by Shanks and Franses [20]: (1) the confinement of a fraction of the counterions onto the micellar surface results in an effective loss of ionic charges and (2) the micelles can

contribute to the charge transport to a lesser extent than the free ions owing to their lower mobility. Figure 2 shows examples of the variation of κ with the surfactant concentration for one dicationic surfactant (specifically $(C_{10}Im)_2C_{12}-2Br$) and one tricationic surfactant (specifically $(C_8Im)_3Bn-3Br$). The change in the gradient of κ versus IL-based surfactant concentration has also been plotted in Figure 2 (dotted curve in grey). The CMC can also be determined as the concentration corresponding to the maximum change in the gradient of κ versus surfactant concentration. There were not significant differences in the calculated CMC values for the IL-based surfactant studied if the CMC were estimated by the break-point of the two slopes or by the maximum change in the gradient above mentioned.

The CMC values obtained by conductivity measurements are also shown in Table 1, and their corresponding premicellar and postmicellar curves in Table S1. The CMC values varied from $0.19 \pm 0.05 \text{ mmol}\cdot\text{L}^{-1}$ for the dicationic $(C_{16}Im)_2C_{12}-2Br$ to $4.15 \pm 0.85 \text{ mmol}\cdot\text{L}^{-1}$ for the tricationic $(C_8Im)_3Am-3Br$. In general, lower CMC values were obtained with the dicationic surfactants, with the exception being $(C_4Im)_2C_{12}-2Br$.

Regarding dicationic IL-based surfactants, the same trend was observed as with conventional surfactants: a decrease in the CMC values when the lateral chain length of the surfactant is increased (keeping constant the spacer). Thus, they decrease from 58.56 ± 11.30 with to the butyl side chain to $0.19 \pm 0.05 \text{ mmol}\cdot\text{L}^{-1}$ with to the hexadecyl side chain. In general, low CMC values have been reported for Gemini surfactants. For example, the CMC of the dicationic surfactant butyl bis(dimethyltetradecylammonium) dibromide $(C_{14}M_2N)_2C_4-2Br$ is of 0.17 mM [21], which is similar to the 0.19 mM value obtained by conductivity in this work for $(C_{16}Im)_2C_{12}-2Br$.

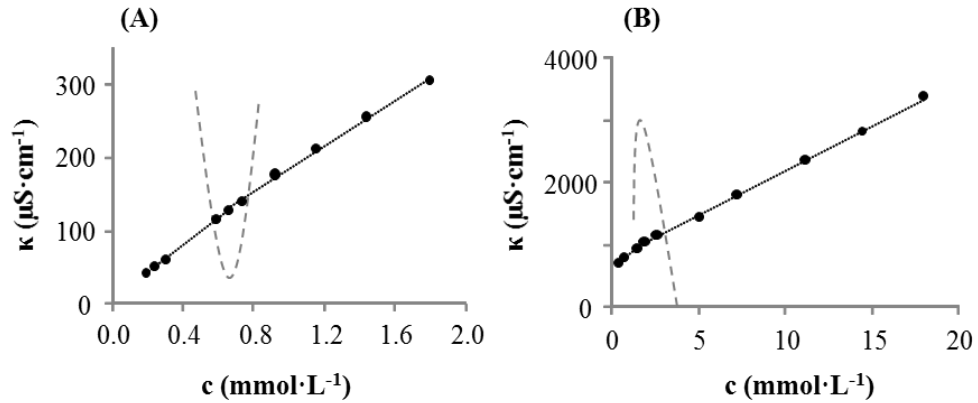


Figure 2. Plots of the variation of the specific conductivity (κ) with the IL-based surfactant concentration (c) (isotherms in black), altogether with the change in the gradient of κ versus c (dotted grey) for a representative dicationic surfactant, $(C_{10}Im)_2C_{12}-2Br$ (A), and a tricationic surfactant, $(C_8Im)_3Bn-3Br$ (B).

For the two tricationic IL-based surfactants considered, it can be concluded that the increase in aromaticity and volume of the spacer (keeping constant the same lateral chains) induce lower CMC values; from 1.87 ± 0.20 $mmol \cdot L^{-1}$ for the tricationic surfactant with a Bn spacer to 4.15 ± 0.85 $mmol \cdot L^{-1}$ for the surfactant with Am spacer.

5.6.2.2 Determination of the degree of micelle dissociation (α) and the degree of counterion binding to micelles (β)

The degree of micelle dissociation (α) can be determined from the ratio of the slopes of the postmicellar (S_2) and the premicellar (S_1) linear regions (Table S1) in supplemental information of Appendix D.

$\alpha = \frac{S_2}{S_1}$ The degree of the counterion binding to micelles (β) is obtained by subtracting

$$\text{the } \alpha \text{ values to 1 (1-}\alpha\text{). } \beta = 1-\alpha$$

Tables 1 and S1 also includes α and β values for each surfactant studied. The obtained α values oscillates between 0.41 ± 0.04 for $(C_{16}Im)_2C_{12}-2Br$ and 0.84 ± 0.03 for $(C_{10}Im)_2C_{12}-2Br$. Regarding β , there are several values reported in literature for the dicationic surfactants $(C_{10}Im)_2C_4-2Br$, $(C_{12}Im)_2C_4-2Br$, and $(C_{14}Im)_2C_4-2Br$, being of 0.67, 0.70 and 0.57 at 298 K [22], respectively.

Table 1 CMC, α , and β values for the studied IL-based surfactants, obtained from conductivity measurements, and as a function of the content of acetonitrile in the micellar solution (298 K).

IL-based surfactant	acetonitrile (%_{v/v})	$\alpha \pm \text{error}^a$	$\beta \pm \text{error}^a$	CMC $\pm \text{error}^b$ (mmol·L⁻¹)
<u>Dicationic surfactants</u>				
(C ₄ Im) ₂ C ₁₂ -2Br	0	0.82 ± 0.01	0.18 ± 0.01	58.6 ± 11.3
	5	0.71 ± 0.05	0.29 ± 0.05	64.2 ± 13.6
	10	0.55 ± 0.04	0.45 ± 0.04	70.1 ± 12.0
	15	0.67 ± 0.12	0.33 ± 0.12	78.3 ± 21.4
(C ₁₀ Im) ₂ C ₁₂ -2Br	0	0.84 ± 0.03	0.16 ± 0.03	0.66 ± 0.24
	5	0.81 ± 0.07	0.19 ± 0.07	1.67 ± 0.67
	10	0.32 ± 0.04	0.68 ± 0.04	2.14 ± 1.56
	15	0.98 ± 0.05	0.02 ± 0.05	3.18 ± 1.32
(C ₁₆ Im) ₂ C ₁₂ -2Br	0	0.41 ± 0.04	0.59 ± 0.04	0.19 ± 0.05
	5	0.46 ± 0.09	0.54 ± 0.09	1.21 ± 0.80
	10	0.58 ± 0.05	0.42 ± 0.05	2.82 ± 0.45
	15	0.44 ± 0.06	0.56 ± 0.06	3.20 ± 2.36
<u>Tricationic surfactants</u>				
(C ₈ Im) ₃ Am-3Br	0	0.52 ± 0.06	0.48 ± 0.06	4.15 ± 0.85
	5	0.70 ± 0.15	0.30 ± 0.15	4.46 ± 1.18
	10	0.75 ± 0.04	0.25 ± 0.04	4.94 ± 0.66
	15	0.92 ± 0.04	0.08 ± 0.04	6.47 ± 0.62
(C ₈ Im) ₃ Bn-3Br	0	0.62 ± 0.04	0.38 ± 0.04	1.87 ± 0.20
	5	0.72 ± 0.09	0.28 ± 0.09	2.70 ± 0.50
	10	0.88 ± 0.03	0.12 ± 0.03	4.01 ± 0.84
	15	0.85 ± 0.03	0.15 ± 0.03	5.60 ± 0.44

^aError in the determination of α and β , calculated from mathematical propagation of the errors, and also considering the errors of S₁ and S₂

^bCMC error, calculated from mathematical propagation of the error in the prediction of the CMC concentration

A longer spacer is probably accompanied by a lower density of effective positive charge and therefore by a lower attraction of counterions. With respect to the observed differences between β values among dicationic IL-based surfactants, this could be related to the fact

that bigger lateral chains like C₁₆ can provide a non-spherical 3D structure of the micelle. This structural arrangement can involve an increasing attraction of the counterion with respect to (C₁₀Im)₂C₁₂-2Br and (C₄Im)₂C₁₂-2Br.

Table 2 CMC values obtained by fluorescence measurements for the group of IL-based surfactants studied at 298 K and the corresponding polynomial equations obtained.

IL-based surfactant	Polynomial equation ^a	R ^b	CMC (mmol·L ⁻¹)
<u>Dicationic surfactants</u>			
(C ₄ Im) ₂ C ₁₂ -2Br	$I_1/I_3 = -4.2 \times \log^4 c - 34.6 \times \log^3 c - 106.9 \times \log^2 c - 146.6 \times \log c - 74.3$	0.997	58.5
(C ₁₀ Im) ₂ C ₁₂ -2Br	$I_1/I_3 = 4.2 \times \log^4 c + 53.9 \times \log^3 c + 259.8 \times \log^2 c + 552.5 \times \log c + 1.3$	0.995	1.04
(C ₁₆ Im) ₂ C ₁₂ -2Br	$I_1/I_3 = -0.01 \times \log^5 c - 0.2 \times \log^4 c - 1.3 \times \log^3 c - 3.7 \times \log^2 c - 0.5 \times \log c - 1.1$	0.998	0.21
<u>Tricationic surfactants</u>			
(C ₈ Im) ₃ Am-3Br	$I_1/I_3 = 2.7 \times \log^5 c + 36.0 \times \log^4 c + 186.6 \times \log^3 c + 478.1 \times \log^2 c + 603.2 \times \log c + 300.2$	0.992	5.13
(C ₈ Im) ₃ Bn-3Br	$I_1/I_3 = -0.1 \times \log^4 c + 1.2 \times \log^3 c + 5.5 \times \log^2 c + 10.6 \times \log c + 8.7$	0.995	2.30

^aI₁ (375 nm)/I₃ (385 nm) versus log (IL-based surfactant concentration, in mol·L⁻¹), using 8·10⁻⁷ mol·L⁻¹ of pyrene as probe, 2.5 nm excitation and emission slit widths, and data acquisition in the range of 350 to 450 nm

^bCorrelation coefficient

This behavior is not observed with tricationic surfactants probably due to the presence of the Bn and Am spacers. They provide the same effective positive charge densities because they are close to the head groups.

5.6.2.3 Influence of acetonitrile content in micellization parameters

Addition of organic solvents like methanol, acetonitrile or ethanol into aqueous solutions of surfactants delays the process of micellization, thereby increasing the CMC values. This effect can be due to three main reasons: (1) an increase in the hydration of the hydrophilic group due to the rupture of the water structure, (2) a decrease of static dielectric constant of the aqueous solution (ϵ), and (3) an increase in the surfactant solubility. Besides, the micellar aggregation becomes thermodynamically non-favorable at certain organic solvent content and the micelle finally breaks. Acetonitrile was the organic solvent selected in this work because it is widely employed within analytical chemistry; for example, as a mobile phase component in high-performance liquid chromatography (HPLC) or as a solvent in dispersive liquid-liquid microextraction (DLLME). We focused on this solvent given the intended analytical applications of these IL-based surfactants [7].

CMC, α , and β values of dicationic and tricationic surfactants were calculated from conductivity measurements in the presence of different contents of acetonitrile (between 5 and 15%, v/v), as described in section 2.4.2. Results are shown in Table 1. It can be observed that the effect of acetonitrile in the surfactant micelles is similar to that of short chain *n*-alcohols: an increase in their content causes an increase of the CMC value [23]. A decrease in the polarity of the media obviously takes place when acetonitrile is dissolved in the aqueous phase of the surfactants, which in turns is not favorable for the stabilization of the IL-based surfactant monomers (which prefer a polar phase), and therefore higher concentrations of surfactants are needed for successful aggregation.

Table 3 N_{agg} values obtained for the studied dicationic and tricationic IL-based surfactants using fluorescence measurements, including the corresponding quality analytical parameters of the equations employed for their calculations (Equation 3). Pyrene was used as probe ($1.6 \cdot 10^{-6}$ mol·L⁻¹), benzophenone-3 as quencher, and the employed λ_{em} was 375 nm (I_1).

IL-based surfactant	$C_{Surf.}^a$ (mmol·L ⁻¹)	(Slope ^b ± error)×10 ⁻⁴	Intercept ^b ± error	R ^c	$N_{agg} \pm error^d$
<u>Dicationic surfactants</u>					
(C ₄ Im) ₂ C ₁₂ -2Br	121	0.87 ± 0.03	-0.02 ± 0.01	0.996	547 ± 17
(C ₁₀ Im) ₂ C ₁₂ -2Br	1.3	2.196 ± 0.003	0.10 ± 0.02	0.996	4.7 ± 0.1
(C ₁₆ Im) ₂ C ₁₂ -2Br	1.0	12.5 ± 0.7	0.00 ± 0.02	0.993	99.5 ± 5.4
<u>Tricationic surfactants</u>					
(C ₈ Im) ₃ Am-3Br	6.3	2.03 ± 0.05	-0.07 ± 0.02	0.997	24.7 ± 1.1
(C ₈ Im) ₃ Bn-3Br	7.2	1.98 ± 0.06	0.01 ± 0.01	0.997	98.6 ± 3.2

^afixed IL-based surfactant concentration in the study

^bSlope and intercept refer to the linear equation obtained when plotting $\ln(I_0/I)$ versus C_Q (Equation 3)

^cCorrelation coefficient of such plot

^dError in the determination N_{agg} , calculated from mathematical propagation of the error for the slopes and intercepts

It was observed that the variation of the CMC values with the acetonitrile content followed a linear trend, with correlation coefficients between 0.995 and 0.993 for the dicationic $(C_4Im)_2C_{12}-2Br$ and the tricationic $(C_8Im)_3Am-3Br$, respectively. Figure S10 of the supplementary material shows representative plots of such trends. In any case, the maximum variation of the CMC values with the acetonitrile content was observed for the dicationic $(C_4Im)_2C_{12}-2Br$, which is the IL-based surfactant with the highest CMC value of all studied surfactants.

In general, α values of dicationic surfactants decrease when the acetonitrile content increases. There are exceptions at higher contents of acetonitrile (15%, v/v), probably due to the start of the micellar breakdown and to the overall decrease in the polarity of the media. However, the opposite effect takes place for tricationic surfactants: the increase of acetonitrile contents results in an increase of α values. Although this is not common behavior for surfactants, Tiwari *et al.* have observed the same effect with other organic solvents and for several dicationic IL-based surfactants [24]. Similar explanations as those obtained for α , but obviously with opposite trend, are valid for the β values obtained.

5.6.3 Determination of micellization parameters by fluorescence measurements

The utilization of fluorescence probes to study micellar systems is a versatile and widely used approach. Pyrene is a fluorescent hydrophobic compound commonly used as probe, which exhibits different fluorescence characteristics depending upon the properties of the solubilizing medium. Its usefulness to determine solvent environments is due to its excited state, which presents a different non-polar structure compared to the ground state. Certain emission bands are unaffected but others show variations in intensity due to the interaction with the solvent.

5.6.3.1 Determination of CMC

The fluorescence emission spectrum of pyrene in an aqueous medium exhibits five characteristic bands in the region of 370 to 400 nm, as shown in Figure S11 of the supplemental information of Appendix D. The vibronic peak of pyrene corresponding to a I_1 intensity appears with a λ_{em} of ~ 375 nm, and the vibronic peak related to I_3 with λ_{em} of ~ 385 nm. In a polar media, there is an increase of the band intensity 0-0 (peak 1) *versus* others due to vibronic coupling [25]. The emission spectrum of pyrene obtained when working below the CMC of a representative IL-based surfactant (the dicationic $(C_{10}Im)_2C_{12}-2Br$) is shown in Figure S11(B). It can be observed that it is quite similar to that obtained in water (Figure S11(A)), because there are not yet micelles in the environment. When working above the CMC (Figure S11(C)), pyrene is normally dissolved in the interior region of the micelles due to its hydrophobicity and poor solubility in water ($2 - 3 \mu\text{mol}\cdot\text{L}^{-1}$). This change results in an alteration of the ratio of relative band intensities I_1/I_3 [25]. Therefore, CMC values can be estimated by plotting the ratio of the relative band intensities I_1/I_3 *versus* surfactant concentration or logarithm of surfactant concentration, with the curves following a simple sigmoidal expression.

Thus, the determination of the CMC values for the group of dicationic and tricationic IL-based surfactants was performed utilizing an optimum concentration for pyrene of $8\cdot 10^{-7} \text{ mmol}\cdot\text{L}^{-1}$, altogether with the remaining group of conditions described in section 2.4.3. Figure S12(A) of the Supplementary Material shows the typical sinusoidal shape of plots of the variation of the I_1/I_3 ratio *versus* logarithm of surfactant concentration, with the dicationic $(C_{10}Im)_2C_{12}-2Br$ being the plotted representative example. The CMC values correspond to the inflection point of the curves, and can be calculated by using the 2nd derivative method. The obtained CMC values are listed in Table 2. They are accompanied by the corresponding

polynomial equations (I_1/I_3 versus logarithm of surfactant concentration). It can be observed that correlation coefficients higher than 0.99 were obtained in all cases. Regarding the CMC values obtained by fluorescence measurements for the dicationic IL-based surfactants, it can be observed that they decrease when the number of carbons of lateral alkyl chains of surfactants increase, from $58.5 \text{ mmol}\cdot\text{L}^{-1}$ for $(\text{C}_4\text{Im})_2\text{C}_{12}\text{-2Br}$ to $0.21 \text{ mmol}\cdot\text{L}^{-1}$ for $(\text{C}_{16}\text{Im})_2\text{C}_{12}\text{-2Br}$. The obtained CMC values for the tricationic surfactants were very similar among them, being higher than those for dicationics except for $(\text{C}_4\text{Im})_2\text{C}_{12}\text{-2Br}$.

If these CMC values are compared with those obtained by conductometry, it can be observed that they are in agreement and are slightly higher those obtained by fluorescence measurements.

5.6.3.2 Determination of N_{agg}

N_{agg} values of IL-based surfactants were determined by the static luminescence quenching technique, originally proposed by Turro and Yekta [26]. The method requires the use of a micellar system, a probe and a quencher. Several assumptions have to be considered about the probe and the quencher: (1) they are solubilized by micelles, (2) they have a Poisson distribution in the micelles, (3) they remain confined in the micelles during a time longer than the lifetime of the excited probe and, (4) the fluorescence of probe is inhibited when quencher and probe occupy the same micelle [27]. If these assumptions are satisfied, for specific values of λ_{em} and λ_{exc} , the logarithm of the ratio of probe fluorescence intensities in absence (I_0) and presence (I) of the quencher can be plotted versus the concentration of the quencher (C_Q). The slope of such representation is $N_{\text{agg}}/(C_{\text{surf}} - \text{CMC})$, being C_{surf} the surfactant concentration, whereas $\ln\left(\frac{I_0}{I}\right) = \frac{N_{\text{agg}}}{C_{\text{surf}} - \text{CMC}} \cdot C_Q N_{\text{agg}}$ and CMC values refer to each studied IL-based surfactant (using the CMC values already derived from fluorescence measurements: Table 2, section

3.3.1). In this work, pyrene was selected as the probe with an optimum concentration of $1.6 \cdot 10^{-6} \text{ mol} \cdot \text{L}^{-1}$, and benzophenone-3 was selected as quencher. The fluorescence responses were monitored at λ_{em} of 375 nm ($\lambda_{\text{ex}} = 335 \text{ nm}$), corresponding with the highest intensity fluorescence peak of pyrene of (I_1). Figure S12(B) shows a representative plot of such quenching effect for the representative tricationic IL-based surfactant $(\text{C}_8\text{Im})_3\text{Bn-3Br}$ ($7.2 \text{ mmol} \cdot \text{L}^{-1}$). The calculated N_{agg} values for all surfactants studied are listed in Table 3, along with the corresponding quality analytical parameters of the linear least-squares fit of the $\ln(I_0/I)$ versus C_Q plot. The concentration values used for surfactants are also listed in Table 3. In all cases, the molar fraction of benzophenone-3 was always lower than $8.8 \cdot 10^{-3}$.

It can be observed that the N_{agg} values for dicationic IL-based surfactants oscillate between 4.7 ± 0.1 for $(\text{C}_{10}\text{Im})_2\text{C}_{12}\text{-2Br}$ and 547 ± 17 for $(\text{C}_4\text{Im})_2\text{C}_{12}\text{-2Br}$. In general, no trends were observed within the dicationic IL-based surfactants. Nevertheless, it had been described for monocationic surfactants that N_{agg} increases with the increasing size of lateral alkyl chains [27]. This increase is only observed from $(\text{C}_{10}\text{Im})_2\text{C}_{12}\text{-2Br}$ to $(\text{C}_{16}\text{Im})_2\text{C}_{12}\text{-2Br}$, with $(\text{C}_4\text{Im})_2\text{C}_{12}\text{-2Br}$ being an exception.

For tricationic IL-based surfactants, the obtained N_{agg} values were 24.7 ± 1.1 for $(\text{C}_8\text{Im})_3\text{Am-3Br}$ and 98.6 ± 3.2 $(\text{C}_8\text{Im})_3\text{Bn-3Br}$. These results can be explained in terms of aromaticity. In the case of $(\text{C}_8\text{Im})_3\text{Bn-3Br}$, the higher aromaticity due to the Bn spacer implies higher intra-micelle repulsion and so more monomers of surfactant are required for micelle formation.

The literature N_{agg} value for the monocationic $\text{C}_{16}\text{MIm-Br}$ is 66 [27], which is obviously much lower than that of the dicationic $(\text{C}_{16}\text{Im})_2\text{C}_{12}\text{-2Br}$ ($N_{\text{agg}} \sim 104$). There are few literature N_{agg} values for monocationic surfactants containing substituents higher than methyl in the 3-

position of the cation, which makes difficult the comparison with our reported values. To the best of our knowledge, there are not reported N_{agg} values for dicationic surfactants, at least not with similar structures to compare with and clearly not for tricationics.

5.6.4 Determination of micellization behavior by surface tension measurement

As discussed previously, these studies are focused on tricationic IL-based surfactants because the characterization of dicationic surfactants by surface tensiometry has been previously carried out [9].

5.6.4.1 Determination of CMC and surface activity of tricationic IL-based surfactants

Figure 3 shows the surface tension plots obtained for the tricationic surfactants. The absence of a minimum around the breakpoint in the plots confirms the high purity of the surfactants. The CMC values of the two surfactants were mathematically determined from the break points in the $-\log C$ curves, and are listed in Table 4.

It can be observed from Table 4 that $(C_8Im)_3Bn-3Br$ exhibited lower CMC values in comparison with $(C_8Im)_3Am-3Br$ with identical alkyl substituents. This difference in CMC values may be due to the higher hydrophobicity imparted by the benzyl core in $(C_8Im)_3Bn-3Br$. It can also be observed from Table 4 that the tricationic surfactants possess lower CMC values compared to the linear trimeric surfactant methyloctyl bis[3-(dimethyloctylammonio)ethyl]ammonium tribromide (8-2-8-2-8), particularly when compared with the $(C_8Im)_3Am-3Br$ surfactant containing the same hydrocarbon chain length [28]. Similar observations were also found when comparing monocationic surfactants and traditional monomeric quaternary ammonium based surfactants [29].

Surface activity of surfactants is usually expressed in terms of *effectiveness* of the surface tension reduction and *efficiency* of surfactant adsorption. *Effectiveness* is the minimum surface

tension (γ_{CMC}) caused by the surfactant regardless of the concentration. It is also related to the maximum surface adsorption (Γ_{max}) occurring below the CMC. These values are obtained from surface tension plots and are calculated using the Gibbs adsorption isotherm represented by equation 1.

Table 4 Values of CMC, γ_{CMC} , Γ_{max} , A_{min} , pC_{20} and CMC/C_{20} obtained for the tricationic IL-based surfactants examined in this study, and for previously reported traditional trimeric surfactants.

IL-based surfactant	CMC \pm error^a (mM)	γ_{CMC} (mN m⁻¹)	Γ_{max} ($\times 10^6$ mol m⁻²)	A_{min} (nm²)	pC_{20}	CMC/C_{20}
(C ₈ Im) ₃ Am-3Br	4.3 \pm 0.2	33	1.11	1.50	3.13	5.7
(C ₈ Im) ₃ Bn-3Br	2.2 \pm 0.1	40	1.37	1.21	2.81	1.4
8-2-8-2-8	14 ^b	35 ^b	1.07 ^b	1.55 ^b	-	-

^aCMC error, calculated from mathematical propagation of the error in the prediction of the CMC concentration

^bData obtained from [28]

$$\Gamma_{\text{max}} = -\frac{1}{iRT} \left(\frac{\partial \gamma}{\partial \ln C} \right)_{\tau} \quad (\text{Equation 1})$$

In this relationship, the term within parenthesis is the linear slope of the surface tension plots below the CMC; C is the concentration of the surfactant in bulk solution, the value of i for the tricationic IL-based surfactants is 4, R is the gas constant (8.31 J K⁻¹ mol⁻¹), and T is the absolute temperature [28].

The area occupied by a single surfactant molecule at the air–solution interface (A_{\min}) can be calculated by the following equation 2:

$$A_{\min} = \frac{1}{N \cdot \Gamma_{\max}} \quad (\text{Equation 2})$$

with N being Avogadro's constant ($6.022 \times 10^{23} \text{ mol}^{-1}$).

The calculated values for γ_{CMC} , Γ_{\max} , and A_{\min} are also included in Table 4. In comparing the $(\text{C}_8\text{Im})_3\text{Bn-3Br}$ and $(\text{C}_8\text{Im})_3\text{Am-3Br}$ surfactants, the benzyl core surfactant exhibited the higher γ_{CMC} value. This indicates that the triethylamine core surfactants are more effective in reducing the surface tension of water. The lower γ_{CMC} values of $(\text{C}_8\text{Im})_3\text{Am-3Br}$ may be attributed to enhanced interactions of the three alkyl chain moieties around the triethylamine core allowing them to be adsorbed strongly at the air/water interface. The traditional trimeric surfactant 8-2-8-2-8 exhibited similar values to $(\text{C}_8\text{Im})_3\text{Am-3Br}$, which is the IL-based surfactant with closer structure to compare with. The Γ_{\max} values of $(\text{C}_8\text{Im})_3\text{Am-3Br}$ are smaller and A_{\min} values were higher than those of $(\text{C}_8\text{Im})_3\text{Bn-3Br}$. This indicates that the benzene ring exerts a stronger influence, and so the packing density of surfactant molecules at the interface is higher for $(\text{C}_8\text{Im})_3\text{Am-3Br}$ than for $(\text{C}_8\text{Im})_3\text{Bn-3Br}$. Monomers of the $(\text{C}_8\text{Im})_3\text{Bn-3Br}$ may be more compact than $(\text{C}_8\text{Im})_3\text{Am-3Br}$ monomers at the air/solution interface.

An additional parameter that can be obtained from the surface tension plots is pC_{20} , which provides a measure of the adsorption efficiency of the surfactant at the air-water interface. C_{20} is the IL-based surfactant concentration required to reduce the initial surface tension of the pure solvent by 20 mN m^{-1} . The larger the pC_{20} value, the greater the tendency of the surfactant to undergo adsorption rather than forming a micelle in solution [23]. From Table 4, it is clear that pC_{20} values of $(\text{C}_8\text{Im})_3\text{Am-3Br}$ were higher than those of $(\text{C}_8\text{Im})_3\text{Bn-3Br}$, indicating that they

are more efficient in adsorbing at the interface. Recently, Ao *et al.* studied the effect of spacer length on the adsorption efficiency of dicationic surfactants using the ratio of the CMC/C_{20} values [12]. The CMC/C_{20} values provide information about the relative structural and micro-environmental factors of the surfactant on adsorption over micellization [12]. Surfactants with larger CMC/C_{20} ratios indicate a greater tendency of the surfactant to adsorb at the air/water interface *versus* micellization. From Table 4, $(C_8Im)_3Am-3Br$ exhibited higher CMC/C_{20} values, which is concordant with all results derived from the surface tension study accomplished. The CMC/C_{20} values obtained for the tricationic surfactants of the present work are lower or similar to the IL-type Gemini imidazolium-based surfactants with dodecyl hydrocarbon chain substituents [12].

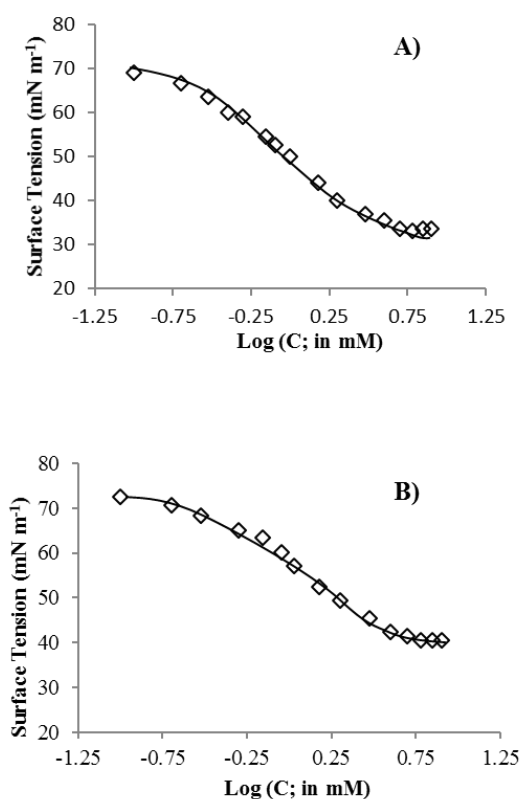


Figure. 3 Surface tension plots of trigonal tricationic IL-based surfactants, (A) $(C_8Im)_3Am-3Br$, and (B) $(C_8Im)_3Bn-3Br$.

5.6.5 Effect of salt additives on solubility and CMC of tricationic IL-based surfactants

Electrolytes are able to screen the charge repulsion between head groups and facilitate the formation of a micelle at lower concentration. As a result, the CMC values of surfactants are often lower in comparison to aqueous surfactant solutions that do not contain electrolytes [30,31]. Several studies have examined the effect of electrolytes on the aggregation of surfactants in aqueous solutions [12,15, 16].. Wang *et al.* studied the aggregation properties of the surface active monocationic surfactant 1-decyl-3-methylimidazolium bromide in aqueous solutions in the presence of 15 different salts [16]. Recently, Yu *et al.* reported the salting-out phenomenon with cationic Gemini surfactants. It was shown that variations in the spacer group resulted in a significant difference in salt concentration required to produce the salting-out effect [30].

In the present study, two inorganic salts (sodium iodide and sodium bromide) and one organic salt (sodium benzoate) were studied to examine their effect on the CMC and surface active properties of the trigonal tricationic surfactants in aqueous solutions, as a preliminary study of their behavior.

The concentration of salts used in aqueous surfactants solutions was dependent on the nature of the surfactant. Furthermore, the concentration of sodium iodide used in the study was lower in comparison with sodium bromide and sodium benzoate salts due to the increased salting-out effect of sodium iodide. For example, it was observed that aqueous solutions of the tricationic $(C_8Im)_3Bn-3Br$ phase separated when the concentration of sodium iodide exceeded 0.1 mM. Therefore, this concentration was not examined. However, this behavior was not observed for the other two salts at similar concentrations. The maximum working

concentration of sodium iodide used in aqueous solutions of the $(C_8Im)_3Am-3Br$ was 2 mM due to the salting-out effect. Aqueous solutions containing high concentrations of sodium bromide (>10 mM) and sodium benzoate (>5 mM) also exhibited the salting-out phenomenon for both tricationic IL-based surfactants. The surface tension plots obtained from the tricationic surfactants and salts studied are included in Figures 4 and S13 of the Supplementary Material. It can be observed from Tables 4 and 5 that the CMC values for both classes of surfactants decreased in the presence of electrolytes. For example, the CMC value of the $(C_8Im)_3Am-3Br$ decreased from 4.3 mM in pure water to 2.1 mM in 2 mM sodium iodide (Figure 4(D)) or in 5 mM sodium benzoate (Figure 4(C)). As shown in Figure S13 for $(C_8Im)_3Bn-3Br$, a clear shift in the break point is observed when the concentration of sodium benzoate was increased from 2 to 5 mM, resulting in a drop in CMC from 1.8 to 0.9 mM.

A comparison of the CMC values for the tricationic surfactants in the presence of similar concentrations of sodium salts provides information into the effects of different counter-ions.

It can be seen from Table 5 that the sodium salts (at the same or similar concentration) lower the CMC values of $(C_8Im)_3Am-3Br$ following the order: $NaI > C_6H_5COONa > NaBr$. At equal concentrations of $NaBr$ and C_6H_5COONa salts, the $(C_8Im)_3Bn-3Br$ surfactant exhibited a lower CMC value in the presence of sodium benzoate. This counter-ion effect on the tricationic surfactant may be rationalized due to difference in hydration and polarizability of the counter-ion. Wang *et al.* studied the effect of electrolytes on the aggregation of monocationic surfactants in aqueous solution using conductivity, fluorescence, and dynamic light scattering techniques. It was reported that aggregation depended on the polarizability and hydrodynamic radius of the counter-ion used as the electrolyte [16]. Thus, the observed effects

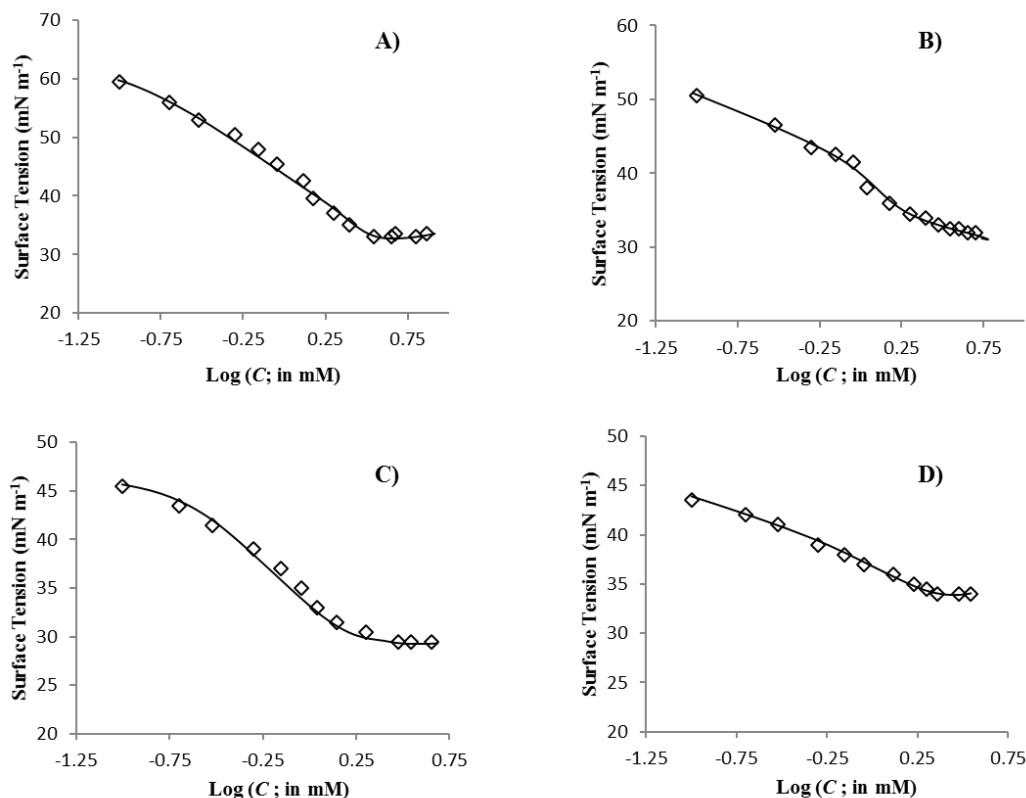


Figure. 4 Surface tension plots of the tricationic IL-based surfactant $(C_8Im)_3Am-3Br$ in presence of: (A) 5 mM sodium bromide, (B) 2 mM sodium benzoate, (C) 5 mM sodium benzoate, and (D) 2 mM sodium iodide.

of electrolytes on the aggregation of tricationic surfactants follow similar trends to those previously observed for monocationics.

5.6.6 Effect of electrolytes on the interfacial adsorption of tricationic IL-based surfactants

The effect of electrolytes on the interfacial adsorption of tricationic surfactants was examined by comparing the surface activity parameters including γ_{CMC} , pC_{20} , and CMC/C_{20} values for pure aqueous solutions of surfactants with those of solutions containing sodium salts. These values are also included in Table 5. It can be observed that the pC_{20} and CMC/C_{20} values increased in the presence of sodium salts. This effect may be due to the enhanced adsorption of tricationic surfactant molecules at the interface. For example, the pC_{20} and CMC/C_{20} values were 3.13 and 5.7, respectively, for the $(C_8Im)_3Am-3Br$ IL-based surfactant

in water. These values increased up to 4.92 and 173, respectively, in the presence of 2 mM sodium iodide. The effect of sodium iodide on this surfactant can be observed by comparing the surface tension plots in Figures 3(A) and 4(D). Thus, at similar surfactant concentrations, the surface tension value of the water dropped from 69.5 to 44.5 mN m⁻¹. This drop in surface tension may be due to the enhanced adsorption of surfactant molecules in the presence of sodium iodide. Similar observations can also be made for sodium bromide and sodium benzoate salts from Figures 4(A) and 4(C), wherein the surface tension of water dropped to 59.5 and 45.5 mN m⁻¹, respectively. A similar electrolyte effect was also observed for the (C₈Im)₃Bn-3Br surfactant. As shown in Figure S13, the surface tension of water decreased significantly as the sodium benzoate concentration increased from 0 to 5 mM.

The pC₂₀ and CMC/C₂₀ values for both tricationic IL-based surfactants depend on the concentration of sodium salt employed. In Table 5, it can be observed for both classes of surfactants that an increase in sodium benzoate concentration resulted in an increase in pC₂₀ and CMC/C₂₀ values. For (C₈Im)₃Am-3Br, the increase in these parameters follows the order: NaI > C₆H₅COONa > NaBr. Similarly, in the case of the (C₈Im)₃Bn-3Br, and at equal concentrations of sodium bromide and sodium benzoate salts, the CMC/C₂₀ and pC₂₀ values were higher in the presence of sodium benzoate. Para *et al.* previously studied the adsorption properties of aqueous solutions of traditional cationic quaternary ammonium-based surfactants in the presence of sodium salts and developed a model to describe their experimental observations [31]. According to this model, adsorption of ionic surfactants is accompanied by the formation of an electric double layer (EDL) at the interface. The surface potential at the EDL hinders further adsorption of ionic surfactants and facilitates the adsorption of the counter-ions. The adsorption of counter-ions at the interface reduces the surface potential and

enhances the adsorption of ionic surfactants. Based on experimental and theoretical studies, these authors claimed that the adsorption of counter-ions is related to the polarizability and size of the counter-ion [31]. Thus, the observed specific-ion effect in the present study may be related to similar observations made in such previous study for traditional cationic surfactants.

At higher concentrations of sodium benzoate salt, the γ_{cmc} values of $(\text{C}_8\text{Im})_3\text{Am}-3\text{Br}$ decreased (see Table 5). For the other two salts, the obtained γ_{cmc} values are similar than those obtained for $(\text{C}_8\text{Im})_3\text{Am}-3\text{Br}$ in water. Recently, Yu *et al.* also observed a decrease in γ_{cmc} values for dicationic Gemini surfactants only in the presence of sodium benzoate, but did not observe this decrease in aqueous solutions of sodium chloride and sodium sulfate. The specific-ion effect was explained based on the additional hydrophobicity imparted by the benzoate anions at the interface [30]. Interestingly, the γ_{cmc} values of the $(\text{C}_8\text{Im})_3\text{Bn}-3\text{Br}$ surfactant solutions only experience a small decrease in the presence of sodium benzoate salts.

5.7 Conclusions

For first time, two trigonal tricationic IL-based surfactants comprised of two different cores were synthesized and their surface activity parameters (interfacial and aggregation behavior) were studied in aqueous solutions using surface tension, conductivity and fluorescence measurements. Three dicationic IL-based surfactants were also characterized using conductivity and fluorescence measurements.

The obtained CMC values of the tricationic surfactants were lower than analogous linear trimeric surfactants. For the two tricationics considered, it seemed that an increase in the aromaticity and size of the linker (Bn *versus* Am), while keeping constant the lateral chains of the surfactants, is accompanied by a decrease in the CMC. The CMC values of dicationic surfactants clearly decreased as a function of the alkyl chain size when maintaining the same

linker. To the best of our knowledge, this is the first time that the aggregation number has been determined for dicationic IL-based surfactants and, obviously, for tricationics. For tricationics, the higher N_{agg} value was obtained for the surfactant containing the Bn core, which can be linked to higher intra-micelle repulsion due to the aromaticity of the ring, and so more monomer are required for micelle formation. Regarding dicationics, there was an increase in the N_{agg} values when increasing the alkyl chain side from butyl to decyl, but then a decrease for the hexadecyl substituent.

The effect of sodium salts in decreasing CMC values of the tricationic surfactants followed the general trend: $NaI > C_6H_5COONa > NaBr$. The observed trend may be rationalized due to difference in hydration and polarizability of the counter-ion. It was observed that pC_{20} and CMC/C_{20} values increased significantly in the presence of sodium salts due to enhanced adsorption of the tricationic surfactant molecules at the air/water interface.

On-going studies in our group are focused on studying mixed micellization of various monocationic surfactants with the tricationic and dicationic IL-based surfactants presented in this study. The goal is to further understand how the molecular structures of surfactants influence co-micellization in aqueous solutions.

Acknowledgements

V.P. thanks the Spanish Ministry of Economy and Competitiveness (MINECO) for the Ramón y Cajal contract with the University of La Laguna (ULL), as well as funding from MINECO ref. MAT2013-43101-R and from the ULL ref. 2013-young researchers modality. A.M.A. acknowledges funding from a Bridge Project and a Consolidated Research Funding Project of ULL. J.L.A. acknowledges funding from the Chemical Measurement and Imaging Program in the Division of Chemistry at the National Science Foundation (CHE-1413199).

A.M.P. thanks his fellowship from the Environmental Service of ULL (SEMALL), and M.J.T.R. thanks her PhD fellowship from “Fundación CajaCanarias”. D.J. Steyer thanks the office of Undergraduate Research at The University of Toledo for funding of an undergraduate research grant.

Supporting information

Figure S1 to Figure S13 and Table S1 are provided in Appendix D

References

- [1] T. Welton, Room-Temperature Ionic Liquids. Solvents for Synthesis and Catalysis, *Chem. Rev.* 99 (1999) 2071–2084.
- [2] T.L. Merrigan, E.D. Bates, S.C. Dorman, J.H. Davis Jr, New fluorosurfactant ionic liquids function as surfactants in conventional room-temperature ionic liquids, *Chem. Commun.* 20 (2000) 2051–2052.
- [3] J.L. Anderson, V. Pino, E.C. Hagberg, V.V. Sheares, D.W. Armstrong, Surfactant solvation effects and micelle formation in ionic liquids, *Chem. Commun.* 19 (2003) 2444–2445.
- [4] J. Bowers, C.P. Butts, P.J. Martin, M.C. Vergara-Gutierrez, R.K. Heenan, Aggregation Behavior of Aqueous Solutions of Ionic Liquids, *Langmuir.* 20 (2004) 2191–2198.
- [5] J. Sirieix-Plénet, L. Gaillon, P. Letellier, Behaviour of a binary solvent mixture constituted by an amphiphilic ionic liquid, 1-decyl-3-methylimidazolium bromide and water: Potentiometric and conductimetric studies, *Talanta*, 63 (2004) 979–986.
- [6] J. Łuczak, J. Hupka, J. Thöming, C. Jungnickel, Self-organization of imidazolium ionic liquids in aqueous solution, *Colloid Surf. A-Physicochem. Eng. Asp.* 329 (2008) 125–133.
- [7] V. Pino, M. Germán-Hernández, A. Martín-Pérez, J.L. Anderson, Ionic Liquid-Based Surfactants in Separation Science, *Sep. Sci. Technol.* 47 (2011) 264–276.
- [8] M. Blesic, M.H. Marques, N.V. Plechkova, K.R. Seddon, L.P.N. Rebelo, A. Lopes, Self-aggregation of ionic liquids: micelle formation in aqueous solution, *Green Chem.* 9 (2007) 481–490.
- [9] Q.Q. Baltazar, J. Chandawalla, K. Sawyer, J.L. Anderson, Interfacial and micellar properties of imidazolium-based monocationic and dicationic ionic liquids, *Colloid Surf. A-Physicochem. Eng. Asp.* 302 (2007) 150–156.

- [10] M.G. Freire, P.J. Carvalho, A.M. Fernandes, I.M. Marrucho, A.J. Queimada, J.A.P. Coutinho, Surface tensions of imidazolium based ionic liquids: Anion, cation, temperature and water effect, *J. Colloid Interface Sci.* 314 (2007) 621–630.
- [11] B.L. Bhargava, M.L. Klein, Formation of Interconnected Aggregates in Aqueous Dicationic Ionic Liquid Solutions, *J. Chem. Theory Comput.* 6 (2010) 873–879.
- [12] M. Ao, P. Huang, G. Xu, X. Yang, Y. Wang, Aggregation and thermodynamic properties of ionic liquid-type Gemini imidazolium surfactants with different spacer length, *Colloid Polym Sci.* 287 (2009) 395–402.
- [13] A. Modaressi, H. Sifaoui, M. Mielcarz, U. Domańska, M. Rogalski, Influence of the molecular structure on the aggregation of imidazolium ionic liquids in aqueous solutions, *Colloids and Surfaces A: Physicochem. Eng. Asp.* 302 (2007) 181–185.
- [14] H. Wang, J. Wang, S. Zhang, X. Xuan, Structural effects of anions and cations on the aggregation behavior of ionic liquids in aqueous solutions, *J. Phys. Chem. B* 112 (2008) 16682–16689.
- [15] J. Jiao, Y. Zhang, L. Fang, L. Yu, L. Sun, R. Wang, N. Cheng, Electrolyte effect on the aggregation behavior of 1-butyl-3-methylimidazolium dodecylsulfate in aqueous solution, *J. Colloid Interface Sci.* 402 (2013) 139–145.
- [16] H. Wang, Q. Feng, J. Wang, H. Zhang, Salt Effect on the Aggregation Behavior of 1-Decyl-3-methylimidazolium Bromide in Aqueous Solutions, *J. Phys. Chem. B* 114 (2010) 1380–1387.
- [17] M. Planellas, R. Pleixats, A. Shafir, Palladium Nanoparticles in Suzuki Cross-Couplings: Tapping into the Potential of Tris-Imidazolium Salts for Nanoparticle Stabilization, *Adv. Synth. Catal.* 354 (2012) 651–662.
- [18] T. Yoshimura, T. Kusano, H. Iwase, M. Shibayama, T. Ogawa, H. Kurata, Star-Shaped Trimeric Quaternary Ammonium Bromide Surfactants: Adsorption and Aggregation Properties, *Langmuir* 28 (2012) 9322–9331.
- [19] Y. Yuan, I. Thomé, S.H. Kim, D. Chen, A. Beyer, J. Bonnamour, E. Zuidema, S. Chang, C. Bolm, Dimethyl Sulfoxide/Potassium Hydroxide: A Superbase for the Transition Metal-Free Preparation of Cross-Coupling Products, *Adv. Synth. Catal.* 352 (2010) 2892–2898.
- [20] P.C. Shanks, E.I. Franses, Estimation of Micellization Parameters of Aqueous Sodium Dodecyl Sulfate from Conductivity Data, *J. Phys. Chem.* 96 (1992) 1794–1805.
- [21] P.A. Koya, K. Ismail, K.u. Din, T.A. Wagay, Influence of 1,4-dioxane on the aggregation of bis(tetradecyldimethylammonium)butane dibromide Gemini surfactant, *J. Mol. Liq.* 177 (2013) 288–294.

- [22] M. Ao, G. Xu, Y. Zhu, Y. Bai, Synthesis and properties of ionic liquid-type Gemini imidazolium surfactants, *J. Colloid Interface Sci.* 326 (2008) 490–495.
- [23] V. Pino, C. Yao, J.L. Anderson, Micellization and interfacial behavior of imidazolium-based ionic liquids in organic solvent–water mixtures, *J. Colloid Interface Sci.* 333 (2009) 548–556.
- [24] A.K. Tiwari, S.M. Sowmiya, S.K. Saha, Micellization behavior of gemini surfactants with hydroxyl substituted spacers in water and water-organic solvent mixed media: The spacer effect, *J. Mol. Liq.* 167 (2012) 18–27.
- [25] B. Dong, X. Zhao, L. Zheng, J. Zhang, N. Li, T. Inoue, Aggregation behavior of long-chain imidazolium ionic liquids in aqueous solution: Micellization and characterization of micelle microenvironment, *Colloid Surf. A-Physicochem. Eng. Asp.* 317 (2008) 666–672.
- [26] N.J. Turro, A. Yekta, Luminescent probes for detergent solutions. A simple procedure for determination of the mean aggregation number of micelles, *J. Am. Chem. Soc.* 100 (1978) 5951–5952.
- [27] R. Vanyúr, L. Biczók, Z. Miskolczy, Micelle formation of 1-alkyl-3-methylimidazolium bromide ionic liquids in aqueous solution, *Colloid Surf. A-Physicochem. Eng. Asp.* 299 (2007) 256–261.
- [28] T. Yoshimura, H. Yoshida, A. Ohno, K. Esumi, Physicochemical properties of quaternary ammonium bromide-type trimeric surfactants, *J. Colloid Interface Sci.* 267 (2003) 167–172.
- [29] T. Inoue, H. Ebina, B. Dong, L. Zheng, Electrical conductivity study on micelle formation of long-chain imidazolium ionic liquids in aqueous solution, *J. Colloid Interface Sci.* 314 (2007) 236–241.
- [30] D. Yu, X. Huang, M. Deng, Y. Lin, L. Jiang, J. Huang, Y. Wang, Effects of Inorganic and Organic Salts on Aggregation Behavior of Cationic Gemini Surfactants, *J. Phys. Chem. B* 114 (2010) 14955–14964.
- [31] G. Para, E. Jarek, P. Warszynski, The Hofmeister series effect in adsorption of cationic surfactants-theoretical description and experimental results, *Adv. Colloid Interface Sci.* 122 (2006) 39–55.

CHAPTER 6
ANALYSIS OF BACTERIAL PLASMID DNA BY SOLID-PHASE
MICROEXTRACTION

Reproduced from *Analytical Methods* **2015**, 7, 7202-7207 with permission from the Royal Society of Chemistry

Omprakash Nacham, Kevin D. Clark, and Jared L. Anderson

Abstract

The extraction and preconcentration of DNA is a critical step in the analysis of microorganisms. In this study, a polymeric ionic liquid (PIL) sorbent coating was applied for the preconcentration of plasmid DNA (pDNA) from bacterial cells using solid-phase microextraction (SPME). PIL-based SPME devices were prepared by ultraviolet photoinitiated polymerization of a dicationic ionic liquid (IL)-based cross-linker and IL monomer on a nitinol support. pDNA was extracted from buffered aqueous solution using the PIL-based sorbent coating followed by the amplification of a target gene by polymerase chain reaction (PCR). Extraction conditions for the method were optimized based on the relative intensities of PCR amplicon bands visualized on an agarose gel. Compared to a commercial polyacrylate sorbent coating, the PIL sorbent coating extracted greater quantities of pDNA. With an extraction time of 5 min, the PIL-based SPME technique was capable of preconcentrating a sufficient amount of template pDNA from a 20 ng/mL solution to allow detection of the PCR product on an agarose gel. Sequence analysis demonstrated that the sequence of the pDNA was unaltered following PIL-based SPME. The developed method was successfully employed for the analysis of pDNA from two different *E. coli* transformants in a dilute aqueous solution.

6.1 Introduction

The analysis of deoxyribonucleic acid (DNA) plays a central role in a variety of applications ranging from the determination of microbial diversity in environmental samples,¹ identifying pathogens in food,² monitoring the levels of cell free nucleic acids in cancer prognosis (liquid biopsies),³ bioprospecting,⁴ and phylogenetic studies.⁵ Techniques such as polymerase chain reaction (PCR) and DNA sequencing enable the analysis of extremely small quantities of DNA. However, the reliability and reproducibility of these methods largely depends on the quality of the sample. Complex environmental and biological samples often contain compounds such as humic acids, proteins, or lipids that can inhibit PCR amplification or DNA sequencing reactions.⁵⁻⁸ In these circumstances, a proper sample preparation technique is necessary to purify and preconcentrate DNA for accurate and reproducible analysis.

Various sample preparation techniques have been developed for DNA purification including phenol-chloroform alkaline extraction,⁹ cesium chloride-based density gradient ultracentrifugation,¹⁰ and solid phase extraction (SPE) methods.¹¹ Although useful in many cases, these conventional DNA purification approaches often involve large sample volumes, the use of organic solvents, time-consuming and laborious centrifugation steps, or multiple sample transfer steps that increase the risk of contamination.⁶ DNA extraction based on commercial SPE kits reduces the volume of organic solvent consumed as well as the time required for analysis, but the cost per sample remains high and the number of extractions that can be performed is limited.¹² In some cases, the yield and purity of DNA obtained using different commercial extraction kits can be highly variable.¹³ Consequently, new methods that address the deficiencies of existing DNA sample preparation techniques are particularly desirable.

Solid-phase microextraction (SPME) is a non-exhaustive and solvent free sample preparation technique developed by Pawliszyn and co-workers. SPME possesses a significant advantage over traditional sample preparation methods by merging sampling and sample preparation into a single step.¹⁴ In this technique, target analytes adsorb or partition to a thin layer of polymeric sorbent coating immobilized on a solid support. SPME has been successfully employed in different areas within the field of analytical chemistry including bioanalysis,¹⁵ drug analysis,¹⁶ environmental analysis,¹⁷ and *in vivo* metabolomic studies.¹⁸ Although SPME has been applied for the extraction and preconcentration of numerous important biomolecules, it has yet to be extended to the analysis of DNA.

An increasing number of investigations have been recently reported involving the application of ionic liquids (ILs) in DNA technologies. ILs are molten organic salts composed of unsymmetrical organic cations and inorganic/organic anions with low melting points (≤ 100 °C).¹⁹ Customization of the IL structure has led to the development of IL coated capillaries for DNA separations,²⁰ ion conductive DNA films,²¹ long-term DNA storage media,²² and solvents for stabilizing triplex DNA.²³ Recently, our group and others have applied ILs as novel solvents for the extraction of DNA from aqueous samples. Electrostatic, hydrogen bonding, and hydrophobic interactions between the IL cationic component and the negatively charged phosphate group of DNA were shown to facilitate DNA extraction.^{12, 24, 25} In addition to conventional ILs, Wang and co-workers demonstrated the use of polymeric ionic liquid (PIL) microspheres in the highly efficient extraction of DNA from aqueous solution.²⁶ However, the reusability of the microspheres for subsequent DNA extractions was not discussed in the study.

In this study, a cross-linked PIL sorbent coating consisting of a dicationic IL-based cross-linker 1,12-bis(3-vinylimidazolium) dodecane dibromide ($[(\text{VIM})_2\text{C}_{12}^{2+}] 2[\text{Br}^-]$) and 1-vinyl-3-hexylimidazolium chloride ($[\text{VHIM}^+] [\text{Cl}^-]$) monomer was used for the extraction and preconcentration of plasmid DNA (pDNA) from bacterial cells. The PIL-based SPME method was capable of extracting sufficient template pDNA after 5 min from a 20 ng/mL solution for subsequent PCR amplification and visualization on an agarose gel. Due to favorable electrostatic interactions afforded by the PIL-based sorbent coating, a greater quantity of template pDNA was extracted from aqueous solution compared to a commercial polyacrylate (PA)-based sorbent coating under similar extraction conditions. The PIL sorbent was successfully applied for the extraction of two different plasmids from a mixture of *E. coli* transformants.

6.2 Experimental

6.2.1 Reagents. 1-vinylimidazole, 1-chlorohexane, 1,12-dibromododecane, 2-hydroxy-2-methylpropiophenone (DAROCUR 1173), and vinyltrimethoxysilane (VTMS) were purchased from Sigma-Aldrich (Milwaukee, WI, USA). Methanol, concentrated hydrogen peroxide (30 % (w/w)), hydrochloric acid, sodium chloride, tris(hydroxymethyl)aminomethane hydrochloride (Tris-HCl), acetic acid, boric acid, phosphoric acid, and sodium hydroxide were obtained from Fisher Scientific (Fair Lawn, NJ, USA). Deionized water (18.2 M Ω cm) was obtained from a Milli-Q water purification system (Millipore, Bedford, MA, USA). Elastic nitinol wires with an outer diameter of 125 μm were purchased from Nitinol Devices & Components (Fremont, CA, USA). A UV reactor equipped with a spinning carousel was obtained from Southern New England Ultraviolet Company (Bradford, CT, USA). Amber glass vials (10 mL), screw caps with polytetrafluoroethylene

septa, and an 85 μm polyacrylate (PA) fiber were obtained from Supelco (Bellefonte, PA, USA). Polypropylene microcentrifuge tubes were purchased from Fischer Scientific. Modified pET-32 plasmids were obtained from EMD Millipore (Billerica, MA, USA). NEB 5-alpha Competent *E. coli* cells and Phusion High-Fidelity DNA Polymerase and 5X Phusion HF buffer were obtained from New England Biolabs (Ipswich, MA, USA). A deoxyribonucleoside triphosphate (dNTP) mix (10 mM each) was obtained from Thermo Scientific (Pittsburgh, PA, USA). Agarose and tris(hydroxymethyl)aminomethane (Tris) were purchased from P212121 (Ypsilanti, MI, USA). A 1 Kb Plus DNA Ladder (250-25,000 bp) was obtained from Gold Biotechnology, Inc. (St. Louis MO, USA). SYBR[®] Safe DNA gel stain was supplied by Life Technologies (Carlsbad, CA, USA) and bromophenol blue was purchased from Santa Cruz Biotech (Dallas, TX, USA).

6.2.2 Preparation of PIL-based SPME fiber. The IL monomer ($[\text{VHIM}^+][\text{Cl}^-]$) and the dicationic IL cross-linker ($[(\text{VIM})_2\text{C}_{12}^{2+}] 2[\text{Br}^-]$) were synthesized according to previously reported procedures. Cross-linked PIL-based SPME fibers were prepared as previously described by our group.^{27, 28} Briefly, the nitinol support was immersed in boiling hydrogen peroxide at 70-75 °C for 2 h to generate free hydroxyl groups on the surface of the substrate. The derivatized surface was then reacted with neat VTMS at 85 °C for 2 h. A 1 cm length of the metallic alloy fiber was then dip-coated with a mixture containing the IL monomer, 50% (w/w) cross-linker with respect to monomer, and 3% (w/w) DAROCUR 1173. Afterwards, the fiber was exposed to 254 nm UV light for 2 h. The PIL-based SPME fiber was then immersed in 100 μL of methanol for 15 min, followed by washing in 10 mL of 20 mM Tris-HCl for 30 min. A JEOL JSM-7500F scanning electron microscope (SEM) was used to characterize the PIL-based SPME fiber. A SEM image of a PIL-based fiber after 40 extractions is shown in

Figure 1. The average film thickness of the PIL sorbent coating was found to be 65 μm , which is slightly less than the film thickness of the commercial PA fiber (85 μm) examined in this study.

6.2.3 Cell cultures. Competent *E. coli* cells were transformed with a modified pET-32 plasmid (5.9 kbp) containing either the 879 bp human 5'-methylthioadenosine phosphorylase (MTAP) gene or the 1275 bp vaccinia virus K4 gene. The transformed cells were cultured in 120 mL of Luria Bertani (LB) media with 100 $\mu\text{g}/\text{mL}$ carbenicillin at 37 $^{\circ}\text{C}$ for 20 h. Optical density measurements were performed at 600 nm using a Nicolet Evolution 300 UV-vis spectrophotometer from Thermo Scientific. Purified pDNA was obtained from the culture with a QIAprep Spin Miniprep Kit (Qiagen, Valencia, CA, USA) according to the manufacturer's instructions. The concentration of the pDNA standards were measured using a Synergy H4 Hybrid Microplate Reader from BioTek (Winooski, VT, USA).

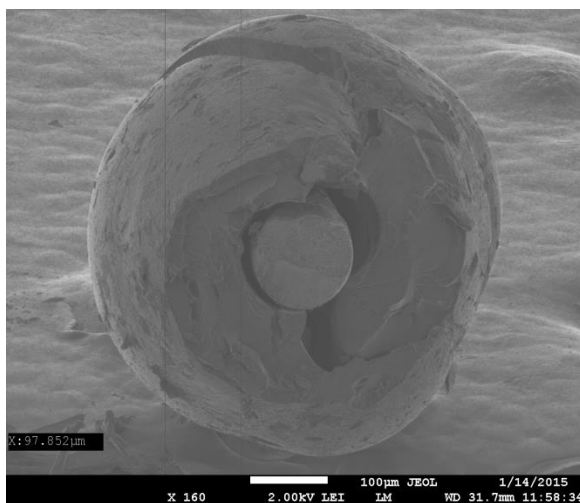


Figure 1. SEM image showing the cross-section of the PIL sorbent coating used for extracting pDNA from aqueous solution after 40 extractions.

6.2.4 PIL-based SPME of pDNA. The buffer used in this study was prepared using a mixture of 0.04 M of boric acid, phosphoric acid, and acetic acid. The desired pH was obtained by adjusting with sodium hydroxide or hydrochloric acid. Solutions containing either *E. coli* cells or purified pDNA were prepared in 10 mL of the buffer immediately prior to PIL-based SPME. The number of cells added to solution was approximated using OD₆₀₀ values. pDNA was extracted by immersing the SPME fiber in the solution under agitation at 650 rpm. Following extraction, the pDNA was desorbed by placing the PIL fiber in a solution containing 50 µL of 1 M NaCl and 20 mM Tris-HCl for 15 min. A 2 µL aliquot of the desorption solution was then subjected to PCR amplification. The PIL fiber was washed using 2 × 10 mL of 1 M NaCl in the buffer for 5 min before further use.

6.2.5 PCR and amplicon visualization. Immediately prior to PCR amplification, 0.03% (w/v) of Brij-700 was added to the desorption solution and allowed to incubate at room temperature for 15 min with gentle mixing to prevent adsorption of the nucleic acid to the polypropylene tube. A 2 µL aliquot of the desorption solution was then transferred to a PCR tube containing 34.5 µL of deionized water and 10 µL of 5X Phusion HF buffer. The MTAP and K4 genes were amplified using the primers 5'- TGC TGT TCC AGG GAC CT -3' and 5'- GAA TTC GGA TCC GGA CGC -3' at a final concentration of 0.2 µM. Finally, 1 µL from a 10 mM stock solution of dNTPs was added to the reaction mixture along with 1 unit of Phusion High Fidelity DNA Polymerase. Amplification of the MTAP and K4 genes was performed using a Techne FTgene2D thermal cycler (Burlington, NJ, USA). Thermal conditions for the amplification of both genes consisted of 5 min initial denaturation at 95 °C followed by 30 cycles of denaturation (95 °C for 30 s), annealing (54 °C for 45 s), and elongation (72 °C for 45 s). PCR products were loaded onto a 1% agarose gel and separated using a BRL H4

Horizontal Gel Electrophoresis System from Life Technologies with a Neo/Sci dual output power supply (Rochester, NY, USA). Gels were visualized on a Safe Imager™ 2.0 blue-light transilluminator from Life Technologies. The intensities of the DNA bands were measured using ImageJ software (National Institutes of Health).

6.3 Results and discussion

6.3.1 Preconcentration of pDNA using SPME fibers. The analysis of extremely small quantities of DNA invariably requires sample purification and preconcentration prior to downstream procedures. Conventional DNA sample preparation methods involve numerous steps that are time consuming and often require manual operation. The development of SPME sorbent coatings for DNA sample preparation is an important advancement that not only facilitates preconcentration, but also constitutes a platform that is amenable to laboratory, clinical, or field sampling.

In this study, pDNA containing the MTAP gene (879 bp) was chosen as a model DNA biomolecule to investigate the extraction performance of the cross-linked PIL and commercial PA SPME fibers. Figure 2 shows the PCR amplification of the MTAP gene from pDNA extracted from aqueous solution using PIL and PA SPME fibers. As shown in Lane 1, the amplicon is not observed after directly loading 2 μ L of the 20 ng/mL pDNA solution onto the gel. This is attributed to an insufficient amount of template to detect the amplicon after 30 cycles of PCR amplification. In contrast, preconcentration of pDNA by the PIL or PA fiber provides sufficient template DNA for detection of the PCR product in Lanes 2 and 3, respectively. The intensity of the PCR product band obtained after PIL extraction was calculated to be 4.2 times greater than the band observed for the PA fiber indicating that a greater quantity of pDNA was extracted by the PIL coating. Previous studies have suggested

that IL-based substrates are capable of engaging in electrostatic interactions with the negatively charged phosphate backbone of DNA molecules.^{20, 26, 29} Unlike the PA sorbent coating, the cross-linked PIL coating possesses ion-exchange sites that favor electrostatic interactions and lead to superior enrichment of pDNA.

6.3.2 Optimization of extraction and desorption conditions. The nature of the desorption solution has a profound influence on the recovery of pDNA from the PIL-based SPME fiber. As shown in Figure S1 of the electronic supplementary information (ESI), desorption of the PIL fiber in a solution of 20 mM Tris-HCl after extraction from a 20 ng/mL pDNA solution resulted in no observable amplicon. However, the addition of 1 M NaCl to the desorption solution provided a dramatic improvement in the recovery of pDNA from the sorbent coating. At NaCl concentrations greater than 1 M, inhibition of PCR was observed. In an effort to maximize the recovery of pDNA from the PIL coating while maintaining PCR amplification, 1 M NaCl was used as the desorption solution in all subsequent experiments.

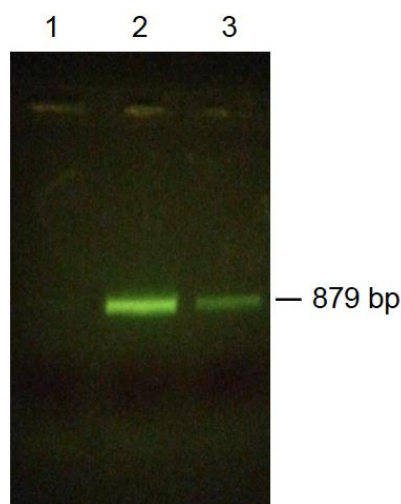


Figure 2. Amplicon obtained following the preconcentration of 6.7 kbp pDNA from aqueous solution using PIL and commercial PA SPME fibers. Lane (1): PCR product from a 2 μ L aliquot of 20 ng/mL of pDNA solution; Lane (2): PCR product following extraction/preconcentration using PIL-based sorbent coating; Lane (3): PCR product following extraction using PA sorbent coating. Extraction conditions: pDNA concentration: 20 ng/mL; total solution volume: 10 mL; desorption solution: 1 M NaCl in 20 mM Tris HCl; desorption solution volume: 50 μ L; pH 4.0; extraction time: 30 min; desorption time: 15 min

To avoid carryover of pDNA, the PIL-based SPME fiber was washed after each extraction using 2×10 mL of 1 M NaCl in buffer for 5 min. The PIL fiber was then desorbed in 50 μ L of 1 M NaCl for 15 min and a 2 μ L aliquot of the desorption solution was subjected to PCR. After washing the PIL sorbent, no amplicon band was observed.

An aqueous solution containing 20 ng/mL of pDNA was used to investigate the effect of extraction time on PIL-based SPME. The extraction time was varied from 5 to 30 min while the desorption time was held constant at 15 min. As shown in Figure 3, an increasing amount of amplicon was obtained as the extraction time was increased. However, beyond an extraction time of 30 min, no significant increase in the amount of pDNA extracted was observed. An extraction time of 20 min was selected for further experiments as a compromise between extraction time and the amount of pDNA extracted.

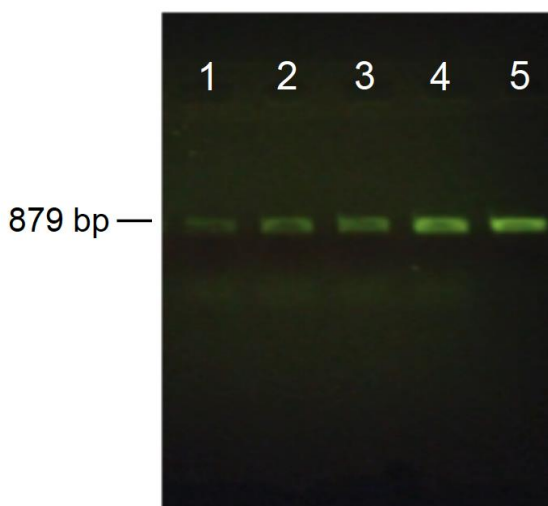


Figure 3. Effect of extraction time on the extraction of 6.7 kbp pDNA containing the MTAP gene (879 bp). Lane (1): 5 min; Lane (2): 10 min; Lane (3): 15 min; Lane (4): 30 min. Lane (5) represents a 390 ng MTAP gene standard. Extraction conditions: pDNA concentration: 20 ng/mL; total solution volume: 10 mL; desorption solution: 1 M NaCl in 20 mM Tris HCl; desorption solution volume: 50 μ L; pH 4.0; desorption time: 15 min.

The effect of solution pH on the extraction of pDNA using the PIL-based sorbent coating was studied. Aqueous solutions containing 20 ng/mL of pDNA and pH values ranging from 2 to 8 were examined. As shown in Figure S2 (ESI), modest differences in the amount of amplicon were observed from pH 4 to 8 with a slightly higher amount of pDNA being extracted at pH 4.0. In contrast, extraction at pH 2.0 generated the lowest intensity amplicon band, most likely due to degradation of the template pDNA.³⁰ The limit of detection for the PIL-based SPME method at pH 4 was found to be 1 ng/mL of pDNA.

In order to ensure that the sequence of the pDNA remained unaltered following extraction by the PIL coating, the amplified MTAP gene was subjected to sequence analysis. The sequence of the PCR amplified MTAP gene obtained after PIL-based SPME and the sequence of a MTAP gene standard are shown in Figures S3 and S4 of supplemental information of Appendix E, respectively. Comparison of the MTAP gene sequence after PIL-based extraction to the standard revealed no detectable differences, demonstrating the feasibility of PIL-based SPME as a DNA sample preparation technique.

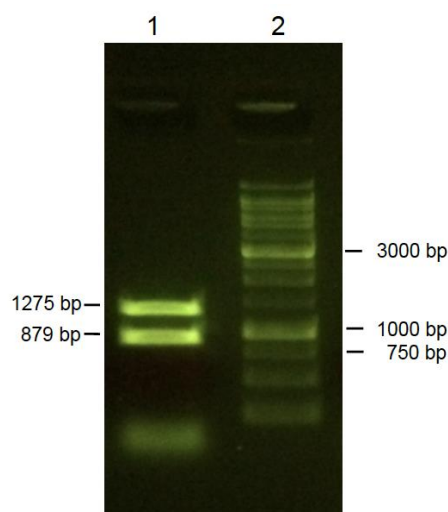


Figure 4. PCR products obtained following PIL-based SPME of a 1:1 mixture of *E. coli* cells transformed with pDNA containing either the 1275 bp K4 gene or the 879 bp MTAP gene. Lane (1) shows the PCR products following PIL-based SPME and Lane (2) includes a DNA ladder. Conditions: total solution volume: 10 mL; desorption solution: 1 M NaCl; 20 mM Tris HCl; desorption solution volume: 50 μ L; pH 4.0; extraction time: 20 min; desorption time: 15 min.

6.3.3 Direct extraction of pDNA from a bacterial cell culture. The sampling of bacterial DNA from environmental, food, and biological samples is a vital step for the identification of microbial communities and pathogen detection.^{2, 3, 5} Frequently, the population of microorganisms in a given sample is diverse. To determine whether the PIL-based SPME method is capable of detecting bacteria from independent cell cultures, *E. coli* cells transformed with either the MTAP or K4 plasmids were mixed in a 1:1 ratio and diluted to 10 mL with buffer. The total number of cells in solution containing the MTAP plasmid was calculated to be 1.44×10^8 , while 1.35×10^8 cells contained the K4 plasmid. Figure 4 shows the PCR products obtained from the desorption solution following PIL-based SPME of the diluted bacterial cells. The bands for the amplified MTAP and K4 genes are of similar intensity, indicating that the length of the gene insert does not affect the relative proportions of pDNA extracted.

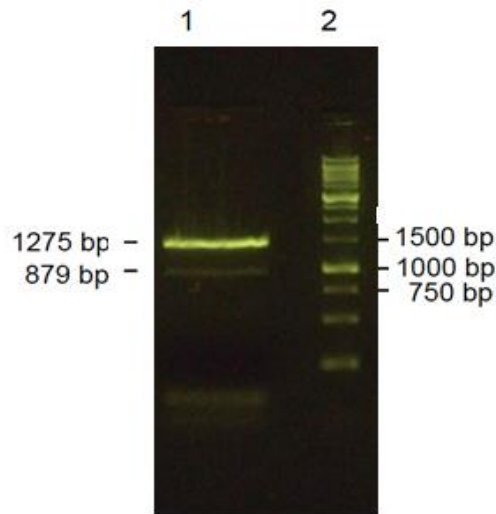


Figure 5. Detection of pDNA from *E. coli* cells containing either the 1275 bp K4 gene or the 879 bp MTAP gene using the PIL-based SPME method. Lane (1): PCR products obtained following the extraction of an aqueous solution spiked with 1.36×10^8 cells containing K4 and 1.44×10^6 cells containing MTAP. Conditions: total solution volume: 10 mL; desorption solution: 1 M NaCl in 20 mM Tris HCl; desorption solution volume: 50 μ L; pH 4.0; extraction time: 20 min; desorption time: 15 min. Lane (2): DNA ladder

During extraction of pDNA from cell culture-based sample solution, the source of pDNA can be either from ruptured dead cells or whole *E. coli* cell that may adsorb onto the surface of the PIL sorbent coating. In order to investigate this issue, two independent experiment were performed. Firstly, prior to SPME, *E. coli* cell culture containing pDNA with MTAP gene was filtered through the 0.22 μm sterilized syringe filter in order to retain the whole cells. Then, 100 μL of the filtrate was used for extraction. Following desorption and PCR, a band was observed for corresponding to the MTAP gene. Secondly, in order to confirm whether *E. coli* cells adsorbed on to the PIL sorbent coating was a major source of template in PCR, following SPME the PIL sorbent coating was subjected to SEM. It can be observed from SEM images on Figure 6 that a significant number of *E. coli* cells from sample solution were adsorbed on to the PIL sorbent coating. These two experiments illustrate that source of pDNA for PCR can be from both adsorbed *E. coli* cells and pDNA from the dead cells.

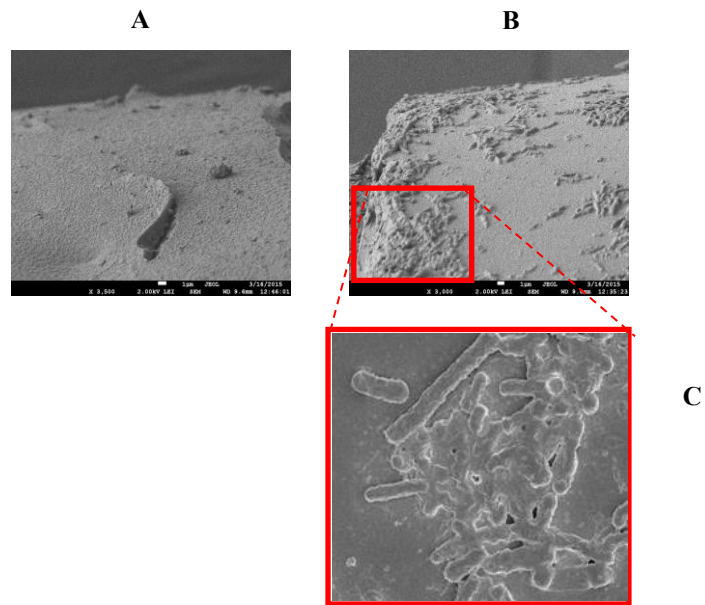


Figure 6. Scanning electron micrographs showing the surface of the PIL sorbent coating before and after immersion in aqueous solution containing 100 μL of *E. coli* cells transformed with pDNA possessing 879 bp MTAP gene. (A) Surface of PIL sorbent coating before immersion in sample solution. (B and C) Surface of PIL sorbent coating after immersion in sample solution.

A recurrent cause of bias in the analysis of microbial communities occurs during sampling procedures as a result of disproportionate quantities of unique specimens in the sample.^{31, 32} A 10 mL aqueous solution of *E. coli* transformants possessing either the K4 gene or the MTAP gene (100:1, respectively) was extracted using the PIL sorbent coating. The number of *E. coli* cells in solution containing the K4 and MTAP genes was 1.36×10^8 and 1.44×10^6 , respectively. As shown in Figure 5, bands for both the MTAP and K4 genes were observed following PCR amplification. Normalizing the band intensity for the K4 gene to 1, the MTAP gene produced a band with an intensity of 0.086, reflecting the 100-fold fewer *E. coli* cells possessing the MTAP gene in solution. Based on these results, the PIL-based SPME method shows promise for the rapid analysis of bacterial contamination in food samples or the determination of microbial diversity in environmental samples. Moreover, the SPME platform is well suited for applications requiring field sampling, further expanding the applicability of the method.

6.4 Conclusions

In this study, PIL-based sorbent coatings were used in SPME for the isolation and preconcentration of pDNA from bacterial cells. The PIL sorbent phase exhibited superior extraction of pDNA from aqueous solution compared to a commercial PA sorbent coating. The optimized SPME technique was capable of preconcentrating sufficient pDNA within 5 min for PCR amplification and detection on an agarose gel. Sequence analysis of a target gene from the extracted pDNA confirmed that the integrity of the pDNA sequence was preserved after PIL-based SPME. The developed method was successfully employed for the analysis of two different *E. coli* transformants from a dilute solution.

Acknowledgements

The authors acknowledge funding from the Chemical Measurement and Imaging Program at the National Science Foundation (Grant number CHE-1413199). Ali Najafi and Cheng Zhang are thanked for their assistance in preparing the PIL-based SPME fibers. Don Ronning, Michael Banco, and Chris Goins are thanked for their advice and discussions. K.D.C. thanks the University of Toledo College of Graduate Studies for a graduate fellowship.

Supporting information

Figure S1 to Figure S4 are provided in Appendix E.

References

1. F. V. Wintzingerode, U. B. Göbel and E. Stackebrandt, *FEMS Microbiol. Rev.*, 1997, **21**, 213-229.
2. F. Postollec, H. Falentin, S. Pavan, J. Combrisson and D. Sohier, *Food Microbiol.*, 2011, **28**, 848-861.
3. E. Gormally, E. Caboux, P. Vineis and P. Hainaut, *Mutat. Res. Rev. Mutat. Res.*, 2007, **635**, 105-117.
4. G. Strobel and B. Daisy, *Microbiol. Mol. Biol. Rev.*, 2003, **67**, 491-502.
5. S. G. Tringe and E. M. Rubin, *Nat. Rev. Genet.*, 2005, **6**, 805-814.
6. M. M. Rahman and A. Elaissari, *Drug Discov. Today*, 2012, **17**, 1199-1207.
7. P. Rådström, R. Knutsson, P. Wolffs, M. Dahlenborg and C. Löfström, K. Sachse and J. Frey, in *PCR Detection of Microbial Pathogens*, ed. K. Sachse and J. Frey, Humana Press, 2003, vol. 216, pp. 31-50.
8. L. A. Marshall, C. M. Han and J. G. Santiago, *Anal. Chem.*, 2011, **83**, 9715-9718.
9. R. Patel, J. T. Kvach and P. Mounts, *J. Gen. Microbiol.*, 1986, **132**, 541-551.
10. V. Glisin, R. Crkvenjakov and C. Byus, *Biochemistry*, 1974, **13**, 2633-2637.
11. T. Poeckh, S. Lopez, A. O. Fuller, M. J. Solomon and R. G. Larson, *Anal. Biochem.*, 2008, **373**, 253-262.

12. T. Li, M. D. Joshi, D. R. Ronning and J. L. Anderson, *J. Chromatogr. A*, 2013, **1272**, 8-14
13. J. Löffler, H. Hebart, U. Schumacher, H. Reitze and H. Einsele, *J. Clin. Microbiol.*, 1997, **35**, 3311-3312.
14. C. L. Arthur and J. Pawliszyn, *Anal. Chem.*, 1990, **62**, 2145-2148.
15. E. Cudjoe, B. Bojko, P. Togunde and J. Pawliszyn, *Bioanalysis*, 2012, **4**, 2605-2619.
16. H. Kataoka and K. Saito, *J. Pharm. Biomed. Anal.*, 2011, **54**, 926-950.
17. M. Chai and J. Pawliszyn, *Environ. Sci. Technol.*, 1995, **29**, 693-701.
18. D. Vuckovic, S. Risticovic and J. Pawliszyn, *Angew. Chem., Int. Ed.*, 2011, **50**, 5618-5628.
19. J. P. Hallett and T. Welton, *Chem. Rev.*, 2011, **111**, 3508-3576.
20. S. F. YauáLi, *Analyst*, 2003, **128**, 37-41.
21. N. Nishimura, Y. Nomura, N. Nakamura and H. Ohno, *Biomaterials*, 2005, **26**, 5558-5563.
22. R. Vijayaraghavan, A. Izgorodin, V. Ganesh, M. Surianarayanan and D. R. MacFarlane, *Angew. Chem., Int. Ed.*, 2010, **49**, 1631-1633.
23. H. Tateishi-Karimata, M. Nakano and N. Sugimoto, *Sci. Rep.*, 2014, **4**, 3593.
24. J.-H. Wang, D.-H. Cheng, X.-W. Chen, Z. Du and Z.-L. Fang, *Anal. Chem.*, 2007, **79**, 620-625.
25. K. D. Clark, O. Nacham, H. Yu, T. Li, M. M. Yamsek, D. R. Ronning and J. L. Anderson, *Anal. Chem.*, 2015, **87**, 1552-1559.
26. X. Wang, L. Xing, Y. Shu, X. Chen and J. Wang, *Anal. Chim. Acta*, 2014, **837**, 64-69.
27. T. D. Ho, B. R. Toledo, L. W. Hantao and J. L. Anderson, *Anal. Chim. Acta*, 2014, **843**, 18-26.
28. T. D. Ho, H. Yu, W. T. Cole and J. L. Anderson, *Anal. Chem.*, 2012, **84**, 9520-9528.
29. Y.-N. Xie, S.-F. Wang, Z.-L. Zhang and D.-W. Pang, *J. Phys. Chem. B*, 2008, **112**, 9864-9868.

30. T. Suzuki, S. Ohsumi and K. Makino, *Nucleic Acids Res.*, 1994, **22**, 4997-5003.
31. F. Martin-Laurent, L. Philippot, S. Hallet, R. Chaussod, J. Germon, G. Soulas and G. Catroux, *Appl. Environ. Microbiol.*, 2001, **67**, 2354-2359.
32. D. Ercolini, *J. Microbiol. Meth.*, 2004, **56**, 297-314.

CHAPTER 7**EXTRACTION AND PURIFICATION OF DNA FROM COMPLEX BIOLOGICAL SAMPLE MATRICES USING SOLID-PHASE MICROEXTRACTION COUPLED WITH REAL-TIME PCR**

Reprinted with permission from *Analytical Chemistry* **2016**, 88, 7813-7820

Copyright © 2016, American Chemical Society

Omprakash Nacham, Kevin D. Clark, and Jared L. Anderson

Abstract

The determination of extremely small quantities of DNA from complex biological sample matrices represents a significant bottleneck in nucleic acid analysis. In this study, polymeric ionic liquid (PIL)-based solid-phase microextraction (SPME) was applied for the extraction and purification of DNA from crude bacterial cell lysate with subsequent quantification by real-time PCR (qPCR) analysis. Using an on-fiber ultraviolet initiated polymerization technique, eight different PIL sorbent coatings were generated and their DNA extraction performance evaluated using qPCR. The PIL sorbent coating featuring halide anions and carboxylic acid groups in the cationic portion exhibited superior DNA extraction capabilities when compared to the other studied PILs and a commercial polyacrylate SPME fiber. Electrostatic interactions as well as an ion-exchange mechanism were identified as the driving forces in DNA extraction by the PIL sorbents. The selectivity of the PIL sorbent coating for DNA was demonstrated in the presence of PCR inhibitors at high concentration, where a quantifiable amount of template DNA was extracted from aqueous samples containing CaCl_2 and FeCl_3 . Furthermore, the PIL-based SPME method was successfully applied for the extraction of DNA from crude bacterial cell lysate spiked with 1 pg mL^{-1} template DNA

without requiring the use of organic solvents or centrifugation steps. Following PIL-based SPME of DNA from a dilute cell lysate, the qPCR amplification efficiency was determined to be 100.3%, demonstrating the feasibility of the developed method to extract high purity DNA from complex sample matrices.

7.1 Introduction

Deoxyribonucleic acid (DNA) analysis holds great promise in a variety of applications including clinical diagnostics,¹ forensics,² genomics,³ and food safety.⁴ Valuable diagnostic information is often provided by subjecting DNA samples to the polymerase chain reaction (PCR) and/or sequencing methods. These sensitive bioanalytical techniques require the input of highly pure nucleic acids, particularly for the detection of extremely small quantities of target DNA.^{5,6} Therefore, the isolation and preconcentration of DNA from complex cellular or environmental sample matrices is an important prerequisite for successful downstream analysis.

Conventional DNA purification methods have relied on phenol-chloroform liquid-liquid extraction (LLE) with modifications including surfactants,⁷ sonication, fine grinding of the sample under liquid nitrogen using mortar and pestle,⁸ and enzymatic degradation to assist in the removal of interfering agents.⁹ However, these sample preparation procedures are often time consuming, labor-intensive, and require multiple sample transfer steps that may result in the loss of target DNA. Furthermore, phenol-chloroform LLE methods often consume large volumes of organic solvent and are incompatible with automation. Solid phase extraction (SPE) techniques have reduced analysis times and organic solvent consumption in DNA purification by applying samples to a sorbent material that reversibly binds DNA.¹⁰ However, SPE methods require tedious centrifugation steps, lack reusability, and suffer from high cost

per sample.¹¹ In order to address the limitations associated with existing DNA purification methodologies, new sample preparation techniques that enable high throughput analysis must be explored.

Solid-phase microextraction (SPME) is a solvent-less, non-exhaustive sample preparation technique developed by Pawliszyn and co-workers.¹² In practice, a thin layer of polymeric sorbent coating is immobilized on a solid support and exposed to either the headspace of the sample or directly immersed in the sample solution. Analytes that partition to the sorbent coating can then be desorbed and analyzed by an appropriate technique. SPME possesses a unique advantage over other methods because sampling and sample preparation are combined into a single step, often reducing the overall time required for analysis. SPME has been successfully applied in numerous areas of chemical research including environmental analysis,¹³ drug analysis,¹⁴ and biomolecule analysis.¹⁵

Ionic liquid (IL)-based materials are becoming increasingly popular substrates in nucleic acid applications. ILs are molten organic salts possessing melting points below 100 °C. The physicochemical properties of ILs can be controlled by tailoring the structure of the IL cation and anion.¹⁶ ILs have been applied as DNA preservation media,¹⁷ solvents for stabilizing triplex DNA,¹⁸ ion-conductive DNA films,¹⁹ additives for enhancing the rate of DNA amplification in PCR,²⁰ and stationary phases for the separation of DNA in capillary electrophoresis.²¹ Recently, our group and others have investigated various IL solvents in aqueous DNA extraction systems.²²⁻²⁴ Hydrogen bonding, hydrophobic interactions, and electrostatic interactions between the cationic portion of the IL and the negatively charged phosphate groups of DNA are thought to be the driving forces for the extraction.

Polymeric ionic liquids (PILs) are a sub-class of ILs generated by incorporating polymerizable groups within the cation/anion of the IL structure. Owing to their structural tunability, enhanced thermal stability, and resistance toward harsh matrix conditions, PILs have been applied as sorbent coatings in SPME. A core advantage of PILs in SPME is the ability to modify the chemical composition of the PIL sorbent to facilitate the extraction of a broad range of analytes from complex sample matrices.²⁵ Careful design and modification of the PIL chemical structure through imparting functional groups that engage in favorable interactions with DNA may provide enhanced DNA extraction efficiency and selectivity. Previously, Wang and co-workers investigated the application of PIL-based microspheres for the extraction of DNA from aqueous solution and demonstrated the feasibility of utilizing the PIL scaffold for DNA enrichment.²⁶ Until now, the PIL-based SPME platform has not been exploited extensively in the sample preparation of nucleic acids from biological samples. In a recent study, our group demonstrated the application of PIL-based SPME for the analysis of bacterial plasmid DNA (pDNA) from aqueous solution.²⁷ In this approach, pDNA was extracted using a PIL-based SPME device and subjected to end-point PCR amplification followed by digital imaging densitometry. Although semi-quantitative end-point PCR amplification methods are useful in many cases, post-PCR steps required for amplicon detection (e.g., gel electrophoresis) are time consuming and require numerous sample transfer steps. Moreover, accurate and reliable quantification of nucleic acids at low concentrations is not achievable using end-point methods.²⁸ Real-time quantitative PCR (qPCR) amplification is a technique wherein the accumulating amplicon is detected after each cycle using fluorescent DNA probes. In addition to reducing analysis time by circumventing the need for gel electrophoresis, qPCR addresses the limitations associated with quantification in end-point PCR.^{29, 30}

This study constitutes the first report in the application of SPME sorbent coatings interfaced with qPCR for the extraction of bacterial pDNA from crude cell lysate. In this study, eight different PIL-based sorbent coatings were prepared and their DNA extraction performance evaluated using qPCR. By systematically modifying the PIL sorbent coating composition and observing the resulting DNA extraction performance, electrostatic interactions as well as exchangeable anions were found to play important roles in DNA extraction. The binding capacity and selectivity of the PIL-based sorbent coating for template DNA was investigated in the presence of PCR inhibitors. Under optimal conditions, the developed PIL-based SPME approach was capable of preconcentrating pDNA from crude bacterial cell lysate with sufficient quality and quantity for qPCR analysis. The fiber-based DNA extraction platform provides a simple, rapid, and automatable technique that is highly suitable for laboratory or field sampling applications.

7.2 Experimental

7.2.1 Materials and Measurements. NEB 5-alpha Competent Escherichia coli cells, 50 mM magnesium chloride solution, and dimethylsulfoxide (100%) were obtained from New England Biolabs (Ipswich, MA, USA). The QIAquick Gel Extraction Kit and QIAprep Spin Miniprep Kit were purchased from QIAGEN (Valencia, CA, USA). Deionized water (18.2 MΩ cm) obtained from a Milli-Q water purification system was used for the preparation of all solutions (Millipore, Bedford, MA, USA). SsoAdvanced universal SYBR Green supermix for real-time PCR assays was obtained from Bio-Rad Laboratories (Hercules, CA, USA). DNA LoBind polypropylene microcentrifuge tubes were purchased from Fisher Scientific. An 85 μm polyacrylate (PA) SPME fiber was obtained from Supelco (Bellefonte, PA, USA).

$^1\text{H-NMR}$ spectra were recorded using Bruker 500 MHz nuclear magnetic resonance spectrometer. The film thickness of the PIL sorbent coatings was determined using a JEOL JSM-6060 LV low vacuum scanning electron microscope (SEM).

7.2.2 Preparation of DNA Samples. A modified plasmid with a 135 bp DNA insert was used for the transformation of competent *E. coli* cells by heat shock. The transformed cells were cultured in 120 mL of Luria Bertani (LB) media with $100 \mu\text{g mL}^{-1}$ ampicillin at 37°C for 24 h. pDNA was then purified from the cell culture using a QIAprep Spin Miniprep kit by following the manufacturer's instructions. The concentration of the pDNA was measured using a NanoDrop 2000c spectrophotometer from Thermo Scientific (Wilmington, DE, USA). Purified pDNA containing the 135 bp target sequence was amplified by PCR using primers with sequences of 5'-CAC GCT TAC ATT CAC GCC CT-3' and 5'-CGA GCG TCC CAA AAC CTT CT-3'. Following amplification, the amplicon was subjected to agarose gel electrophoresis using a BRL H4 Horizontal Gel Electrophoresis System from Life Technologies with a Neo/Sci dual output power supply (Rochester, NY, USA). The 135 bp amplicon was excised from the gel and purified using a QIAquick Gel Extraction kit by following the manufacturer's instructions. The concentration of DNA was measured using a NanoDrop 2000c spectrophotometer. A standard solution of $2.89 \text{ ng } \mu\text{L}^{-1}$ of DNA was prepared in 1X TE buffer (pH 8.0) and serially diluted with 1X TE buffer (pH 8.0). All DNA standard solutions used in the study were stored at -80°C and thawed on ice prior to use.

7.2.3 Real-time quantitative PCR Assays. Real-time quantitative PCR (qPCR) assays were performed on a CFX96 Touch Real-Time PCR Detection System from Bio-Rad Laboratories (Hercules, CA, USA) according to the following thermal cycling protocol: initial denaturation step of 3 min at 95.0°C , followed by 40 cycles of 10 sec at 95.0°C and 30 sec at 64.0°C . All

amplification reactions were performed in triplicate. For each reaction, 1 μL template DNA was mixed with 19 μL reaction mix containing 10 μL of SsoAdvanced universal SYBR Green supermix (2x), 2.6 μL of 50 mM MgCl_2 , 1 μL of DMSO, 0.8 μL of 10 μM forward and reverse primers, and 3.8 μL of deionized water. For the external calibration curve, an additional 10 mM NaCl was also included in the reaction mixture. Quantification cycle (C_q) values were used to calculate the amount of DNA that was extracted using the SPME fibers.

As shown in Figure S1, in order to evaluate the amplification efficiency, a four-point calibration curve with a tenfold dilution series was developed. The amplification efficiency was calculated using Equation 1, where the slope is the slope of the linear regression in the calibration curve.

$$\text{Efficiency} = [10^{(\frac{-1}{\text{slope}})} - 1] \times 100 \quad (1)$$

The qPCR amplification efficiency was found to be 98.3% under the conditions employed in this study.

7.2.4 Extraction of DNA using SPME Devices. A schematic for the general procedure employed in DNA extraction using PIL-based SPME followed by qPCR assay is depicted in Figure 1. A 10 pg mL^{-1} solution of DNA was prepared in 10 mL of 1X TE buffer (pH 8) immediately prior to extraction. DNA was then extracted by immersing a SPME sorbent in the sample solution under agitation at 650 rpm. Following SPME, DNA was desorbed from the sorbent coating by immersion in 50 μL of 1 M NaCl desorption solution for 30 min. To relieve the inhibition caused from 1 M NaCl, 20 μL of a desorption solution was diluted five times with deionized water prior to the qPCR assay. Finally, a 1 μL aliquot of the diluted desorption solution was subjected to qPCR amplification, resulting in a final NaCl concentration of 10 mM. Prior to the next extraction, the SPME sorbent was washed using 2 x 10 mL of 1X TE

7.3 Results and Discussion

7.3.1 Structural Design of PIL Sorbent Coatings to Enhance DNA Extraction. In this study, eight different PIL sorbent coatings were prepared by combination of different IL monomers and crosslinkers, as shown in Table 1. IL monomers and crosslinkers were produced according to the reported procedures from the literature.³¹⁻³³ ¹H-NMR was used to characterize the IL monomers and crosslinkers, as shown in Figures S2-S11 of the supplemental information of Appendix F. Materials and detailed procedures employed for the fabrication of PIL-based SPME devices are described in supplemental information of Appendix F. The approximate film thickness values of all PIL sorbent coatings are shown in Table 1 and a representative SEM micrograph of a PIL-based sorbent coating (Fiber 4) is shown in Figure S12.

In SPME, the chemical composition of the sorbent coating has a profound influence on the extraction of target analytes from a sample matrix. An optimal sorbent coating can enhance the extraction performance as well as improve the sensitivity of the developed extraction procedure. To investigate the effect of the PIL sorbent coating composition on DNA extraction, the structures of IL monomers and crosslinkers were modified with different anions and a variety of functional groups appended to the IL cations. The extraction performance of the PIL sorbent coatings was examined under similar experimental conditions using qPCR as the method of analysis. The amount of DNA extracted by the sorbent coating is correlated to a C_q value obtained from qPCR analysis. A lower C_q value indicates a greater quantity of extracted template DNA. A difference in one C_q value corresponds to a two-fold difference in the amount of extracted DNA when the amplification efficiency is 100%.

Figure 2 illustrates the DNA extraction performance of different PIL fibers and a commercial PA fiber. For PIL Fibers 3 and 8 as well as the commercial PA fiber, the mass of

template DNA extracted was not determined as the high C_q values obtained were out of the calibration range indicating the poor extraction efficiency of these fibers. As shown in Figure 2, the incorporation of benzyl moieties within the crosslinker of Fiber 2 resulted in a diminished DNA extraction efficiency compared to Fiber 1. Further tailoring of the PIL sorbent coatings by incorporating polar functional groups into the cationic structure, such as a carboxylic acid (Fiber 4) or alcohol moieties (Fiber 7), resulted in higher DNA extraction than PIL sorbents lacking polar moieties. For example, the average C_q value obtained from extractions using Fiber 1 was 30.42 ± 0.22 , whereas Fibers 4 and 7 exhibited superior DNA extraction capabilities with C_q values of 27.89 ± 0.73 and 29.25 ± 0.16 , respectively. Intra-day fiber-to-fiber extraction reproducibility was determined using a set of three fibers for PIL Fibers 1 and 4, resulting in C_q values with relative standard deviations (RSD) of 1.8% and 4.6%, respectively.

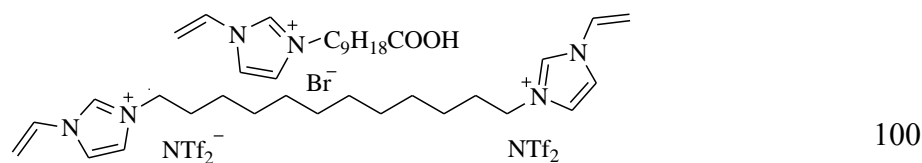
The anionic component of the PIL-based sorbent coating was observed to have a major influence on DNA extraction. As shown in Figure 2, substitution of halide-based anions (Fiber 1) with NTf₂⁻ anions (Fiber 3) within the PIL sorbent coatings of similar cationic composition resulted in a 4.5 cycle increase in the C_q value, indicating a dramatic decrease in DNA extraction performance. With a cation composition identical to Fiber 4, two sorbent coatings were prepared by replacing the halide anions with NTf₂⁻ anions in either the monomer (Fiber 5) or the monomer and crosslinker (Fiber 6). From Figure 2, the amount of DNA extracted using Fibers 5 and 6 was lower than that observed for Fiber 4. The diminished extraction performance of Fibers 5 and 6 suggests that the halide anions in Fiber 4 play a crucial role in extracting higher amounts of DNA from aqueous solutions.

7.3.2 Optimization of Extraction Parameters for PIL Fiber 4. On the basis of its superior DNA extraction performance in comparison to the other six PIL fibers studied, Fiber 4 was selected for optimization of the PIL-based SPME method. Previous investigations of DNA extraction using PIL sorbents established that a desorption solution containing 1 M NaCl was essential for recovering DNA from the sorptive phase.²⁷ However, when a similar concentration of NaCl was employed for desorption of DNA in PIL-based SPME interfaced with qPCR analysis, amplification was inhibited due to the high salt concentration within the qPCR solution (data not shown). qPCR amplification was recovered by performing a five-fold dilution of the desorption solution prior to analysis.

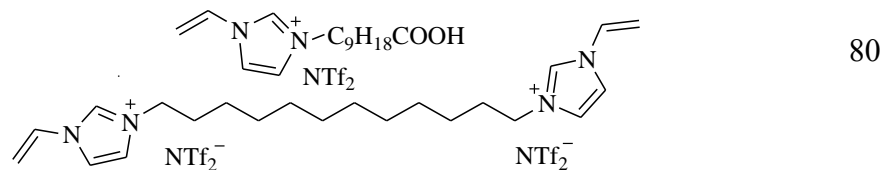
Table 1 Chemical composition of all PIL-based SPME sorbent coatings examined in this study for

Fiber	IL monomer and crosslinker composition ^a	Approximate film thickness (μm)
Fiber 1		81
Fiber 2		80
Fiber 3		82
Fiber 4		69

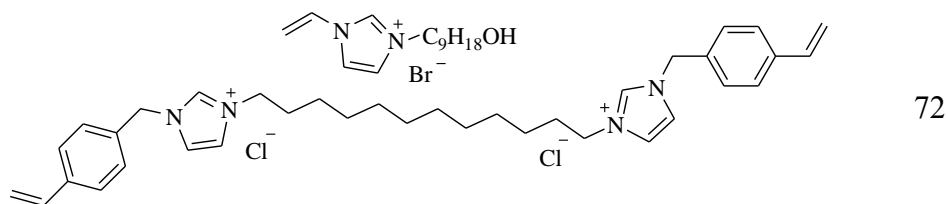
Fiber 5



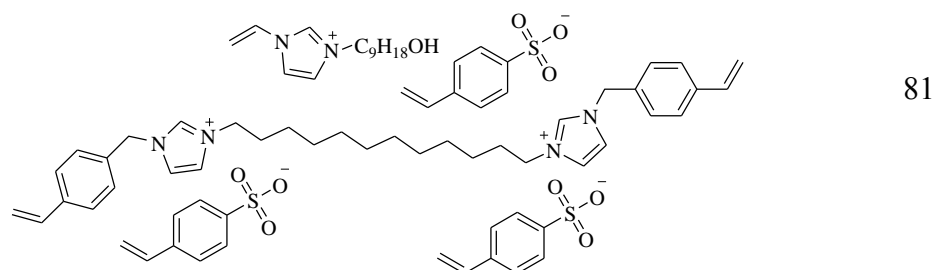
Fiber 6



Fiber 7



Fiber 8



^aThe dicationic IL crosslinker employed within each sorbent coating was 50% by weight with respect to the weight of IL monomer.

To reduce carry-over effects as well as minimize the number of washing steps prior to the subsequent extraction, a desorption time of 30 min was chosen for all extractions. Figure S13 depicts typical qPCR amplification plots obtained from a diluted desorption solution following PIL-based SPME (Fiber 4) and a washing fraction prior to subsequent extraction, demonstrating good DNA recovery and reusability of PIL sorbent coating with no detectable carry-over.

The effect of extraction time on the amount of DNA extracted from an aqueous solution containing 10 pg mL^{-1} DNA was examined from 5 to 90 min using Fiber 4. As shown in Figure S14, the amount of DNA extracted increased with an increase of the extraction time from 5 to 60 min. However, beyond an extraction time of 60 min, no significant increase in the amount of DNA extracted was observed. In an effort to maintain a compromise between overall analysis time and the amount of DNA extracted, an extraction time of 30 min was chosen for all subsequent experiments.

The extraction of biological samples is heavily influenced by the pH of the sample solution. Careful optimization of sample solution pH often minimizes the co-extraction of interfering components and enhances the extraction of target analytes.⁸⁵ In this study, the effect of pH on DNA

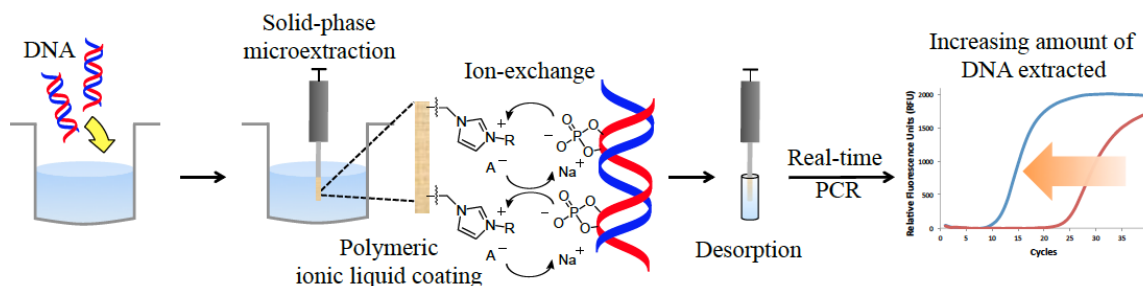


Figure 1. Schematic representation of template DNA extraction using PIL-based SPME approach and subsequent quantification utilizing a real-time PCR assay

extraction was examined by varying the pH from 2 to 10. An aqueous solution containing 10 pg mL^{-1} of DNA was employed to investigate the effect of pH on PIL-based SPME using Fiber 4. The desired sample solution pH was obtained by adjustment with either HCl or NaOH. As shown in Figure S15, higher amounts of DNA were extracted when performing extractions at pH 8 and 10 compared to pH 4 and 6.

The amount of DNA extracted did not vary significantly from pH 4 to 6. However, a very high Cq value was obtained at pH 2 and may be due to depurination of the template DNA in acidic solutions.^{86,87} In order to achieve high extraction efficiency while minimizing the deleterious effects of acidic pH, sample solutions were adjusted to pH 8 in all extractions.

7.3.3 Insight into the Extraction Mechanism of PIL Sorbent Coatings. Previous studies have postulated that hydrophobic and electrostatic interactions between ILs and DNA play a significant role in extracting DNA from aqueous solutions. In order to gain insight toward the mechanism of DNA extraction by the PIL-based sorbent coatings, the DNA extraction performance of the PIL sorbent coatings were first compared to a commercial PA sorbent phase. As shown in Figure 2, the PIL-based sorbent coatings extracted a higher amount of the template DNA compared to the PA fiber under similar experimental conditions. These results are in good agreement with a previous comparison of PIL and PA sorbents for DNA extraction.²⁷ Unlike the PA fiber, PIL sorbent coating possesses a cross-linked cationic framework that is capable of engaging in electrostatic interactions with the negatively charged phosphate backbone of the template DNA.

Apart from electrostatic interactions playing a significant role in extracting DNA, it is conceivable that an ion-exchange mechanism between the anions of the PIL sorbent coating and negatively charged DNA molecules may also occur. To investigate the possibility of ion-exchange, a non-exchangeable anion component was incorporated into the PIL sorbent. Previously, Feng and co-workers investigated anion exchange between a PIL sorbent coating containing p-styrenesulfonate anions and high ionic strength solutions (30% w/v NaCl) over an extended period of time. By co-polymerizing p-styrenesulfonate anions with the cationic moieties of the PIL sorbent, exposure of the PIL to salt solutions for 3 h resulted in no

significant variation in the sulfur composition of the PIL as determined by elemental analysis, indicating that the PIL anions were not exchanged with the salt solution.⁸⁴ In order to evaluate the ion-exchange interactions between the PIL sorbent coating and template DNA molecules, a similar approach was applied in which the halide-based anions of Fiber 7 were substituted with polymerizable p-styrenesulfonate anions to yield Fiber 8. Although the fibers possessed identical cationic composition, Figure 2 shows a dramatic decrease in the amount of DNA extracted by Fiber 8 compared to Fiber 7. The diminished extraction performance observed for Fiber 8 may be due to the lack of exchangeable anions within the PIL sorbent coating due to copolymerization of the anion with the cationic framework.⁸⁴ The results indicate that a combination of electrostatic interactions and ion-exchange comprise the driving forces for the extraction of DNA by PIL-based sorbent coatings. Since ion-exchange processes occur rapidly, the data in Figure S14 seem to indicate that the electrostatic interactions between the PIL and DNA may contribute to longer extraction times.

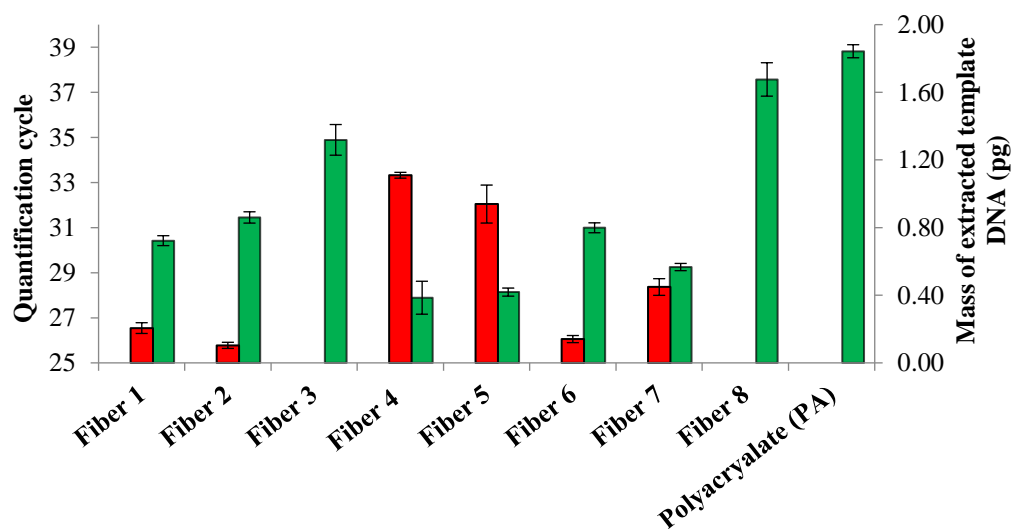


Figure 2. Comparison of extraction performance of different PIL-based sorbent coatings. All experiments were performed in triplicate ($n = 3$); concentration of 135 bp DNA: 10 pg mL^{-1} ; sample solution: 1X TE buffer (pH 8.0); extraction time: 10 min; desorption time: 30 min; desorption solvent: 1 M NaCl; desorption solvent volume: $50 \text{ }\mu\text{L}$; (■) represents quantification cycles; (■) denotes mass of extracted template DNA. *Mass of template DNA extracted by PIL Fibers 3 and 8 and a commercial polyacrylate fiber was not determined as the Cq values obtained were out of the calibration range.

7.3.4 Effect of PCR Inhibitors on DNA Extraction using PIL-based SPME. qPCR is an extremely powerful, rapid, and sensitive diagnostic tool for the analysis of nucleic acids. However, when applied to biological samples the sensitivity and reproducibility of the technique can be drastically reduced, owing to the presence of PCR inhibitory components such as metal ions.^{6, 37}

Since the ion-exchange mechanism between the PIL sorbent coating and DNA may also be influenced by the presence of metal salts, the DNA extraction capability of Fiber 4 was evaluated in the presence of FeCl₃ and CaCl₂. A complex sample matrix was simulated by the addition of varying amounts of metal salts to a 10 pg mL⁻¹ aqueous DNA solution. Under the studied qPCR conditions, the minimum inhibitory concentrations of FeCl₃ and CaCl₂ were determined to be 30 μM and 5 mM, respectively (data not shown), which also represent metal ion concentrations found within clinically relevant samples⁶⁰ and food samples.⁸⁸ However, to evaluate the DNA extraction performance of the PIL sorbent coating (Fiber 4) in rigorous sample environments, higher concentrations of FeCl₃·6H₂O and CaCl₂·2H₂O were employed in aqueous DNA solutions. As shown in Figure 3A, by increasing the concentration of CaCl₂·2H₂O from 0 to 100 mM, the amount of template DNA extracted by Fiber 4 decreased slightly and produced a 0.35 unit increase in C_q value. A gradual decrease in the extraction performance of the fiber was observed when the concentration was increased to 700 mM; unfortunately, at concentrations higher than 700 mM, no amplicon was detected. This may be attributed to either the lower amount of DNA extracted by the sorbent coating or co-extraction of calcium ions and subsequent inhibition of qPCR amplification. Figure 3B illustrates the effect of FeCl₃·6H₂O

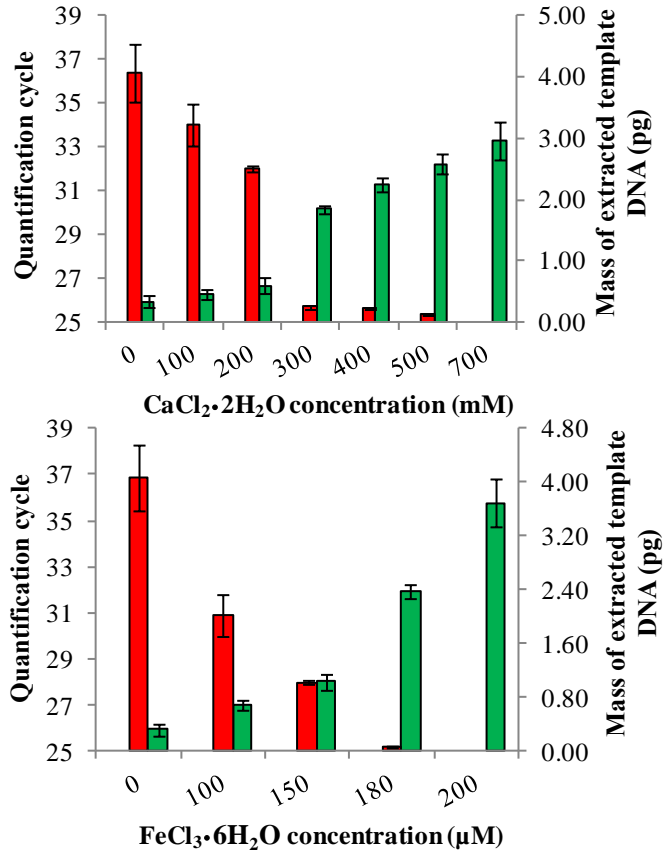


Figure 3. DNA extraction using Fiber 4 in the presence of two known PCR inhibitors (A) CaCl₂·2H₂O and (B) FeCl₃·6H₂O. All experiments were performed in triplicate (n = 3); concentration of 135 bp DNA: 10 pg mL⁻¹; sample solution: 1X TE buffer (pH 8.0); extraction time: 30 min; desorption time: 30 min; desorption solvent: 1 M NaCl; desorption solvent volume: 50 μL. *Mass of extracted template DNA was not determined as the C_q value obtained was out of the calibration range. (■) represents mass of extracted DNA; (■) denotes quantification cycle.

concentration on DNA extraction using Fiber 4. By increasing the concentration of FeCl₃·6H₂O to 100 μM, approximately 50% less DNA was extracted when compared to an aqueous DNA solution without metal ions. Nevertheless, a quantifiable amount of template DNA was extracted by the fiber even at concentrations as high as 180 μM FeCl₃·6H₂O.

Further addition of $\text{FeCl}_3 \cdot 6\text{H}_2\text{O}$ resulted in a drop of the sample solution pH ($\text{pH} < 3$) and no amplicon was detected following PIL-based SPME. These results demonstrate that the PIL-based SPME platform can function as a viable sample preparation tool in selectively extracting DNA from metal rich biological samples.

7.3.5 Extraction of DNA from Bacterial Cell Lysate. The extraction and purification of extremely small quantities of DNA from complex biological or environmental samples represents a significant bottleneck in nucleic acid analysis. The PIL-based SPME platform provides a simple and rapid technique for DNA extraction that eliminates the tedious, multi-step sample pretreatment procedures required for conventional methods. Because interfering constituents within complex sample matrices may influence the DNA binding capacity of the SPME sorbent coating and/or alter extraction performance, the effects of a bacterial cell lysate sample matrix on the PIL-based SPME method were investigated. Initially, the DNA binding capacity of Fiber 4 was studied in 1X TE buffer. As shown in Figure S16, an increase in the amount of DNA extracted was observed upon increasing the concentration of template DNA from 0 to 6 pg mL^{-1} , after which no significant change in Cq value was detected. This suggests that Fiber 4 reached a saturation point in extracting template DNA from buffered aqueous solution at around 6 pg mL^{-1} .

To evaluate the effect of matrix components on DNA extraction using the PIL-based SPME approach, a complex sample matrix consisting of crude bacterial cell lysate was prepared by subjecting *E. coli* cells (approximately 8.12×10^8 cells) to alkaline lysis. Detailed procedures for cell cultures and cell lysis conditions are described in the Supporting Information. Template DNA

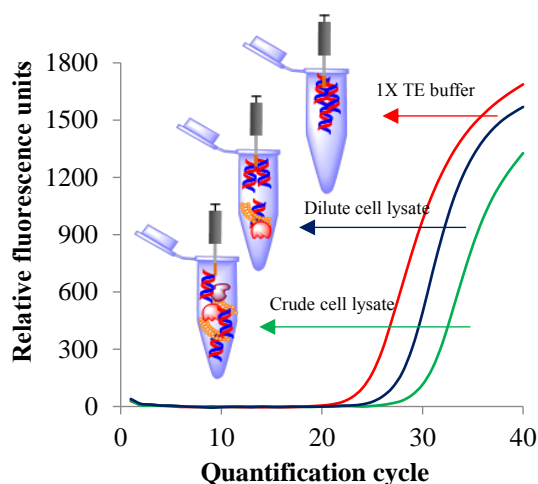


Figure 4. Representative qPCR amplification plot following PIL-based SPME using Fiber 4 from different sample matrices (A) 1X TE buffer (pH 8) (B) dilute *E. coli* cell lysate with 1X TE buffer in 1:0.5 ratio (C) *E. coli* crude cell lysate. Spiked 135 bp DNA concentration: 8 pg mL⁻¹; extraction time: 30 min; desorption time: 30 min; desorption solvent: 1 M NaCl; desorption solvent volume: 50 μL

was spiked at three concentration levels in crude cell lysate, dilute cell lysate, and an aqueous sample matrix, and subsequently extracted using Fiber 4. As shown in Table S1, DNA concentrations of 1, 4, and 8 pg mL⁻¹ in crude cell lysate samples yielded Cq values that were significantly higher than the corresponding aqueous sample solutions, indicating a strong matrix effect on DNA extraction. The DNA extraction performance of Fiber 4 was compared to a commercially available SPE kit, which provided Cq values of 18.31 ± 0.32 following the DNA extraction protocol described by the manufacturer. Nevertheless, a quantifiable amount of template DNA was extracted using SPME with good reproducibility in a process that did not require centrifugation or the use of organic solvent to extract DNA. In an effort to minimize the effect of the sample matrix, crude bacterial cell lysate samples were diluted with 1X TE buffer in a 1:0.5 ratio prior to DNA extraction. Figure 4 shows a comparison of the qPCR amplification plots following PIL-based SPME of the three studied sample matrices spiked with 8 pg mL⁻¹ template DNA. A significant increase in the amount of amplifiable DNA was

extracted following dilution of the crude bacterial cell lysate. Table S1 shows a similar increase in the amount of amplifiable DNA for all spike concentrations upon diluting the crude cell lysate with 1X TE buffer. Inter-day extraction reproducibility was evaluated at a spiked template DNA concentration of 8 pg mL⁻¹ in dilute cell lysate samples, resulting in Cq values with RSD of 2.9% (n = 6). As shown in Figure S17, to evaluate the quality of template DNA extracted from dilute cell lysate sample (spiked template DNA concentration of 8 pg mL⁻¹), a four-point calibration curve with two-fold dilution series was developed. The amplification efficiency and linearity of the calibration curve were found to be 100.2% and R² = 0.98, respectively. Furthermore, as shown in Figure S18, when a melting point analysis was performed on the qPCR amplified product following PIL-based SPME on the dilute cell lysate sample (spiked template DNA concentration 8 pg mL⁻¹), no significant variation in melting point was detected from the standard (1 pg mL⁻¹ in 1X TE buffer), indicating the quality of template DNA extracted from dilute cell lysate remains identical to the standard sample.

Encouraged by these results, the PIL-based SPME method was applied for the extraction of 6 kb pDNA containing a 135 bp DNA insert from the crude lysate of approximately 5.12×10⁷ *E. coli* cells. Detailed procedures for cell culture and lysis are described in the Supporting Information. It is worthwhile to mention that no amplification was observed after direct analysis of 1 μL of the crude cell lysate sample by qPCR. However, amplification was detected following PIL-based SPME of the bacterial cell lysate with a Cq value of 23.22 ± 0.32 (n = 3) as determined from the qPCR amplification plot, demonstrating the suitability of this technique for the extraction of DNA from complex samples.

After performing the aforementioned experiments as described in the previous sections (approximately 85 extractions), fiber reusability was investigated by determining the DNA

extraction capability in aqueous solution. The RSD of the C_q values obtained for triplicate extractions using the PIL-based SPME approach was 2.7%. Because of its simplicity, reusability, and portability, PIL-based SPME represents an alternative to existing technologies that require organic solvents and time-consuming centrifugation steps for DNA extraction, particularly in resource limited settings and field sampling applications.

Table 2. Features of PIL-based SPME and commercial SPE DNA extraction methods

Method	Quantification	Preparative applications	Organic solvent	Vacuum manifold/centrifugation	Reusability ^a	Sorbent
PIL-based SPME	Yes	No	Not required	Not required	~50 extractions	Tunable polymeric ionic liquid
SPE kit	Yes	Yes	Ethanol/isopropanol	Required	Not recommended	Silica

^a Extraction of DNA from bacterial cell lysate

7.4 Conclusion

As the nucleic acid field trends toward faster, more selective, and more portable analysis methods, a major bottleneck is represented by the lack of sample preparation techniques that satisfy these criteria. This study demonstrates, for the first time, the coupling of SPME with real-time qPCR for the analysis of DNA. By modifying the chemical composition of the PIL-based sorbent coating to include halide anions and polar groups in the cation component, the DNA extraction performance of the PIL-based method was enhanced relative to six other PILs and a commercial sorbent. The DNA extraction mechanism of the PIL sorbent coatings was investigated by incorporating a polymerizable anion component incapable of undergoing ion-exchange into the PIL fiber. The diminished DNA extraction performance of the PIL fiber

bearing polymerizable anions compared to PIL fibers with exchangeable anions established the importance of ion-exchange in the mechanism of DNA extraction by PIL sorbents. To evaluate the selectivity of the best performing PIL Fiber 4, DNA was extracted from aqueous solutions spiked with metal salts at concentrations higher than the qPCR minimum inhibitory concentration. Amplification was detectable for $\text{FeCl}_3 \cdot 6\text{H}_2\text{O}$ and $\text{CaCl}_2 \cdot 2\text{H}_2\text{O}$ concentrations as high as 180 μM and 700 mM, respectively, demonstrating the applicability of the PIL-based SPME method for DNA extraction from samples with high metal salt content (e.g., blood or milk samples). Furthermore, PIL-based SPME was applied for the extraction of DNA from bacterial cell lysate, where the isolated DNA was of sufficient quantity and purity for high efficiency amplification in qPCR. The results demonstrate that PIL-based SPME constitutes a selective and portable nucleic acid extraction technique that can be readily interfaced with qPCR for the rapid and sensitive analysis of DNA.

Acknowledgements

The authors acknowledge funding from Chemical Measurement and Imaging Program at the National Science Foundation (Grant number CHE-1413199).

Supporting information

Figures S1-S17, Table S1, materials and fabrication procedures for preparing PIL fibers, conditions for cell cultures and lysis protocols are provided in Appendix F.

References

1. Lofton-Day, C.; Model, F.; DeVos, T.; Tetzner, R.; Distler, J.; Schuster, M.; Song, X.; Lesche, R.; Liebenberg, V.; Ebert, M. *Clin. Chem.* **2008**, 54, 414-423.
2. Jobling, M. A.; Gill, P. *Nat. Rev. Genet.* **2004**, 5, 739-751.
3. Garrouste-Orgeas, M.; Chevret, S.; Arlet, G.; Marie, O.; Rouveau, M.; Popoff, N.; Schlemmer, B. *Am. J. Respir. Crit. Care Med.* **1997**, 156, 1647-1655.

4. Dwivedi, H. P.; Jaykus, L.-A. *Crit. Rev. Microbiol.* **2011**, 37, 40-63.
5. Rossen, L.; Nørskov, P.; Holmstrøm, K.; Rasmussen, O. F. *Int. J. Food. Microbiol.* **1992**, 17, 37-45.
6. Al-Soud, W. A.; Rådström, P. *J. Clin. Microbiol.* **2001**, 39, 485-493.
7. Li, W.; Hartung, J. S.; Levy, L. *J. Microbiol. Methods* **2006**, 66, 104-115.
8. Wilson, I. G. *Appl. Environ. Microbiol.* **1997**, 63, 3741.
9. Demeke, T.; Jenkins, G. R. *Anal. Bioanal. Chem.* **2010**, 396, 1977-1990.
10. Rimola, A.; Costa, D.; Sodupe, M.; Lambert, J.-F.; Ugliengo, P. *Chem. Rev.* **2013**, 113, 4216-4313.
11. Löffler, J.; Hebart, H.; Schumacher, U.; Reitze, H.; Einsele, H. *J. Clin. Microbiol.* **1997**, 35, 3311-3312.
12. Arthur, C. L.; Pawliszyn, J. *Anal. Chem.* **1990**, 62, 2145-2148.
13. Chai, M.; Pawliszyn, J. *Environ. Sci. Technol.* **1995**, 29, 693-701.
14. Kataoka, H.; Saito, K. *J. Pharm. Biomed. Anal.* **2011**, 54, 926-950.
15. Vuckovic, D.; Risticovic, S.; Pawliszyn, J. *Angew. Chem. Int. Ed.* **2011**, 50, 5618-5628.
16. Hallett, J. P.; Welton, T. *Chem. Rev.* **2011**, 111, 3508-3576.
17. Vijayaraghavan, R.; Izgorodin, A.; Ganesh, V.; Surianarayanan, M.; MacFarlane, D. R. *Angew. Chem. Int. Ed.* **2010**, 49, 1631-1633.
18. Tateishi-Karimata, H.; Nakano, M.; Sugimoto, N. *Sci. Rep.* **2014**, 4, 3593.
19. Nishimura, N.; Nomura, Y.; Nakamura, N.; Ohno, H. *Biomaterials* **2005**, 26, 5558-5563.
20. Shi, Y.; Liu, Y.-L.; Lai, P.-Y.; Tseng, M.-C.; Tseng, M.-J.; Li, Y.; Chu, Y.-H. *Chem Commun.* **2012**, 48, 5325-5327.
21. YauáLi, S. F. *Analyst* **2003**, 128, 37-41.
22. Wang, J.-H.; Cheng, D.-H.; Chen, X.-W.; Du, Z.; Fang, Z.-L. *Anal. Chem.* **2007**, 79, 620-625.
23. Li, T.; Joshi, M. D.; Ronning, D. R.; Anderson, J. L. *J. Chromatogr. A* **2013**, 1272, 8-14.
24. Clark, K. D.; Nacham, O.; Yu, H.; Li, T.; Yamsek, M. M.; Ronning, D. R.; Anderson, J. L. *Anal. Chem.* **2015**, 87, 1552-1559.

25. Yu, H.; Ho, T. D.; Anderson, J. L. *Trends Anal. Chem.* **2013**, 45, 219-232.
26. Wang, X.; Xing, L.; Shu, Y.; Chen, X.; Wang, J. *Anal. Chim. Acta* **2014**, 837, 64-69.
27. Nacham, O.; Clark, K. D.; Anderson, J. L. *Anal. Methods* **2015**, 7, 7202-7207.
28. Valasek, M. A.; Repa, J. J. *Adv. Physiol. Ed.* **2005**, 29, 151-159.
29. Heid, C. A.; Stevens, J.; Livak, K. J.; Williams, P. M. *Genome Res.* **1996**, 6, 986-994.
30. Ginzinger, D. G. *Exp. Hematol.* **2002**, 30, 503-512.
31. Baltazar, Q. Q.; Chandawalla, J.; Sawyer, K.; Anderson, J. L. *Colloids and Surf. A: Physicochem. Eng. Asp.* **2007**, 302, 150-156.
32. Zhao, F.; Meng, Y.; Anderson, J. L. *J. Chromatogr. A* **2008**, 1208, 1-9.
33. Feng, J.; Sun, M.; Xu, L.; Wang, S.; Liu, X.; Jiang, S. *J. Chromatogr. A* **2012**, 1268, 16-21.
34. Purohit, H. J.; Kapley, A.; Moharikar, A. A.; Narde, G. *J. Microbiol. Methods* **2003**, 52, 315-323.
35. Gates, K. S. *Chem. Res. Toxicol.* **2009**, 22, 1747-1760.
36. Zoltewicz, J. A.; Clark, D. F.; Sharpless, T. W.; Grahe, G. *J. Am. Chem. Soc.* **1970**, 92, 1741-1750.
37. Bickley, J.; Short, J.; McDowell, D.; Parkes, H. *Lett. Appl. Microbiol.* **1996**, 22, 153-158.

CHAPTER 8**RAPID AND SELECTIVE RNA ANALYSIS BY SOLID-PHASE
MICROEXTRACTION**

(Manuscript in preparation)

Omprakash Nacham, Kevin D. Clark, Marcelino Varona, and Jared L. Anderson

Abstract

In this study, a solid-phase microextraction (SPME) method was developed for purification of messenger RNA (mRNA) from complex biological samples. The real-time reverse transcription quantitative polymerase chain reaction (RT-qPCR) assay was employed to quantify the amount of mRNA extracted by SPME devices. Of all studied SPME sorbent coatings, the PIL sorbent phase containing carboxylic acid groups within IL monomer and halide-based anions extracted the highest amount of mRNA, whereas the native PA fiber demonstrated the lowest extraction efficiency. On basis of RT-qPCR data, electrostatic interactions and an ion-exchange mechanism between negatively charged phosphate backbone of RNA and PIL cation framework are major driving force for mRNA extraction. The optimized PIL-based SPME method purified a high quantity of mRNA from crude yeast cell lysate compared to phenol/chloroform liquid liquid extraction (LLE) method. The reusability and robustness of PIL-based SPME toward RNA analysis represent as significant advantage over conventional silica-based solid-phase RNA extraction kits. The selectivity of SPME method toward mRNA was enhanced by functionalization of PA sorbent surface with oligo dT₂₀ using carbodimide-based amide linker chemistry. A fluorescein (FAM)-based microplate fluorescence was developed to determine the amount of oligo dT₂₀ immobilized on surface of PA sorbent coating. In comparison to native PA sorbent coating, an approximately 1000-fold

higher mass of mRNA extracted by oligo dT₂₀ modified PA sorbent coating. In addition, the modified PA sorbent coating extracted sufficient quantity of mRNA from total RNA at concentrations as low as 5 ng μL^{-1} in aqueous solutions without the use of organic solvents or time-consuming multiple centrifugation steps that are essential for LLE and SPE procedures.

8.1 Introduction

The analysis of ribonucleic acid (RNA) is an essential component of gene expression studies and disease prognosis in biomedical applications. Analytical techniques including Northern blotting,¹ ribonuclease protection assays,² and real-time reverse transcription quantitative polymerase chain reaction (RT-qPCR)³ are commonly employed for the detection and quantification of messenger RNA (mRNA). However, the co-extraction of proteins, phospholipids, or chemically similar DNA from biological sources results in poor method accuracy, irreproducible measurements, or may inhibit mRNA assays altogether.⁴ When combined with the complexity of detecting low abundance mRNA transcripts, the purification and preconcentration of mRNA represents a major bottleneck in the bioanalytical workflow.

Traditional approaches to RNA purification involve liquid-liquid extraction (LLE) with phenol-chloroform and rely on the differential partitioning of RNA and contaminants between an aqueous phase and organic layer. Although there are numerous variations of LLE that utilize surfactant additives, chaotropic salts, or enzymes to improve yields/purity of RNA extracts, the excessive use of organic solvent, time-consuming centrifugation procedures, and multiple sample transfer steps are significant drawbacks to this classical method. To decrease analysis time and reduce organic solvent consumption, solid phase extraction (SPE) methods were developed that rely on the reversible binding of RNA to a silica-based sorbent. The solid matrix can also be functionalized with oligo deoxythymine (dT) for the specific capture of mRNA

from total RNA samples *via* hybridization with the naturally occurring 3' polyadenylated tails of mRNA.⁵ However, SPE relies heavily on centrifugation or applied vacuum to flow the sample over the sorbent material making this method difficult to automate and unsuitable for point-of-care diagnostics. Furthermore, the extraction media provided in commercial SPE kits are not recommended for reuse, dramatically increasing the cost of analyzing multiple samples. From point-of-care diagnostics to high-throughput laboratories, the limitations of LLE and SPE are unsustainable and require the development of new sample preparation techniques to facilitate rapid, selective, and sensitive mRNA analysis.

Solid-phase microextraction (SPME) is a solvent-free, non-exhaustive sample preparation technique that utilizes a thin layer of sorbent material immobilized on a solid support.⁶ In SPME, target molecules are extracted from a sample solution or headspace and subsequently desorbed from the SPME sorbent under appropriate conditions prior to chemical analysis. By combining sampling and sample preparation into a single step, SPME represents a convenient approach to speed up analysis times without compromising the sensitivity of the method. SPME has been employed for the extraction and quantification of peptides,⁷ drug substances,⁸ and metabolites⁹ *in vitro* and *in vivo* to provide insight toward biological systems. The partitioning of analytes in SPME is inextricably related to the chemical composition of the sorbent material. Polymeric ionic liquids (PILs) consist of readily interchangeable cations/anions with polymerizable groups that have recently been investigated as sorbents for the extraction and analysis of DNA.^{10, 11} The PIL-based SPME method was capable of preconcentrating DNA from complex biological sample matrices for analysis by qPCR amplification.¹² Owing to the tunability of the sorbent, reusable extraction device, and centrifuge-free experimental setup, the PIL-based SPME approach addressed several important

shortcomings of existing DNA sample preparation methods. Contrary to DNA, RNA is chemically less stable and highly susceptible to enzymatic degradation.¹³ In addition to purification challenges, RNA quantification is not straightforward and involves multi-step protocols (e.g., reverse transcription and qPCR) that increase the overall complexity of the analysis. Given the success of SPME toward DNA analysis, the development of SPME-based purification technologies for RNA has following advantages: (1) unlike silica-based extraction media, the chemical composition of PIL-based sorbent phases can be readily customized to enhance the RNA extraction performance; (2) since electrostatic and ion-exchange interactions are the major driving forces for RNA extraction, the use of toxic organic solvents, chaotropic salts, and alcohols (known PCR inhibitors) can be eliminated; (3) PIL sorbent coatings are resistant to harsh chemical conditions that would otherwise degrade contemporary silica-based sorbents and can be easily regenerated by exposing the PIL to high ionic strength solutions; (4) owing to its simplicity and portability, SPME-based RNA purification platforms are highly suitable for field sampling and point-of-care diagnostic applications.

To our knowledge, this study constitutes the first report in the development and application of a SPME approach that is coupled to RT-qPCR for selective mRNA analysis from crude yeast cell lysate. The chemical composition of the SPME sorbent coatings including PILs and poly acrylate (PA) were optimized for efficient mRNA extraction. Under similar experimental conditions, the PIL sorbent phase comprised of polar functional groups (carboxylic acids) within IL monomers and halide-based anions extracted the highest amount of mRNA compared to the other studied sorbent phases. Electrostatic interactions and an ion-exchange mechanism between the negatively charged phosphate backbone of RNA and the PIL sorbent phases played a crucial in mRNA extraction. The selectivity of the SPME approach towards

mRNA analysis was enhanced by modifying the surface of a PA sorbent coating with oligo dT₂₀ using carbodiimide-based amide linker chemistry.¹⁴ A fluorescein (FAM)-based microplate fluorescence assay was developed to determine the amount of oligo dT₂₀ that immobilized on the surface of PA sorbent phase. Owing to hybridization between oligo dT₂₀ and the poly A tail of mRNA, an approximately 1000-fold higher mass of mRNA was extracted by oligo dT₂₀ modified-PA sorbent coating compared to an unmodified PA fiber. The mRNA extraction performance of the oligo dT₂₀-modified PA sorbent coating was compared with a commercial spin column-based SPE extraction kit. The developed SPME sorbent coatings demonstrated significant potential for the purification of mRNA from total RNA and yeast cell lysate samples. The results show that SPME-based RNA sample preparation provides a complementary approach to existing RNA purification methodologies and is particularly compatible with field sampling and point-of-care diagnostic applications.

8.2 Experimental

8.2.1 Real-time Reverse Transcription Quantitative PCR Assays. RNA analysis *via* real-time reverse transcription quantitative PCR (RT-qPCR) is a combination of two steps: (1) messenger RNA (mRNA) is first converted into complementary DNA (cDNA) utilizing RNA-dependent DNA polymerase at optimal isothermal conditions and (2) the obtained cDNA is then amplified using qPCR. The RT-qPCR assays employed for evaluating the mRNA extraction performance of SPME fibers were performed according to previously reported procedures with minor modifications.¹⁵ Prior to generation of an external calibration curve, RT and qPCR steps were optimized separately. RT reactions were performed according to the following protocol: initial denaturation step of 5 min at 65 °C, followed by annealing of reverse primers (specific to beta-actin mRNA) at 4 °C for 10 min. The reaction temperature was then

increased to 45 °C and held for 1 h to synthesize cDNA of beta-actin mRNA utilizing SuperScript III reverse transcriptase. The cDNA from the RT reaction was analyzed using real-time quantitative PCR (qPCR) with a CFX96 Touch Real-Time PCR Detection System from Bio-Rad Laboratories (Hercules, CA, USA). The following thermal cycling protocol was employed for qPCR analysis: initial denaturation step of 5 min at 95.0 °C, followed by 40 cycles of 15 sec at 95.0 °C and 30 sec at 67.0 °C. All amplification reactions were performed in triplicate. For each reaction, 1 µL of RT products were mixed with 19 µL of a reaction mixture consisting of 10 µL of SsoAdvanced Universal SYBR Green supermix (2x), 0.6 µL of 10 µM forward and reverse primers, and 7.8 µL of deionized water. For the external calibration curve, an additional 75 mM and 15 mM NaCl was included in RT and qPCR steps, respectively. The quantification cycle (C_q) values obtained for amplification of beta-actin cDNA were used to indicate the amount of mRNA extracted by SPME fibers. All of the mRNA samples used in this study were treated with DNase I at 37 °C for 1 h to eliminate genomic DNA contamination and mRNA was subsequently purified via isopropyl alcohol precipitation. Relevant control experiments to detect the genomic DNA and mRNA/cDNA contamination with RT-qPCR reagents were performed prior to mRNA quantification.

A six-point external calibration curve with a five-fold dilution series (mass of mRNA varied from 1400 to 0.5 pg) was developed to quantify the amount of mRNA extracted by the SPME devices (Figure S1). The RT-qPCR amplification efficiency was calculated using Equation 1, where the slope is the slope of the linear regression within the calibration curve. The amplification efficiency of the beta-actin RT-qPCR assay was found to be 105.1%. Following RT-qPCR analysis, the amplification specificity and presence of primer dimers responsible for false positives were determined using high resolution melting point analysis.

8.2.2 Isolation and Purification of mRNA Using SPME Devices. Figure 1 shows the schematic workflow of SPME-based RNA analysis using RT-qPCR. Aqueous solutions (100 μL) of purified yeast mRNA ($0.1 \text{ ng } \mu\text{L}^{-1}$) were used to examine the applicability of SPME for RNA analysis. The mRNA was extracted by immersing the SPME fiber in the sample solution followed by a desorption step in NaCl to facilitate recovery of the nucleic acid from the sorbent coating. A 3 μL aliquot of the desorption solution was subjected to RT to generate cDNA from beta-actin mRNA using gene specific primers. An aliquot of RT products (4 μL) was used for qPCR amplification, resulting in a final NaCl concentration of 15 mM. Prior to subsequent extractions, the PIL sorbent coating was washed in 100 mM NaOH (100 μL) for 10 min. The chemical composition of the sorbent coating was regenerated by soaking in 2 M NaCl solution for 20 min.

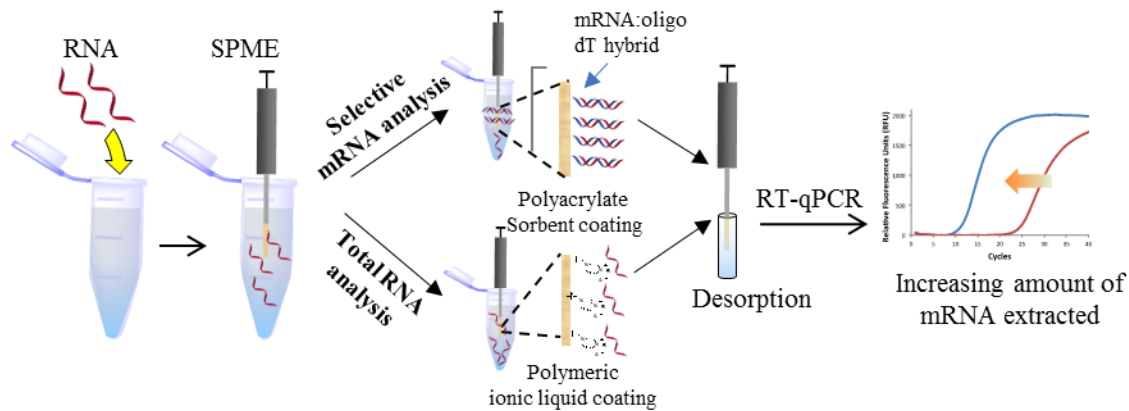


Figure 1. Schematic illustration of RNA analysis using the SPME approach coupled with reverse transcription quantitative polymerase chain reaction (RT-qPCR).

For the extraction of mRNA from total RNA, varying amounts (250 to 2000 ng) of total RNA were spiked into a 100 μL aqueous solution and PIL-based SPME was performed as described above. For extraction of mRNA from yeast cell lysate, approximately 3.0×10^7 *S. cerevisiae* cells (strain BY4735) were suspended in 400 μL of deionized water containing 0.25

g of acid washed glass beads. After vortexing the mixture for 10 min, 200 μ L of the crude cell lysate suspension was added to 200 μ L of deionized water and subjected to PIL-based SPME.

8.2.3 Functionalization of PA Fibers with Amine Linked Oligo dT₂₀. To enhance the selectivity of mRNA analysis, the surface carboxylic acid groups of the PA sorbent coating were modified with amine terminated oligo dT₂₀ via carbodiimide-based amide linker chemistry using reported procedures from literature.¹⁴ Briefly, the PA sorbent coating was soaked in 2 mL of 2-(N-morpholino)ethanesulfonic acid (MES) buffer (pH: 6.2) at room temperature for 6 h. Then the washed PA sorbent coating was exposed to EDC/NHS solution (100 mM EDC and 200 mM NHS in MES buffer) at room temperature for 2 h under agitation at 650 rpm. Subsequently, the NHS ester-functionalized sorbent coating was reacted with 0.5 mM of 5'-/5AmMC12/dT₂₀-3' in 0.1 M sodium carbonate buffer (pH: 9.0; 30 μ L) at room temperature for 12 h. Finally, the oligo dT₂₀ functionalized PA sorbent coatings were washed several times with deionized water and stored in MES buffer at 4.0 °C for future use.

8.2.4 Determination of Oligo dT₂₀ Loading on PA Fiber Using Microplate Fluorescence Assay. A schematic depicting the fluorescein (FAM)-based microplate fluorescence assay used for the determination of the amount of oligo dT₂₀ immobilized onto the PA sorbent coating is illustrated in Figure S2. Subsequent to the EDC/NHS activation step (conditions described above), the PA fiber was subjected to the aminolysis reaction using a fluorophore tagged amine linked oligo dT₂₀ (5'-/5AmMC12/dT₂₀/36-FAM/-3') in 30 μ L of sodium carbonate buffer (pH: 9.0) overnight at room temperature. The FAM-tagged sorbent coating was then washed several times with deionized water (5 x 2 mL) for 12 h to remove adsorbed or unreacted FAM-labeled oligo dT₂₀. Subsequently, the oligo dT₂₀-modified PA sorbent coating was incubated in 100 μ L of aqueous solution containing 10 μ L of 10X DNase buffer and 2 μ L of DNase I (1 U/ μ L)

for 2 h. DNase I nonspecifically cleaves the phosphodiester bonds between dT bases to produce di- and trinucleotide products with FAM tags that are released into solution from the surface of the fiber. Finally, an aliquot of the DNase I reaction products was analyzed by a microplate reader to collect the emitted fluorescence from FAM tags (FAM excitation/emission: 480/525 nm) as shown in Figure S6. The fluorescence from the DNase I reaction is correlated to the mass of amine terminated oligo dT₂₀ that was covalently attached to the PA sorbent coating and was calculated using an external calibration curve as shown in Figure S3 of supplemental information of Appendix G.

8.3 Results and Discussion

8.3.1 Investigating the Applicability of SPME for RNA Analysis. To understand the important structural features of sorbent coatings that can enhance the extraction of mRNA, a variety of SPME sorbent phases were investigated including PILs (see structures and combinations in Figure 2A) and a commercially available PA sorbent phase. The fabrication of PIL-based SPME devices was performed using procedures previously reported in the literature.¹⁶ The mRNA extraction performance of the different SPME sorbent coatings was evaluated by RT-qPCR of beta-actin mRNA from *S. cerevisiae*. Following SPME, an aliquot of NaCl desorption solution (1 M; total volume: 50 μ L) containing mRNA was subjected to RT for cDNA synthesis using beta-actin gene specific primers. Then, an aliquot of RT products was used for a qPCR assay to amplify the beta-actin cDNA. Given that the quantity of cDNA determined by qPCR is proportional to the amount of mRNA extracted by the sorbent coating and subjected to RT, a lower C_q value from the qPCR assay indicates that a high amount of mRNA was extracted. When the qPCR amplification efficiency is 100%, a difference of one C_q value between two different samples indicates a two-fold difference in the amount of

template cDNA. As shown in Figure 2B, the amount of mRNA extracted by the native PA fiber was not determined since the Cq values were higher than the calibration range, suggesting poor mRNA extraction capabilities of the sorbent coating. Recently, our group and other have exploited the unique extraction properties of PILs for DNA analysis.^{10, 11} Although the chemical stability and molecular structure of RNA differs from DNA, it is reasonable to conceive that electrostatic interactions between the negatively charged phosphate back bone of RNA and the PIL cation framework may contribute to mRNA extraction. In order to identify important structural features of the PIL sorbent coating that can aid in RNA analysis, IL monomers substituted with different functional groups and crosslinkers were prepared, as shown in Figure 2A. The effect of the PIL anion on RNA extraction performance was examined using fibers containing the same cationic composition with halide anions (Fiber **2**) and bis[(trifluoromethyl)sulfonyl]imide [NTf₂⁻] anions (Fiber **3**). IL monomers and crosslinkers used in the fabrication of PIL-based SPME were synthesized and characterized using ¹H NMR according to reported procedures from the literature.^{16, 17}

Figure 2B shows the mRNA extraction performance of all PIL fibers and a commercial PA fiber employed in this study. From Figure 2, the amount mRNA extracted by the PIL sorbent coatings (Fiber **1** to **4**) was significantly higher than the PA sorbent coating, suggesting that electrostatic interactions between sorbent coating and RNA molecules are crucial for extraction. Among fibers with the same crosslinker composition (Fibers **1**, **2**, and **4**), the incorporation of carboxylic acid groups within the IL monomer (Fiber **2**) provided a higher extraction performance than Fiber **1** and **4**. For example, the average Cq value of Fiber **1** was 31.07 ± 1.04 , whereas Fiber **2** extracted a higher quantity of mRNA with Cq values of 28.92 ± 0.2 .

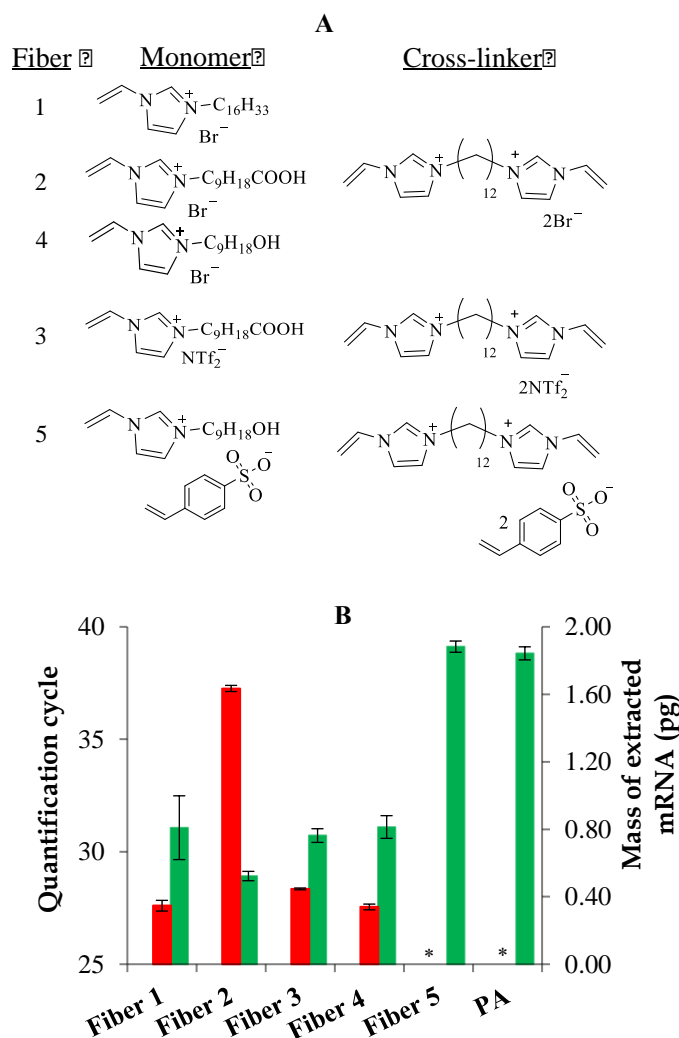


Figure 2. (A) Chemical composition of PIL-based SPME sorbent coatings examined in this study; (B) Effects of sorbent coating composition on mRNA extraction. Concentration of mRNA: $0.1 \text{ ng } \mu\text{L}^{-1}$; sample solution: deionized water ($100 \text{ } \mu\text{L}$); desorption time: 30 min; extraction time: 10 min; desorption solvent: 1 M NaCl; desorption solvent volume: $50 \text{ } \mu\text{L}$; (■) represents quantification cycles; (■) denotes mass of extracted mRNA. Extractions were performed in triplicate ($n = 3$). *Mass of mRNA extracted by PIL Fibers 5 and a commercial polyacrylate fiber was not determined as the Cq values obtained were out of the calibration range.

The replacement of halide anions (Fiber 2) with $[\text{NTf}_2^-]$ anions (Fiber 3) resulted in a 2.18 cycle increase in the Cq value, indicating a dramatic decrease in mRNA extraction performance. This demonstrates that anions within the sorbent coating playing a significant role in enhancing the mRNA extraction performance.

In addition to electrostatic interactions, the ion-exchange mechanism between anions of the PIL sorbent coating and the negatively charged phosphate backbone of mRNA may also contribute to extraction (as previously observed for DNA extraction).^{10, 12} To test this hypothesis, a non-exchangeable styrenesulfonate anion component was incorporated into the PIL sorbent coating (Fiber 5). Previous studies demonstrated that co-polymerization of p-styrenesulfonate anions with PIL cation moieties provided a stable sorbent phase that was incapable of undergoing anion exchange in high ionic strength solutions (30% w/v NaCl).¹⁸ The lack of ion-exchange mechanism for the p-styrenesulfonate-based PIL sorbent coatings was confirmed by determining the sulfur composition of the PIL sorbent phase by elemental analysis. Figure 2 shows that the amount of mRNA extracted by Fiber 5 was significantly lower than all other PIL-based sorbent coatings (Fiber 1 to 4), indicating that an ion-exchange mechanism plays a significant role in mRNA extraction by PIL sorbent coatings.

8.3.2 Optimization of Extraction and Desorption Parameters for PIL-based SPME.

Because of its high extraction performance and good reproducibility (0.7 % RSD for C_q values) compared to other PIL fibers, Fiber 2 was employed for optimization studies. The effects of NaCl concentration on mRNA recovery was evaluated prior to optimization of extraction conditions. As shown in Figure S4, the amount of mRNA recovered from the PIL sorbent coating at a constant desorption time of 30 min increased as the NaCl concentration was increased from 0 to 500 mM. However, beyond 500 mM, no significant enhancement in mRNA recoveries were observed. A 3 μ L desorption solution (500 mM NaCl) was used for RT-qPCR analysis, corresponding to 75 mM and 15 mM of NaCl in RT and qPCR steps, respectively. At higher volumes of desorption solution (>75 mM NaCl in RT), the reproducibility of the RT-qPCR assay was severely compromised (data not shown).

The reusability of the PIL-based SPME device constitutes an important advantage in the purification of RNA samples in comparison to the expensive, single-use commercial silica-based SPE kits. In an effort to minimize carry-over for the SPME method, a 10 min washing step using 100 μ L of 10 mM NaOH (pH 10-11) was employed to remove residual RNA from the PIL sorbent coating (Fiber **2**) by well-established base-catalyzed RNA hydrolysis.¹⁹ Since PILs can undergo ion-exchange interactions in high ionic strength solutions,¹⁸ the sorbent coating was subsequently regenerated by exposure to a 2 M NaCl solution (500 μ L) for 20 min. Figure S5 shows representative RT-qPCR plots for wash fractions prior to the next extraction as well as the desorption fraction following extraction of mRNA using the regenerated sorbent coating (Fiber **2**). These results demonstrate the chemical resistance of the sorbent coating towards harsh pH conditions as well as the reusability of PIL-based SPME devices for RNA analysis.

The sorption-time profile of Fiber **2** was evaluated by varying the extraction time from 5 to 60 min under agitation at 80 rpm using an orbital shaker. From Figure S6, the amount of mRNA extracted by the PIL sorbent coating was dramatically increased from 5 to 45 min, but no obvious improvement in extraction was observed from 45 to 60 min. Although the highest amount of mRNA was extracted at 45 min, an extraction time of 30 min was chosen for all subsequent experiments in order to minimize the overall analysis time.

Under optimized extraction conditions, the fiber-to-fiber reproducibility Fiber **2** was evaluated (using three fibers of Fiber **2**) and resulted in C_q values with a RSD of 3.2%.

8.3.3 Extraction of mRNA from Total RNA Samples and Yeast Cell Lysate. Total RNA is comprised of a pool of different RNA molecules in a cell (e.g., mRNA, ribosomal RNA, transfer RNA). In a typical eukaryotic cell, the quantity of mRNA ranges from 1-2% of the

total RNA.²⁰ The ability of PIL-based SPME to isolate mRNA from total RNA was investigated by spiking varying amounts of total RNA in aqueous solutions over a concentration range typically employed for direct RT-qPCR assays (2.5 to 20 ng/ μ L). As shown in Figure S7, the amount of mRNA extracted by Fiber 2 was extremely small at 2.5 and 5.0 ng/ μ L of total RNA and the obtained C_q values were out of the calibration range. This could be either due to the low amount of mRNA available for extraction or high interference from background total RNA. By increasing the amount of total RNA from 5 to 10 ng/ μ L, a drastic improvement in extraction performance was observed.

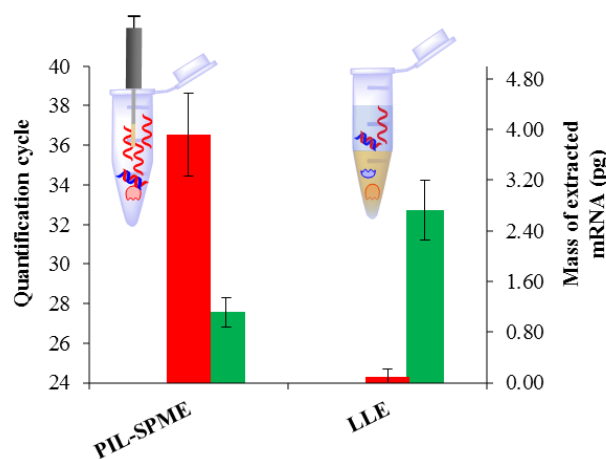


Figure 3. Extraction of mRNA from yeast cell lysate samples using PIL-based SPME (Fiber 2) and phenol/chloroform LLE approaches (n = 3). Approximate number of *S. cerevisiae* cells used for extraction: 3×10^7 cells; (■) represents quantification cycles; (■) denotes mass of extracted mRNA.

However, no significant enhancement in extraction was observed beyond 15 ng/ μ L of total RNA, suggesting a strong effect of background RNA on mRNA extraction. It is important to note that the RNA concentration range where PIL-based SPME can be operated is at least one order of magnitude lower than what is typically used for direct RT-qPCR analysis. Encouraged by these results, the applicability of PIL-based SPME was also investigated for its ability to isolate beta-actin mRNA from the crude lysate of approximately 3.0×10^7 *S. cerevisiae* cells.

The PIL-based SPME method was also compared with a conventional phenol/chloroform liquid liquid extraction (LLE) method. As shown in Figure 3, the amount of mRNA extracted using PIL-based SPME (average Cq value: 27.56 ± 0.75) was significantly higher than the phenol/chloroform LLE method (average Cq value: 32.72 ± 1.51), with superior reproducibility indicated by the lower standard deviation in Cq values. The results demonstrate that the PIL-based SPME method constitutes a simple, faster, and reusable platform that does not require organic solvent or centrifugation for mRNA purification that is anticipated to be highly useful in resource limited settings and high-throughput laboratories.

8.3.4 Selective mRNA Extraction Using Oligo dT₂₀-Modified PA Fiber. Efficient and rapid isolation of mRNA is crucial in the field of genomics, clinical microbiology, and pathology. The functionalization of extraction media with oligo dT₂₀ (poly T tail) that can specifically hybridize with poly A tail of mRNA molecules represents the most common strategy employed in selective mRNA analysis. Methacrylate-based porous polymers, functionalized cellulose powders, and carboxylic acid grafted magnetic beads are few examples of solid-phase substrates that utilized oligo dT:mRNA hybridization approach for the purification of mRNA from complex sample matrices. The development of PIL sorbent coatings for selective mRNA analysis in the presence of total RNA would be challenging due to the nonspecific interactions between total RNA and the PIL sorbent coating (on basis of data from Figure S7) that may result in difficulty quantifying low abundance mRNA samples.

In an attempt to reduce the interference from background total RNA as well as to improve the selectivity of the sorbent coating toward mRNA, the PA sorbent coating was selected for oligo dT₂₀ modification. Since the PA sorbent phase lacks ion-exchange and electrostatic interactions with mRNA molecules (on basis of data from Figure 2B), these types of

interactions between the PA fiber and total RNA may also be minimal and result in reduced interference for mRNA extraction. Importantly, the presence of carboxylate functional groups in the acrylate polymer matrix makes them suitable substrates for oligo dT₂₀ modification *via* carbodiimide-based amide linker chemistry.

Figure 4 shows the comparison of RT-qPCR amplification plots following SPME of aqueous mRNA samples using oligo dT₂₀-modified and unmodified PA fibers (detailed experimental procedures are provided in Supporting Information). The high mRNA extraction performance exhibited by the modified PA fiber (average C_q value: 33.74 ± 0.24 ; $n = 3$) compared to the unmodified PA fiber (C_q value: 39.14) could be due to hybridization between the poly A tail of mRNA and oligo dT₂₀.

It is worthwhile to mention that the concentration range investigated to demonstrate the selectivity of SPME device for mRNA was approximately four-fold lower than what was reported in previous studies.¹⁵ Encouraged by these results, the selectivity of modified PA sorbent coating toward mRNA was also examined in the presence of total RNA (5.0 ng/ μ L in 100 μ L deionized water) and subsequently its extraction performance was compared against a commercial SPE kit. On the basis of RT-qPCR analysis (Figure S8), the average C_q value obtained for modified PA sorbent coating was 32.67 ± 1.31 ($n = 3$), whereas a commercial SPE kit provided a C_q value of 28.93 (triplicate experiments were not performed since the extraction media is not reusable according to manufacturer's guidelines).

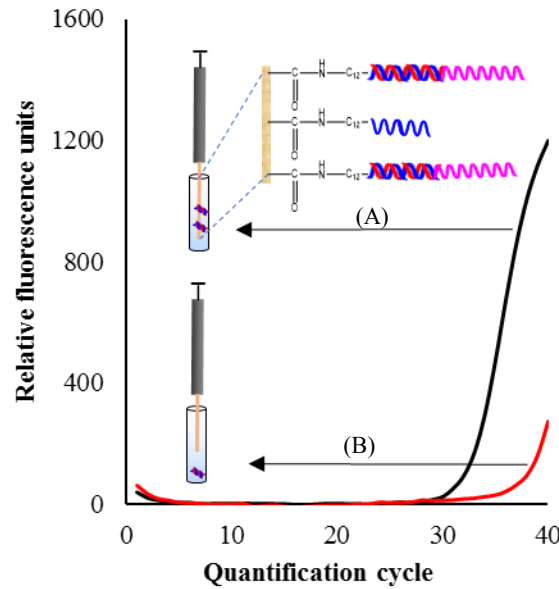


Figure 4. Representative RT-qPCR amplification plot following extraction of mRNA using (A) oligo dT₂₀-modified PA fiber (B) unmodified PA fiber. Extractions were performed in triplicate (n = 3); concentration of mRNA: 0.1 ng μL^{-1} ; sample solution: 100 μL deionized water containing 100 mM NaCl; desorption solvent: 30 μL deionized water. (~~~~~) oligo dT₂₀ complementary to poly A tail of mRNA; (~~~~) mRNA with poly A tail.

The low C_q value of the commercial SPE kit indicates that a high mass of mRNA was extracted when compared to modified PA sorbent coating. Nevertheless, the modified PA-based SPME method preconcentrated the sufficient quantity and quality of mRNA for RT-qPCR assay with low analysis time and minimal experimental setup (i.e., without the use of centrifugation apparatus, binding buffers and elution buffers essential for SPE kits). Furthermore, the oligo dT₂₀ modified PA-based SPME method was applied for the extraction of mRNA from crude cell lysate of approximately 3.5×10^7 *S. cerevisiae* cells. The developed method yielded a C_q value of 26.12 ± 1.21 (n = 3), demonstrating its capability to extract sufficient quantity and quality of mRNA from complex sample matrices. High resolution melting point analysis was performed on the RT-qPCR products to confirm the amplification specificity and purity of the extracted mRNA, as shown in Figure S9 in supplemental information of Appendix G.

The fiber-to-fiber reproducibility of 5'-/5AmMC12/dT₂₀-3' loading on PA fibers was examined using a microplate fluorescence assay (Figure S2). Based on the fluorescence assay, approximately 40.39 and 25.34 ng of oligo dT₂₀ was immobilized on two different PA fibers, indicating a significant difference in their surface composition. This could be due to lot to lot variation in the production of PA fibers, which can result in a difference in the amount of surface acid groups available for the aminolysis reaction. Ongoing studies in our lab are focused on developing new carboxylic acid-based SPME sorbent coatings within a non-ionic polymer matrix in an effort to minimize nonspecific interactions with background total RNA that can potentially address the challenges associated with the commercial PA fiber.

8.4 Conclusions

The feasibility of SPME-based RNA purification methodology was investigated using a variety of sorbent coatings. The structural tunability of PILs enabled to optimize the chemical composition of extraction phase. As a result, the mRNA extraction performance was significantly improved. The optimized PIL-based SPME method demonstrated superior performance in extracting mRNA from crude yeast cell lysate samples compared to phenol/chloroform LLE. The reusability and chemical stability of PIL sorbent coatings constitute an important advantage over expensive and single-use commercial silica-based SPE kits. The selectivity of SPME toward mRNA was enhanced by exploiting oligo dT:mRNA hybridization approach. The modified-PA based SPME method demonstrated its capability to isolate mRNA for RT-qPCR analysis from low quantities of total RNA samples with low analysis time and minimal experimental setup compared to commercial SPE kits.

Acknowledgements

The authors acknowledge funding from Chemical Measurement and Imaging Program at the National Science Foundation (Grant number CHE-1413199).

Supporting information

Figures S1-S7, materials and measurements, preparation of total RNA and messenger RNA samples, preconcentration of mRNA using oligo dT₂₀ modified-PA fibers are provided in Appendix G.

References

1. Alwine, J. C.; Kemp, D. J.; Stark, G. R., *Proc. Natl. Acad. Sci. USA* **1977**, 74, 5350-5354.
2. Gilman, M., *Current protocols in molecular biology* **1993**, 4.7. 1-4.7. 8.
3. Schmittgen, T. D.; Livak, K. J., *Nat. Protoc.* **2008**, 3, 1101-1108.
4. Fleige, S.; Pfaffl, M. W., *Mol. Aspects. Med.* **2006**, 27, 126-139.
5. Wen, J.; Legendre, L. A.; Bienvenue, J. M.; Landers, J. P., *Anal. Chem.* **2008**, 80, 6472-6479.
6. Arthur, C. L.; Pawliszyn, J., *Anal. Chem.* **1990**, 62, 2145-2148.
7. Wang, Y.; Schneider, B. B.; Covey, T. R.; Pawliszyn, J., *Anal. Chem.* **2005**, 77, 8095-8101.
8. Goryński, K.; Kiedrowicz, A.; Bojko, B., *J. Pharm. Biomed. Anal.* **2016**, 127, 147-155.
9. Vuckovic, D.; de Lannoy, I.; Gien, B.; Shirey, R. E.; Sidisky, L. M.; Dutta, S.; Pawliszyn, J., *Angew. Chem., Int. Ed.*, **2011**, 50, 5344-5348.
10. Wang, X.; Xing, L.; Shu, Y.; Chen, X.; Wang, J., *Anal. Chim. Acta* **2014**, 837, 64-69.
11. Nacham, O.; Clark, K. D.; Anderson, J. L., *Anal. Methods* **2015**, 7, 7202-7207.
12. Nacham, O.; Clark, K. D.; Anderson, J. L., *Anal. Chem.* **2016**, 88, 7813-7820.
13. Rogacs, A.; Qu, Y.; Santiago, J. G., *Anal. Chem.* **2012**, 84, 5858-5863.

14. Wang, C.; Yan, Q.; Liu, H.-B.; Zhou, X.-H.; Xiao, S.-J., *Langmuir* **2011**, 27, 12058-12068.
15. Nestorova, G. G.; Hasenstein, K.; Nguyen, N.; DeCoster, M. A.; Crews, N. D. *Lab Chip* **2017**, 17, 1128-1136.
16. Ho, T. D.; Toledo, B. R.; Hantao, L. W.; Anderson, J. L., *Anal. Chim. Acta* **2014**, 843, 18-26.
17. Baltazar, Q. Q.; Chandawalla, J.; Sawyer, K.; Anderson, J. L., *Colloid Surf. A* **2007**, 302, 150-156.
18. Feng, J.; Sun, M.; Xu, L.; Wang, S.; Liu, X.; Jiang, S., *J. Chromatogr. A* **2012**, 1268, 16-21.
19. Oivanen, M.; Kuusela, S.; Lönnberg, H., *Chem. Rev.* **1998**, 98, 961-990.
20. Iyer, V.; Struhl, K. *Proc. Natl. Acad. Sci. USA*, **1996**, 93, (11), 5208-5212.

CHAPTER 9

GENERAL CONCLUSIONS

The first part of dissertation describes the different synthetic methodologies applied for the preparation of hydrophobic MILs. The low aqueous solubility as well as high paramagnetic susceptibility is an important prerequisite for application of MILs in LLEs. Three different classes of hydrophobic MILs with different cation motifs including monocationic, dicationic, and tricationic MILs with $[\text{FeCl}_3\text{Br}^-]$ anions were synthesized. Within these MILs, the incorporation of long hydrocarbon chains, benzyl groups, and perfluoroalkyl moieties significantly increased their hydrophobicity. The multicationic framework of MILs provided the opportunity to control the physicochemical and paramagnetic properties of resulting MILs. The cation asymmetry and chemical properties of anions ($[\text{NTf}_2^-]$) played a crucial in regulating the melting point of resulting MILs. Tricationic imidazolium-based MILs containing three $[\text{FeCl}_3\text{Br}^-]$ anions exhibited an effective magnetic moment (μ_{eff}) as high as 11.76 Bohr magneton (μ_B), representing the highest magnetic moments ever reported for MILs. The functionalization of imidazolium cations with carboxyl ligands that can chelate iron (III) centers enabled to produce a new class of hydrophobic MILs. In contrast to conventional magnetoactive anion-based MILs ($[\text{FeCl}_3\text{Br}^-]$), carboxylate-based MILs provide the opportunity to incorporate task-specific anions such as $[\text{NTf}_2^-]$ into the resulting MILs. In particular, this strategy has potential to impart dual functionality to MILs. The developed MILs were insoluble in aqueous solutions at concentrations as low as 0.1% w/v and provided sufficient paramagnetic susceptibilities to control their molecular motion using an external magnetic field (1T). Consequently, few of those developed hydrophobic MILs (with low viscosity and high hydrophobicity) were employed in dispersive liquid liquid microextractions.

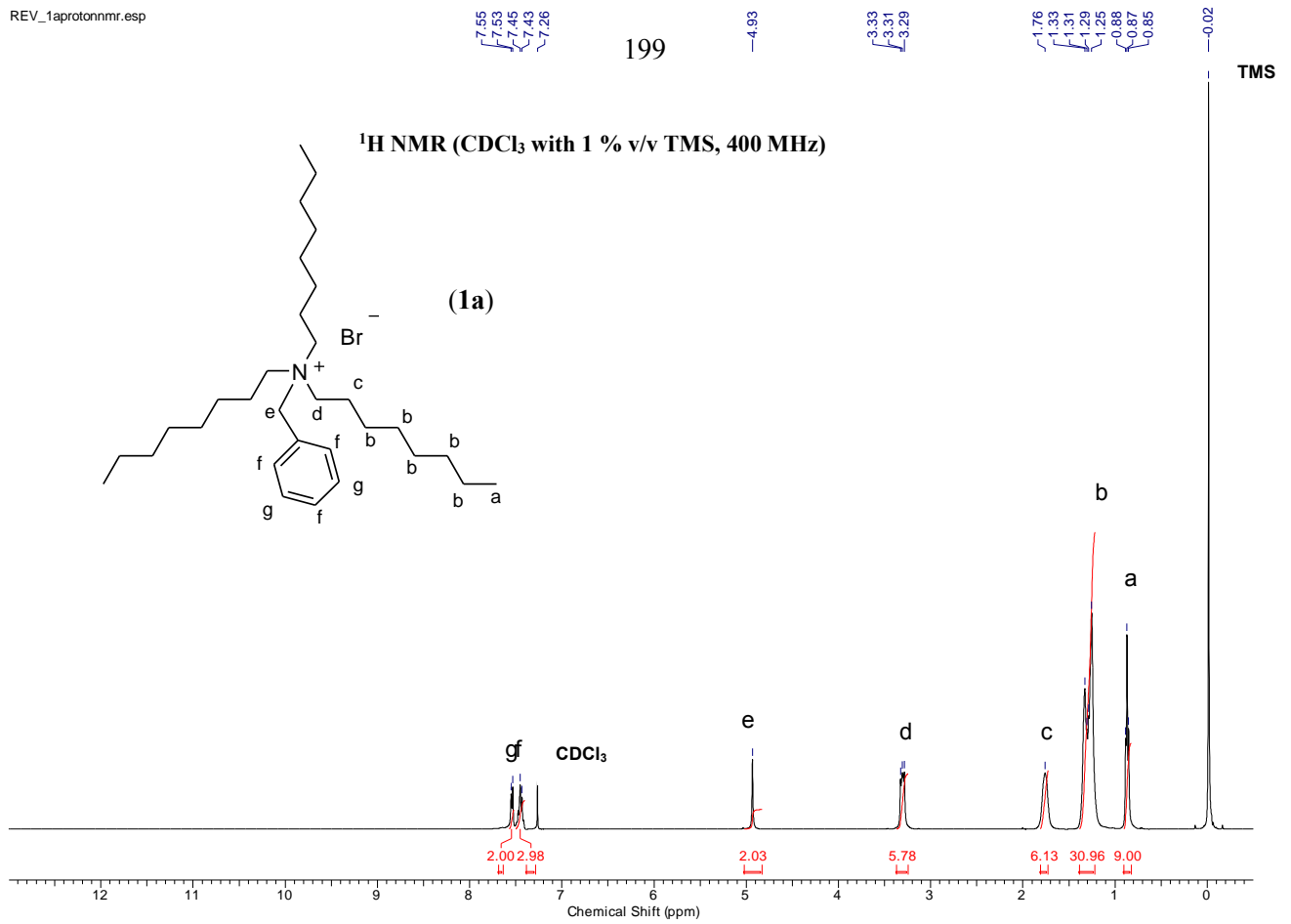
The second part of the dissertation describes the surface active and bulk aggregation properties of two different classes of IL-based surfactants in aqueous solutions. The interfacial and micellar properties of IL-based surfactants were investigated using fluorescence spectroscopy, conductometry, and surface tensiometry techniques. The CMC values of selected IL-based surfactants showed a good correlation between the different measurement techniques. Similar to conventional cationic surfactants, the CMC values and surface adsorption (e.g., pC_{20} and CMC/C_{20}) properties are affected in the presence of added inorganic and organic salts. The CMC values of tricationic surfactants are found to decrease by increasing the concentration of sodium salts in aqueous solutions. In addition, the effects of acetonitrile content on the stability of dicationic and tricationic surfactants were examined. The presence of acetonitrile in IL-based surfactant solutions tends to destabilize the IL micelles. As a result, high CMC values were observed compared to neat solutions.

The third part of dissertation describes the application of ILs as HS-GC diluents for the analysis of residual solvents in APIs. Owing to their high thermal stability and low vapor pressure at room temperatures, IL-based diluents enabled to perform the HS-GC analysis of residual solvents at relatively high temperatures as well as low extraction times. The analytical performance of IL ([BMIM][NTf₂]) was evaluated by determining the reproducibility, linearity and, accuracy of the method. The applicability of the developed method was investigated by spiking different level of residual solvents in selected APIs, and thereby the recovery studies were performed to evaluate the matrix effect on the method. At optimized HS-GC parameters, IL-based method yielded higher sensitivities, require low amount of sample, and provided better throughput than conventional organic solvent (N-methylpyrrolidone, NMP)-based residual solvent methods.

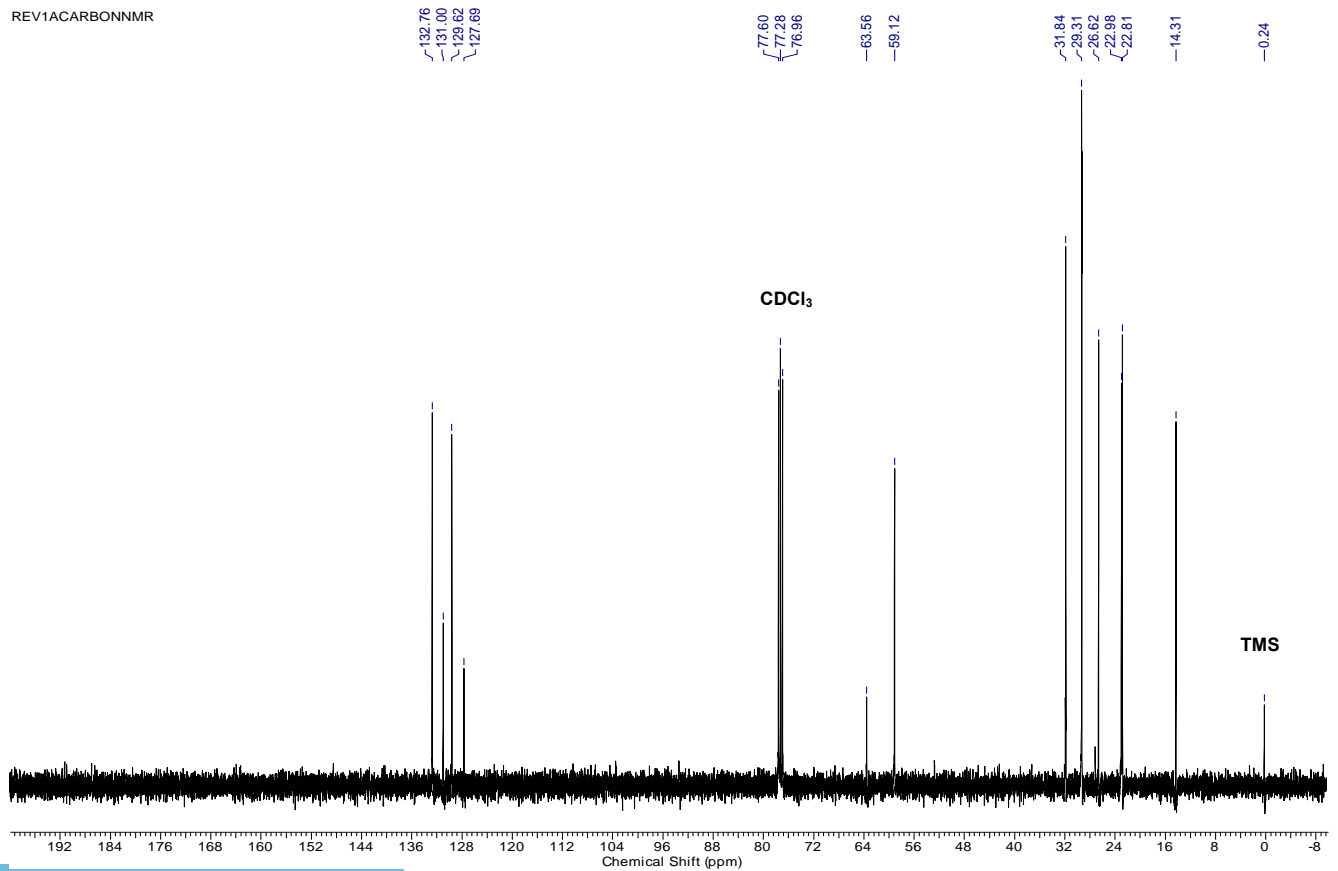
The last part of dissertation describes the SPME of nucleic acids using a range of sorbent coatings including PILs and commercial poly acrylate. Electrostatic interactions between negatively charged phosphate groups of DNA and cation component of ILs are major driving force for DNA extraction by ILs. On basis of this principle, PILs have been developed as sorbent coatings for nucleic acid analysis. The core advantage of PILs relies on the ability to tailor their chemical composition to enhance the nucleic acid extraction. The reusability and resistance toward harsh pH conditions of PIL sorbent coatings constitute an important advantage compared to silica-based SPE kits for nucleic acid purifications. A PIL-based SPME method was applied for the analysis of DNA and RNA from complex sample matrices. The chemical composition of PIL sorbent coatings was optimized to enhance the extraction performance. The PIL-based SPME method was coupled with endpoint PCR, qPCR, and RT-qPCR amplification techniques for analysis of purified nucleic acids. The optimized PIL-sorbent coating featuring carboxylic acid within IL monomer and halide-based anions provided the highest amount DNA/mRNA for downstream applications compared to analogous PIL sorbent coatings. In addition, the PIL-based SPME method extracted sufficient quality and quantity of nucleic acids from bacterial and yeast cell lysate samples without the use of organic solvents and time-consuming centrifugation apparatus. This could be due to their unique mechanism of extraction. Furthermore, the selectivity of SPME device toward mRNA was enhanced by functionalization of PA sorbent coating surface with oligo dT₂₀, which can specifically hybridize with poly A tail of mRNA molecules.

Since SPME is a non-exhaustive sample preparation technique, the mass of nucleic acid extracted by SPME devices was considerably lower than exhaustive SPE platforms. Nevertheless, the simplicity, portability, as well as reusability aspects of SPME are highly useful in resource limited and field sampling applications.

APPENDIX A
SUPPORTING INFORMATION ACCOMPANYING
CHAPTER 2



REV1ACARBONNMR



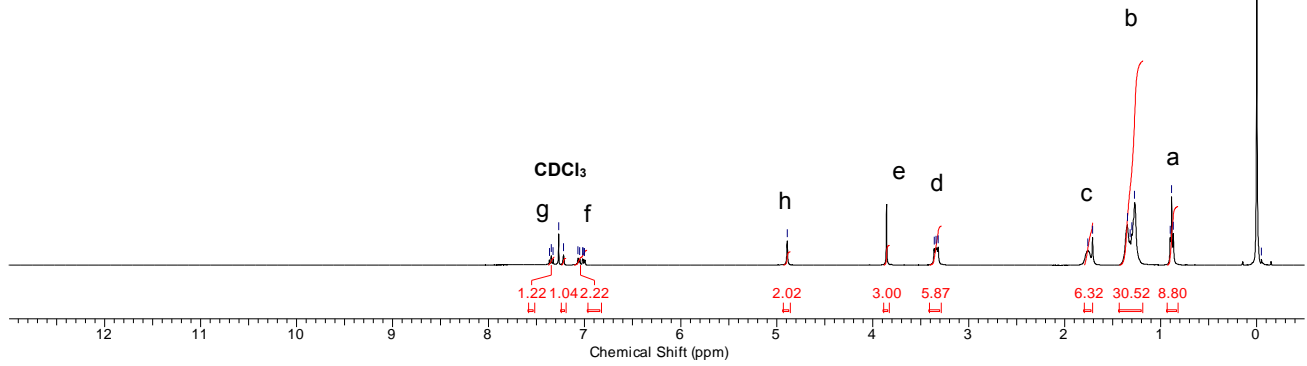
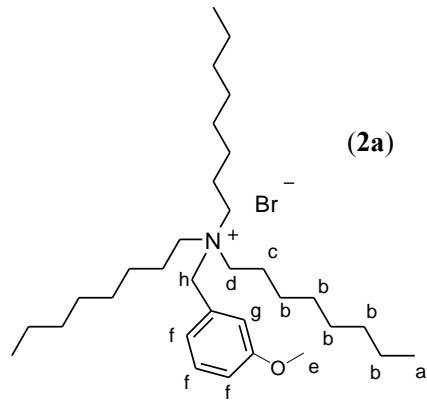
7.37
7.35
7.33
7.27
7.22
7.07
7.05
7.02

200

-4.89

-3.86
-3.36
-3.34
-3.32-1.76
-1.71
-1.35
-1.32
-1.30
-1.27
-0.90
-0.89
-0.87-0.00
-0.05¹H NMR (CDCl₃ with 1 % v/v TMS, 400 MHz)

TMS



METHOXYBNTRIC8X2CARBON

-160.43

-130.62

-129.05

-124.61

-118.43

-116.71

77.67

77.35

77.04

-63.62

-59.28

-56.05

31.93

29.41

29.38

29.28

27.16

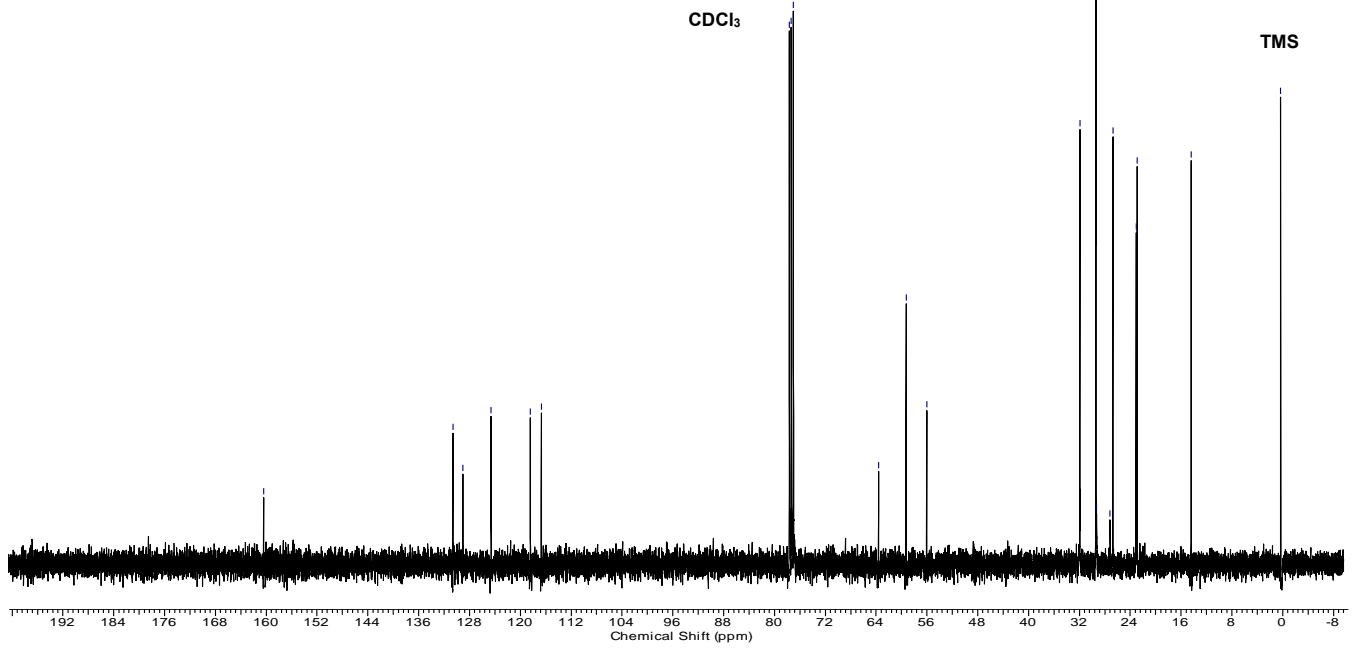
26.72

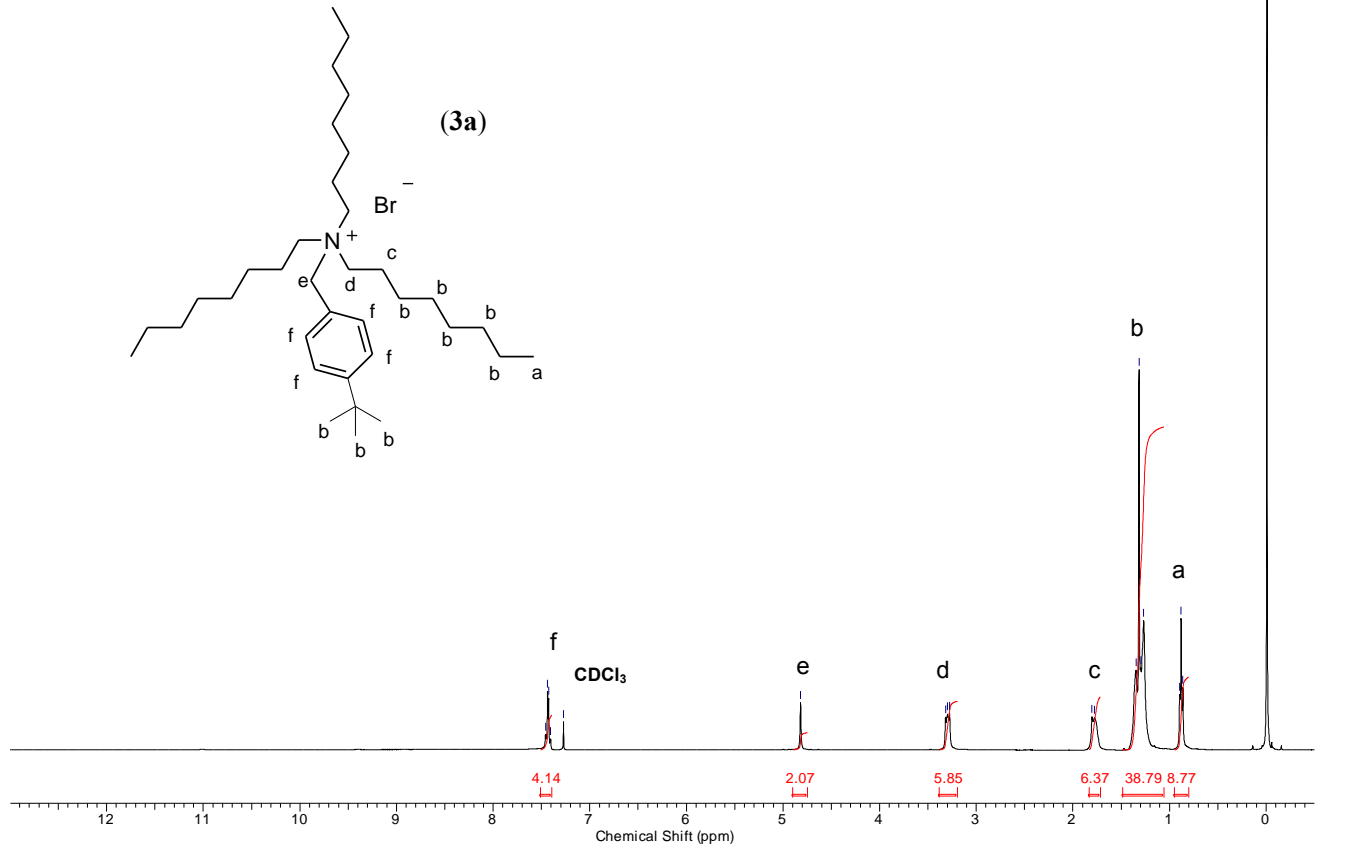
23.08

22.90

-14.41

-0.32



^1H NMR (CDCl_3 with 1 % v/v TMS, 400 MHz)

TBUNTRIC8BRX2CARBON

-154.50

-132.38

-126.61

-124.33

77.57

77.26

76.94

-63.12

-58.86

35.11

31.87

31.36

23.36

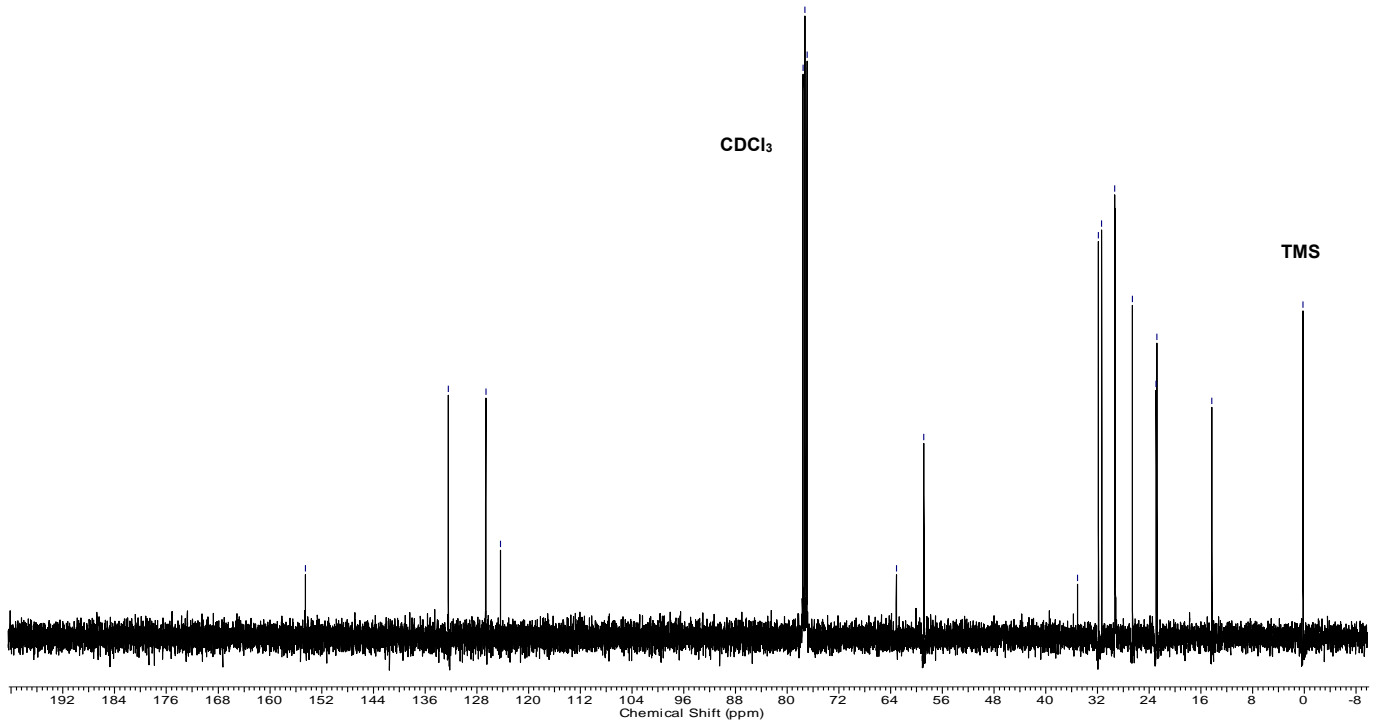
26.62

22.94

22.81

-14.32

-0.24

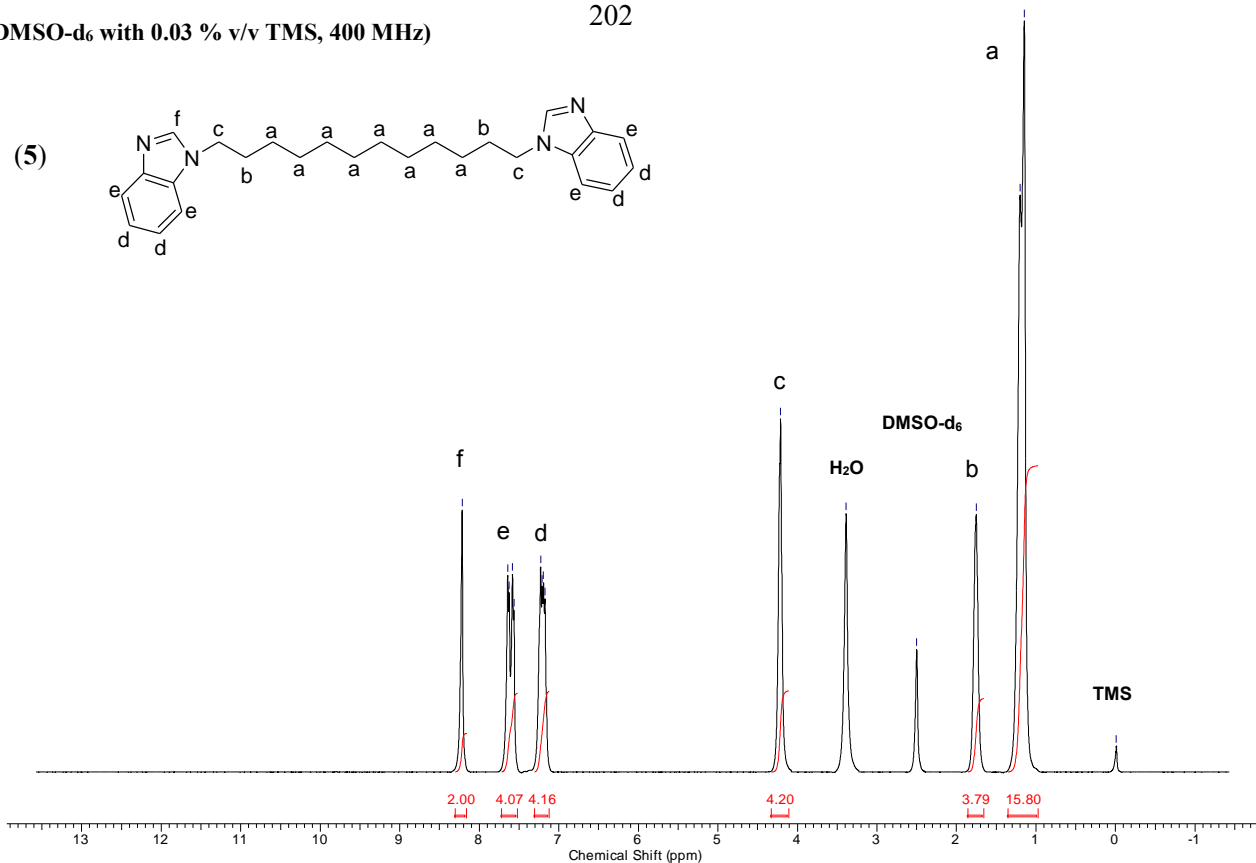
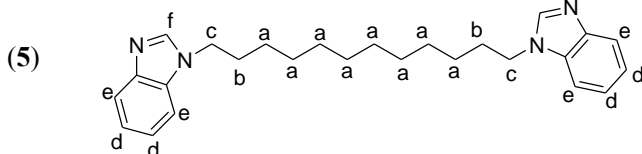


8.22
7.64
7.62
7.58
7.56
7.23
7.21
7.19
7.17

4.21
3.39
2.50
1.75
1.20
1.15
0.01

¹H NMR (DMSO-d₆ with 0.03 % v/v TMS, 400 MHz)

202



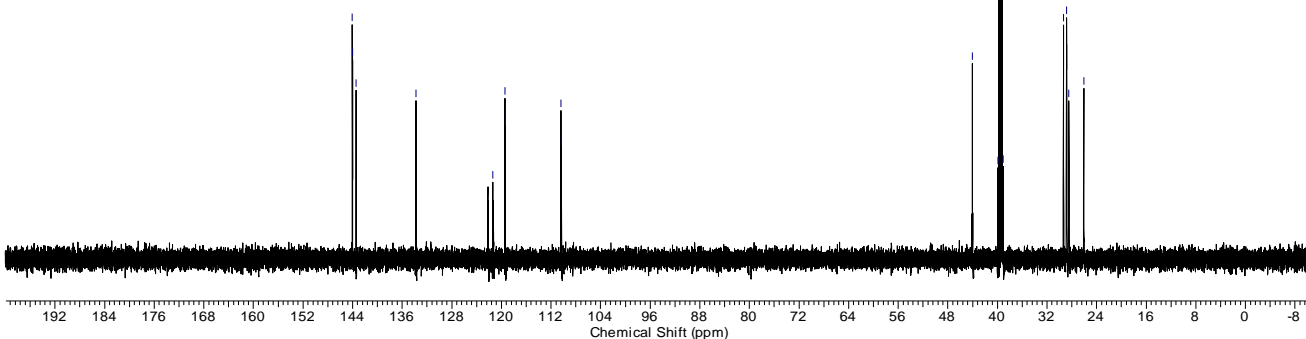
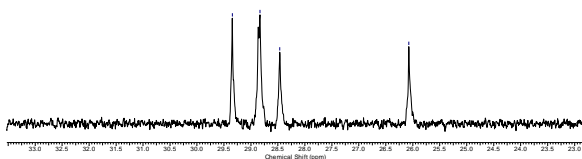
DMLSTEP1BENIMIDAZOLEDODECYLLINKERC13

144.64
144.61
143.46
133.78
121.38
119.45
119.38
110.41
110.32

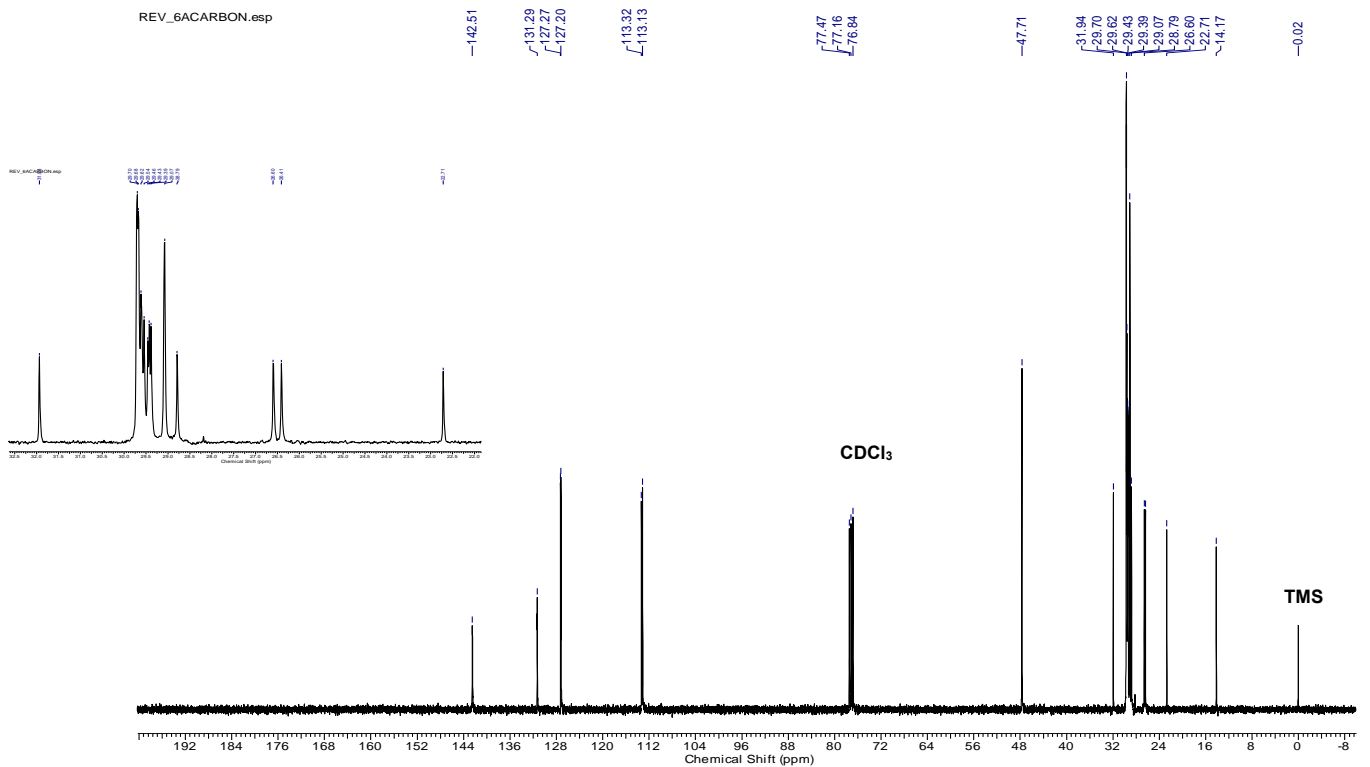
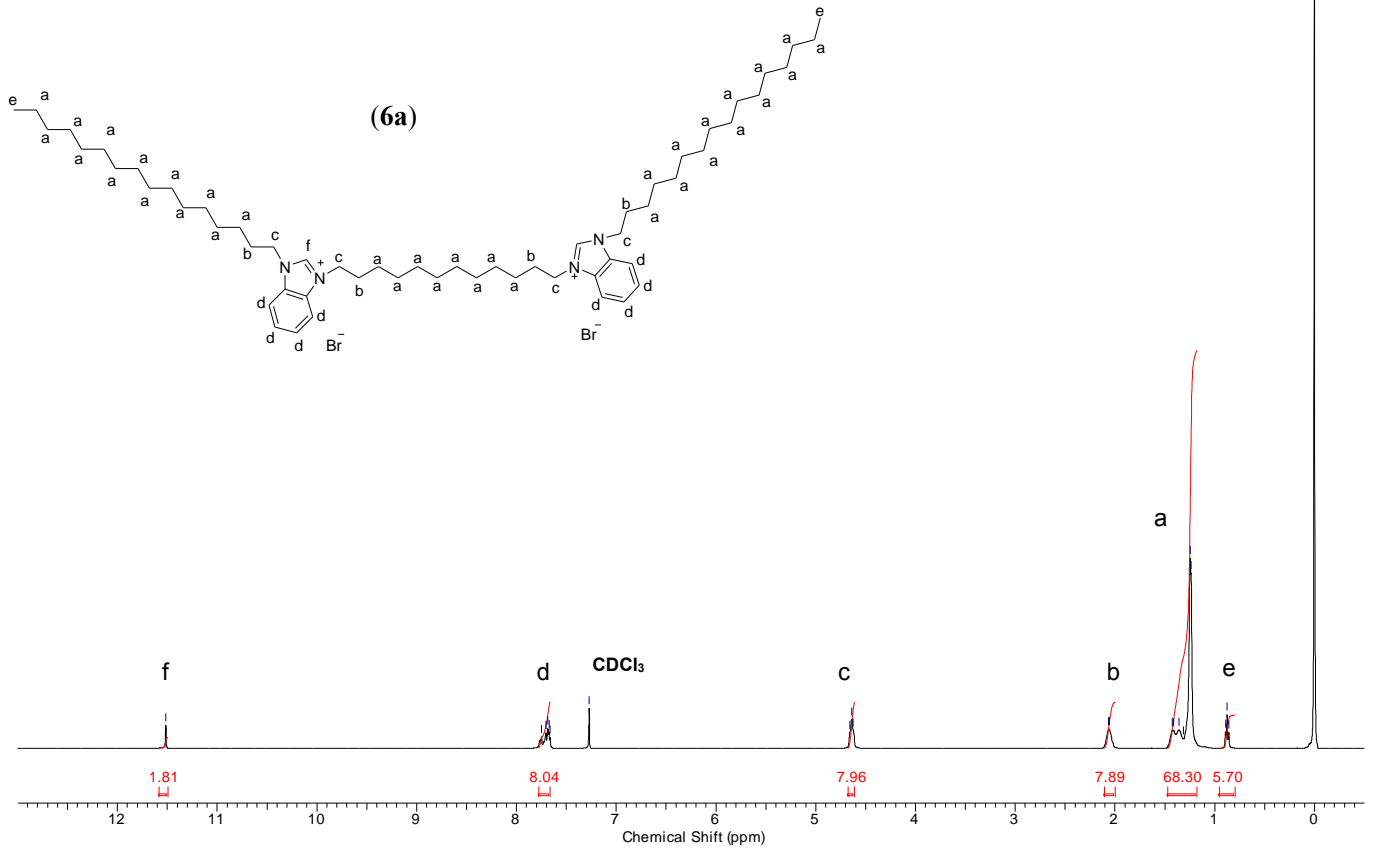
44.04
39.91
39.78
39.64
39.50
39.36
39.22
39.08
29.35
28.83
28.47
26.07

DMLSTEP1BENIMIDAZOLEDODECYLLINKERC13NMR

29.35
28.83
28.47
26.07



¹H NMR (CDCl₃ with 1 % v/v TMS, 400 MHz)



REV_COMPOUND6BPROCESS.ESP

-9.49

7.78
7.73
7.71
7.71
7.70
7.274.51
4.49
4.47

-2.00

-1.38

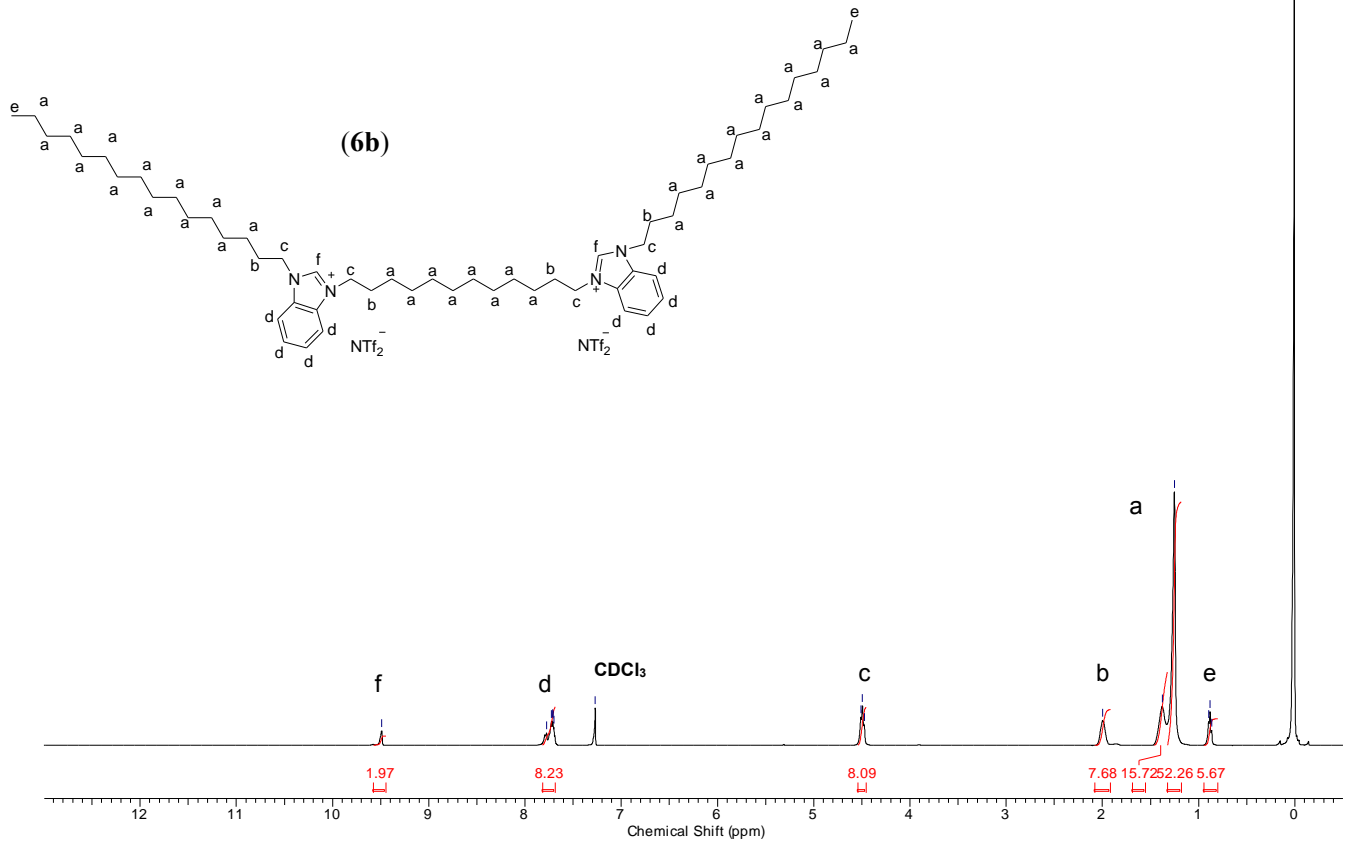
-1.25

-0.90

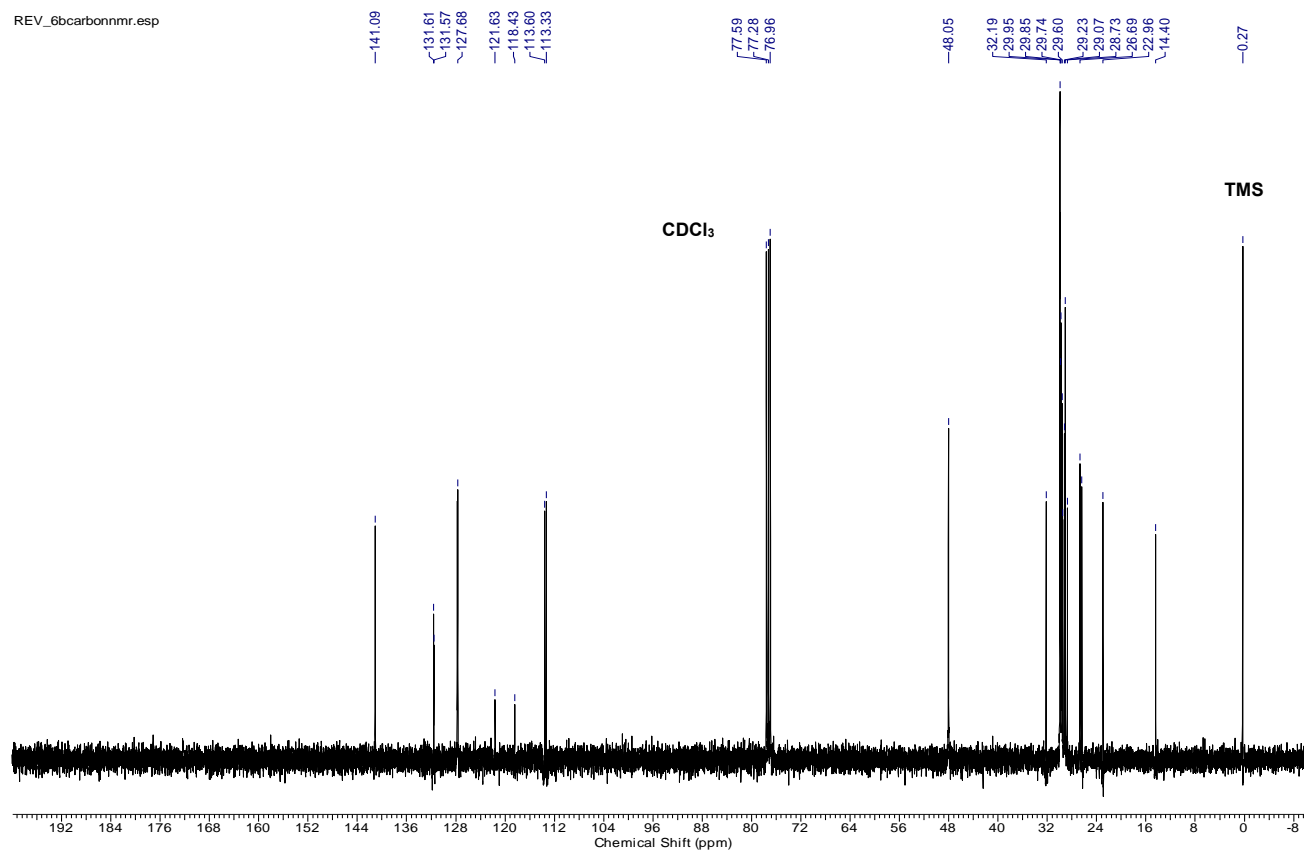
-0.88

-0.86

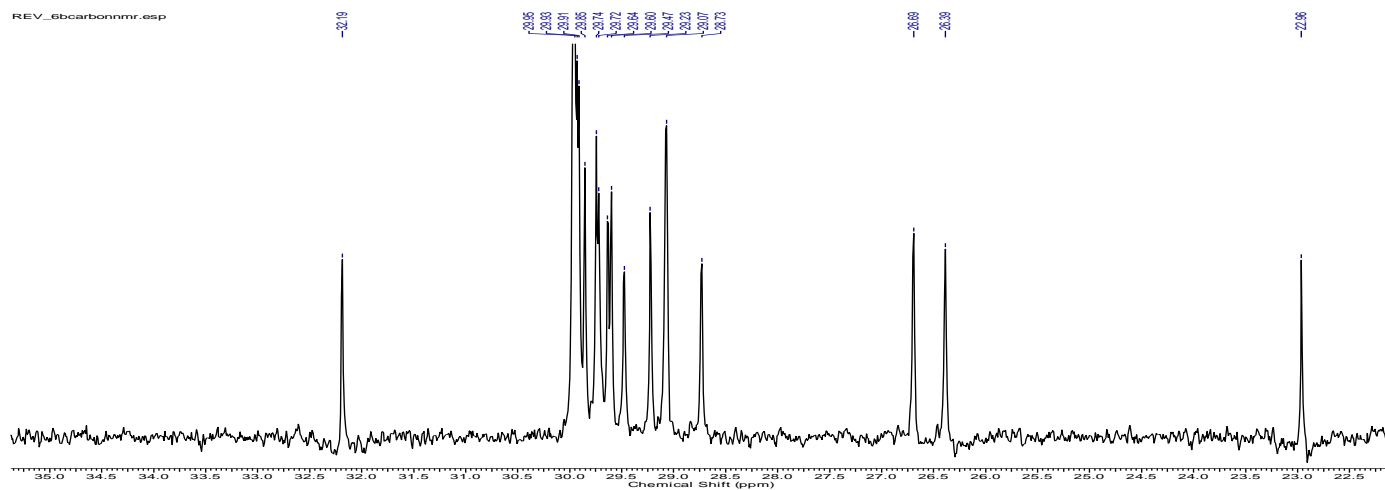
-0.01

¹H NMR (CDCl₃ with 1 % v/v TMS, 400 MHz)

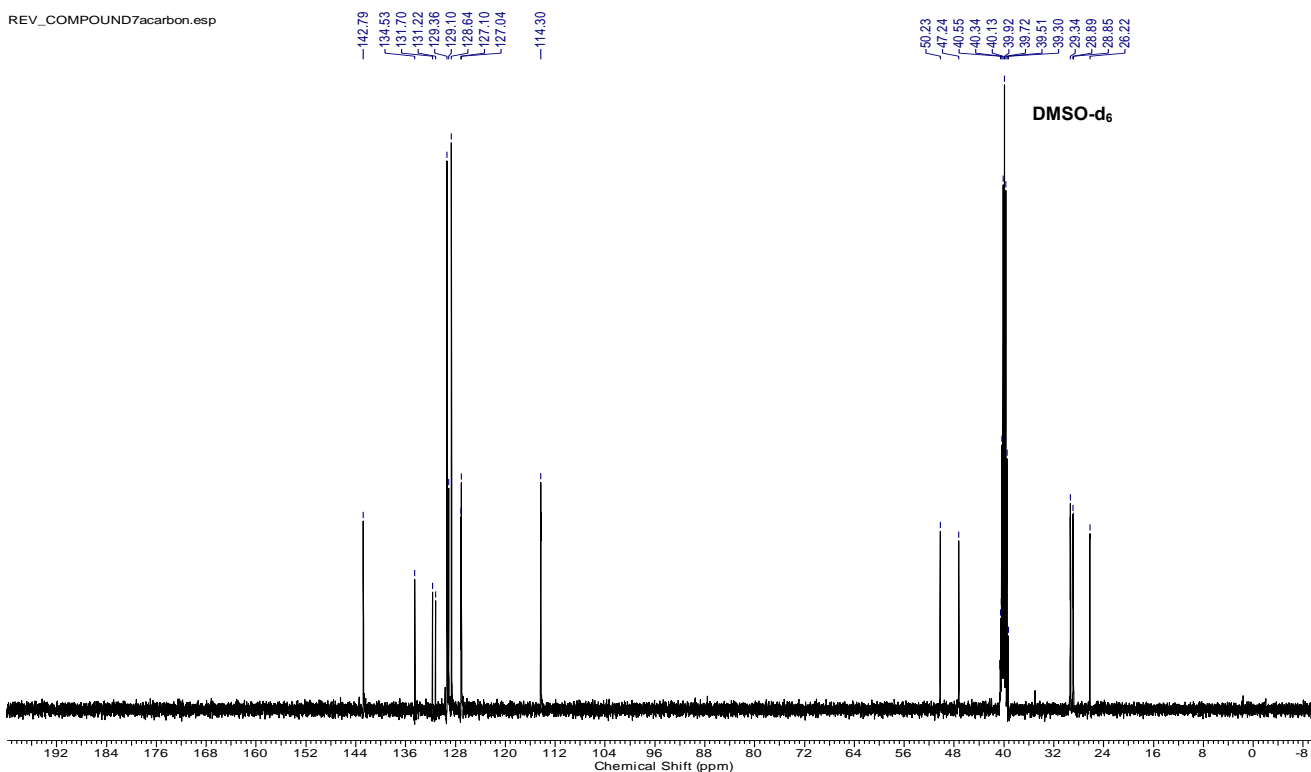
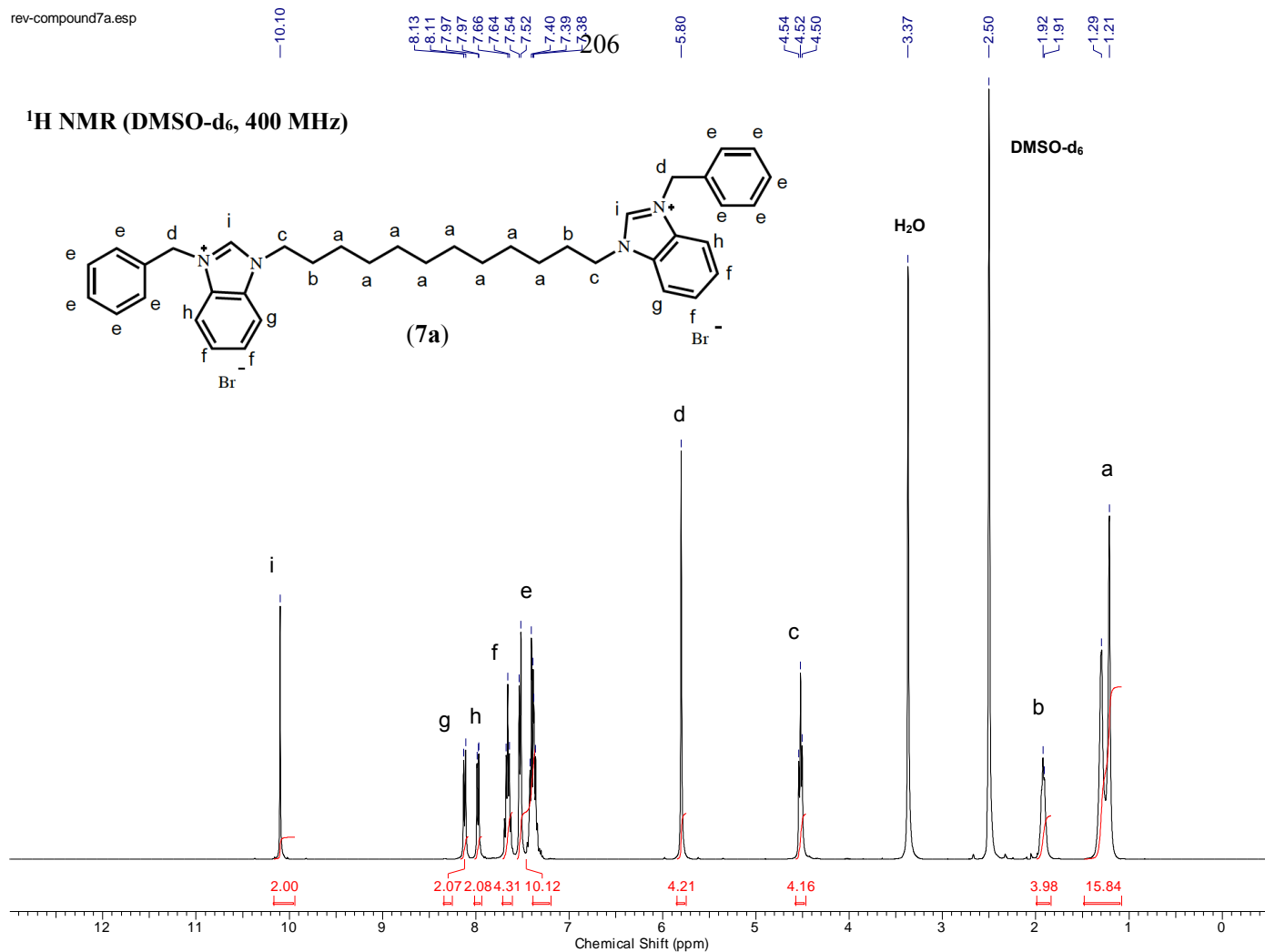
REV_6bcarbonmr.esp



REV_6bcarbonmr.esp



¹H NMR (DMSO-d₆, 400 MHz)



-9.44

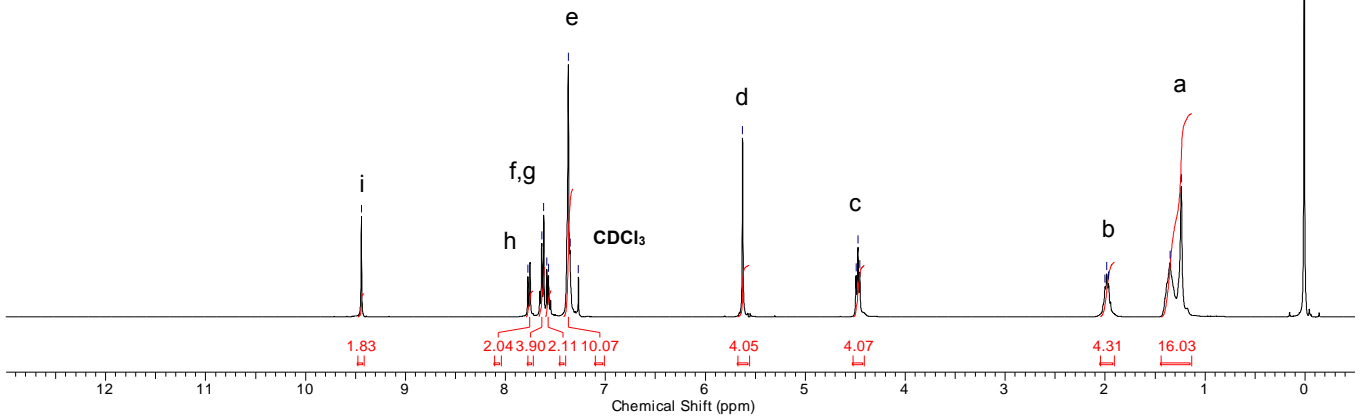
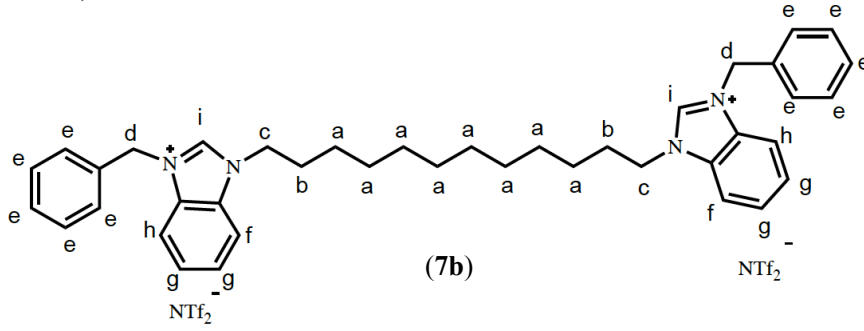
7.78
7.75
7.64
7.62
7.59
7.57
7.37
7.35
7.27

-5.63

4.49
4.47
4.452.00
1.98
1.971.35
1.24

-0.01

^1H NMR (CDCl_3 with 1 % v/v TMS, 400 MHz)



-140.76

132.25
131.49
131.20
129.45
128.09
127.54
121.38
116.19
113.80
113.2877.34
77.02
76.7151.40
47.8629.12
28.87
28.85
28.52
26.14

-0.00

REVCOMPOUND7BC13NMR

1.00

1.00

1.00

1.00

1.00

1.00

1.00

1.00

1.00

1.00

1.00

1.00

1.00

1.00

1.00

1.00

1.00

1.00

1.00

1.00

1.00

1.00

1.00

1.00

1.00

1.00

1.00

1.00

1.00

1.00

1.00

1.00

1.00

1.00

1.00

1.00

1.00

1.00

1.00

1.00

1.00

1.00

1.00

1.00

1.00

1.00

1.00

1.00

1.00

1.00

1.00

1.00

1.00

1.00

1.00

1.00

1.00

1.00

1.00

1.00

1.00

1.00

1.00

1.00

1.00

1.00

1.00

1.00

1.00

1.00

1.00

1.00

1.00

1.00

1.00

1.00

1.00

1.00

1.00

1.00

1.00

1.00

1.00

1.00

1.00

1.00

1.00

1.00

1.00

1.00

1.00

1.00

1.00

1.00

1.00

1.00

1.00

1.00

1.00

1.00

1.00

1.00

1.00

1.00

1.00

1.00

1.00

1.00

1.00

1.00

1.00

1.00

1.00

1.00

1.00

1.00

1.00

1.00

1.00

1.00

1.00

1.00

1.00

1.00

1.00

1.00

1.00

1.00

1.00

1.00

1.00

1.00

1.00

1.00

1.00

1.00

1.00

1.00

1.00

1.00

1.00

1.00

1.00

1.00

1.00

1.00

1.00

1.00

1.00

1.00

1.00

1.00

1.00

1.00

1.00

1.00

1.00

1.00

1.00

1.00

1.00

1.00

1.00

1.00

1.00

1.00

1.00

1.00

1.00

1.00

1.00

1.00

1.00

1.00

1.00

1.00

1.00

1.00

1.00

1.00

1.00

1.00

1.00

1.00

1.00

1.00

1.00

1.00

1.00

1.00

1.00

1.00

1.00

1.00

1.00

1.00

1.00

1.00

1.00

1.00

1.00

1.00

1.00

1.00

1.00

1.00

1.00

1.00

1.00

1.00

1.00

1.00

1.00

1.00

1.00

1.00

1.00

1.00

1.00

1.00

1.00

1.00

1.00

1.00

1.00

1.00

1.00

1.00

1.00

1.00

1.00

1.00

1.00

1.00

1.00

1.00

1.00

1.00

1.00

1.00

1.00

1.00

1.00

1.00

1.00

1.00

1.00

1.00

1.00

1.00

1.00

1.00

1.00

1.00

1.00

1.00

1.00

1.00

1.00

1.00

1.00

1.00

1.00

1.00

1.00

1.00

1.00

1.00

1.00

1.00

1.00

1.00

1.00

1.00

1.00

1.00

1.00

1.00

1.00

1.00

1.00

1.00

1.00

1.00

1.00

1.00

1.00

1.00

1.00

1.00

1.00

1.00

1.00

1.00

1.00

1.00

1.00

1.00

1.00

1.00

1.00

1.00

1.00

1.00

1.00

1.00

1.00

1.00

1.00

1.00

1.00

1.00

1.00

-9.29

7.81
7.43
7.41
7.40
7.39

208

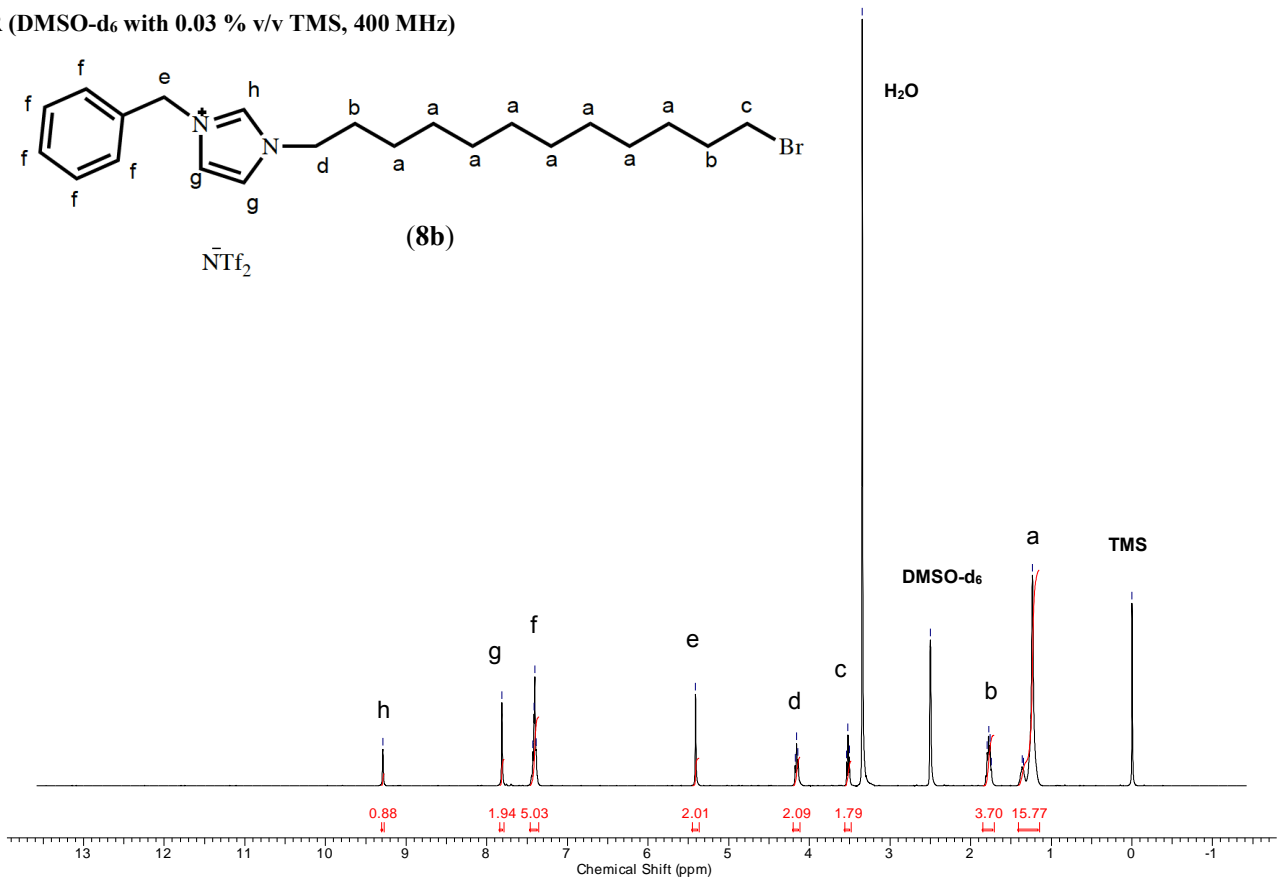
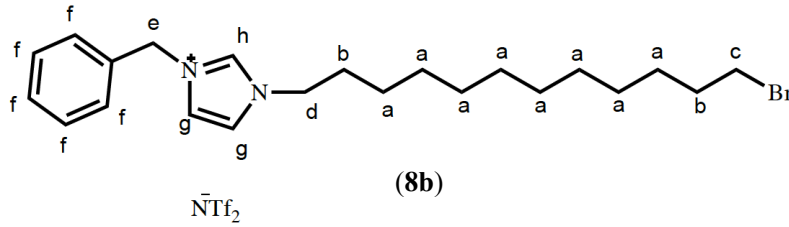
-5.41

4.18
4.16
4.14
3.54
3.52
3.50
3.34

-2.50
-1.80
-1.78
-1.76
-1.74
-1.36
-1.34
-1.23

-0.00

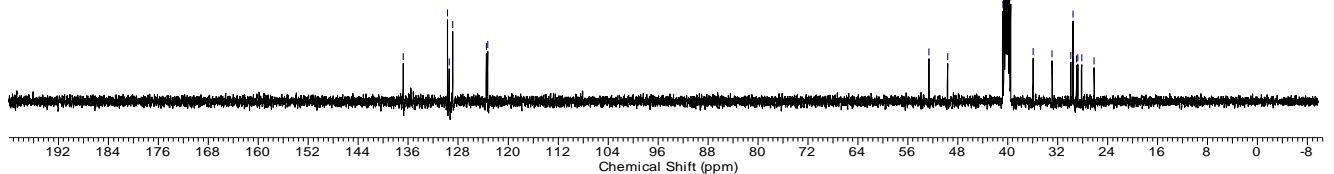
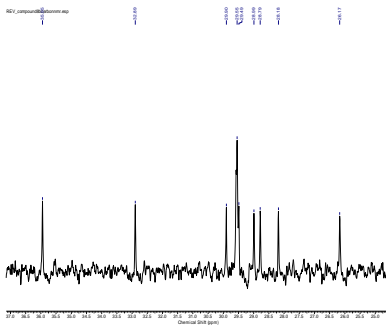
¹H NMR (DMSO-d₆ with 0.03 % v/v TMS, 400 MHz)



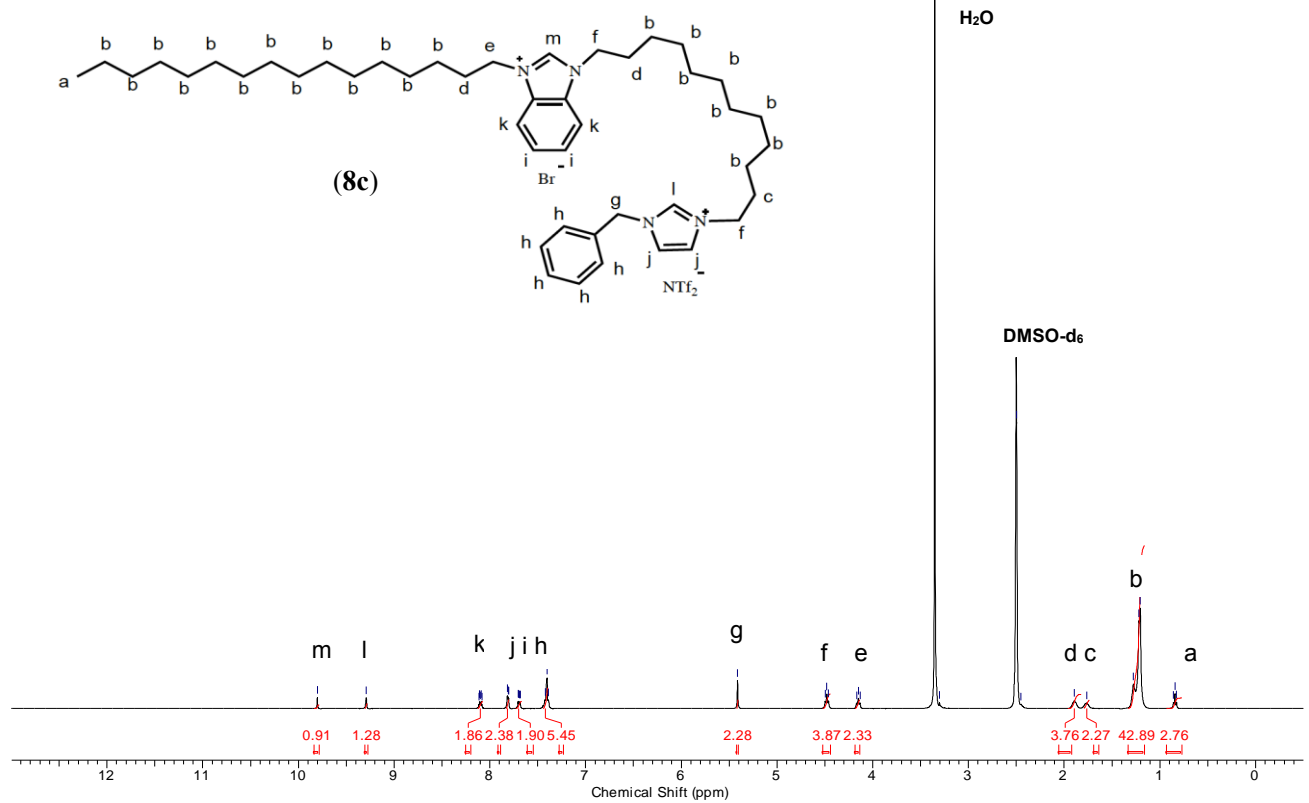
REV_compound8bcarbonmr.esp

136.80
129.69
129.44
128.87
123.50
123.29

52.63
40.80
40.59
40.38
40.17
39.97
39.75
39.55
39.55
35.95
32.89
29.90
29.55
29.49
26.17

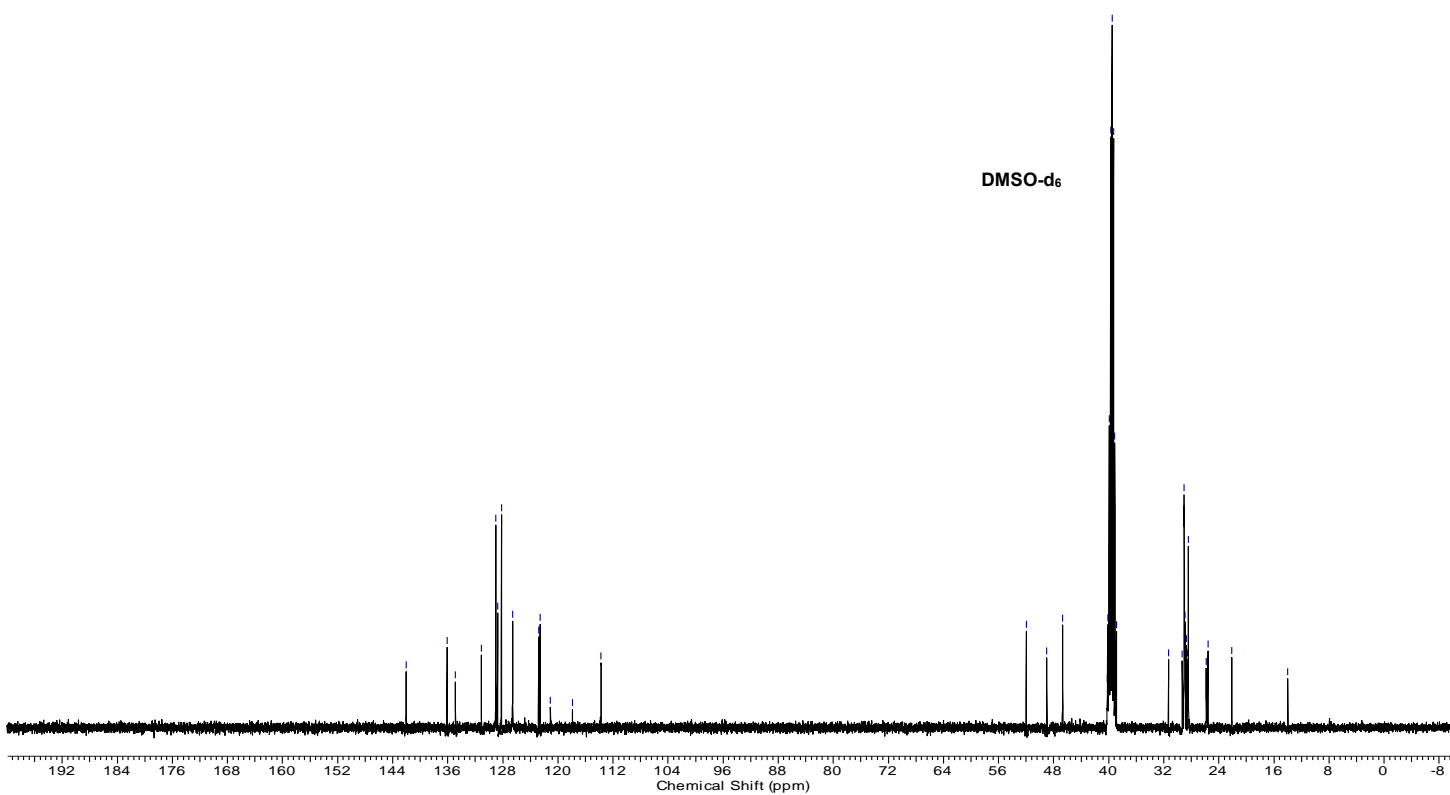


209

¹H NMR (DMSO-d₆, 400 MHz)

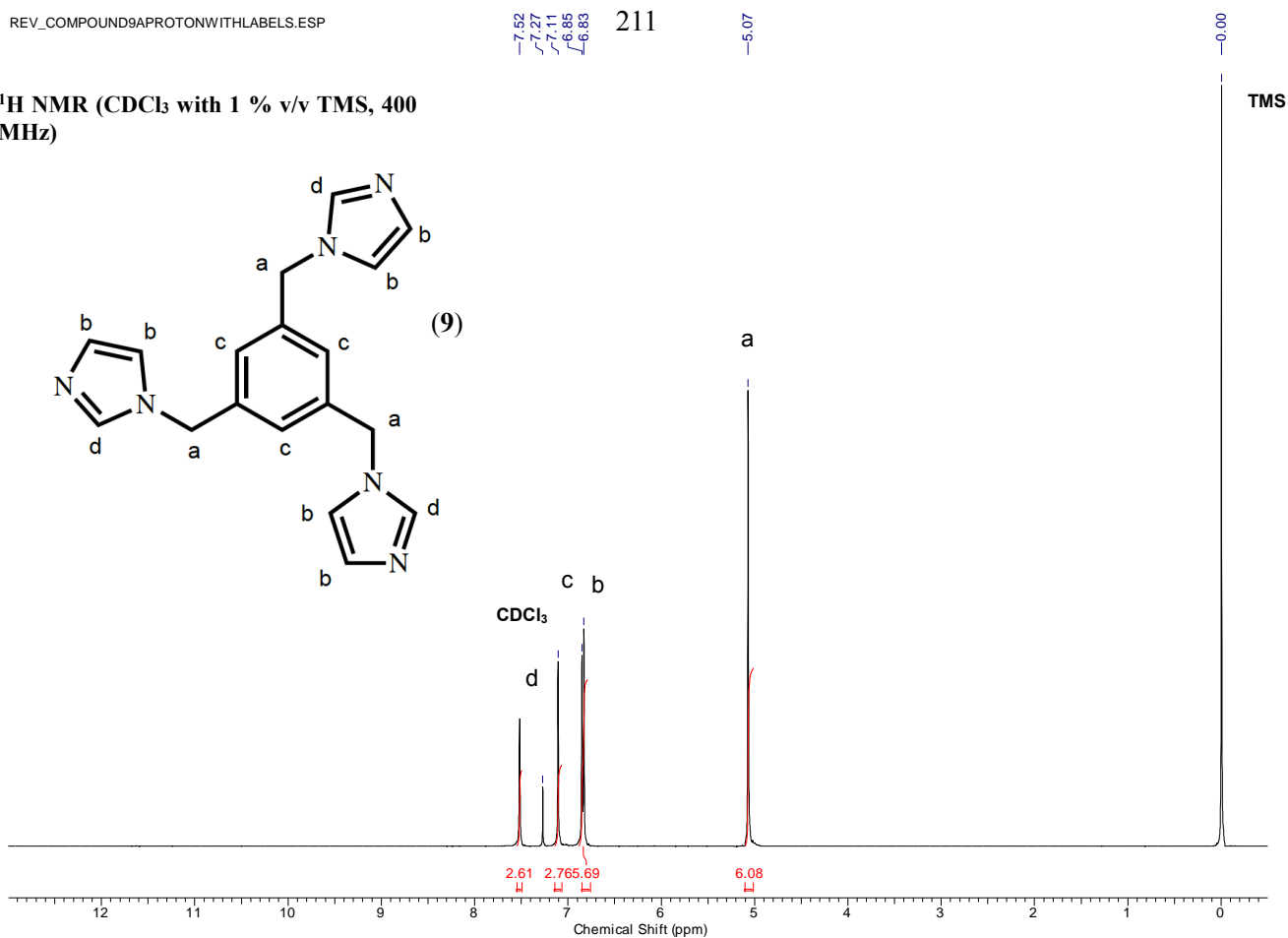
REV_compound8ccarbon.esp

142.04 136.10 134.88 131.10 129.01 128.75 128.21 126.57 122.80 122.61 121.08 117.88 113.74
 51.98 48.99 46.69 40.15 39.94 39.73 39.52 39.31 39.11 38.89 29.06 28.93 28.74 28.43 25.82 25.58 22.13 15.98

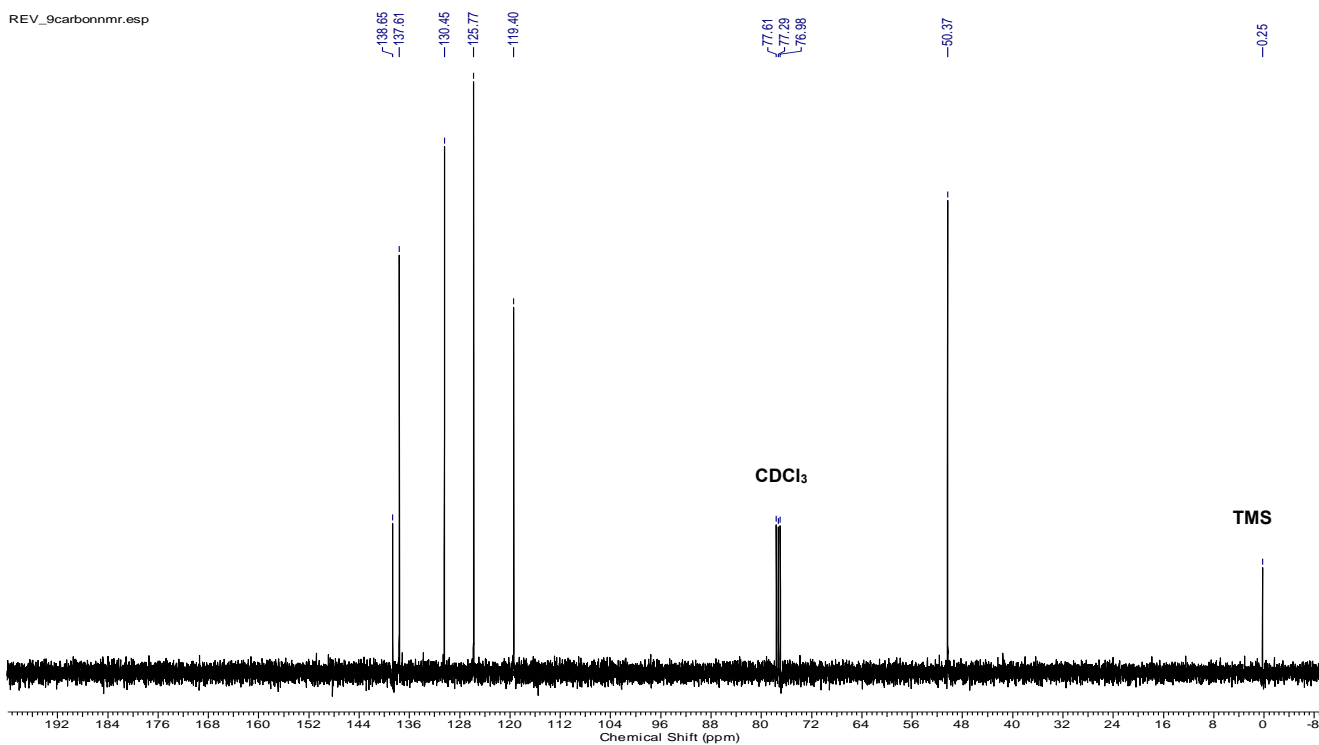


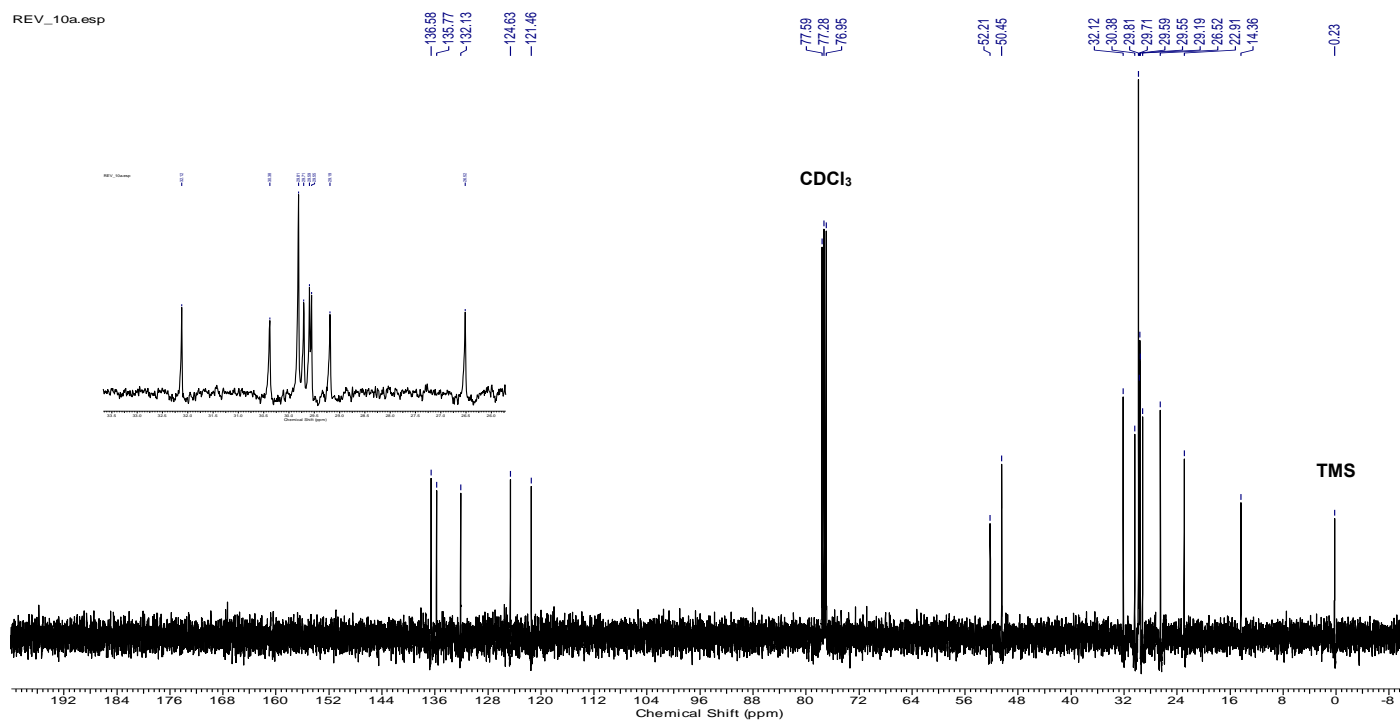
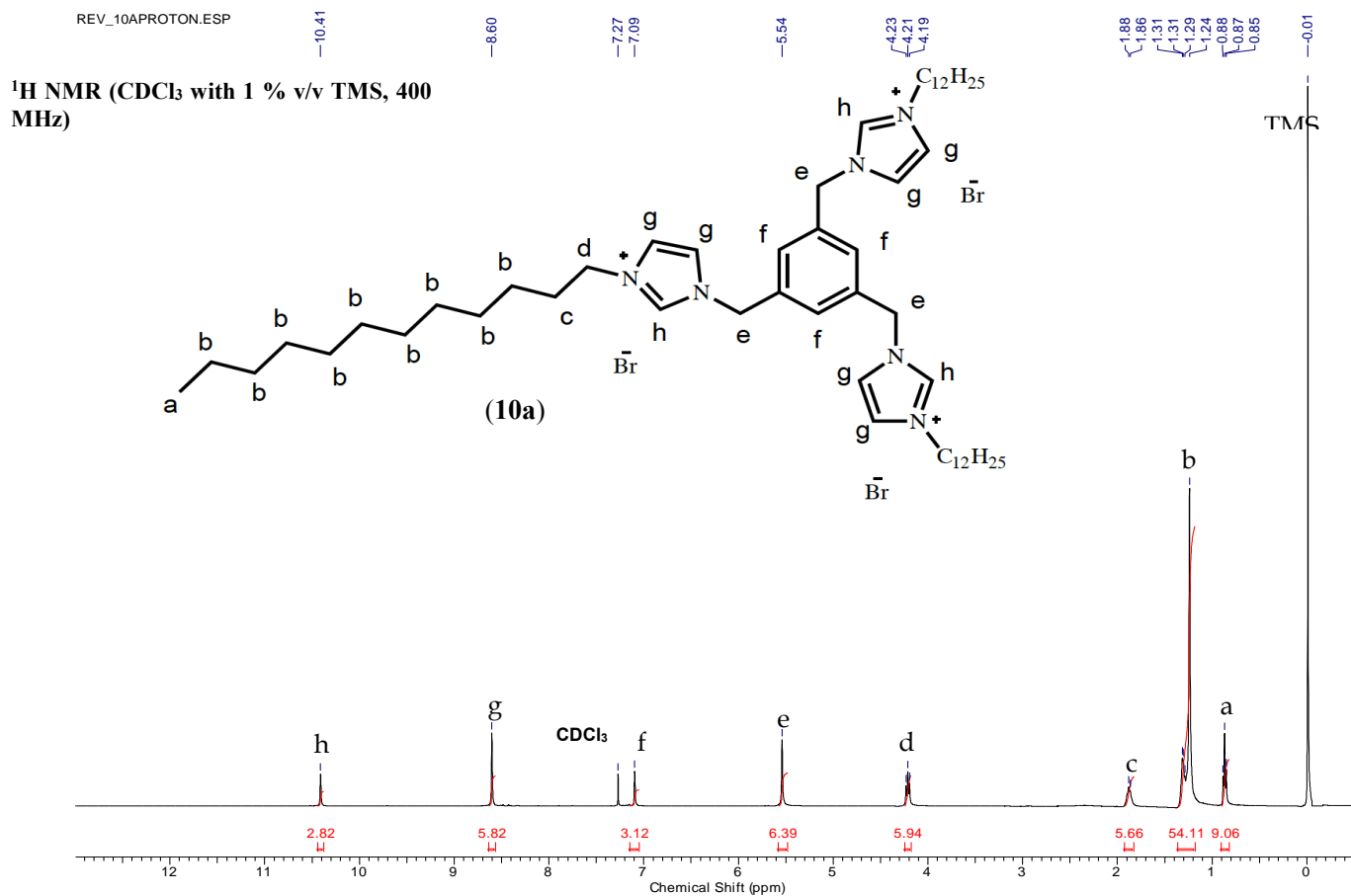
Synthesis of Compound 9. Briefly, imidazole (0.59 g, 8.68 mmol) and potassium hydroxide (2.09 g, 36.96 mmol) were dissolved in DMSO (30 mL) and stirred for 12 h at room temperature. Compound **9** was then obtained by adding 1,3,5-tris(bromomethyl)benzene (1 g, 2.80 mmol) to the reaction flask and stirring for 12 h. Water (30 mL) was added and the reaction mixture subsequently transferred to a separatory funnel and extracted with chloroform (4 x 30 mL). The organic phases were washed several times with water and dried over anhydrous sodium sulfate. After evaporation of the solvent under reduced pressure, compound **9** was dried at 70 °C for 6 h.²¹

^1H NMR (CDCl_3 with 1 % v/v TMS, 400 MHz)

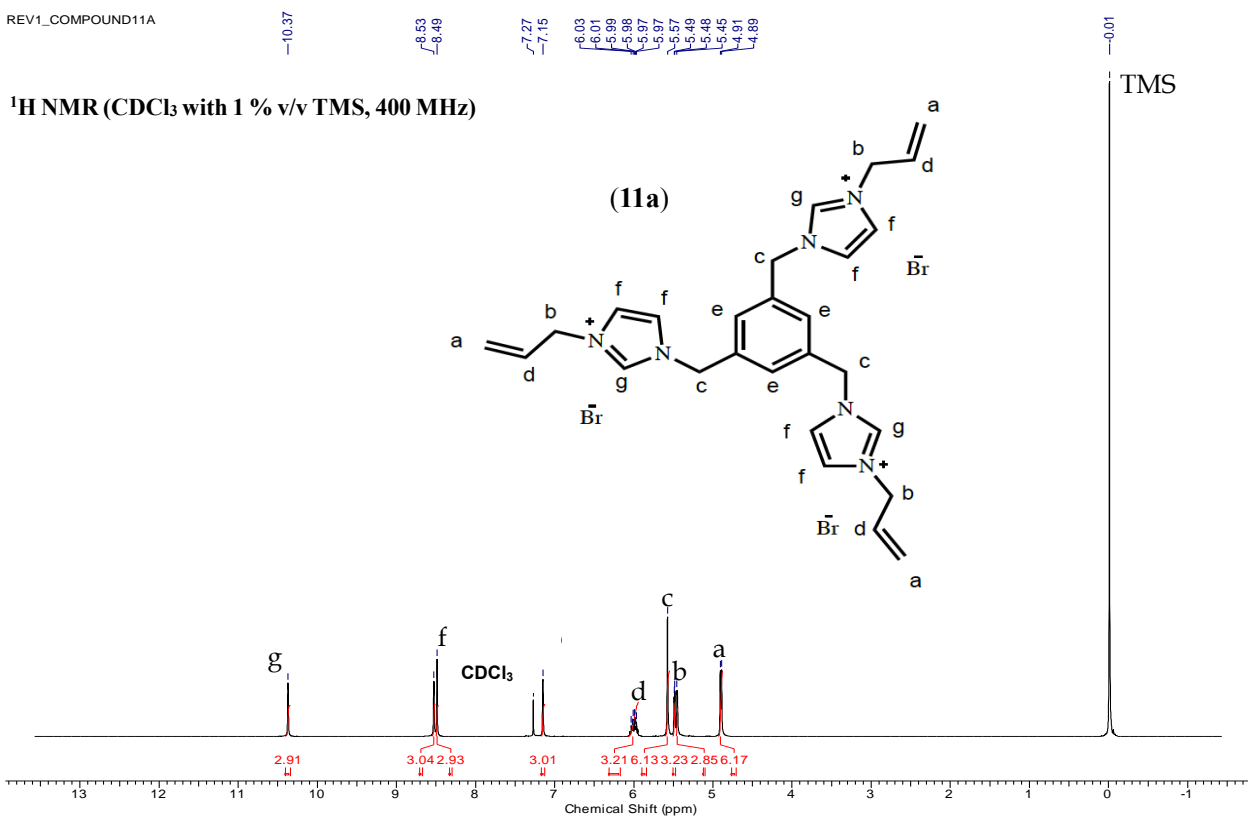


REV_9carbonnmr.esp

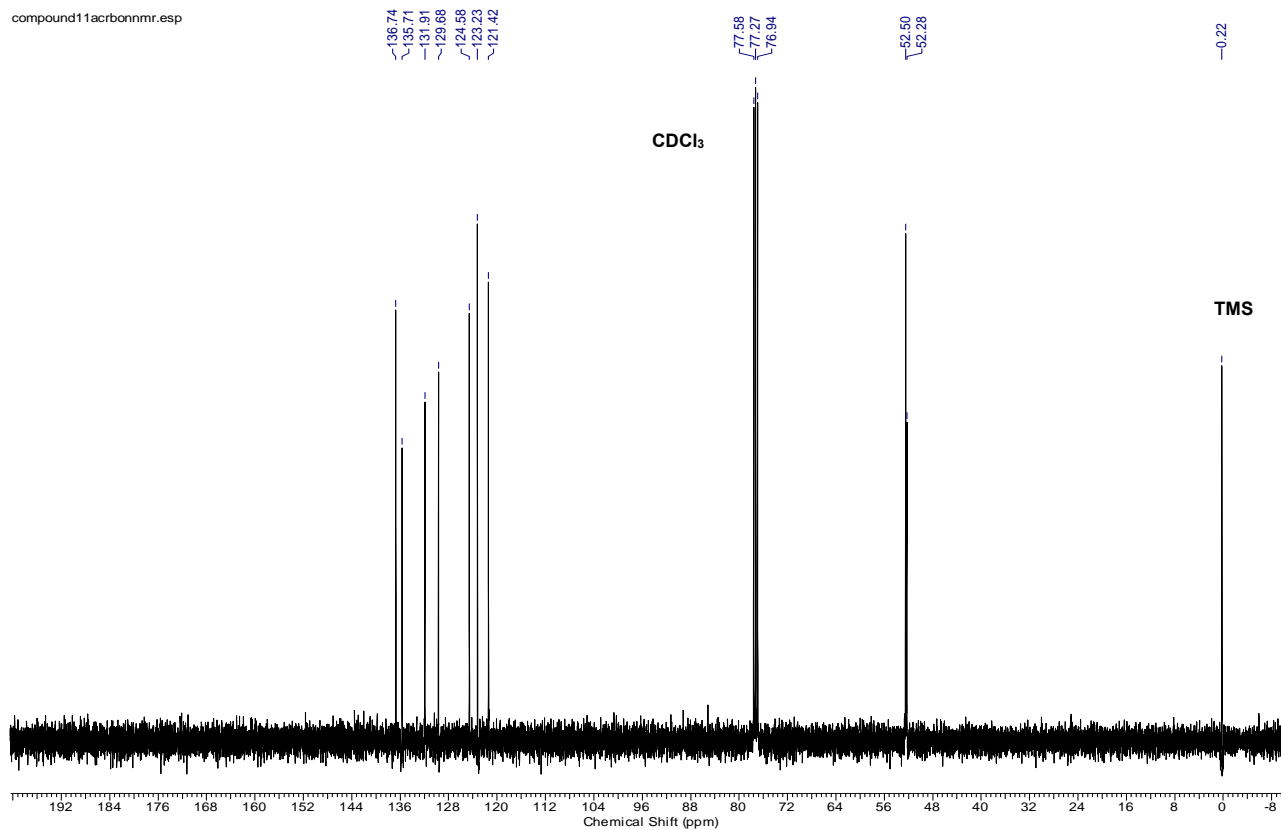


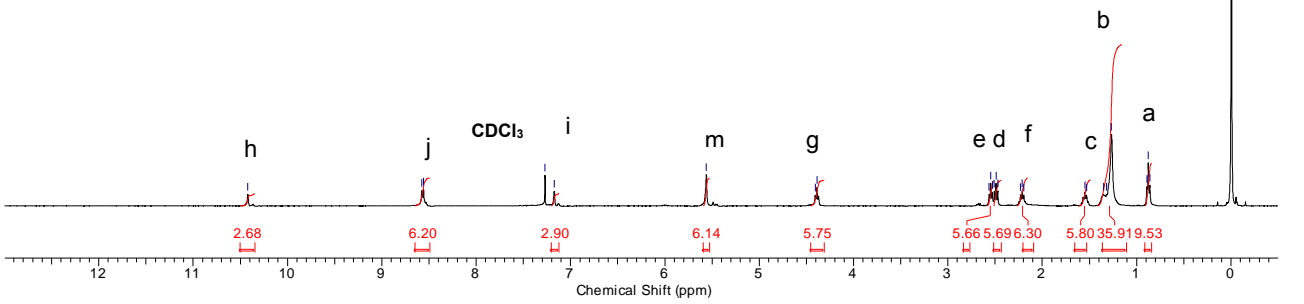
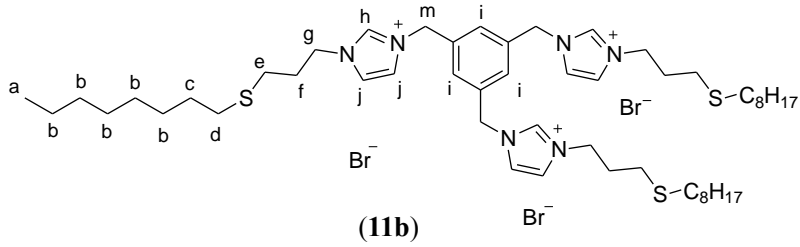


REV1_COMPOUND11A

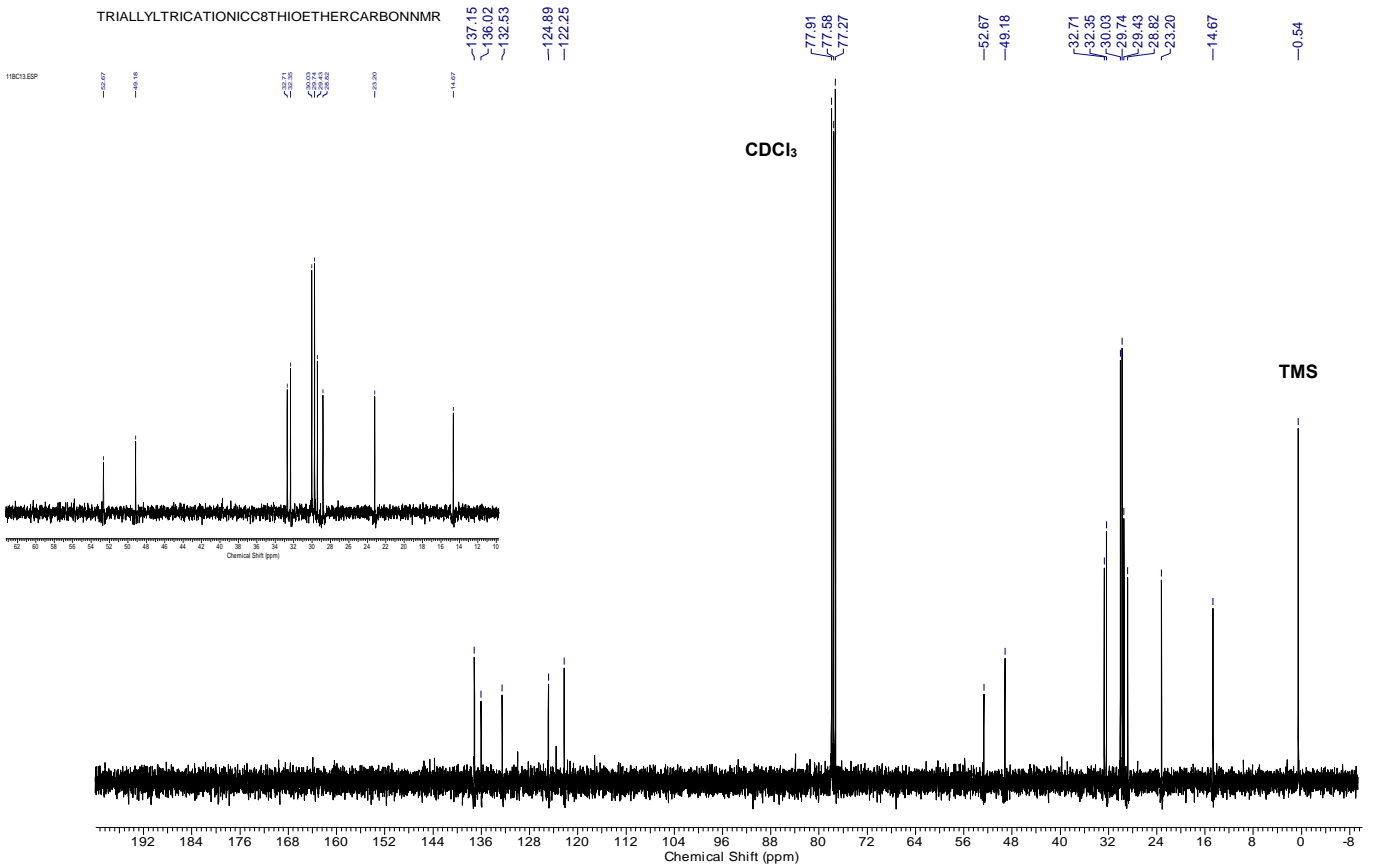


compound11aarbonnmr.esp



¹H NMR (CDCl₃ with 1 % v/v TMS, 400 MHz)

TRIALLYLTRICATIONIC8THIOETHERCARBONNMR



compound12a.esp

-9.53
-9.42

-7.86
-7.82
-7.78
-7.75
-7.67
-7.32
-7.23
-7.00
-6.96
-6.92

-5.47
-5.44
-5.40
-5.22
-5.20
-5.17

-4.21
-4.20
-4.19

-3.35

-2.50

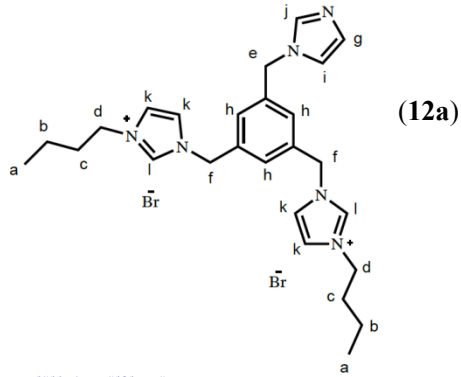
-1.79

-1.27
-1.26
-0.93
-0.91
-0.89

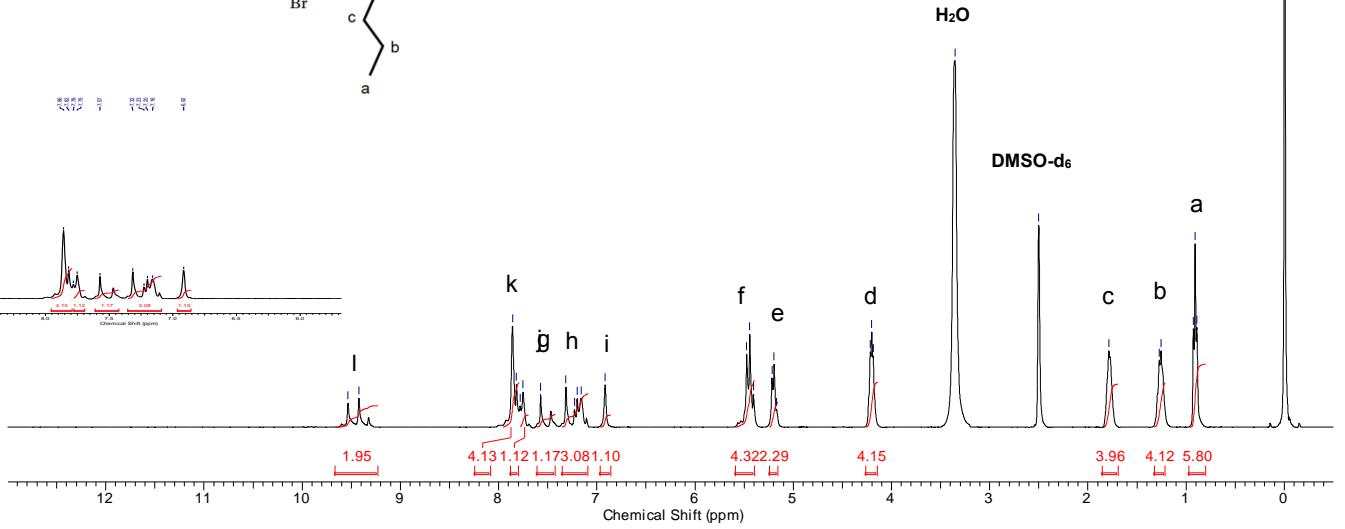
-0.00

¹H NMR (DMSO-d₆ with 1 % v/v TMS, 400 MHz)

TMS



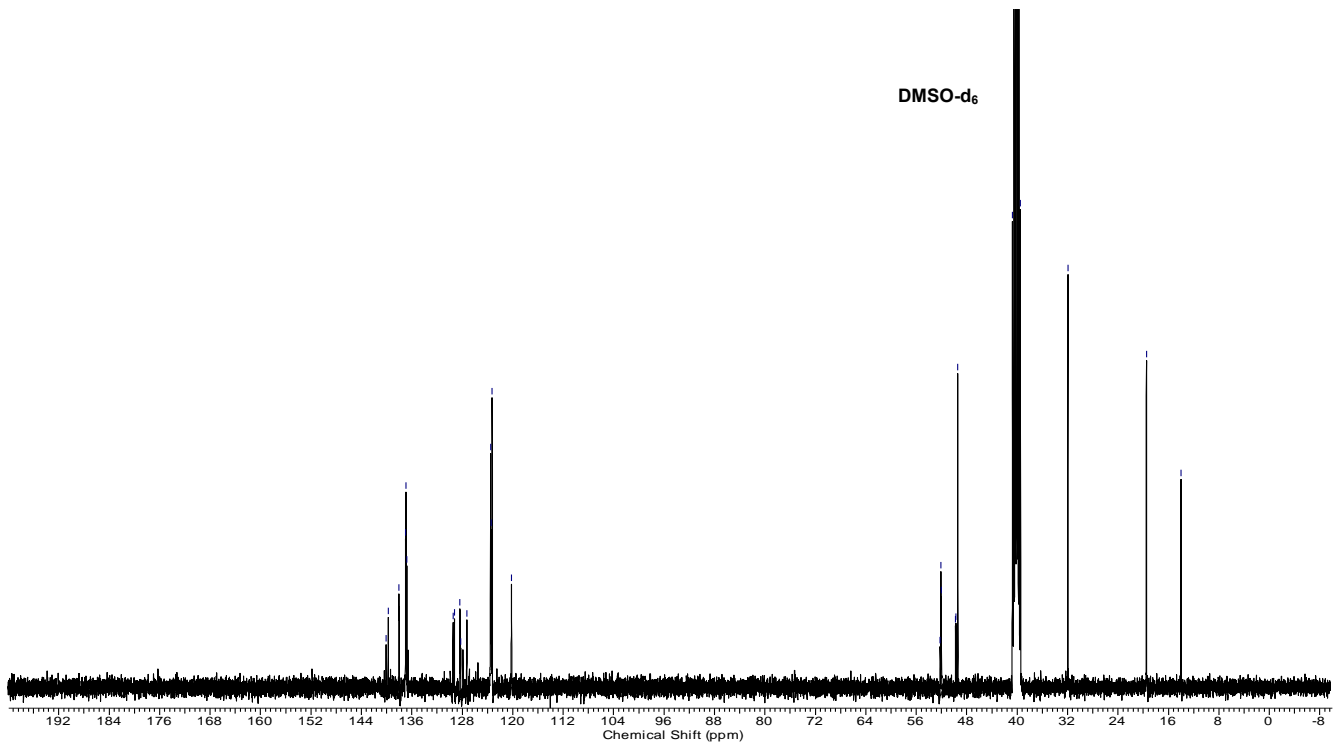
compound12a.esp

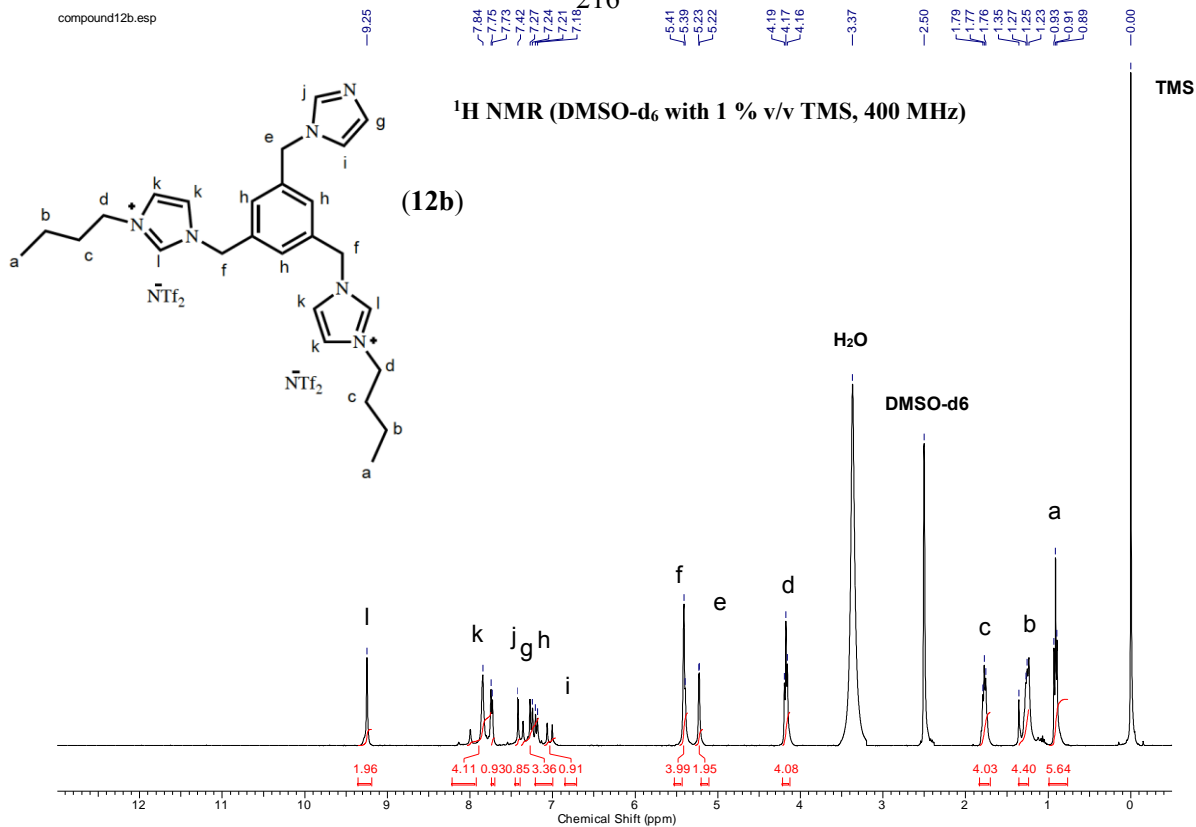


REV_12AC13NMR

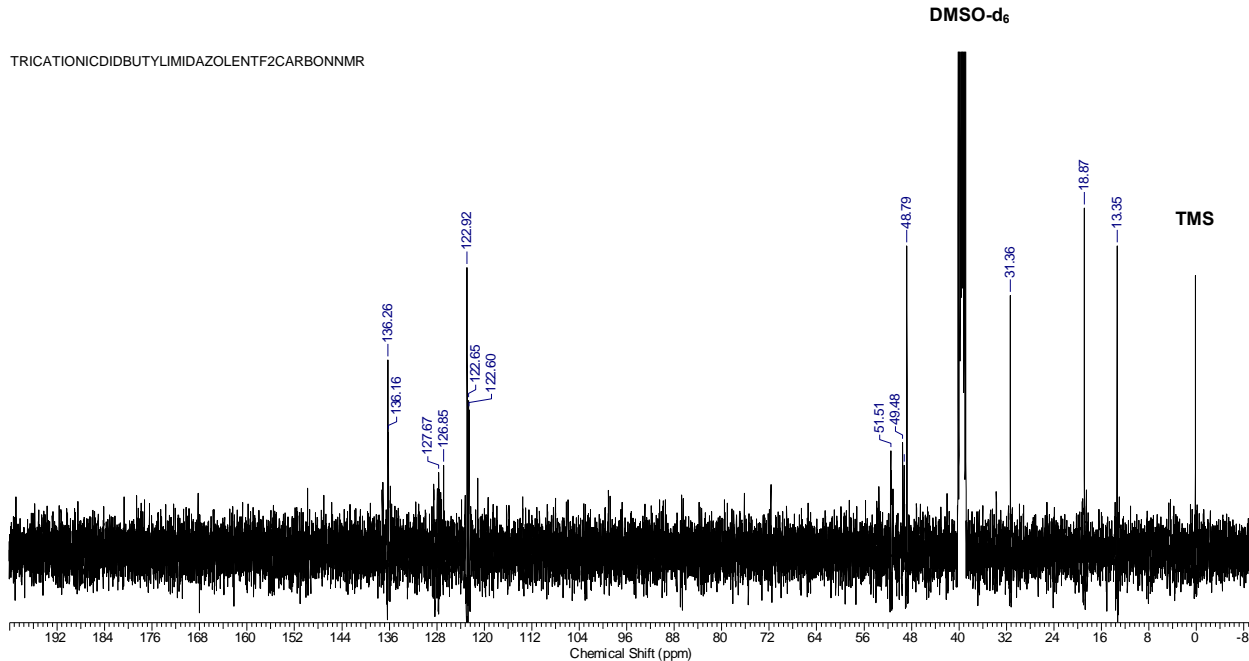
-140.07
-138.74
-136.04
-136.97
-136.91
-136.78
-129.47
-128.26
-128.36
-128.27
-127.28
-123.51
-123.45
-123.25
-120.19

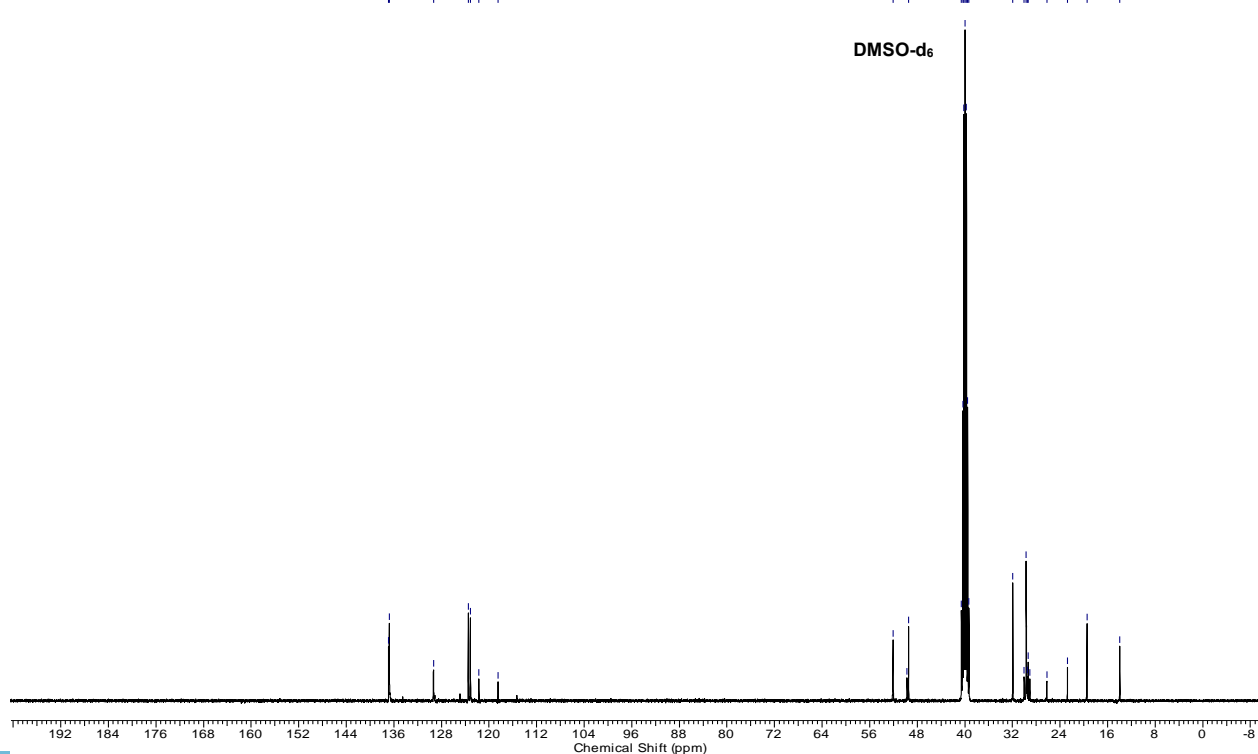
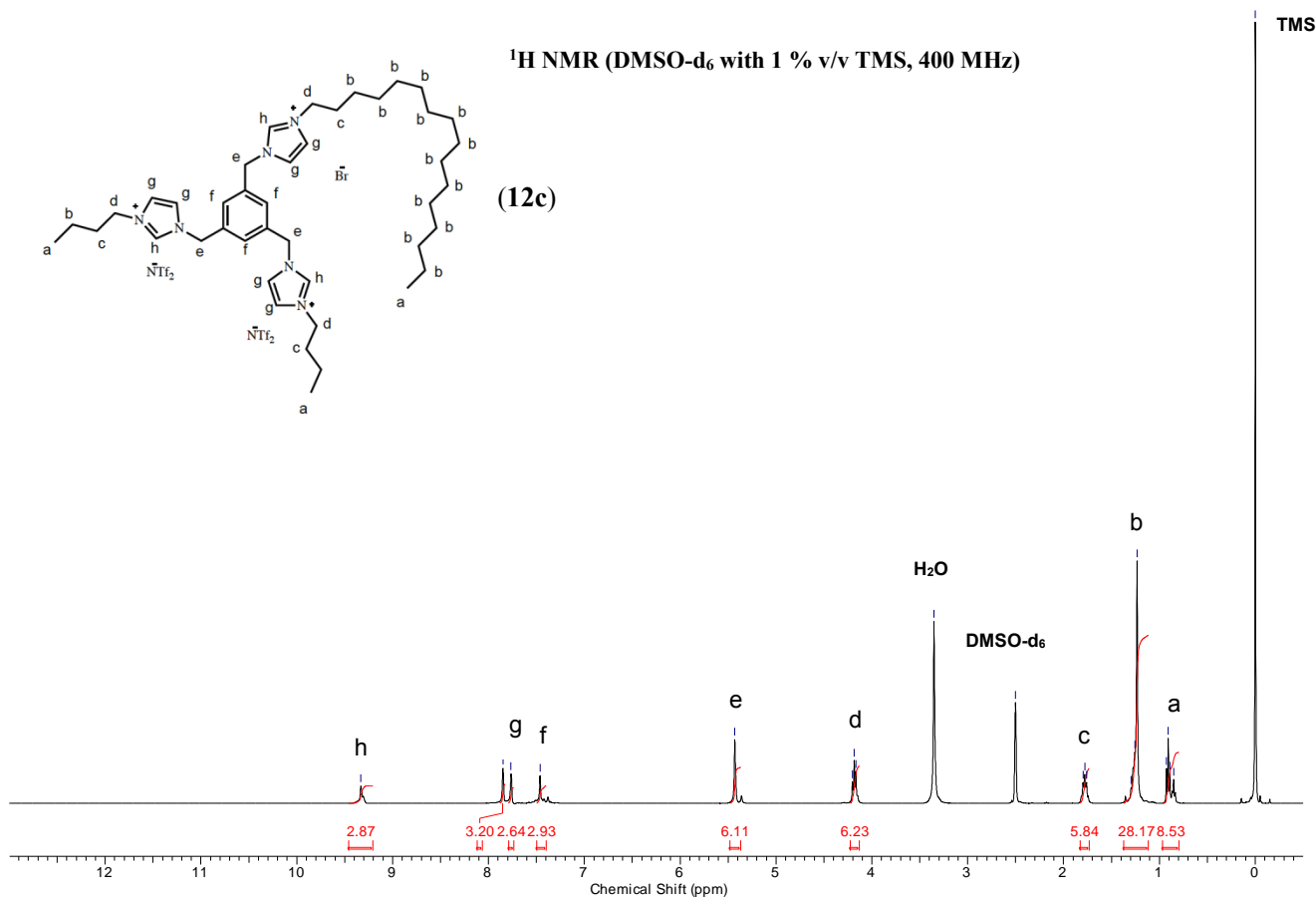
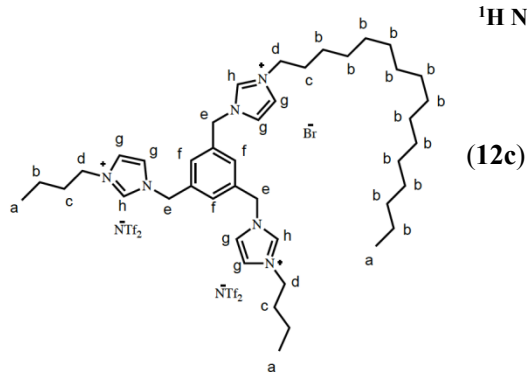
-52.20
-52.10
-52.01
-49.76
-49.43
-40.74
-40.54
-40.32
-40.11
-39.91
-39.69
-39.49
-31.96
-19.50
-14.01





TRICATIONICDIBUTYLIMIDAZOLENTF₂CARBONNMR





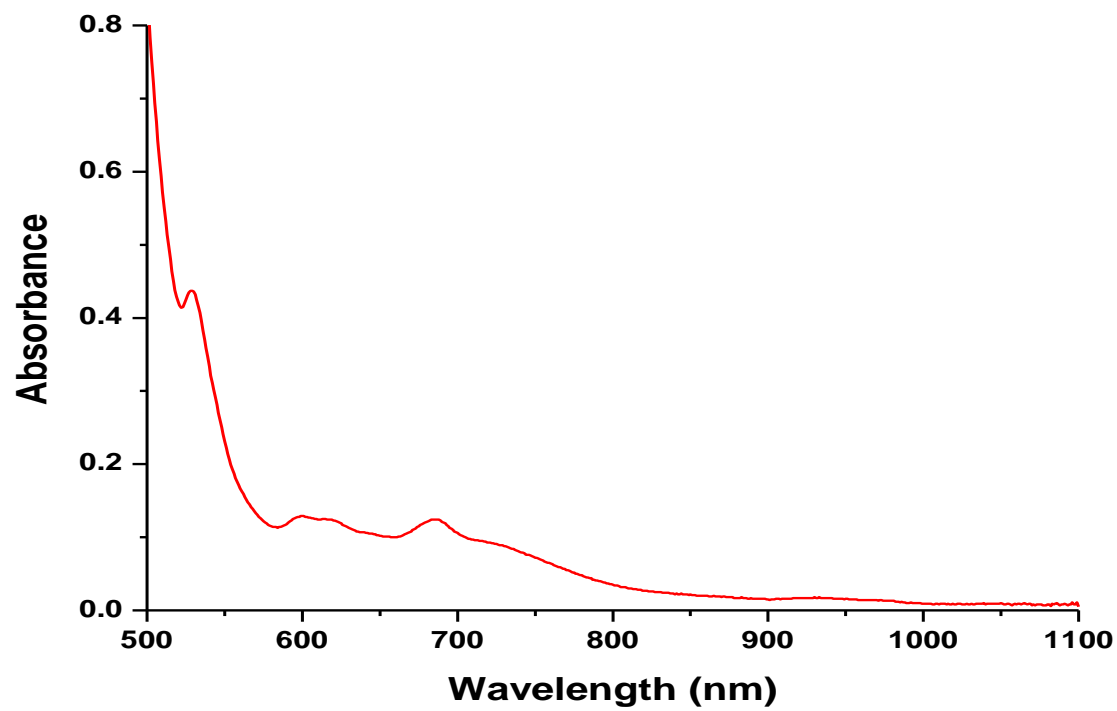
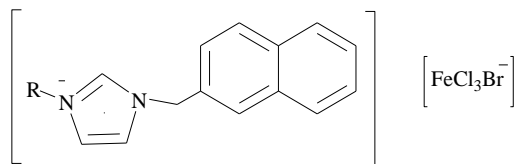
Absorbance spectrum of bromotrichloroferrate $[\text{FeCl}_3\text{Br}^-]$ anion

Table S1. Imidazolium-based monocationic MILs and their corresponding water solubilities.



Entry	R	Miscibility ^a
1	Methyl	M
2	Decyl	M
3	Hexadecyl	M
4	Benzyl	M

^aM = Soluble at 5% (w/v);

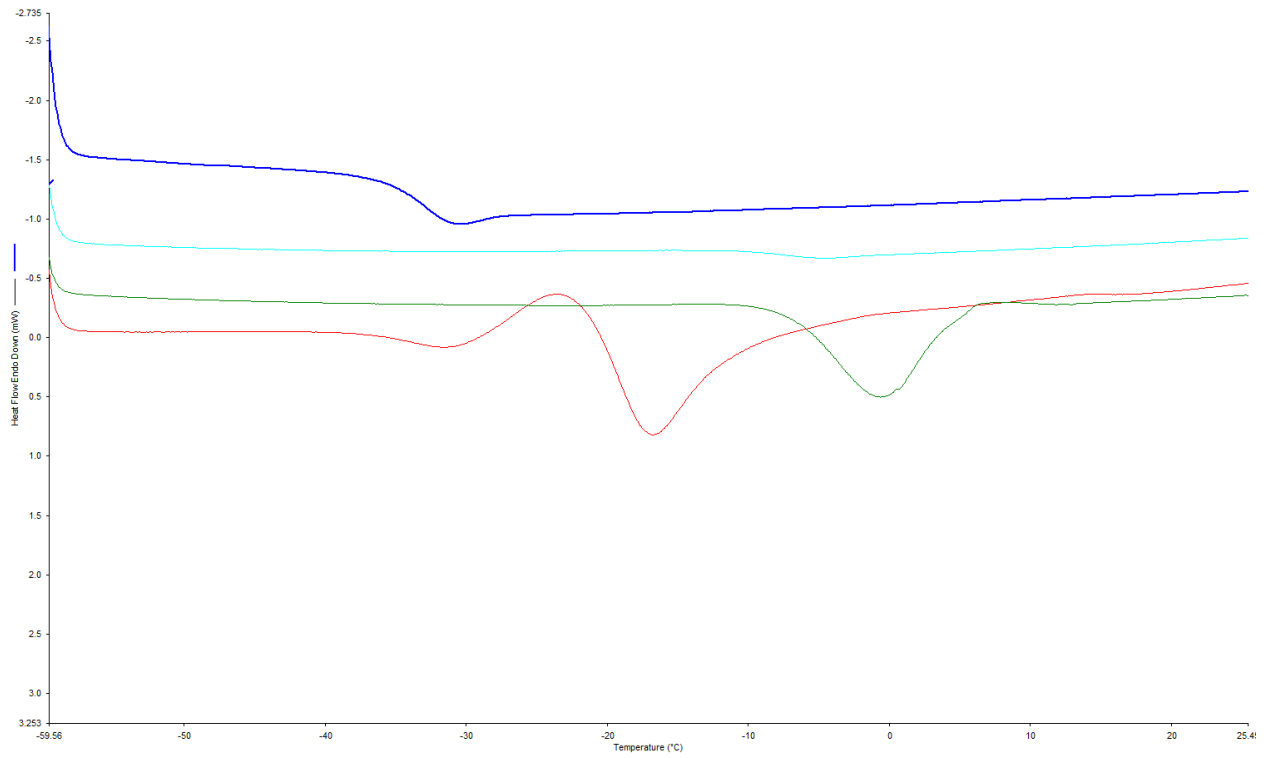


Figure S1. DSC traces of symmetrical/unsymmetrical dicationic hydrophobic MILs

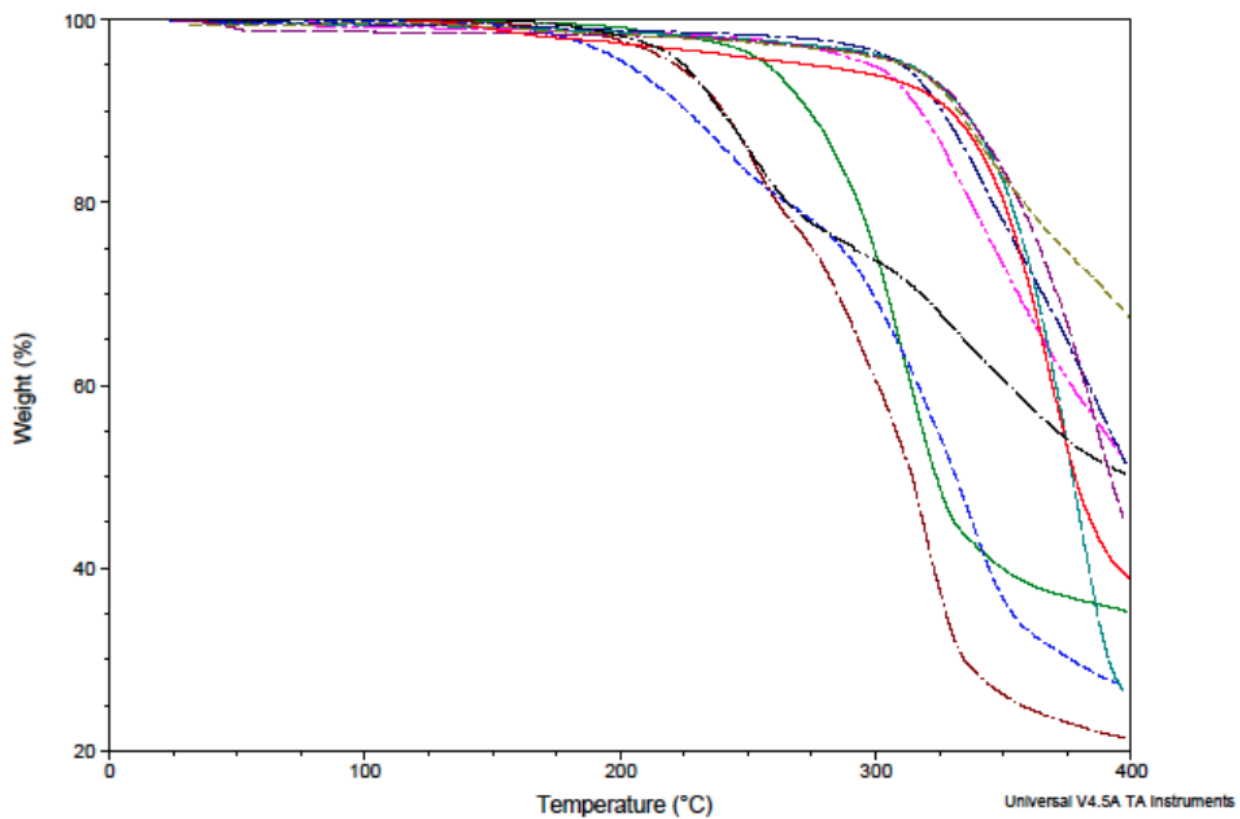
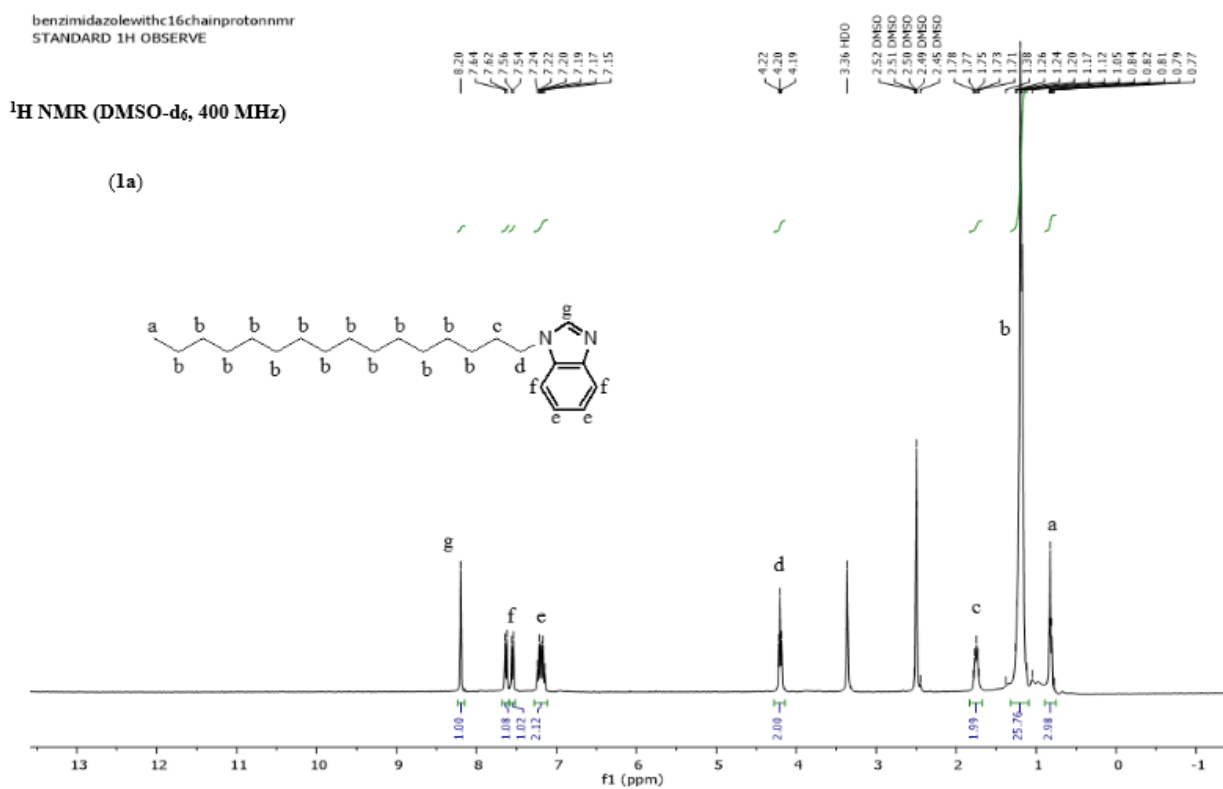


Figure S2. TGA traces for the hydrophobic MILs synthesized in this study.

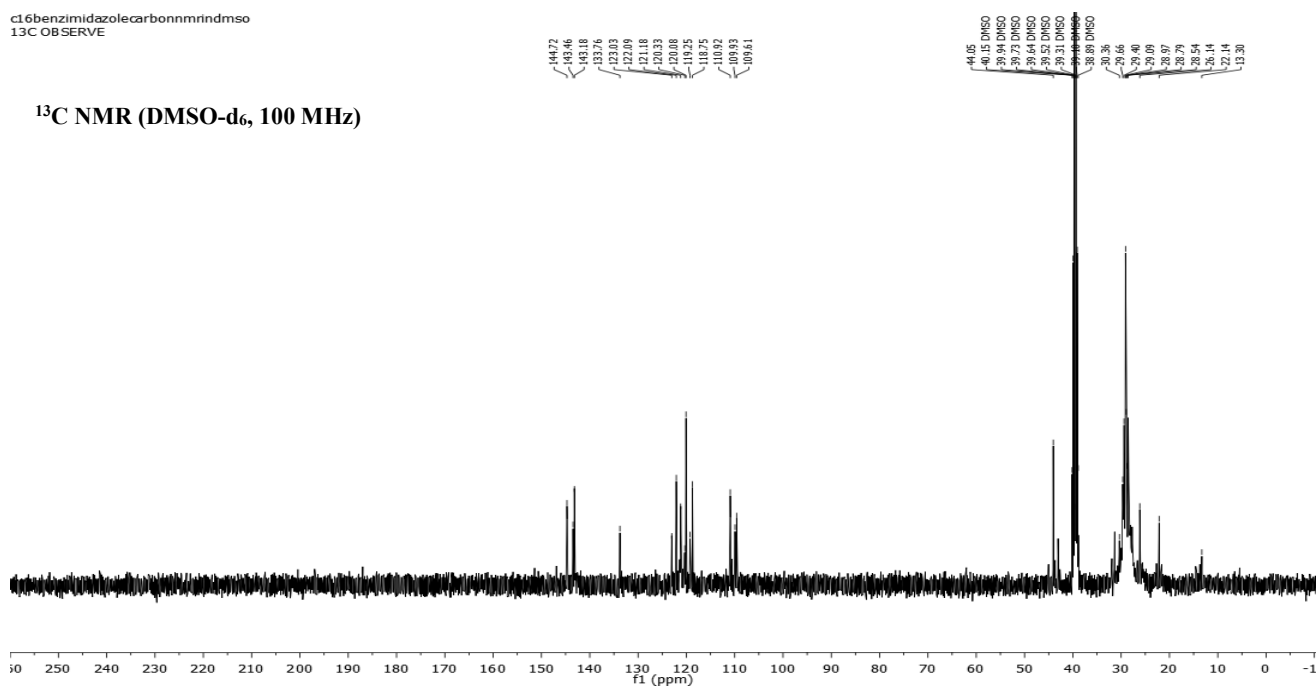
(—) MIL 1; (- - -) MIL 2; (- · -) MIL 3; (- · ·) MIL 6c; (= =) MIL 6; (= · -) MIL 7;
 (- · -) MIL 8; (- - -) MIL 10; (- · -) MIL 11; (—) MIL 12.

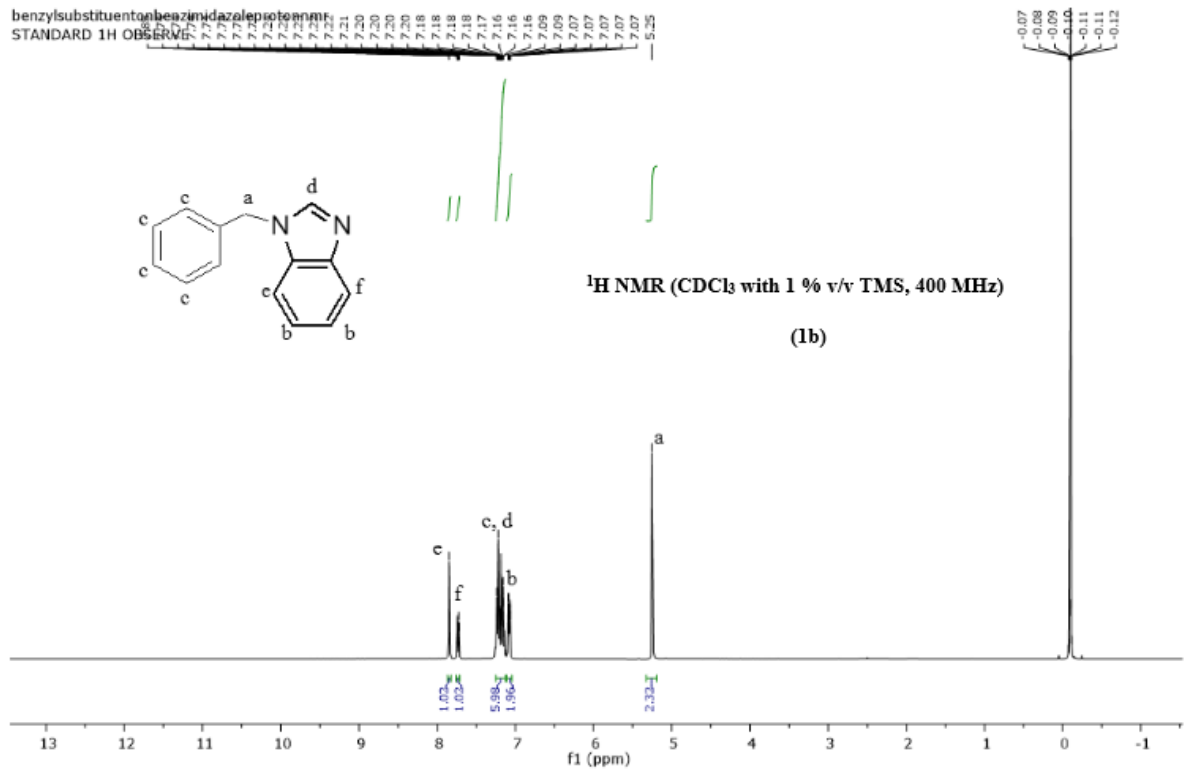
APPENDIX B
SUPPORTING INFORMATION ACCOMPANYING
CHAPTER 3

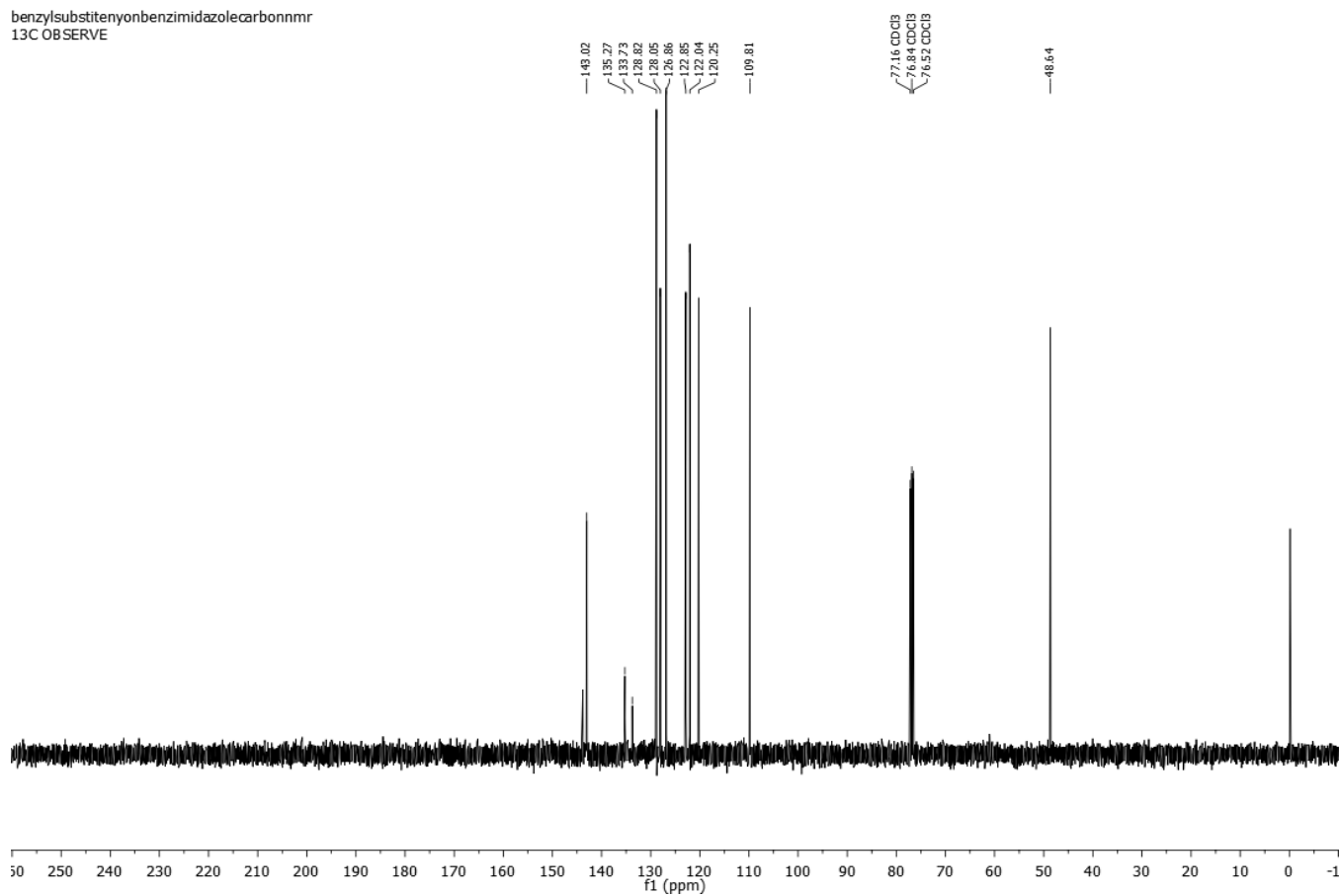


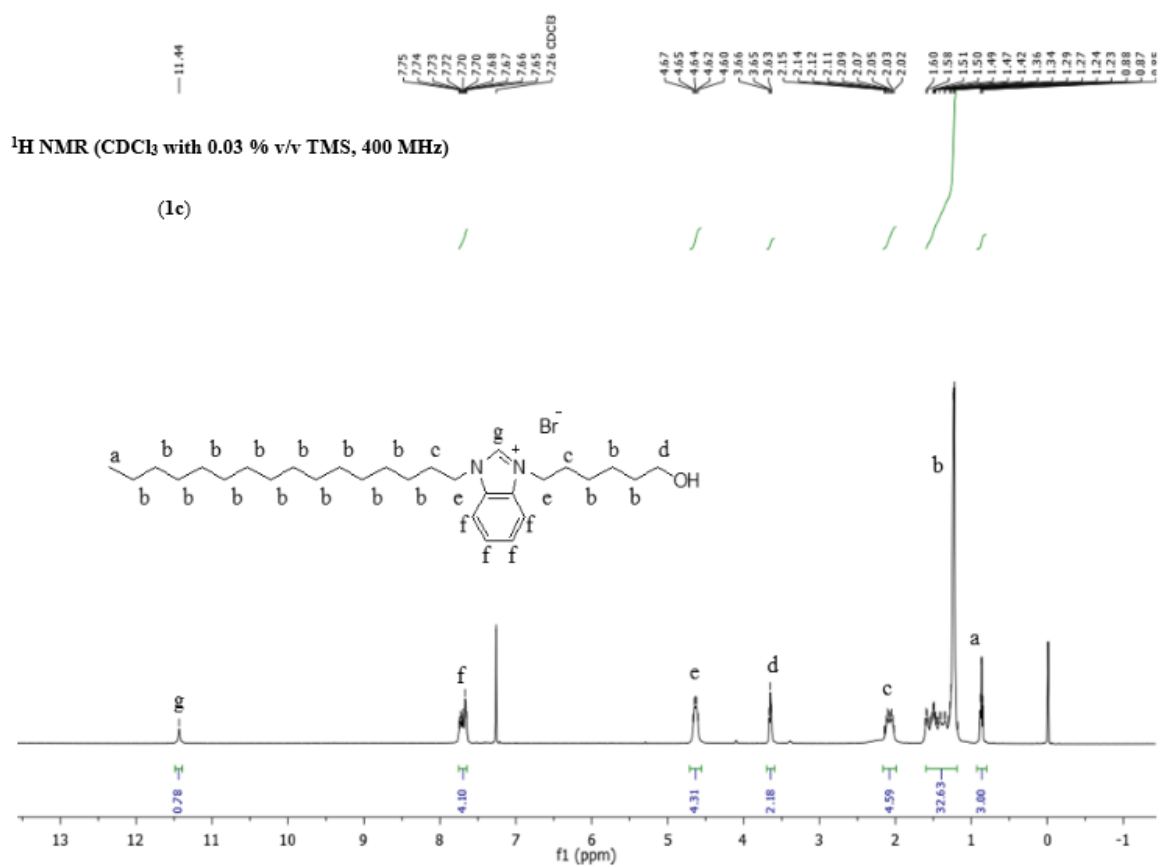
c16benzimidazolecarbonmndmsol
13C OBSERVE

^{13}C NMR (DMSO- d_6 , 100 MHz)



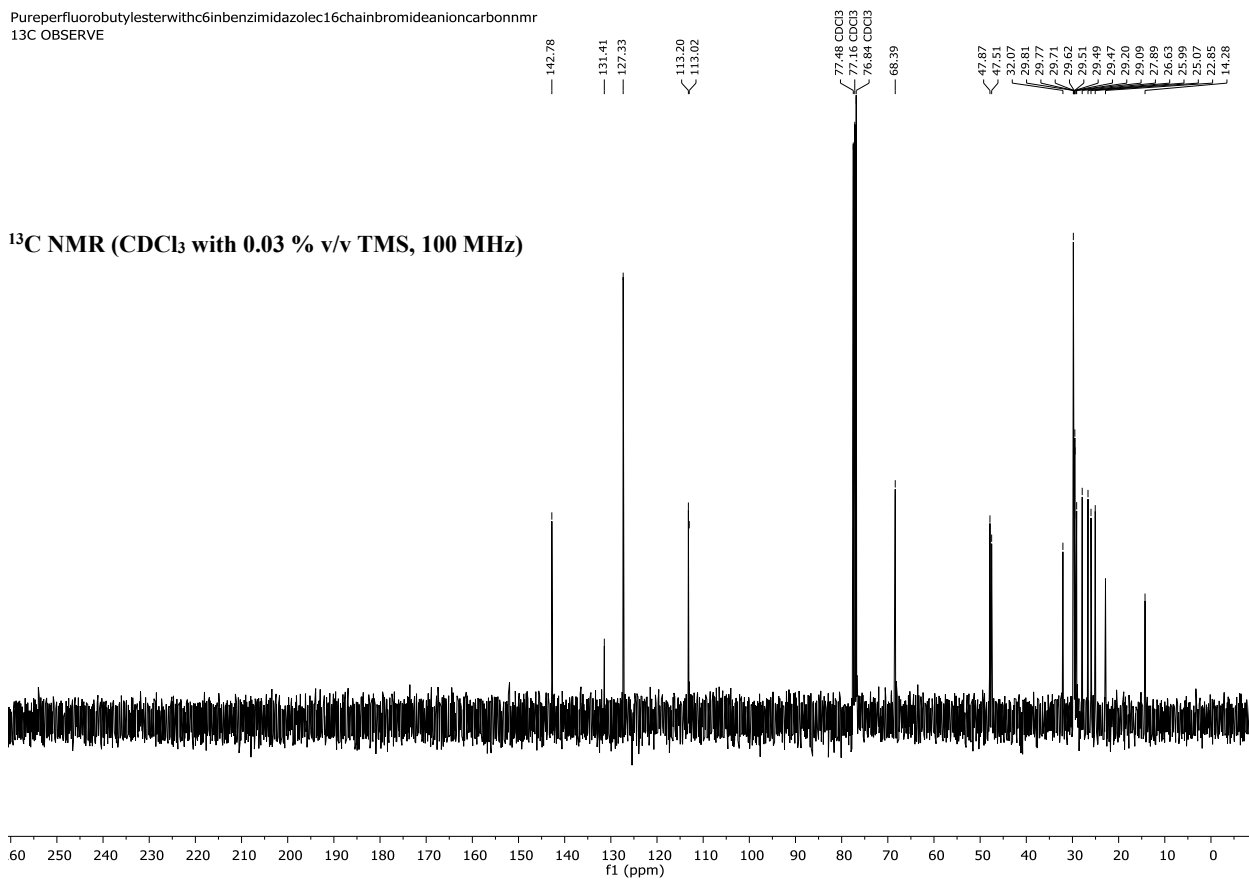


¹³C NMR (CDCl₃ with 0.03 % v/v TMS, 100 MHz)benzylsubstitenyonbenzimidazolecarbonmr
13C OBSERVE



Pureperfluorobutylesterwithc6inbenzimidazolec16chainbromideanioncarbonnmr
13C OBSERVE

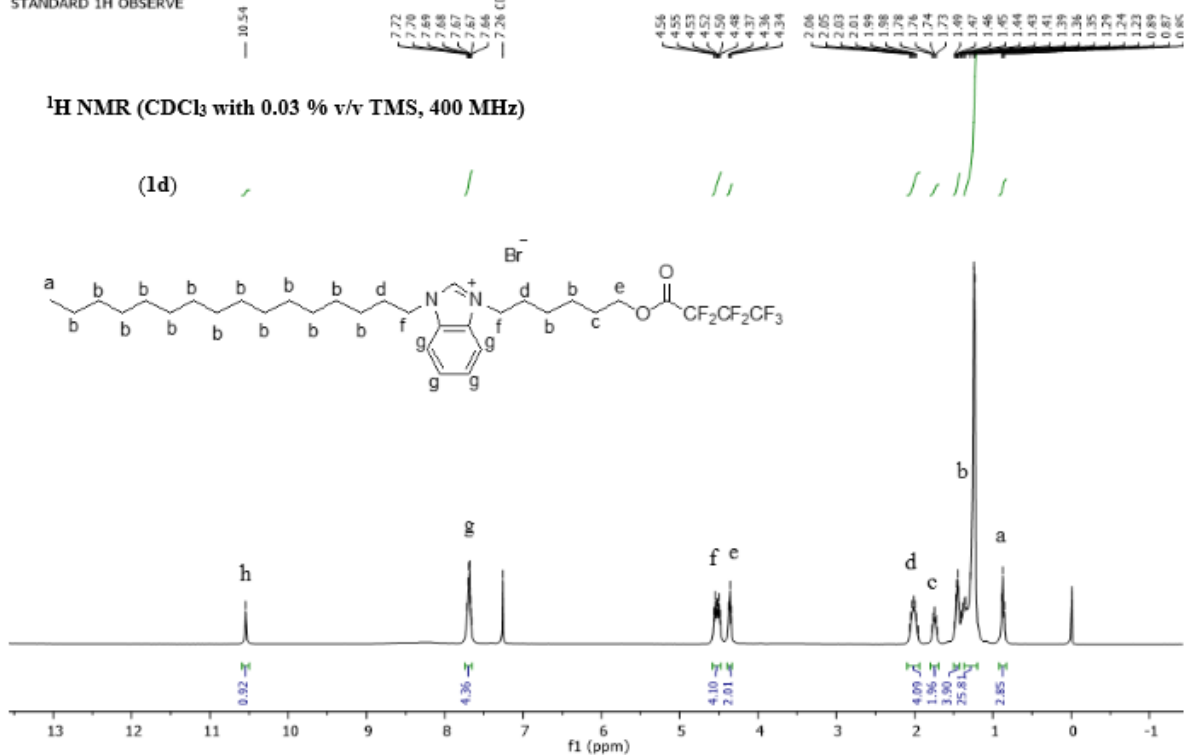
^{13}C NMR (CDCl_3 with 0.03 % v/v TMS, 100 MHz)



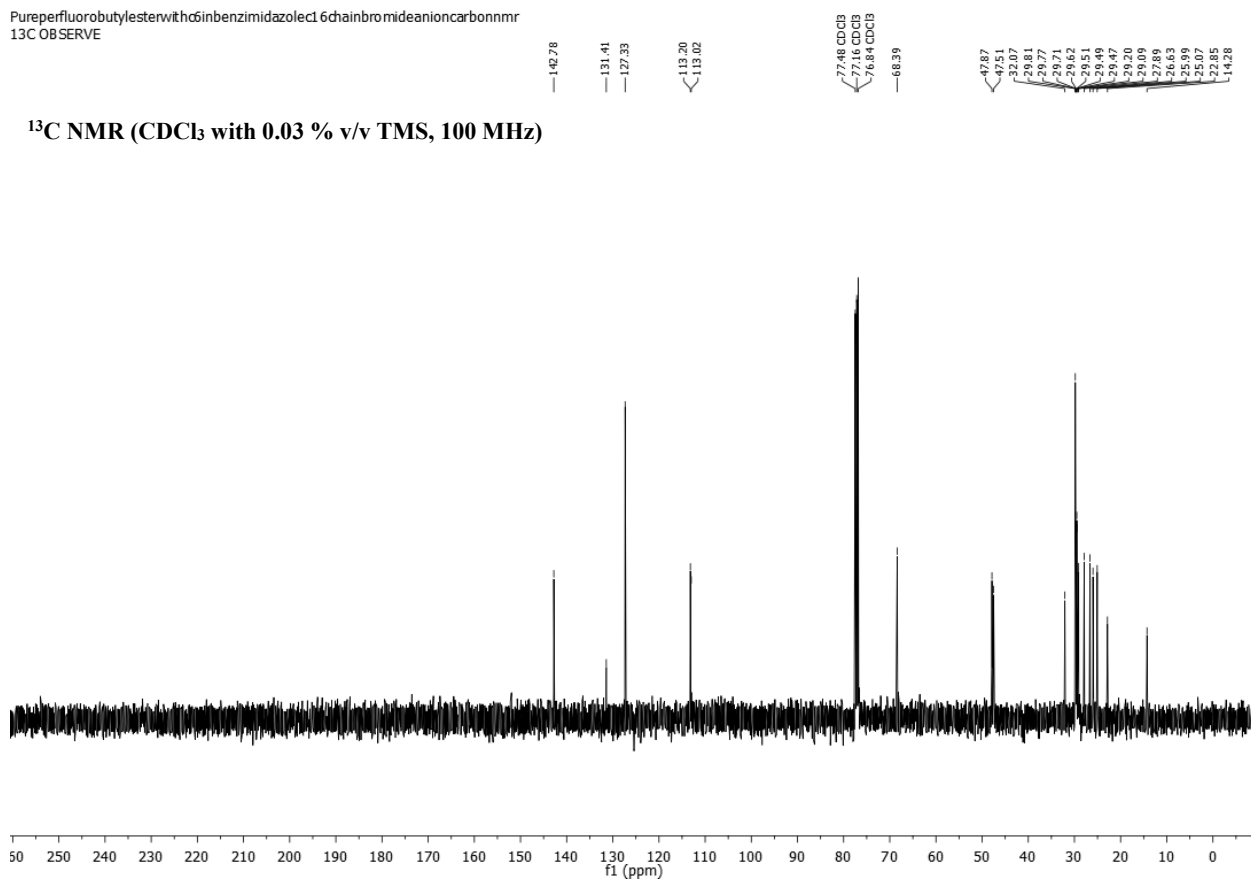
Pureperfluorobutylesterwithc6chaininc16benzimidazolewithbromideanionprotonnmr
STANDARD 1H OBSERVE

$^1\text{H NMR}$ (CDCl_3 with 0.03 % v/v TMS, 400 MHz)

(1d)

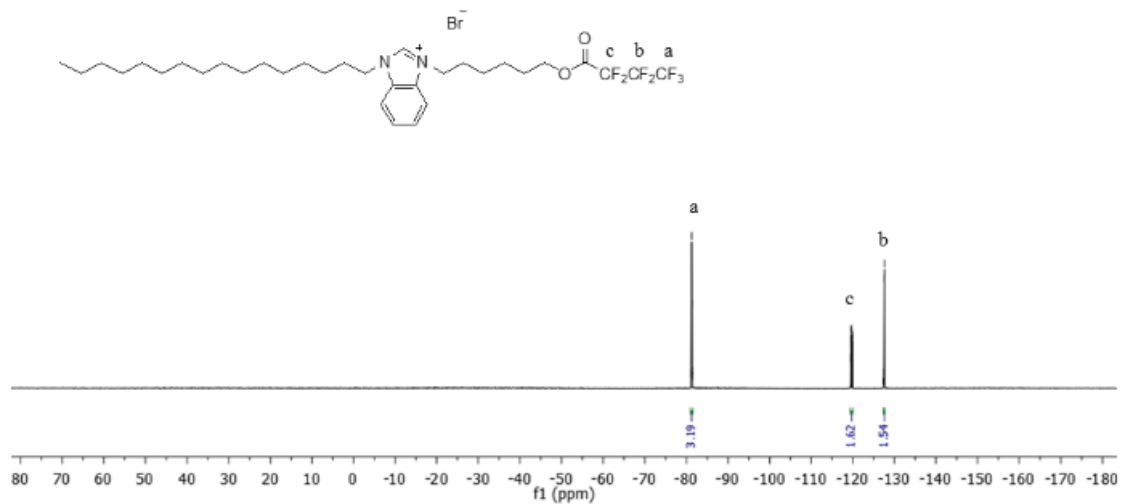


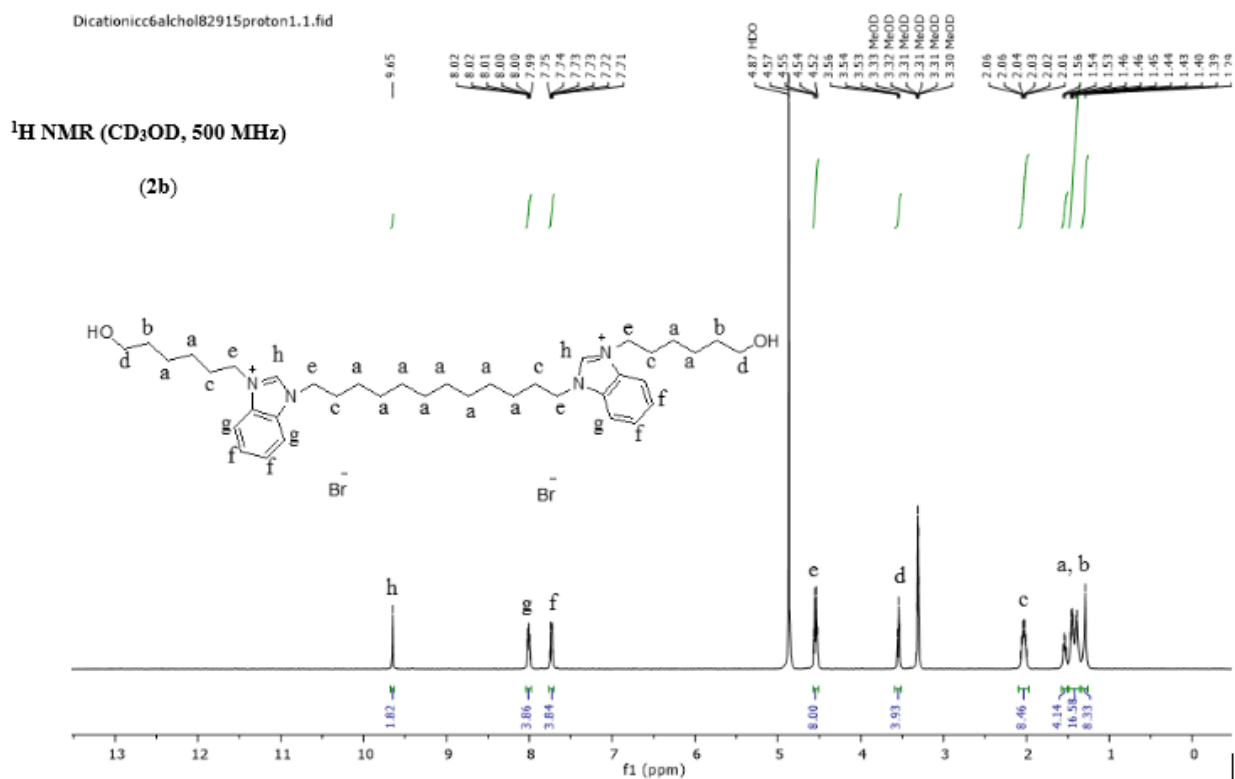
Pureperfluorobutylesterwithh6inbenzimidazolec16chainbromideanioncarbonnmr
13C OBSERVE

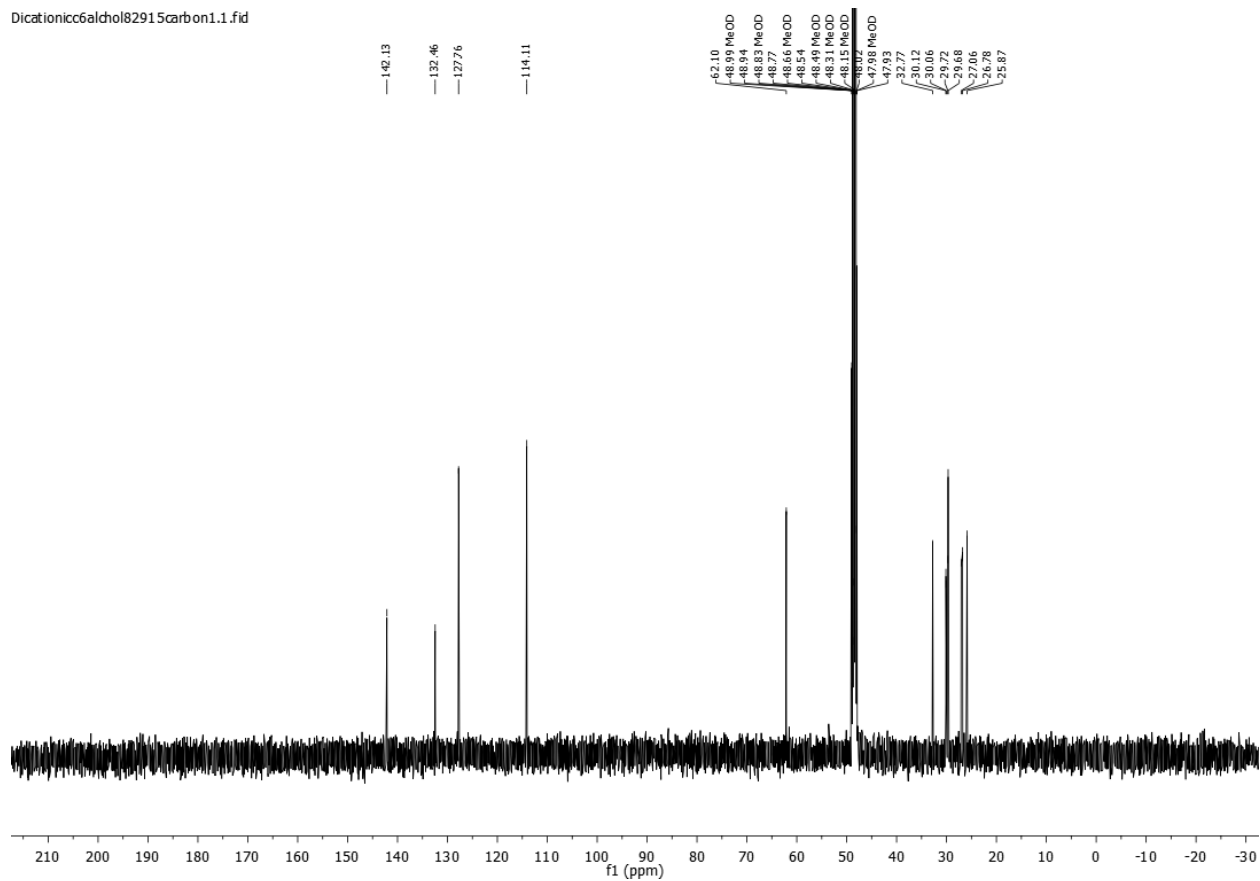


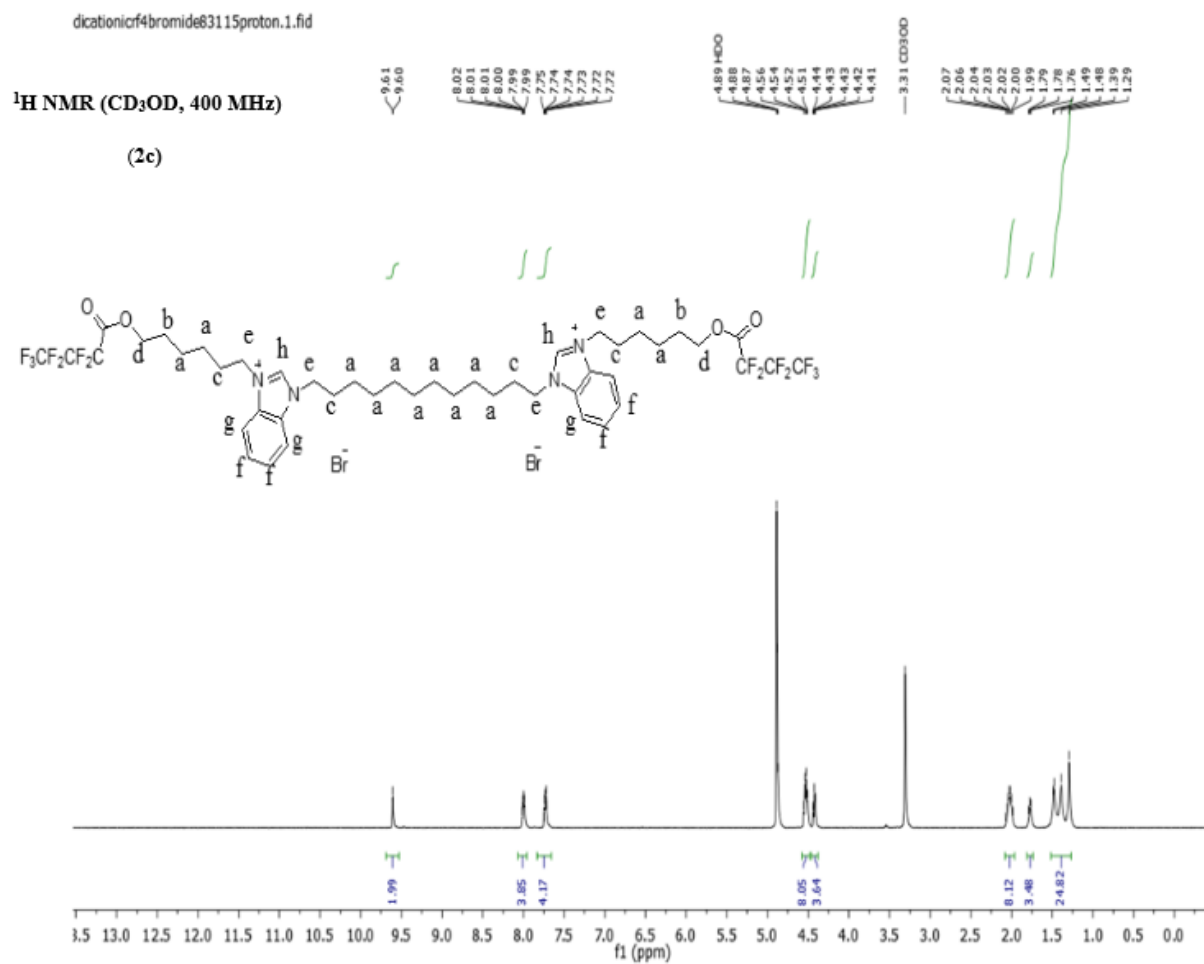
F19NMRforpurefluorobutylesterwith6chaininbenzimidazolewithbromideanionfluorin ppm
 F19 OBSERVE
 STANDARD PARAMETERS

¹⁹F NMR (1d)

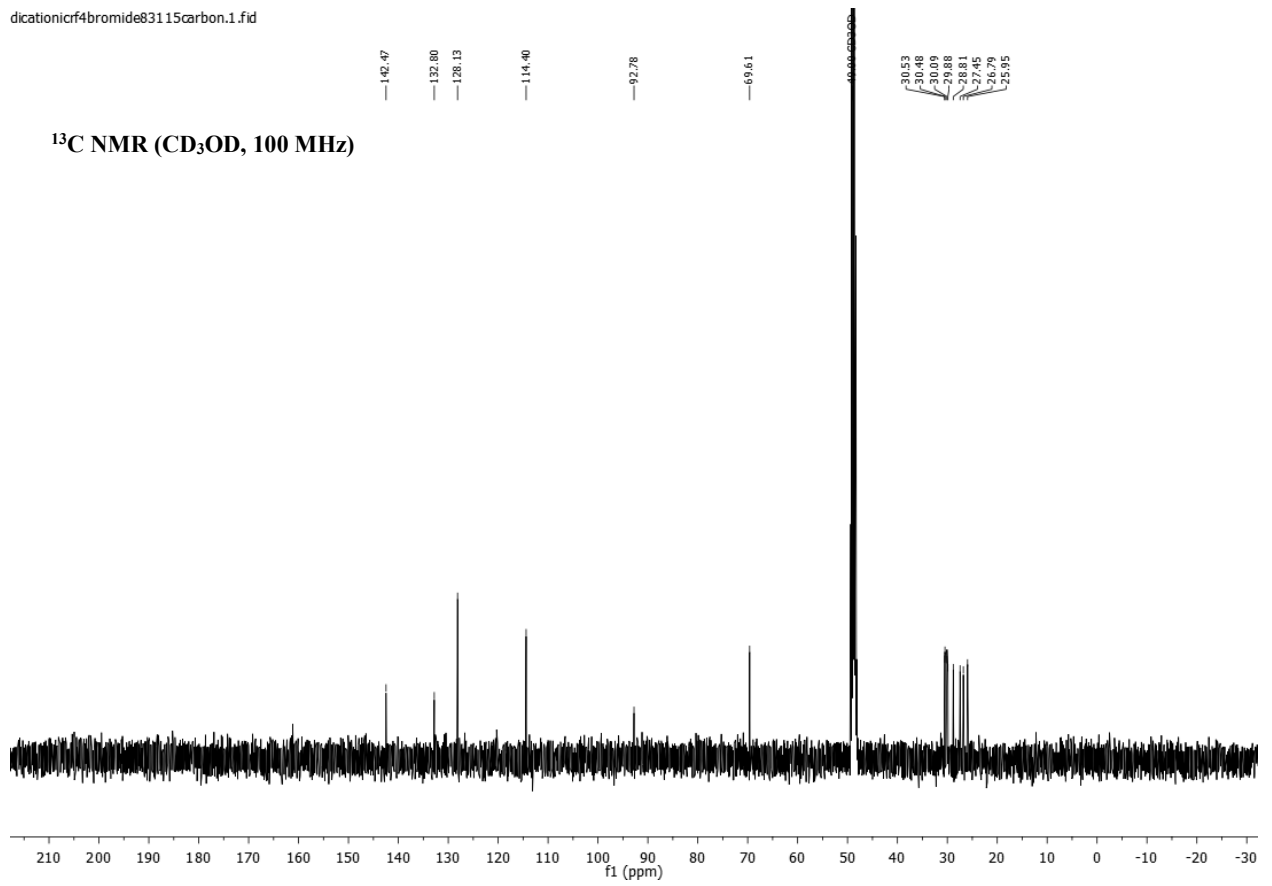




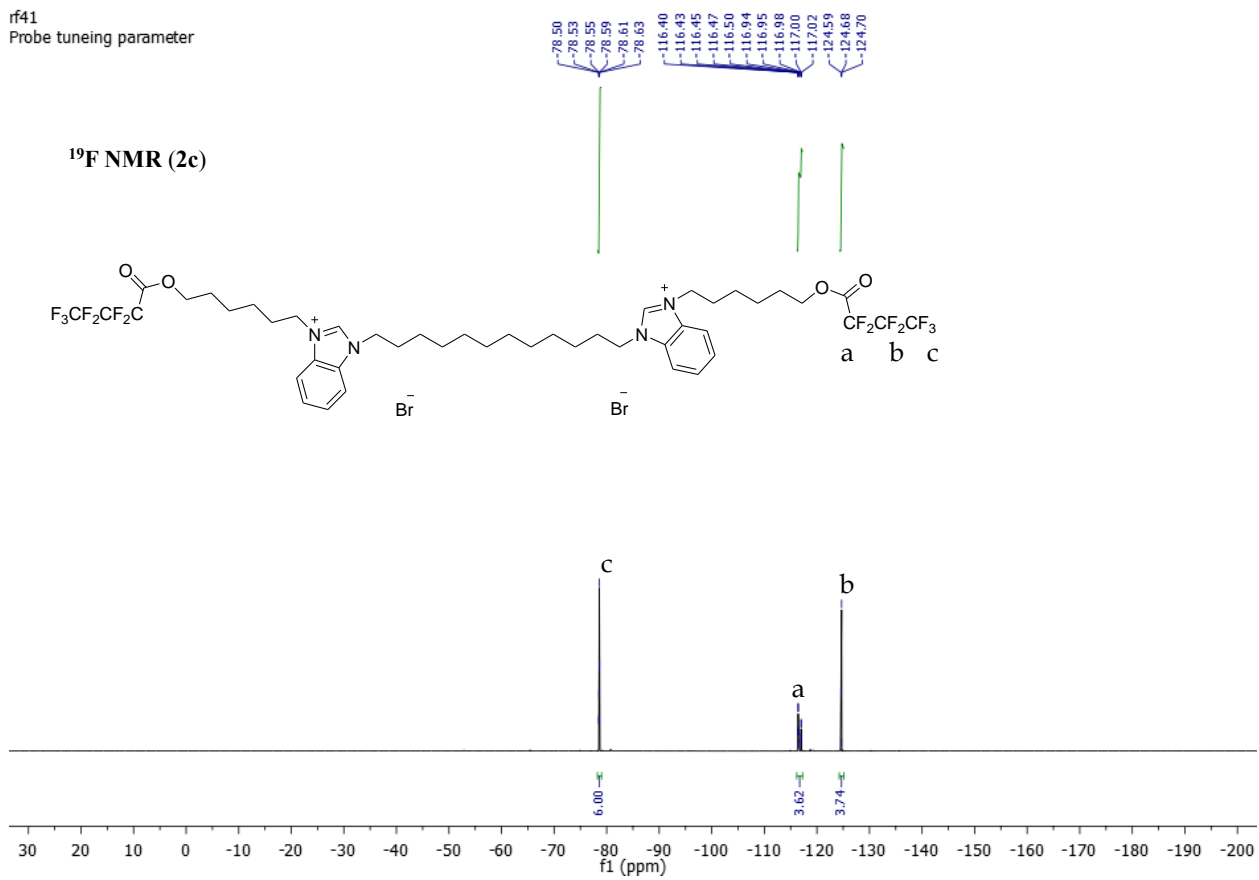
^{13}C NMR (CD_3OD , 400 MHz)



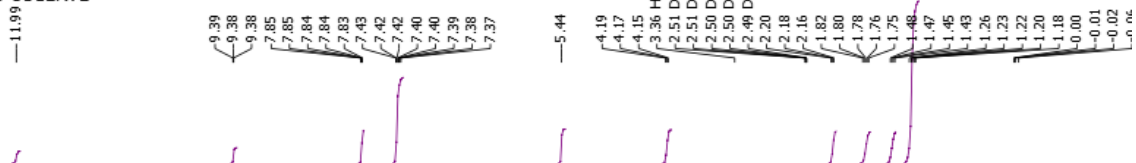
dicationicr4bromide83115carbon.1.fid



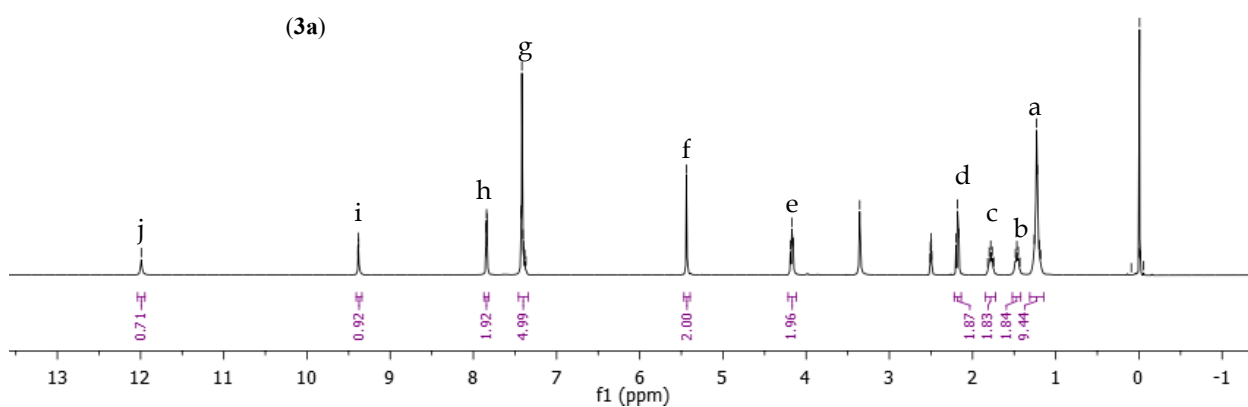
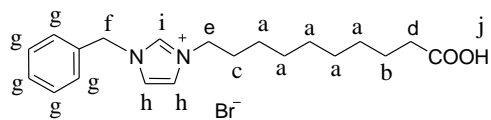
rf41
Probe tuning parameter



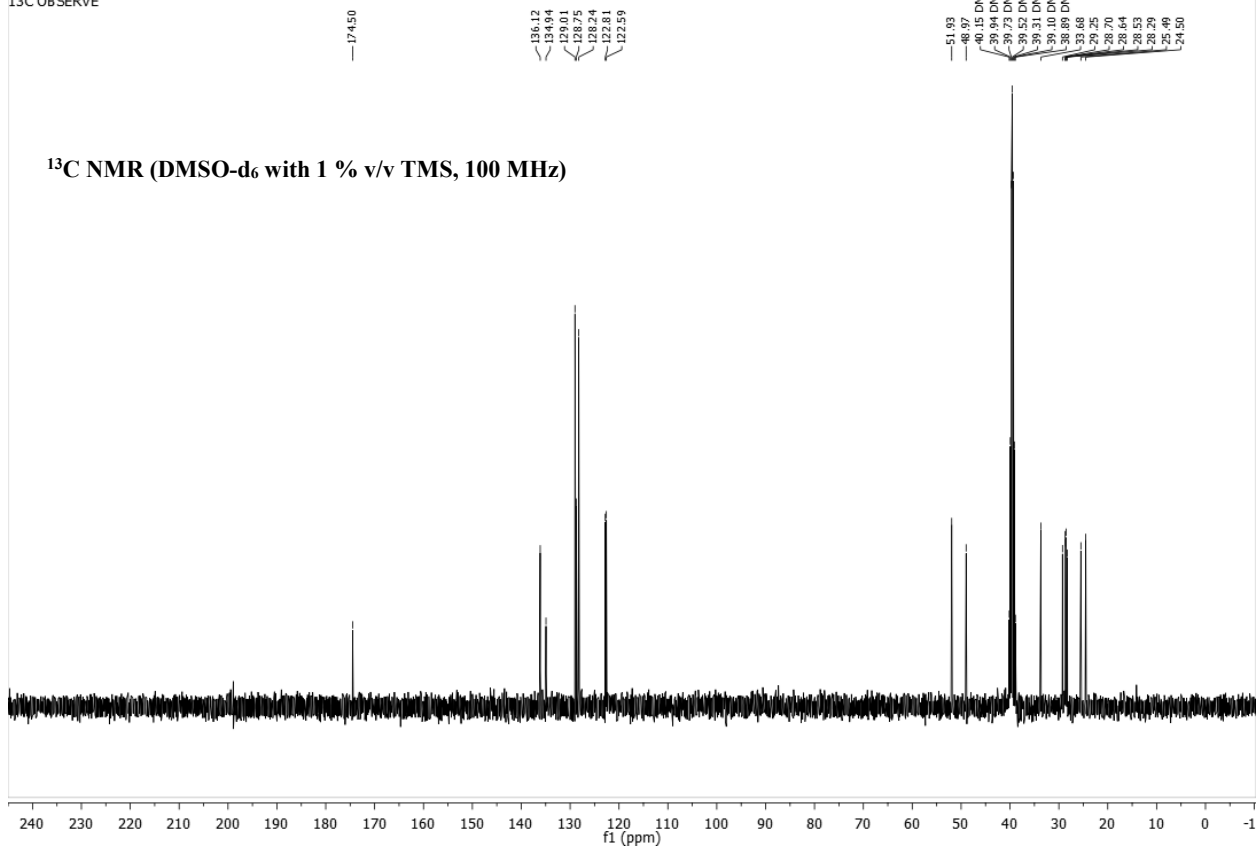
Nbenzylbromodecanoic acid bromide proton mnmr
STANDARD 1H OBSERVE



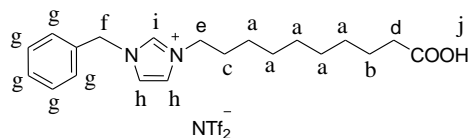
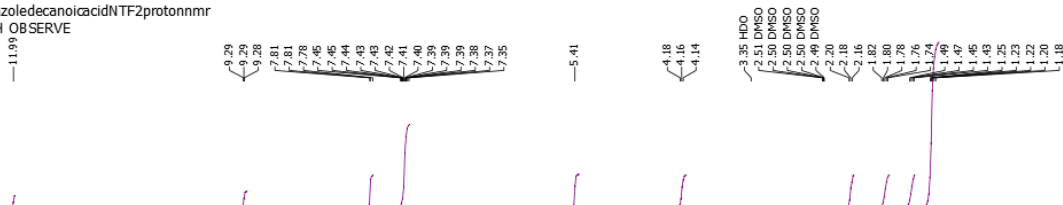
¹H NMR (DMSO-d₆ with 1 % v/v TMS, 400 MHz)



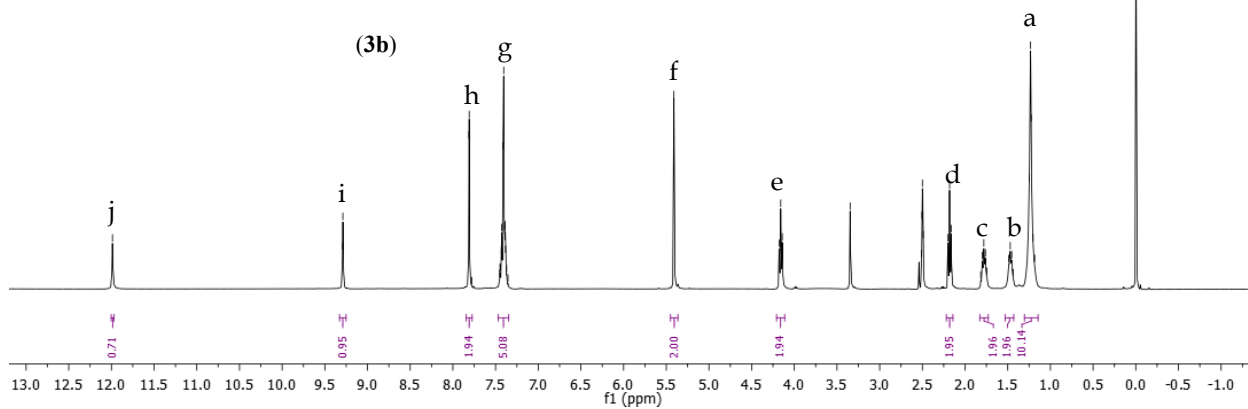
Nbenzylbromodecanoicacidbromidecarbonmr
13C OBSERVE



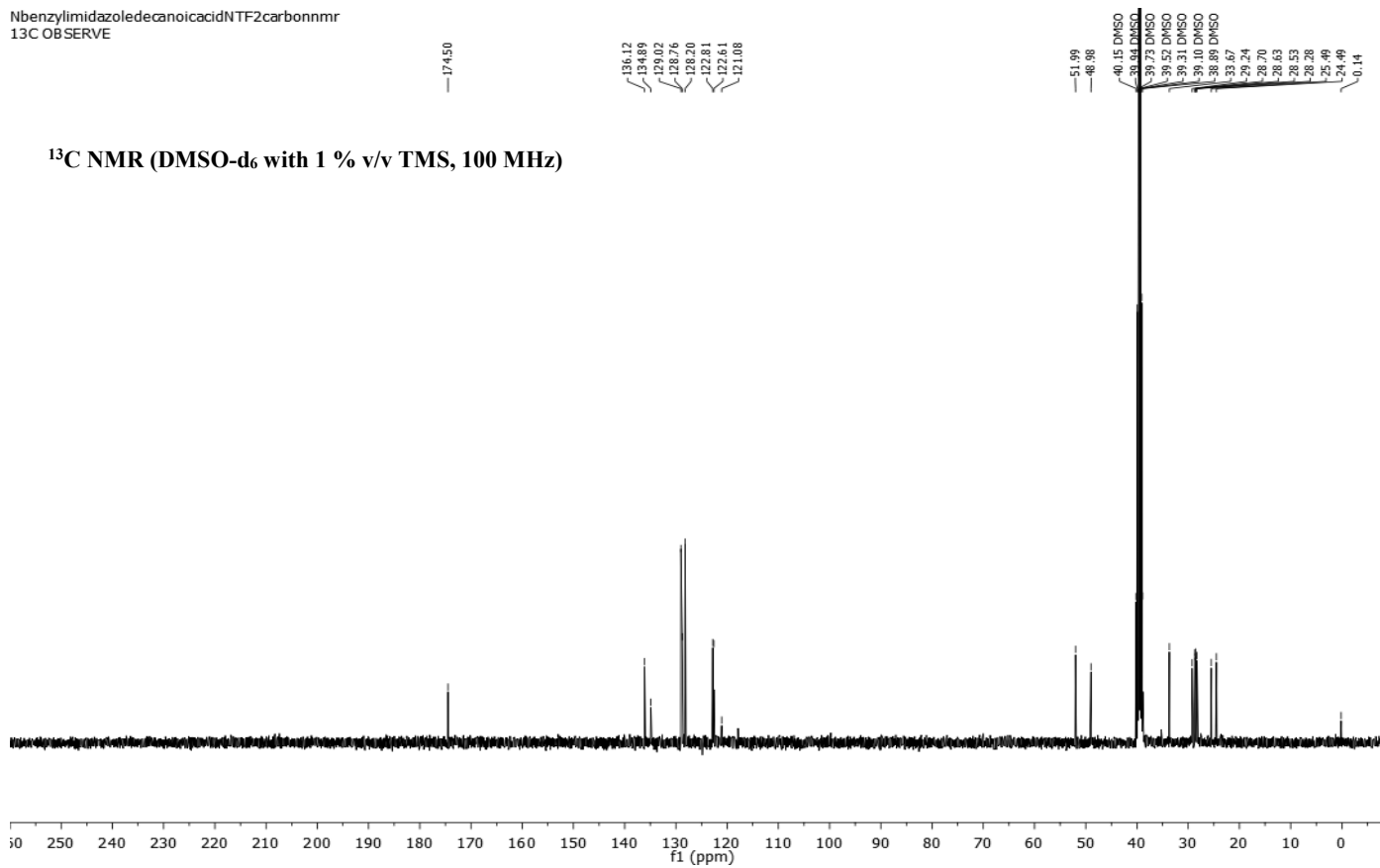
N-benzylimidazoledecanoic acidNTF2protonnmr
STANDARD 1H OBSERVE

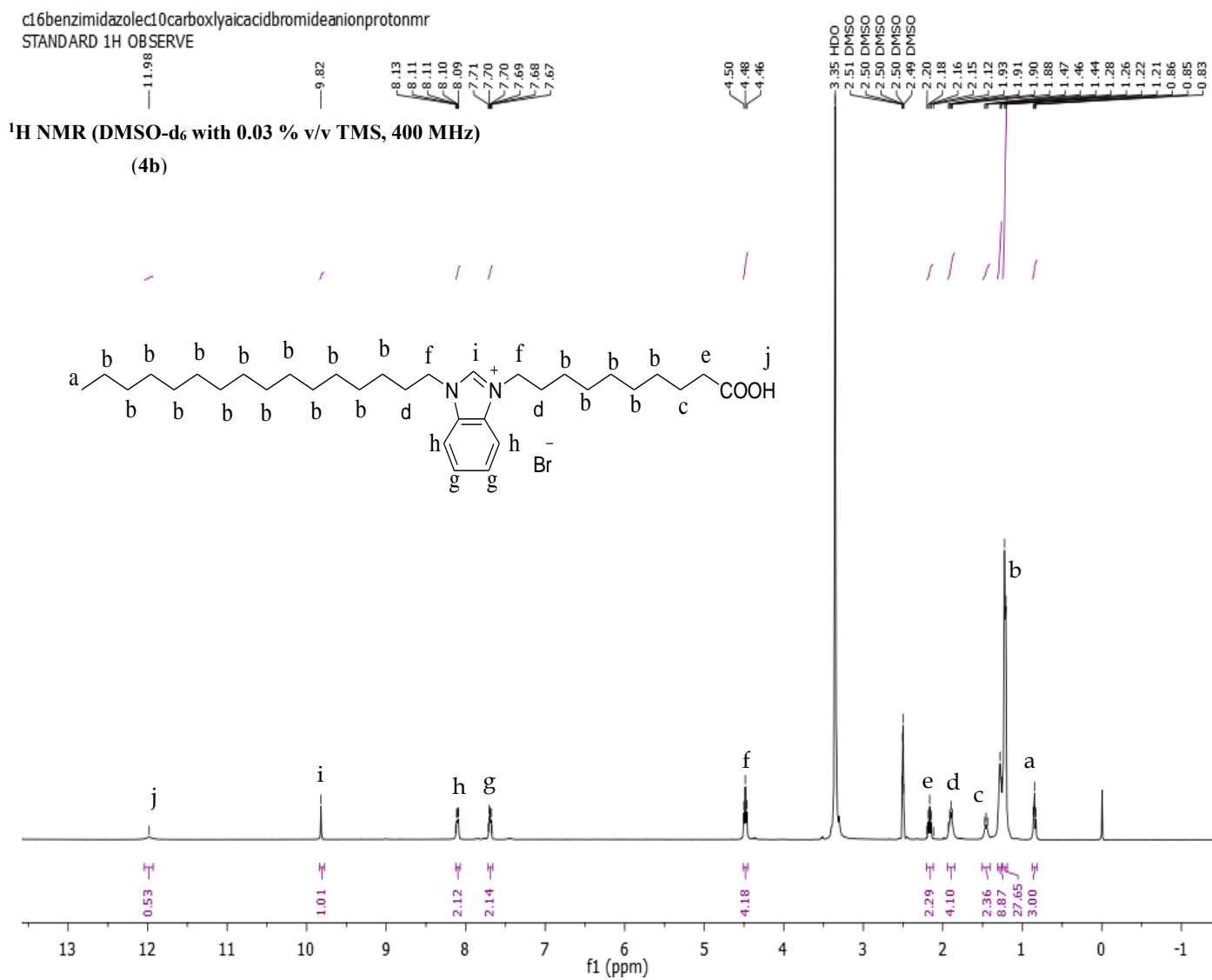


¹H NMR (DMSO-d₆ with 1 % v/v TMS, 400 MHz)

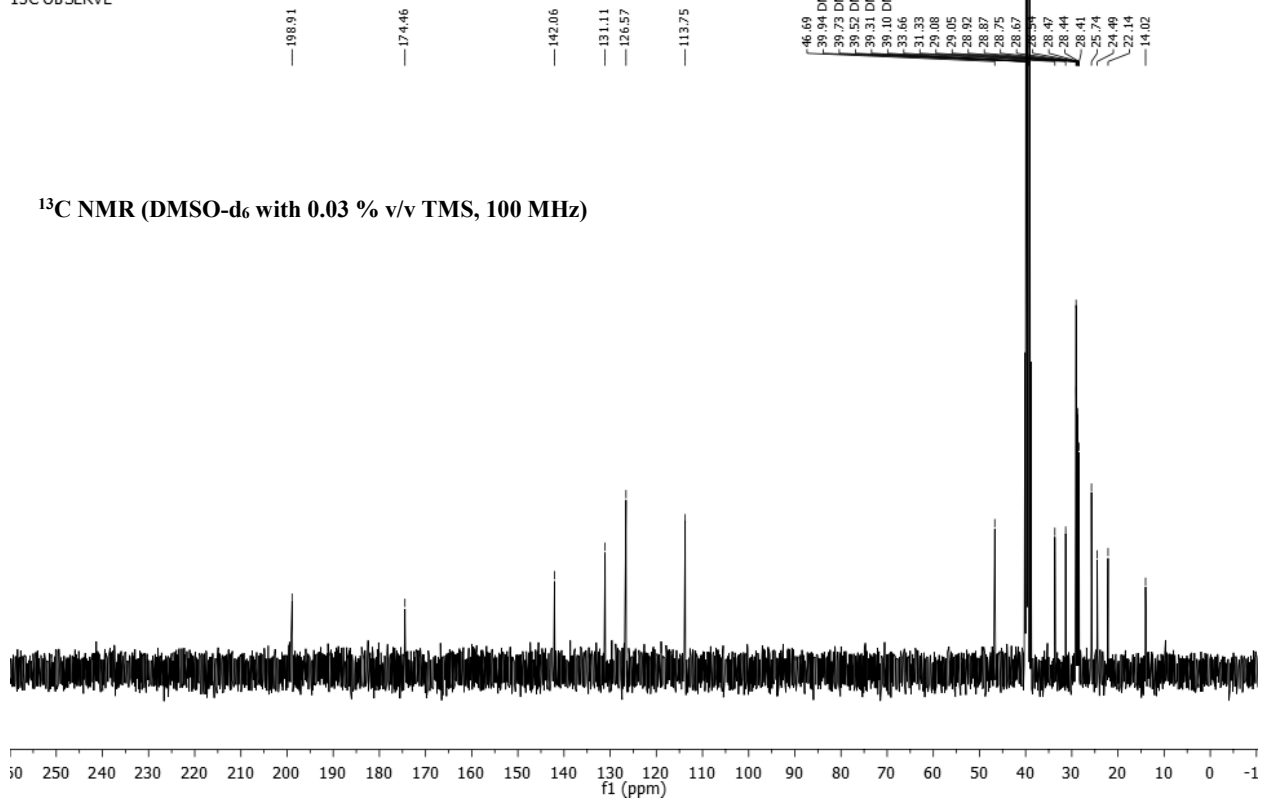


NbenzylimidazoledecanoicacidNTF2carbonnmr
13C OBSERVE





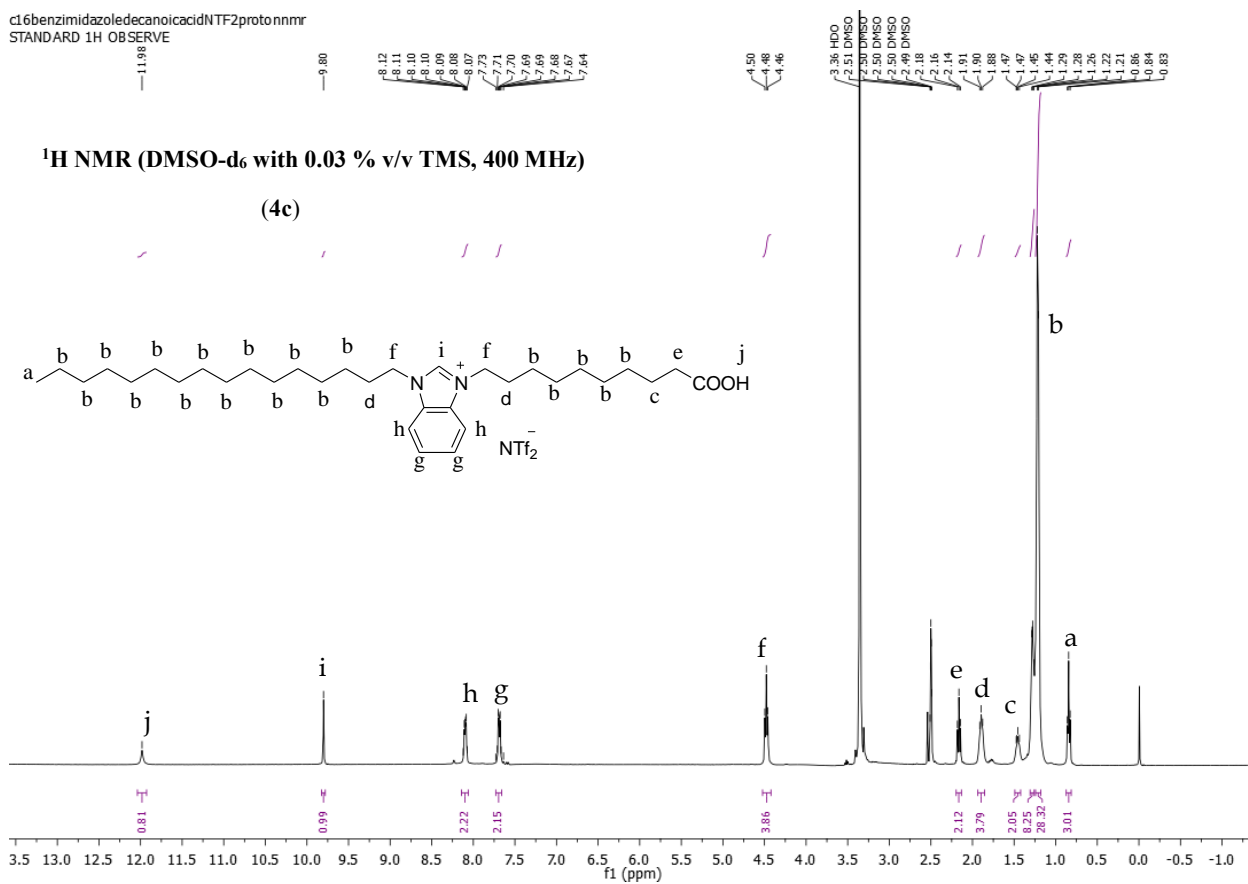
c16benzimidazoledecanoicacidbromideanioncarbonnmr
13C OBSERVE

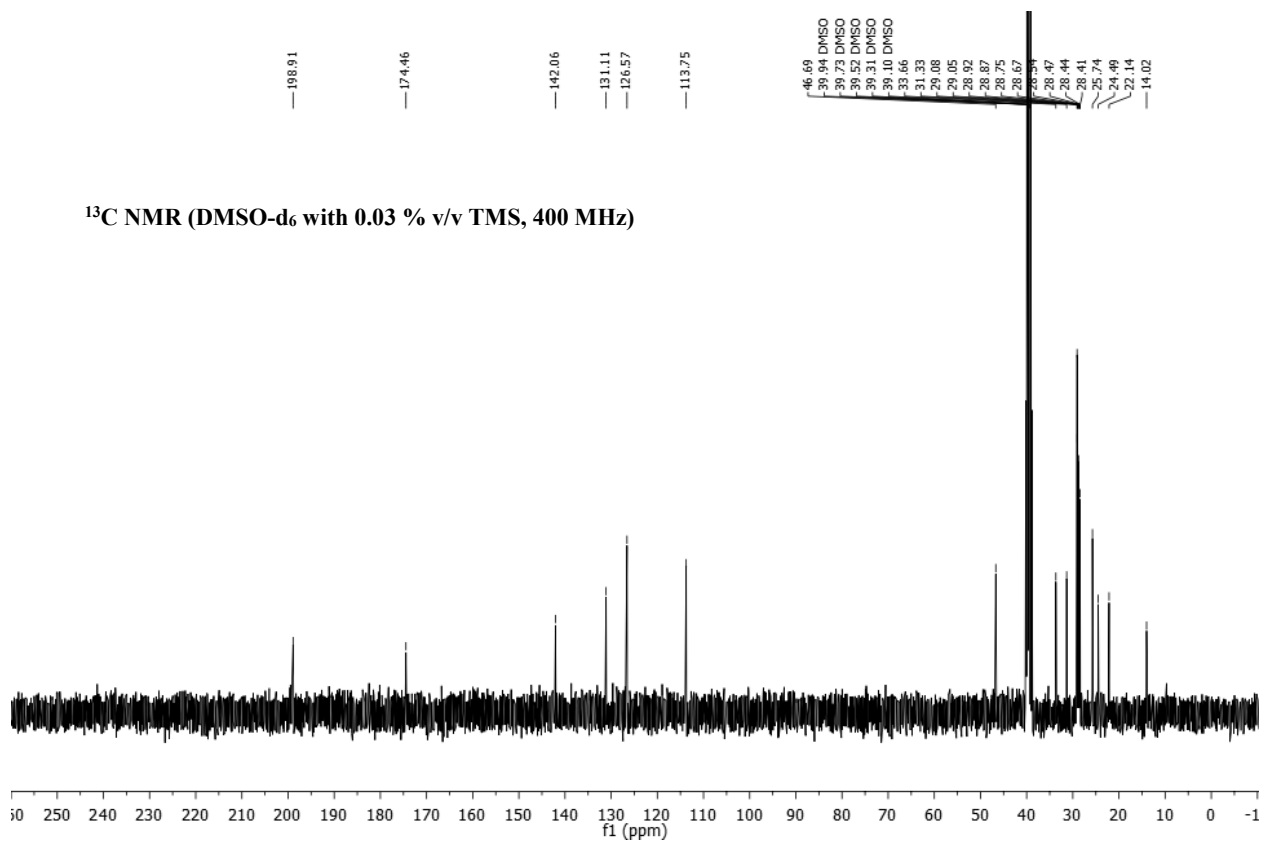


c16benzimidazoledecanoicacidNTF2proto nmr
STANDARD 1H OBSERVE

¹H NMR (DMSO-d₆ with 0.03 % v/v TMS, 400 MHz)

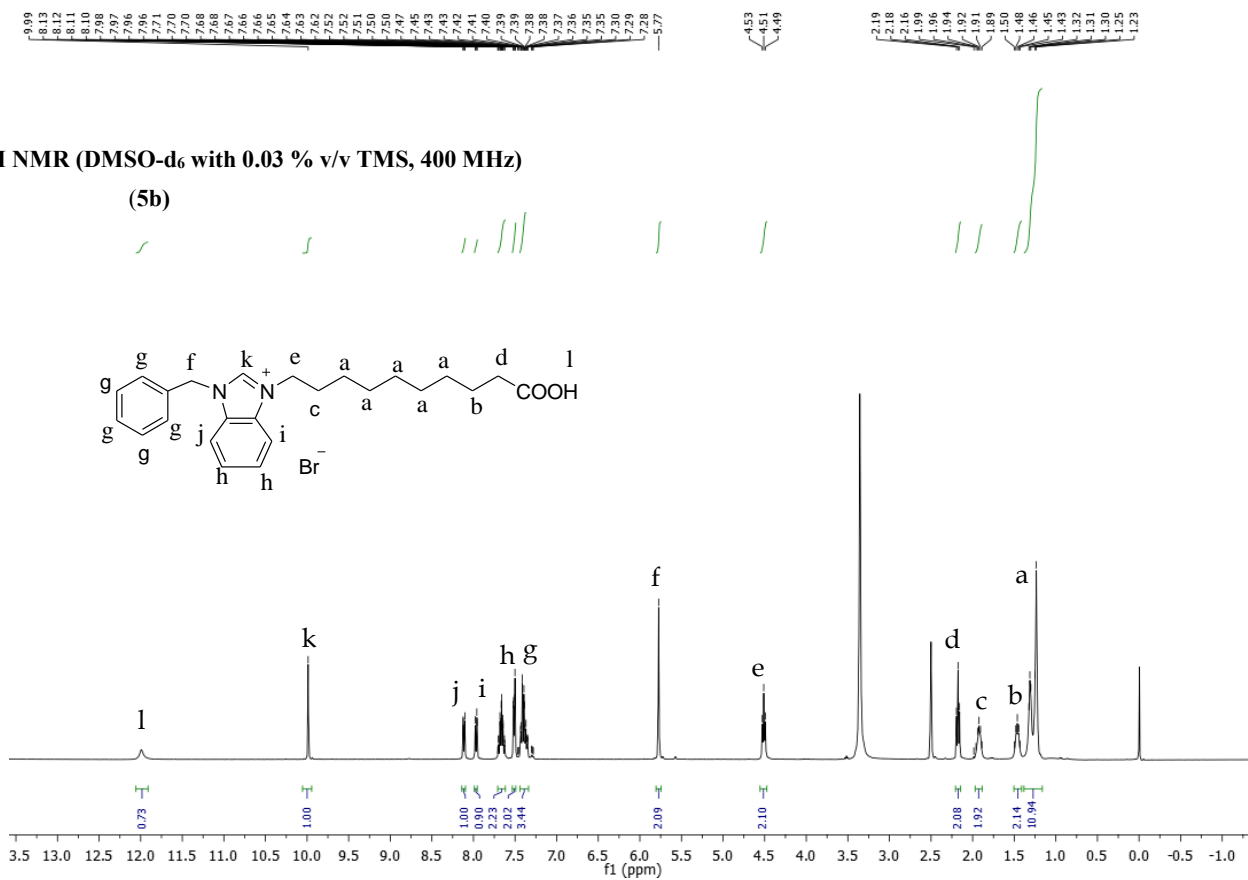
(4c)



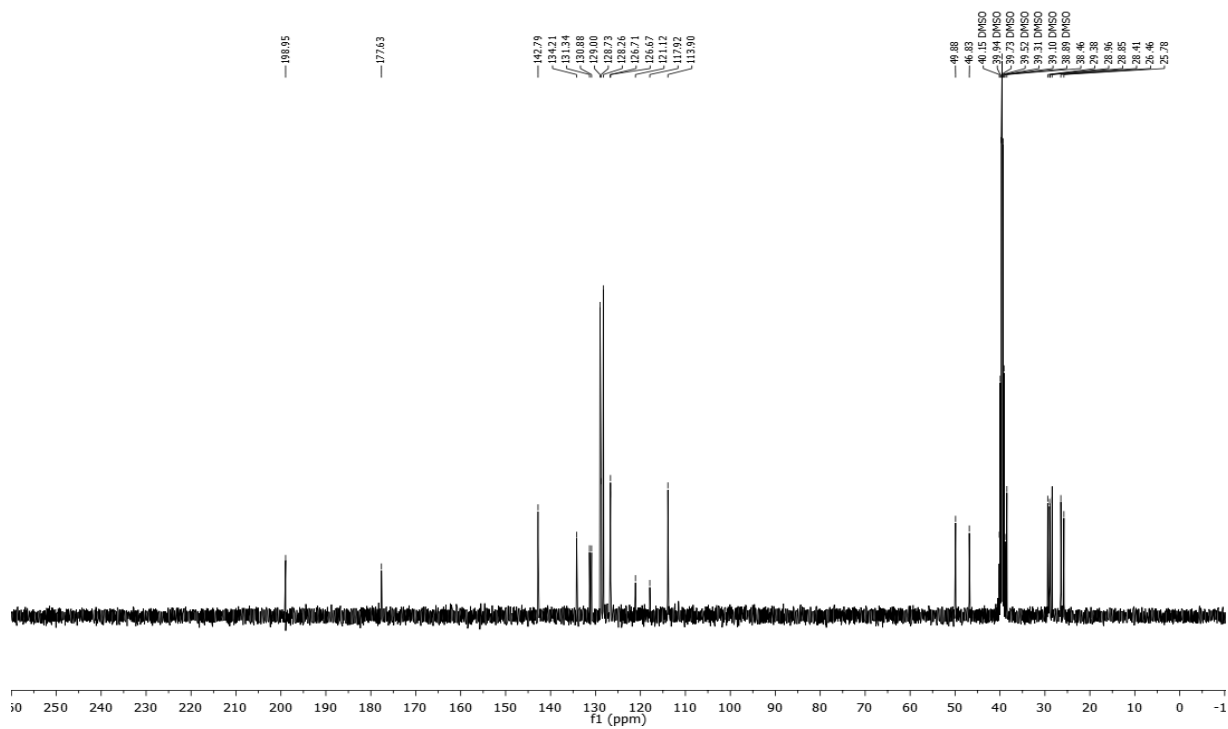


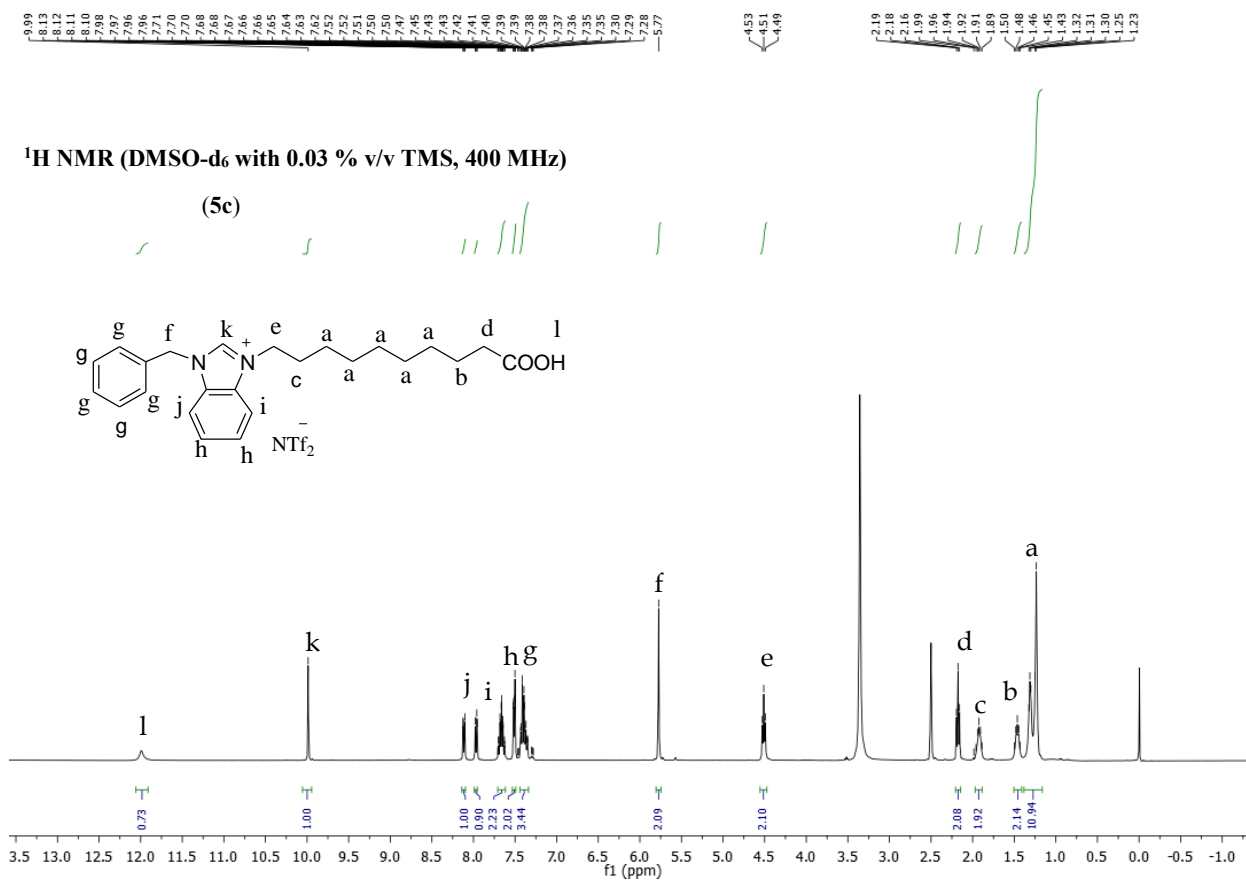
$^1\text{H NMR}$ (DMSO- d_6 with 0.03 % v/v TMS, 400 MHz)

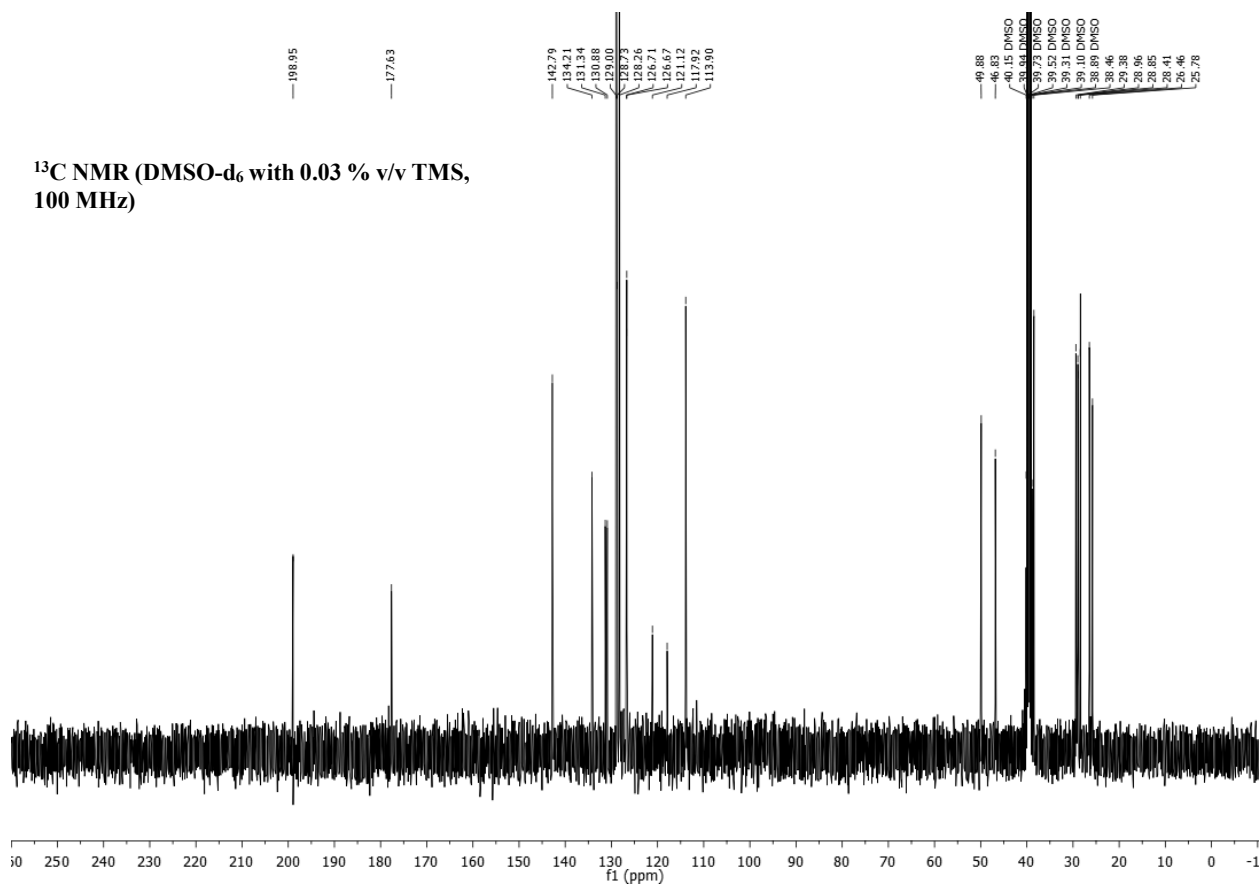
(5b)



^{13}C NMR (DMSO- d_6 with 0.03 % v/v TMS, 100 MHz)







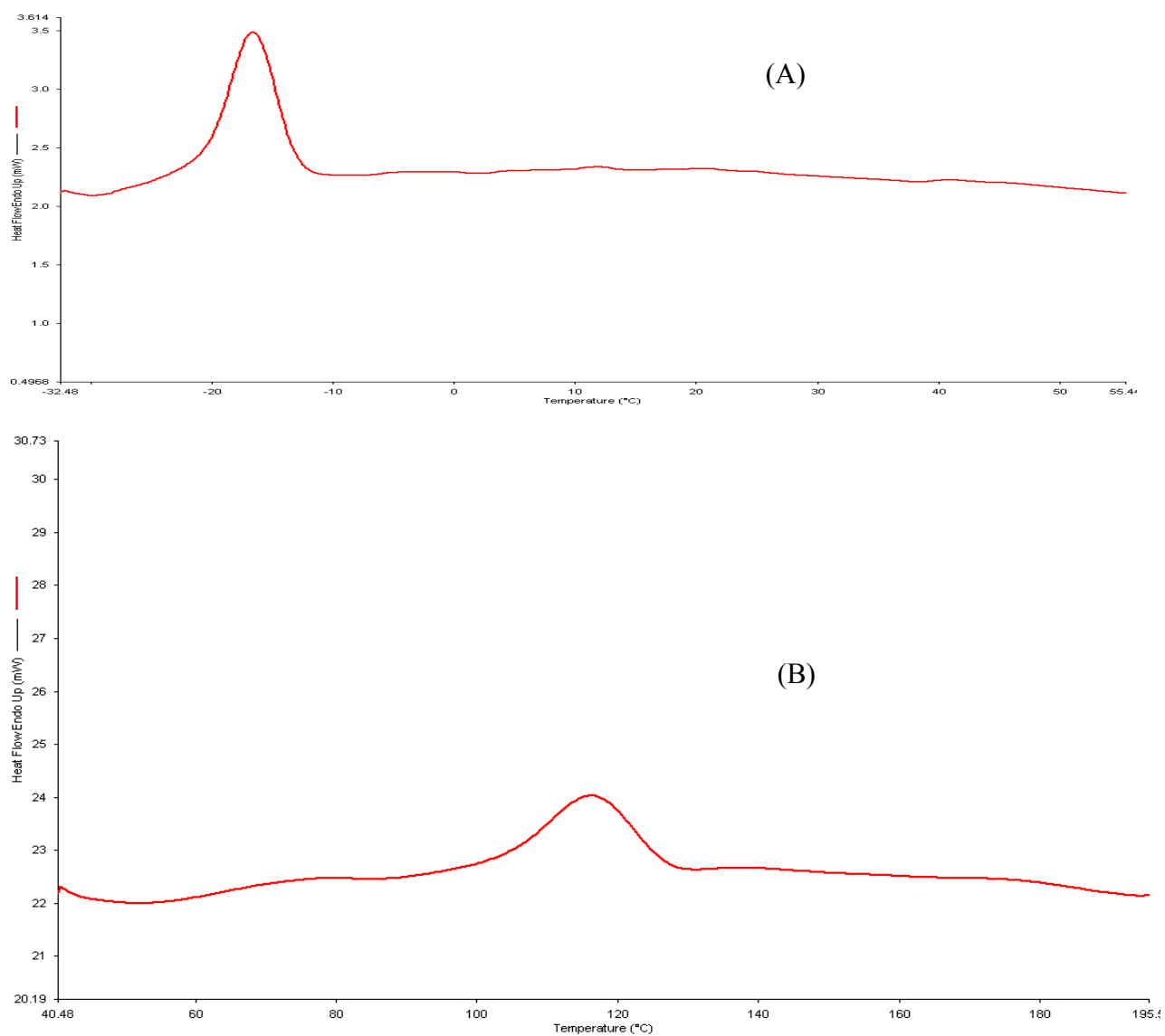


Figure S1. DSC traces of (A) MIL **1**; (B) dicationic MIL intermediate **2b**;

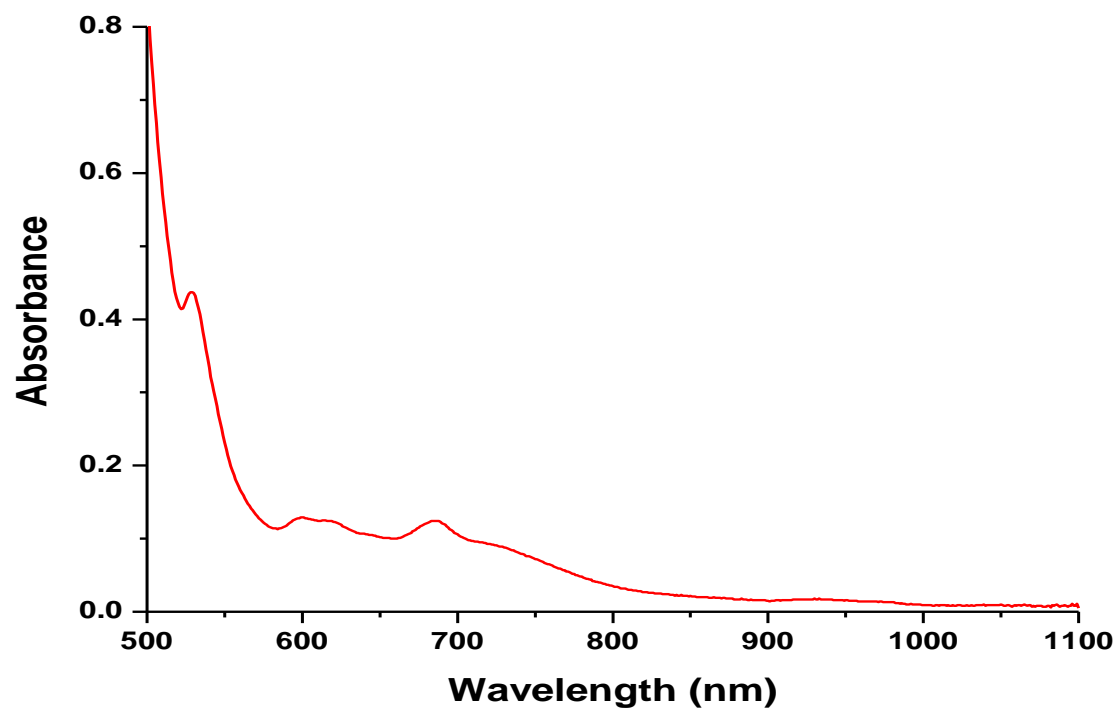


Figure S2. Absorbance spectrum of bromotrichloroferrate $[\text{FeCl}_3\text{Br}^-]$ anion

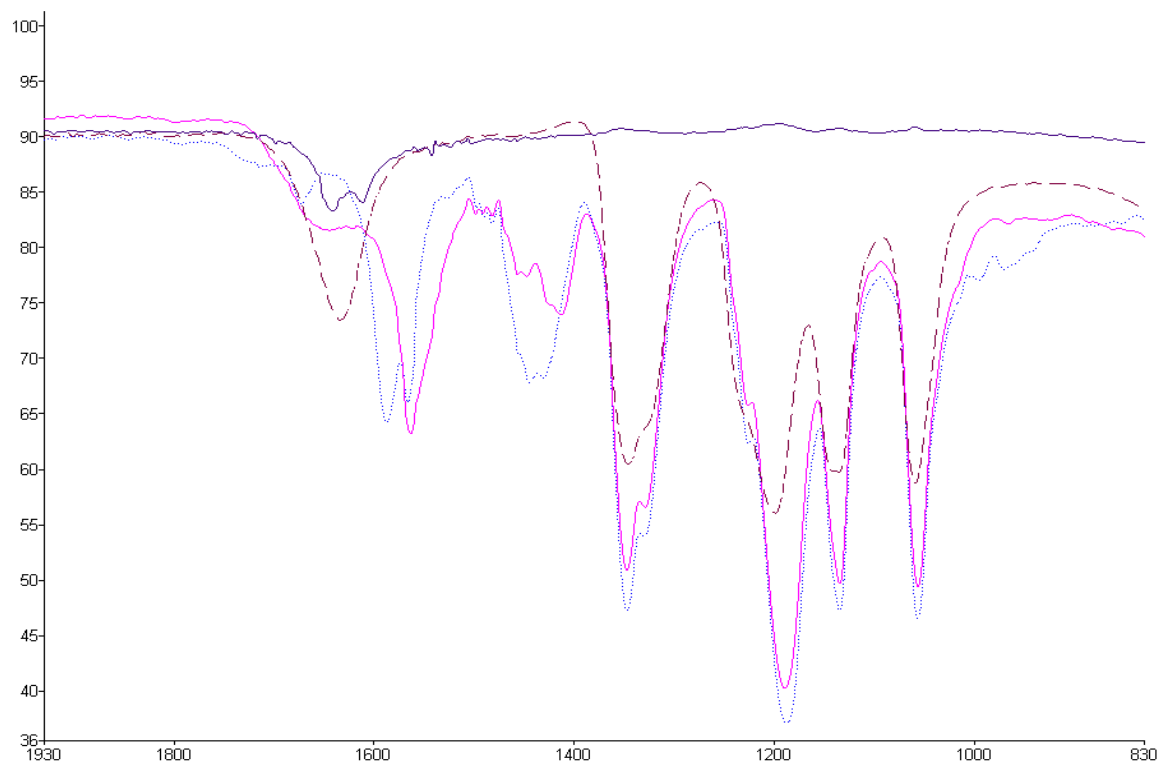


Figure S3. Representative IR overlay for Fe(III) carboxylate-based hydrophobic MIL 4 and compounds involved in its synthesis. FeCl₃·6H₂O (—); LiNTf₂ (- - -); Compound 4d (—); MIL 4 (.....)

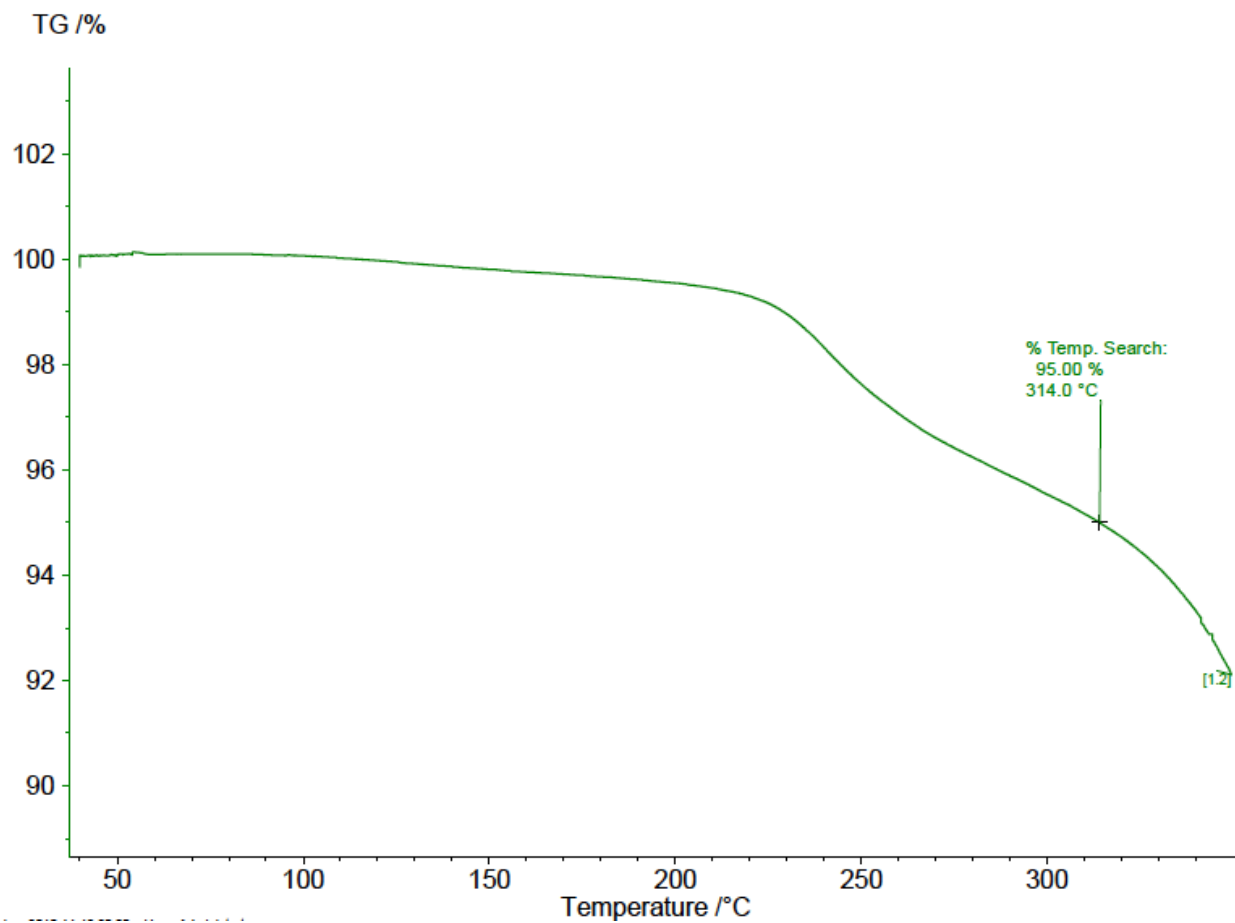


Figure S4. Representative TGA trace for hydrophobic MIL 3.

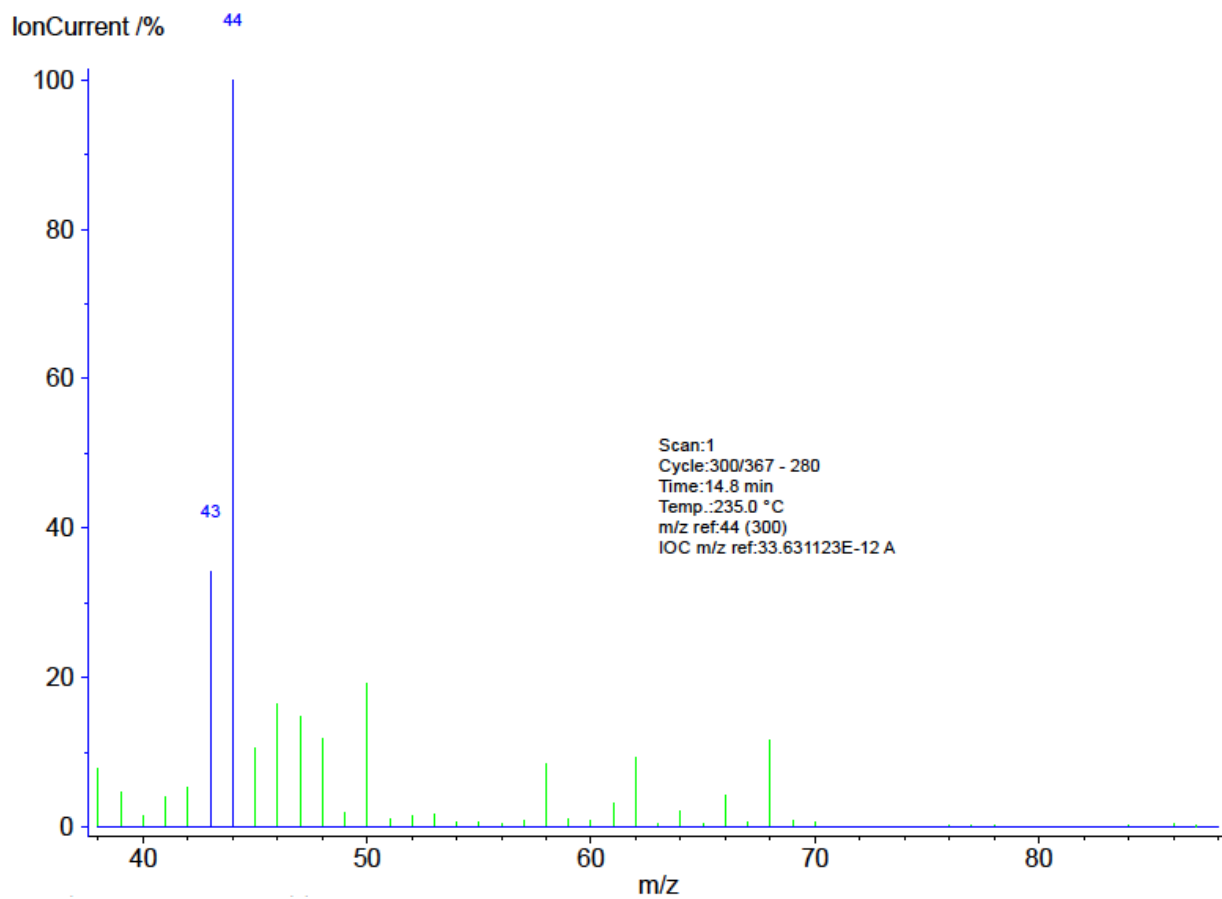


Figure S5. Mass spectrum of the evolved gases during the TGA experiment for the Fe(III) carboxylate-based MIL 3. The spectrum shown was collected when the sample temperature was 235 °C.

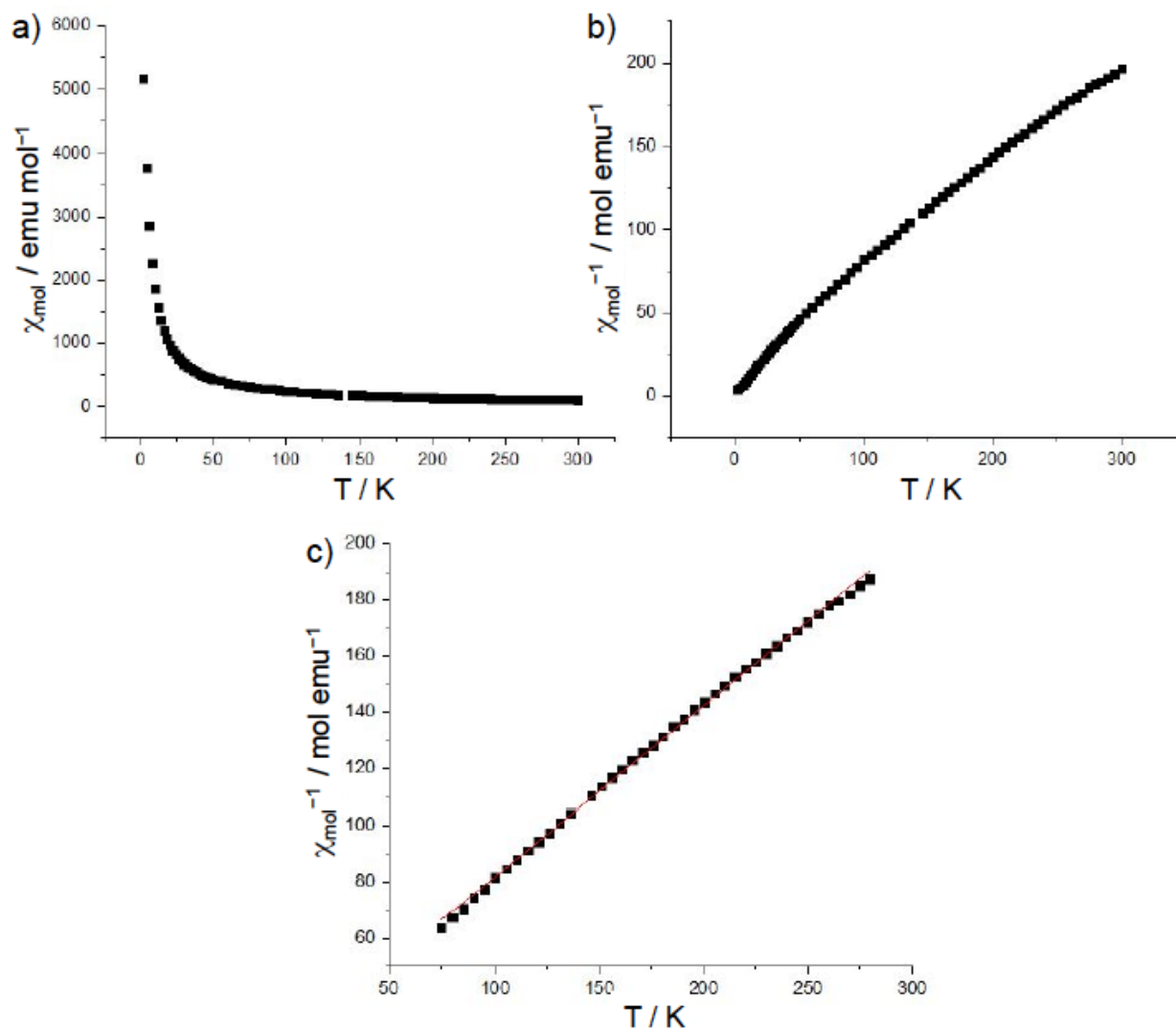


Figure S6. Temperature dependence of the (a) molar magnetic susceptibility and the (b) reciprocal molar susceptibility for MIL 3 using a field of 20,000 Oe. Panel (c) shows the linear fit for reciprocal molar susceptibility versus temperature from 280 K down to 75 K.

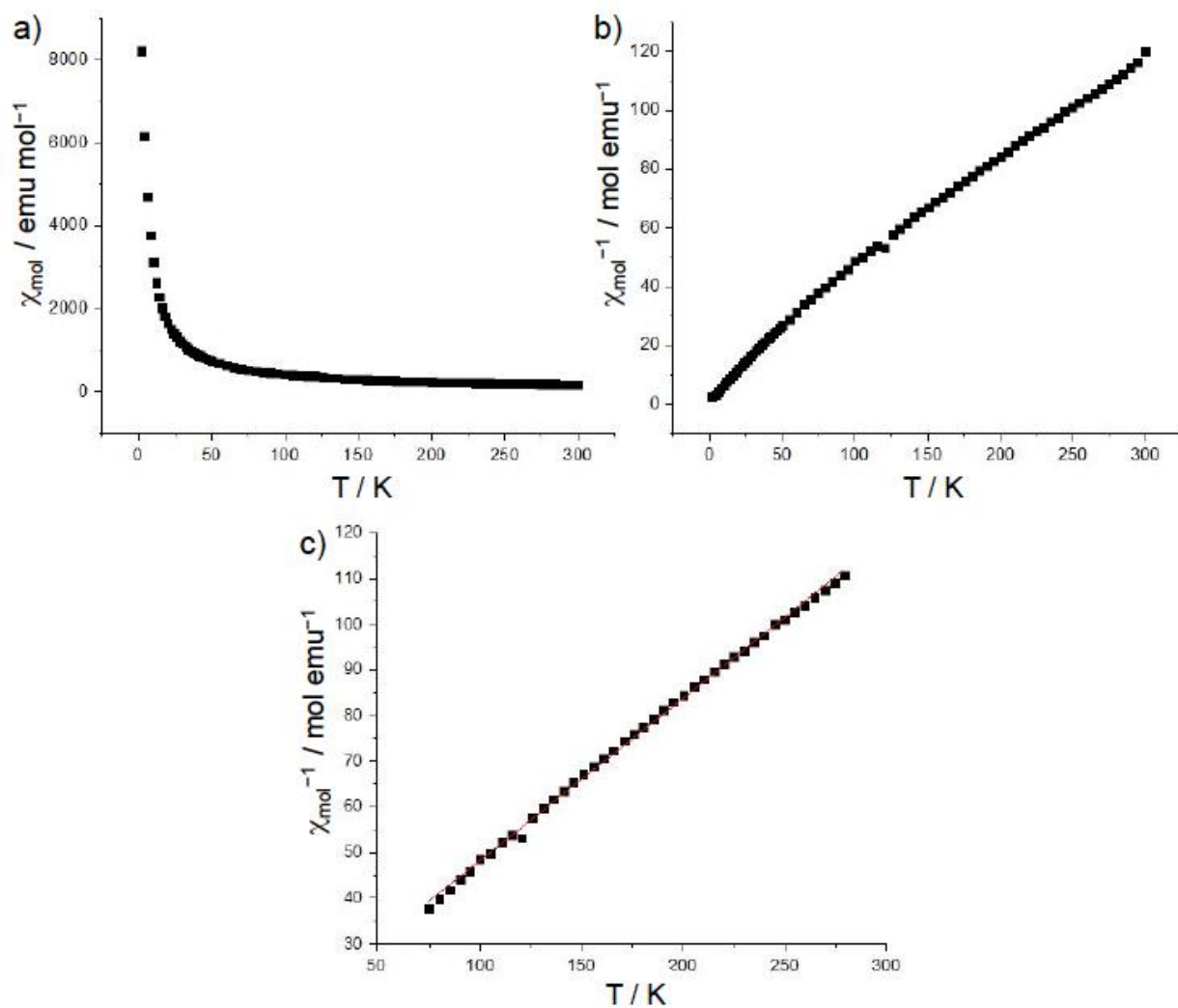


Figure S7. Temperature dependence of the (a) molar magnetic susceptibility, the (b) reciprocal molar susceptibility, and the (c) linear fit for reciprocal molar susceptibility versus temperature from 280 K down to 75 K for MIL 5 using a field of 20,000 Oe.

APPENDIX C
SUPPORTING INFORMATION ACCOMPANYING
CHAPTER 4

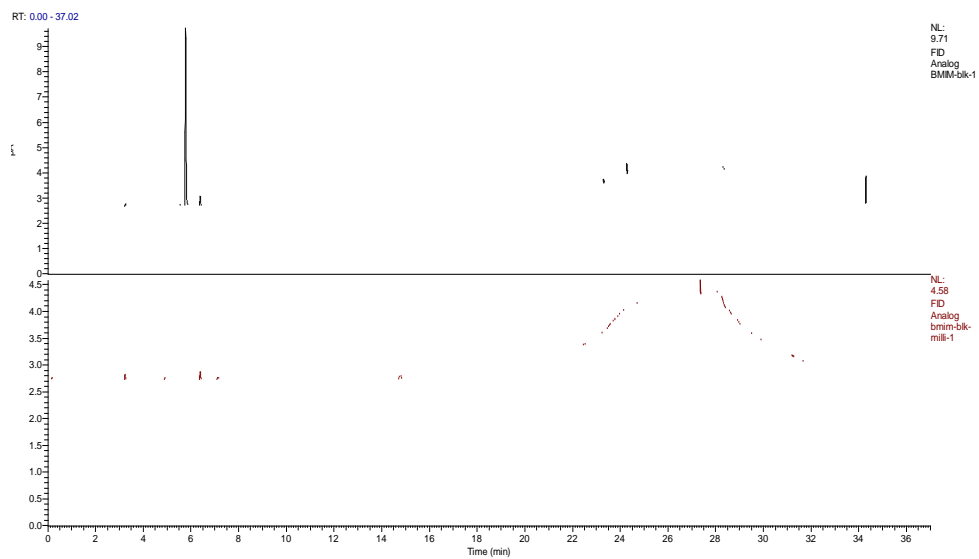


Figure S1. Evaluation of chromatographic background contributions of [BMIM][NTf₂] obtained from different manufacturers (A) IOLITEC and (B) EMD Millipore. Sample volume: 1 mL; incubator temperature: 140 °C; incubation time: 45 min.

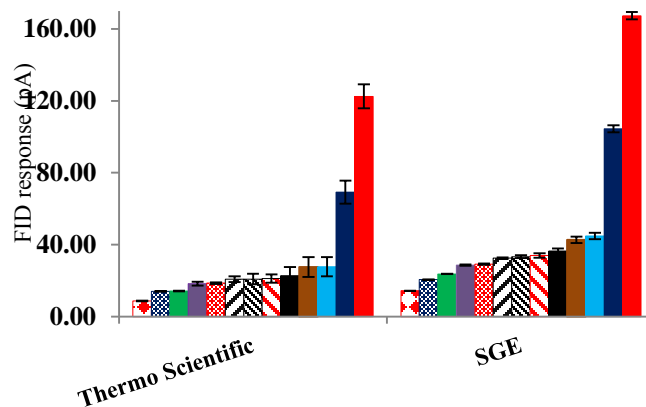


Figure S2. Effect of gastight syringe type on response of the residual solvents in [BMIM][NTf₂] at 145 °C syringe temperature. (■) n-heptane; (■) *tert*-butyl methyl ether; (■) 2-propanol; (■) ethanol; (■) 1-propanol; (■) acetone; (■) 2-methyl-1-propanol; (■) isopropyl acetate; (■) ethyl acetate; (■) methyl ethyl ketone; (■) 1-butanol; (■) methanol; (■) 1-pentanol. Residual solvents concentration: 60% ICH limit (relative to API); incubation temperature: 80 °C; Incubation time: 45 min; Sample volume: 1 mL. Data obtained by performing experiments in triplicate triplicate (n = 3).

APPENDIX D
SUPPORTING INFORMATION ACCOMPANYING
CHAPTER 5

Figure S1. Chemical structures of all the surfactants utilized in this study, including dicationic IL-based surfactants (A), and tricationic IL-based surfactants (B).

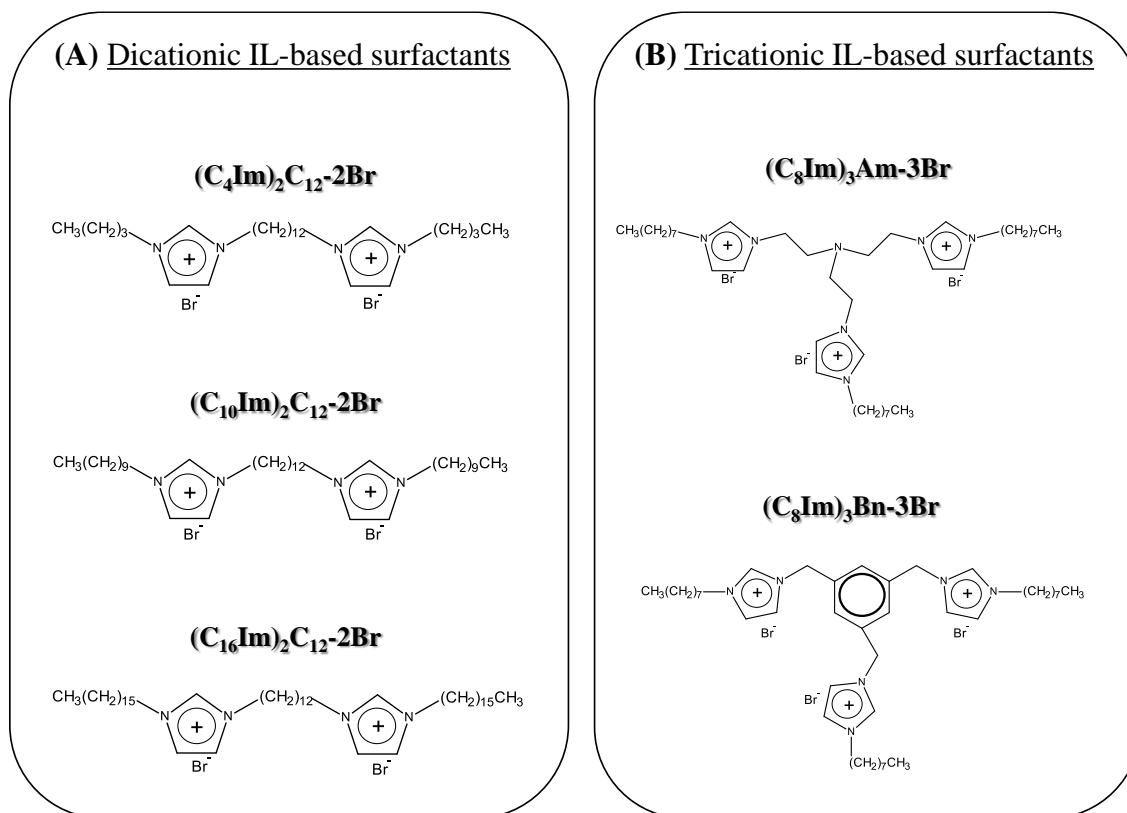
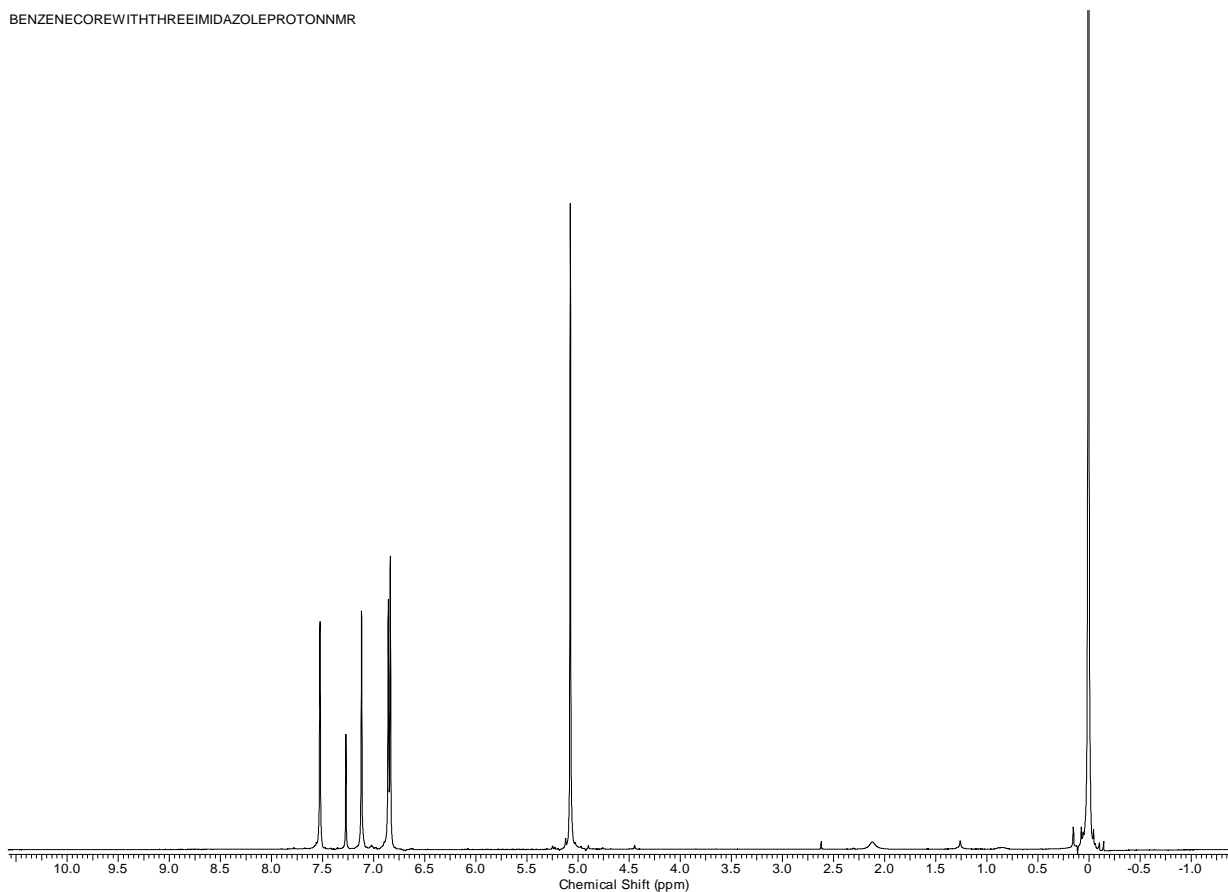


Figure S2. ^1H NMR (A) and ^{13}C NMR (B) spectra for 1-(3,5-bis((1H-imidazol-1-yl)methyl)benzyl)-1H-imidazole (compound 1A)

(A) ^1H NMR

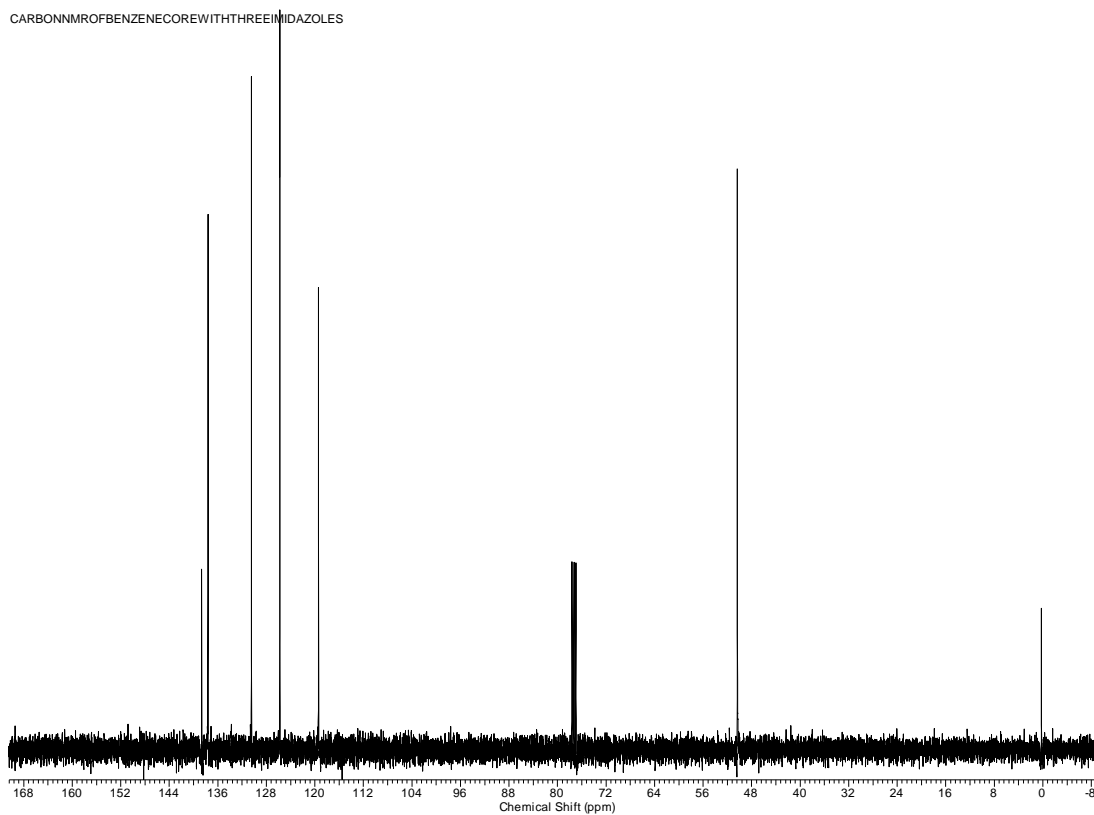
BENZENECOREWITHTHREEIMIDAZOLEPROTONNMR



^1H NMR (CDCl_3 , 400 MHz) δ (ppm): 5.08 (s, 6H), 6.84 (d, $J = 1\text{Hz}$, 3H), 6.86(d, $J = 1\text{Hz}$, 3H), 7.12 (s, 3H), 7.52 (s, 3H).

Figure S2. (continued) ^1H NMR (A) and ^{13}C NMR (B) spectra for 1-(3,5-bis((1H-imidazol-1-yl)methyl)benzyl)-1H-imidazole (compound 1A)

(B) ^{13}C NMR



^{13}C NMR (CDCl_3 , 400 MHz) δ (ppm): 50.37, 119.40, 125.77, 130.45, 137.61, 138.65.

Figure S3. ESI mass spectrum of 1-(3,5-bis((1H-imidazol-1-yl)methyl)benzyl)-1H-imidazole (compound 1A)

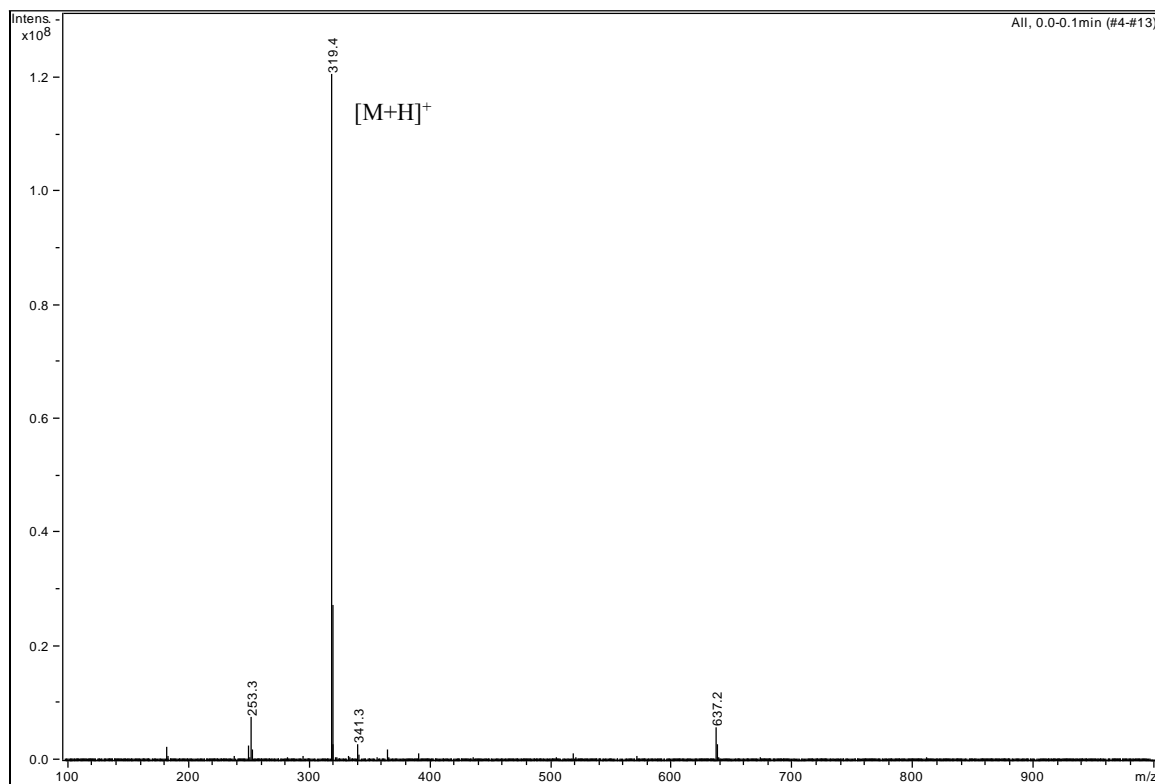
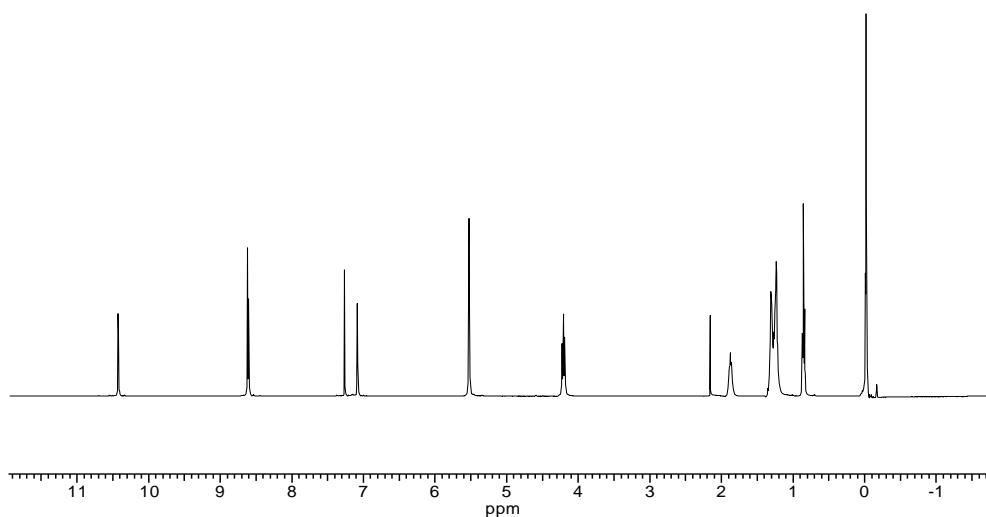


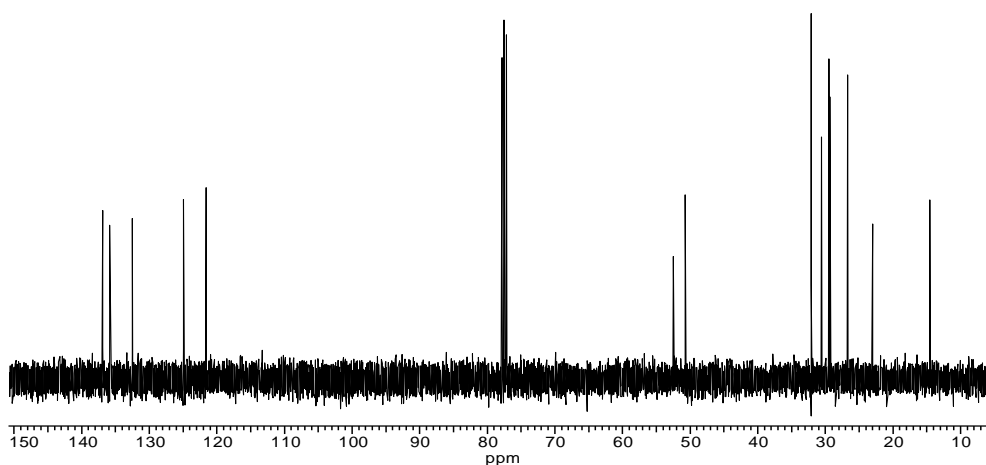
Figure S4. ^1H NMR (A), ^{13}C NMR (B), and elemental analysis data (C) for 3,3',3''-octyl-1,1',1''-(1,3,5)tris (methylene) benzene imidazolium bromide (compound 1B)

(A) ^1H NMR



^1H NMR (CDCl_3 , 400 MHz) δ (ppm): 0.83 (t, $J = 7.32$ Hz, 9H), 1.20 (m, 30H), 1.79 (m, 6H), 4.22 (t, $J = 7.69$ Hz, 6H) 5.58 (s, 6H), 7.08 (s, 3H), 8.61 (d, $J = 2$ Hz, 3H), 8.63 (d, $J = 2$ Hz, 3H), 10.43 (s, 3H)

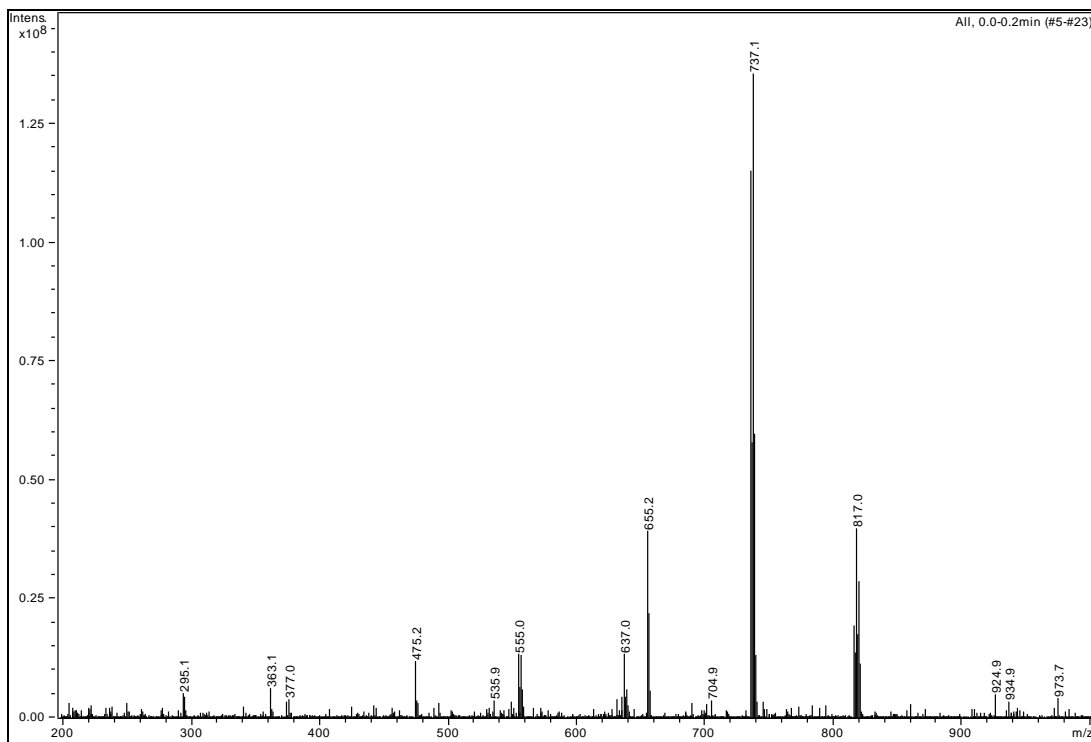
(B) ^{13}C NMR



^{13}C NMR (CDCl_3 , 400 MHz) δ (ppm): 14.29, 22.80, 26.48, 29.11, 30.35, 31.86, 50.45, 52.27, 121.36, 124.69, 132.26, 135.61, 136.65

(C) Elemental analysis calculated for $C_{42}H_{69}Br_3N_6$: 56.19 % C, 7.75 % H, and 9.36 % N; found: 56.21 % C, 8.20 % H, and 9.21 % N

Figure S5. ESI mass spectrum of 3,3',3''-octyl-1, 1', 1''-(1,3,5)tris (methylene) benzene imidazolium bromide (compound 1B)



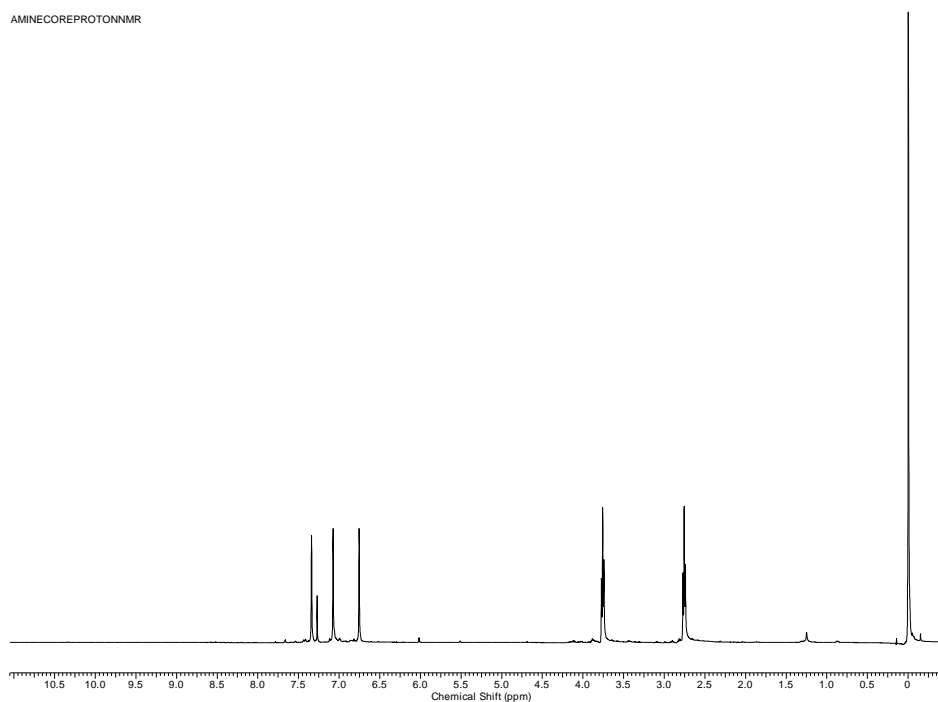
$[Bn(C_8Im)_3 - 2H]^+$: 655.2 amu

$[Bn(C_8Im)_3]^{3+} 2[Br]^-$: 817.1 amu

$[Bn(C_8Im)_3 - H]^{2+} [Br]^-$: 737.1 amu

Figure S6. ^1H NMR (A) and ^{13}C NMR (B) spectra for tris(2-(1H-imidazol-1-yl)ethyl)amine (compound 2A)

(A) ^1H NMR

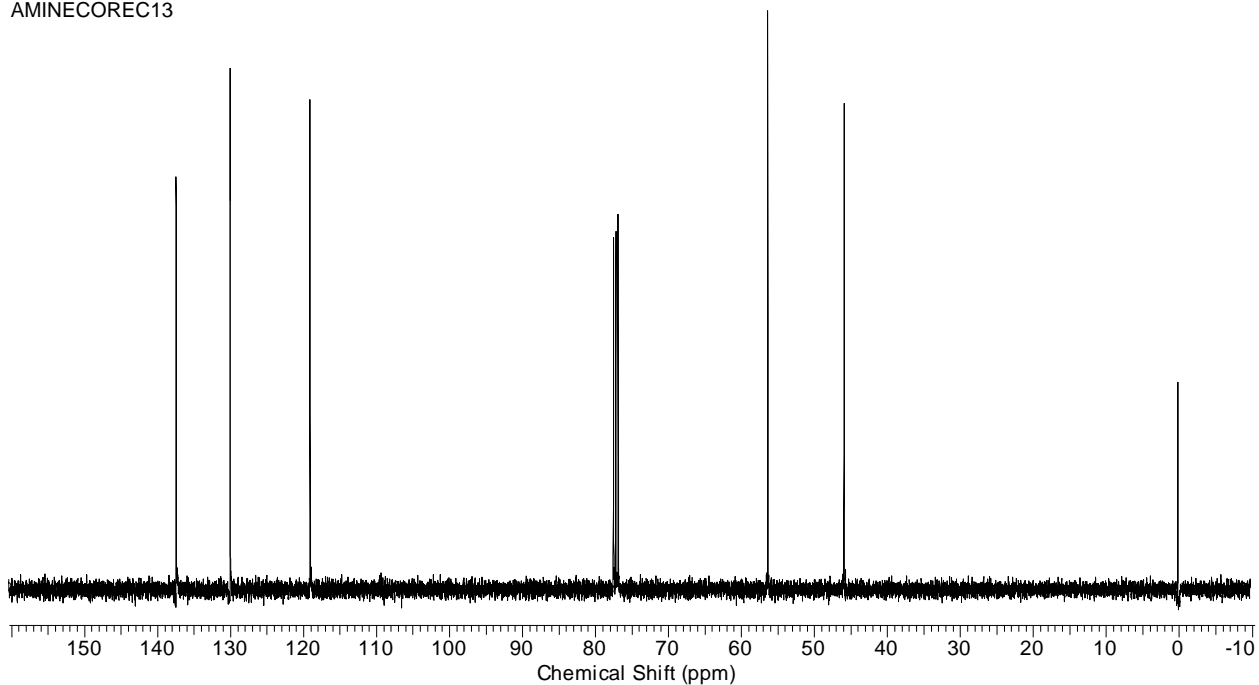


^1H NMR (CDCl_3 , 400 MHz) δ (ppm): 2.76 (t, $J = 5.86$ Hz, 6H), 3.76 (t, $J = 5.86$ Hz, 6H), 6.75 (s, 3H), 7.07 (s, 3H), 7.34 (s, 3H)

Figure S6. (continued) ^1H NMR (A) and ^{13}C NMR (B) spectra for tris(2-(1H-imidazol-1-yl)ethyl)amine (compound 2A)

(B) ^{13}C NMR

AMINECOREC13



^{13}C NMR (CDCl_3 , 400 MHz) δ (ppm): 45.94, 56.39, 119.12, 130.09, 137.47.

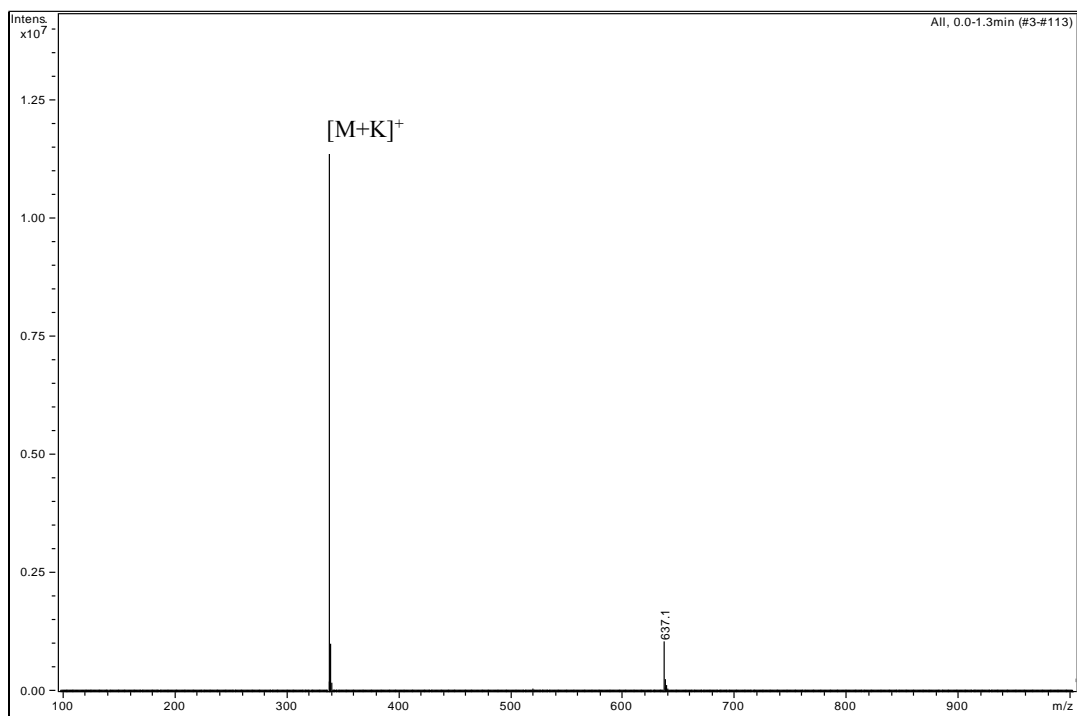
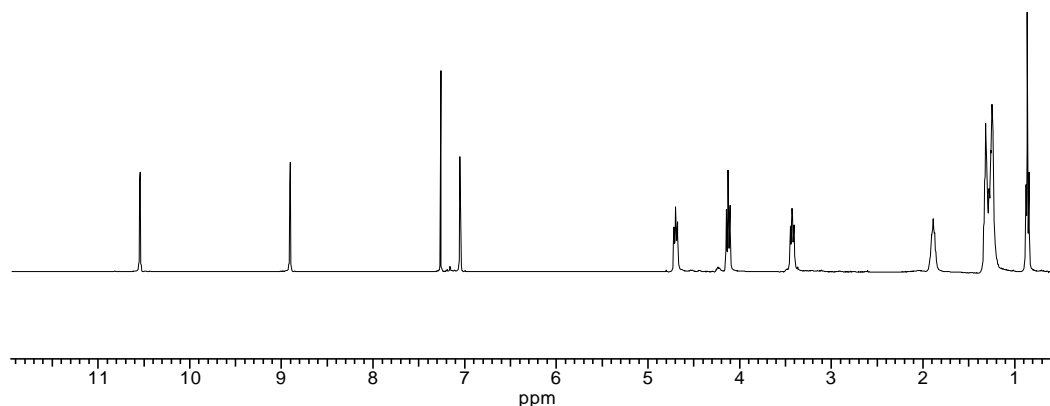
Figure S7. ESI mass spectrum of tris(2-(1H-imidazol-1-yl)ethyl)amine (compound 2A)

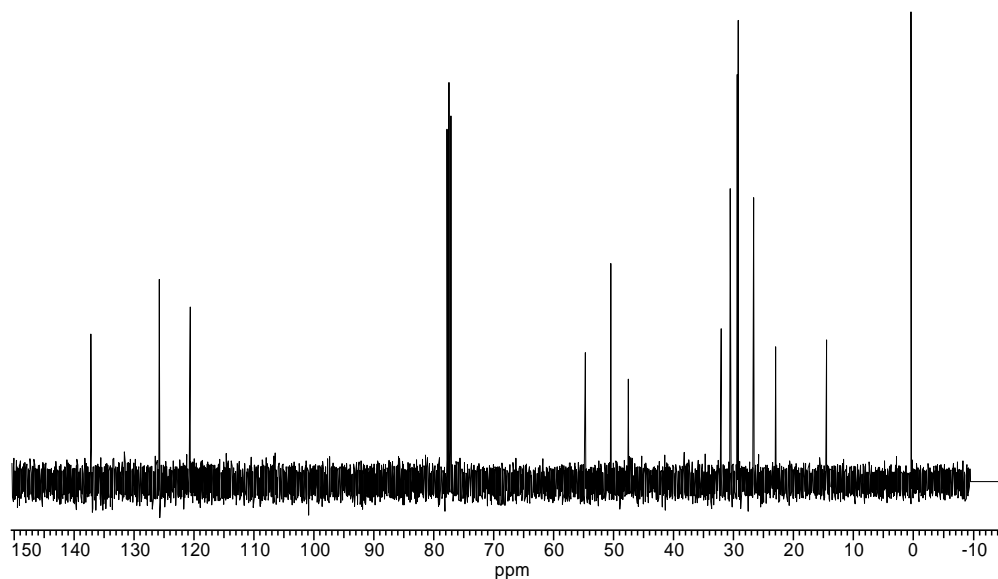
Figure S8. ^1H NMR (A), ^{13}C NMR (B), and elemental analysis data (C) for 3,3',3''-octyl-1,1',1''-(2-ethylamino)imidazolium bromide (compound 2B)

(A) ^1H NMR



^1H NMR (CDCl_3 , 400 MHz) δ (ppm): 0.87 (t, $J = 6.96$ Hz, 9H), 1.27 (m, 30H), 1.90 (m, 6H), 3.44 (t, $J = 7.32$ Hz, 6H), 4.13 (t, $J = 7.32$ Hz, 6H), 4.32 (t, 7.69 Hz, 6H), 7.06 (s, 3H), 8.91 (s, 3H), 10.55 (s, 3H)

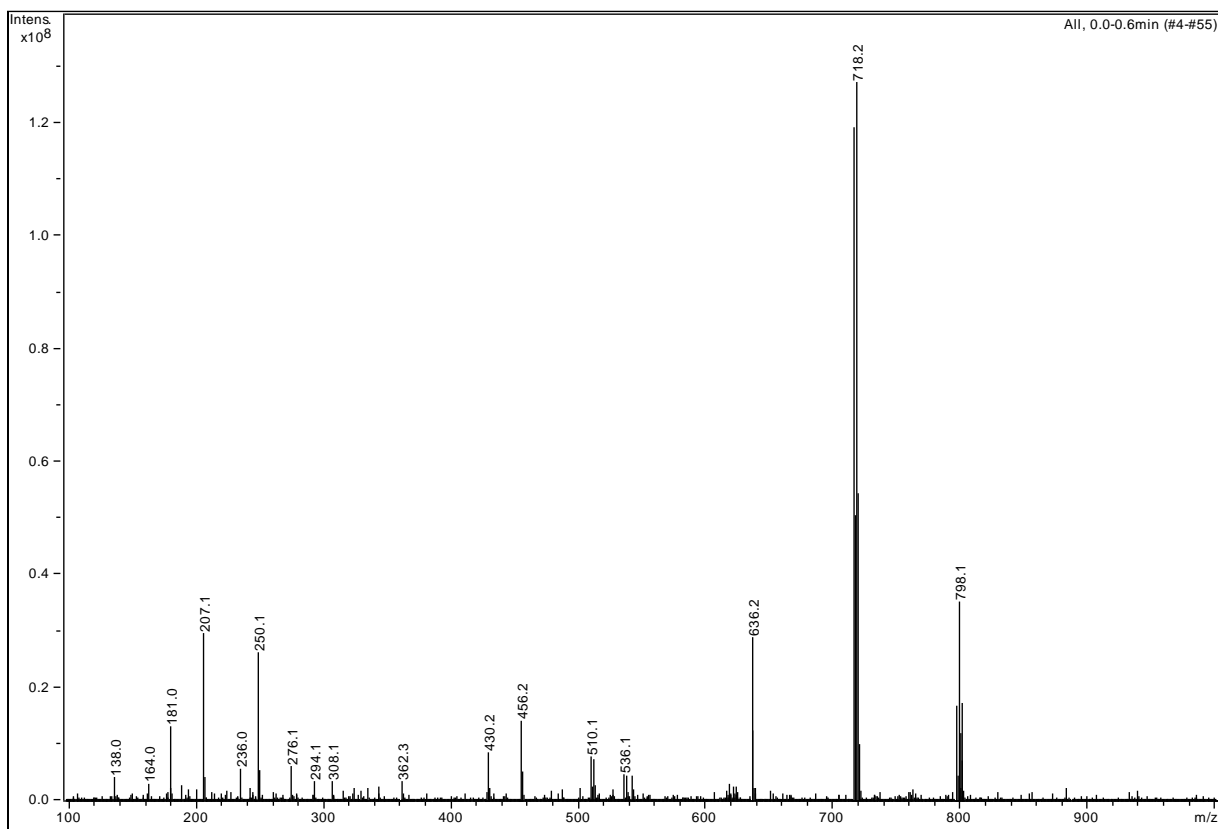
(B) ^{13}C NMR



^{13}C NMR (CDCl_3 , 400 MHz) δ (ppm): 14.30, 22.79, 26.47, 29.06, 29.21, 30.37, 31.85, 47.38, 50.30, 54.51, 120.48, 125.61, 137.02

(C) Elemental analysis calculated for $\text{C}_{39}\text{H}_{72}\text{Br}_3\text{N}_7$: 53.31 % C, 8.26 % H, and 11.16 % N; found: 52.62 % C, 9.14 % H, and 10.92 % N

Figure S9. ESI mass spectrum of 3,3',3''-octyl -1,1',1''- (2-ethyl amino)imidazolium bromide (compound 2B)



$[\text{Am}(\text{C}_8\text{Im})_3 - 2\text{H}]^+$: 636.2 amu

$[\text{Am}(\text{C}_8\text{Im})_3]^{3+} 2[\text{Br}]^-$: 798.1 amu

$[\text{Am}(\text{C}_8\text{Im})_3 - \text{H}]^{2+} [\text{Br}]^-$: 718.1 amu

Figure S10. Variation of the CMC with the acetonitrile content, examples for (A) $(C_4Im)_2C_{12}-2Br$ and (B) $(C_8Im)_3Bn-3Br$. CMC values were determined by conductivity measurements

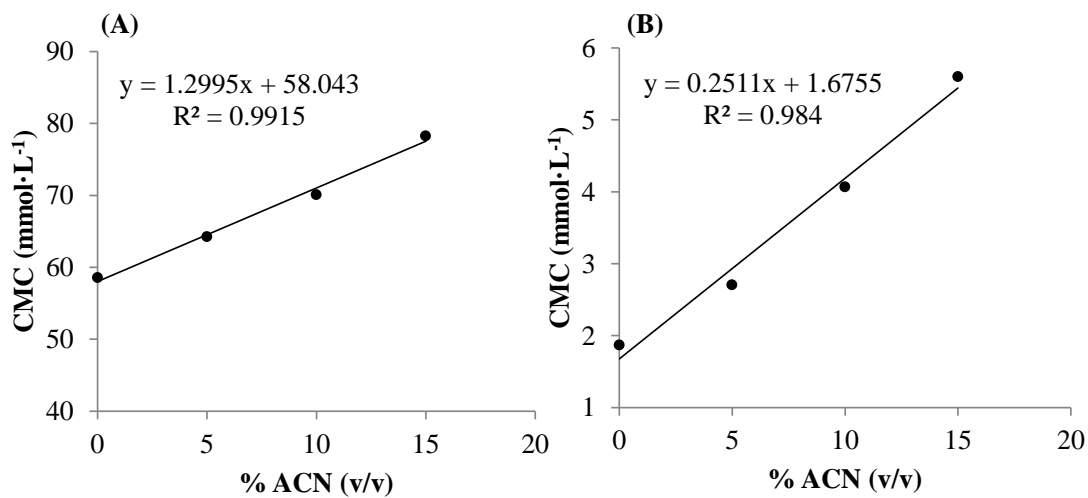


Figure S11. Fluorescence emission spectrum of pyrene: **(A)** in aqueous solution, **(B)** in presence of $(C_{10}Im)_2C_{12}-2Br$ at $0.3 \text{ mmol}\cdot\text{L}^{-1}$ (a concentration below the CMC), and **(C)** in presence of $(C_{10}Im)_2C_{12}-2Br$ at $1.25 \text{ mmol}\cdot\text{L}^{-1}$ (a concentration above the CMC). The excitation wavelength was 335 nm and the remaining conditions are described in section 2.4.3.

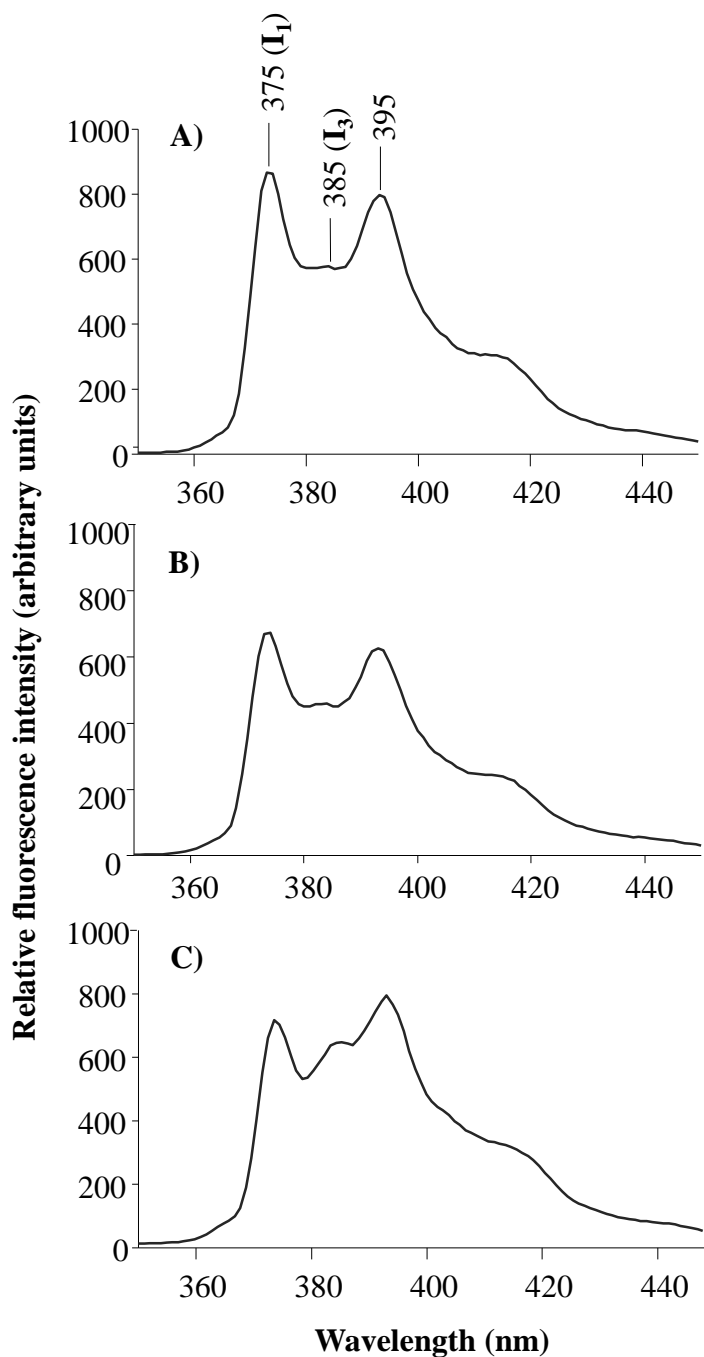


Figure S12. Representative plots obtained by fluorescence measurements for determining the CMC and the N_{agg} . **(A)** Variation of the ratio of band intensities I_1/I_3 of the emission spectrum of pyrene *versus* the logarithm of the concentration for the representative dicationic $(C_{10}Im)_2C_{12}-2Br$. The excitation wavelength was 335 nm and the remaining conditions are described in section 2.4.3. **(B)** Fluorescence quenching of pyrene by benzophenone-3 in $0.05 \text{ mol}\cdot\text{L}^{-1}$ solutions of the representative tricationic $(C_8Im)_3Bn-3Br$. The relative intensities (I and I_0) were recorded at 375 nm. The excitation wavelength was 335 nm and the remaining conditions are described in section 2.4.3.

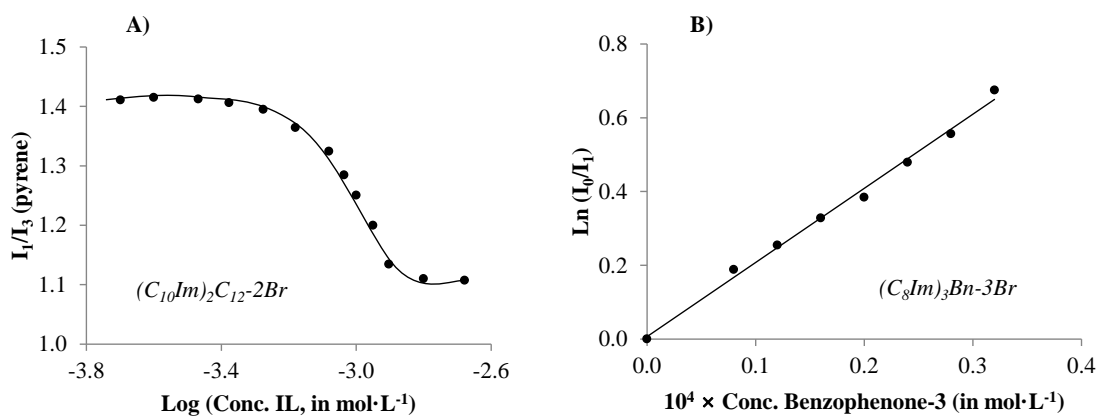


Figure S13. Surface tension plots of the tricationic IL-based surfactant $(C_8Im)_3Bn-3Br$ in presence of: (●) 2 mM of sodium benzoate and (▲) 5 mM of sodium benzoate.

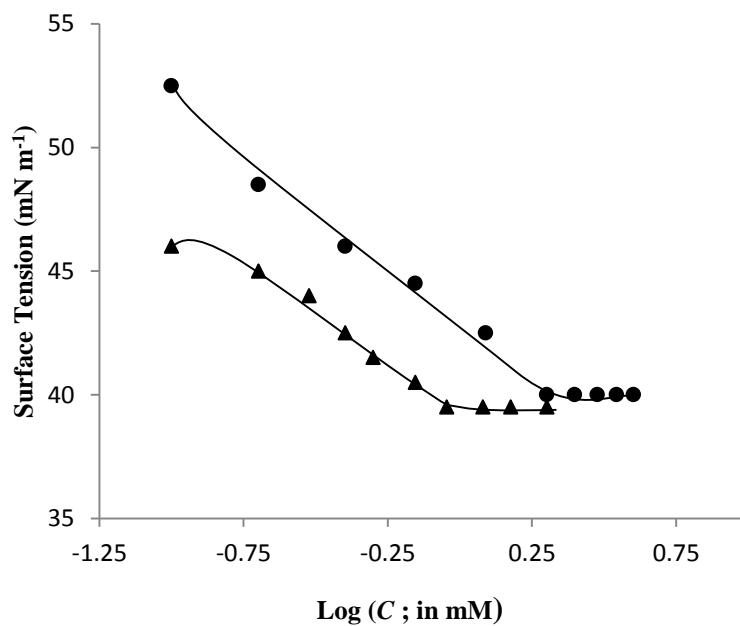


Table S1. CMC, α and β values obtained by conductivity studies (at 298 K) for the selected group of IL-based surfactants, together with the curves employed for the calculations.

IL-based surfactant	CMC (mmol·L ⁻¹) ± error ^a	Premicellar curve (below CMC)			Postmicellar curve (above CMC)			$\alpha \pm \text{error}^f$	$\beta \pm \text{error}^f$
		S ₁ ^b ± SD ^c	interc. ± SD ^d	R	S ₂ ^e ± SD ^c	interc. ± SD ^d	R		
Dicationic surfactants									
(C ₄ Im) ₂ C ₁₂ -2Br	58.56 ± 11.30	0.116 ± 0.003	0.76 ± 0.12	0.999	0.096 ± 0.003	1.98 ± 0.20	0.998	0.82 ± 0.01	0.19 ± 0.01
(C ₁₀ Im) ₂ C ₁₂ -2Br	0.66 ± 0.24	187.1 ± 3.2	4.51 ± 1.37	0.999	156.4 ± 4.5	27.8 ± 5.4	0.998	0.84 ± 0.03	0.17 ± 0.03
(C ₁₆ Im) ₂ C ₁₂ -2Br	0.19 ± 0.05	30.5 ± 2.3	1.52 ± 0.26	0.992	12.5 ± 0.6	7.07 ± 1.31	0.997	0.41 ± 0.04	0.59 ± 0.04
Tricationic surfactants									
(C ₈ Im) ₃ Am-3Br	4.15 ± 0.85	237.2 ± 9.9	430.2 ± 22.7	0.995	123.6 ± 1.6	919.2 ± 24.4	0.999	0.52 ± 0.06	0.48 ± 0.06
(C ₈ Im) ₃ Bn-3Br	1.87 ± 0.20	229.4 ± 8.6	621.2 ± 10.7	0.999	142.9 ± 6.5	760.5 ± 66.3	0.996	0.62 ± 0.04	0.38 ± 0.04

^aCMC error, calculated from the mathematical propagation of the error in the prediction of the concentration

^bPremicellar slope

^cError of the slope of the linear region

^dError of the intercept of the linear region

^ePostmicellar slope

^fError in the determination of α and β , calculated from the mathematical propagation of the error, and also considering the errors of S₁ and S₂

APPENDIX E
SUPPORTING INFORMATION ACCOMPANYING
CHAPTER 6

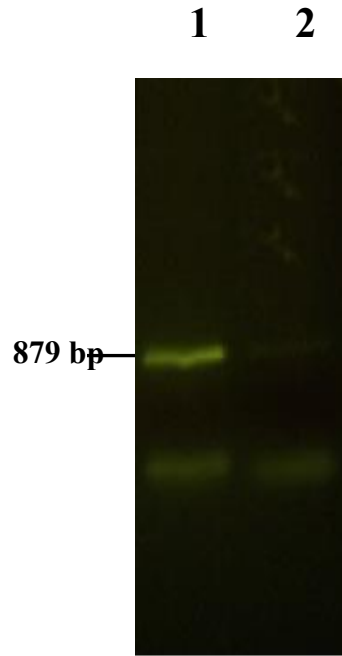


Figure S1. Effect of NaCl on desorption of 6.7 kbp pDNA containing the MTAP gene (879 bp) from PIL fiber. Extraction conditions: pDNA concentration: 20 ng/mL; total solution volume: 10 mL; pH 4.0; extraction time: 20 min; desorption time: 15 min. desorption solution volume: 50 μ L. Lane (1): PCR products obtained following extraction and desorption of PIL fiber in aqueous solution containing 1 M NaCl and 20 mM Tris HCl; Lane (2): PCR products obtained following extraction and desorption of PIL fiber in 20 mM Tris HCl solution.

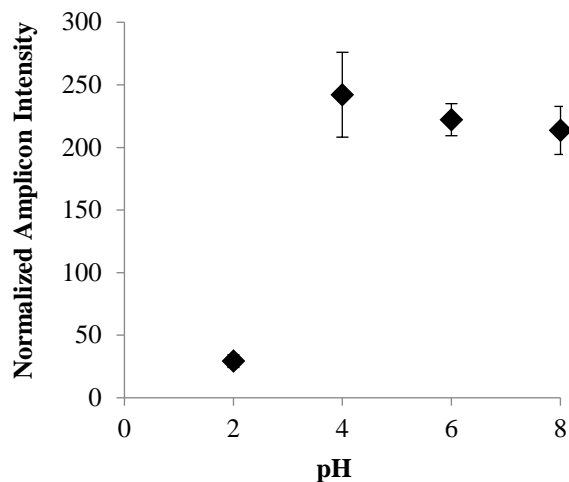


Figure S2. Effect of aqueous solution pH on the intensity of the PCR product obtained following PIL-based SPME of 6.7 kbp pDNA and PCR amplification of an 879 bp gene. The extractions were performed in triplicate. Conditions: pDNA concentration: 20 ng/mL; total solution volume: 10 mL; desorption solution: 1 M NaCl in 20 mM Tris HCl; desorption solution volume: 50 μ L; pH 4.0; extraction time: 20 min; desorption time: 15 min.

APPENDIX F
SUPPORTING INFORMATION ACCOMPANYING
CHAPTER 7

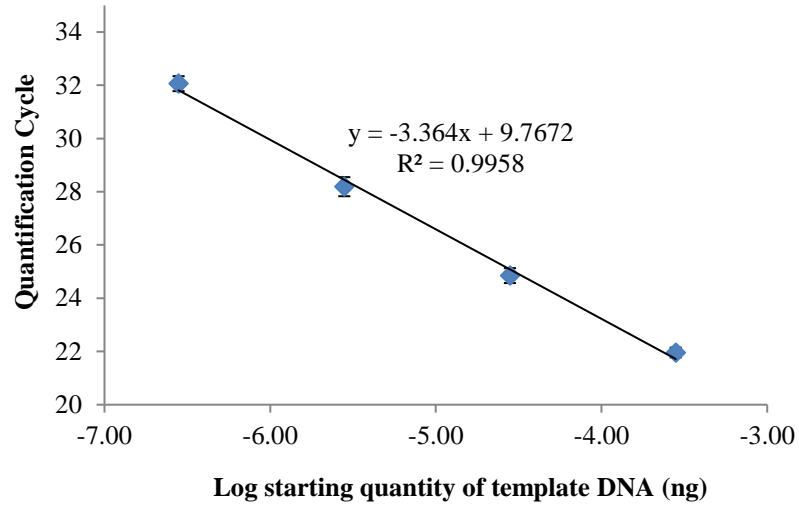


Figure S1. Four-point calibration curve with a tenfold dilution was developed to evaluate the amplification efficiency

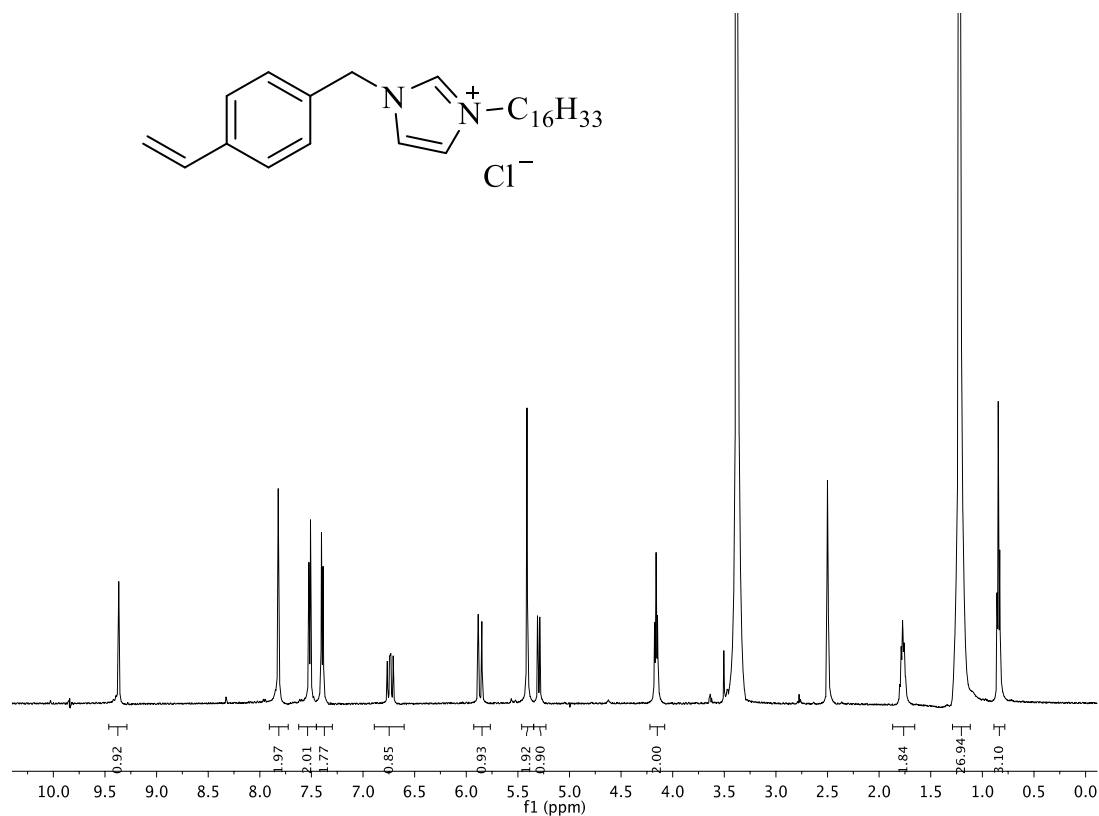


Figure S2 ^1H NMR of IL monomer (Fiber 1) (500 MHz, $\text{DMSO-}d_6$) δ 9.37 (s, 1H), 7.82 (p, $J = 2.0$ Hz, 2H), 7.62 – 7.45 (m, 2H), 7.40 (d, $J = 8.1$ Hz, 2H), 6.74 (dd, $J = 17.7, 11.0$ Hz, 1H), 5.87 (dd, $J = 17.7, 1.0$ Hz, 1H), 5.41 (s, 2H), 5.30 (dd, $J = 10.9, 1.0$ Hz, 1H), 4.16 (t, $J = 7.2$ Hz, 2H), 1.78 (q, $J = 7.9$ Hz, 2H), 1.22 (d, $J = 4.0$ Hz, 26H), 0.89 – 0.78 (m, 3H).

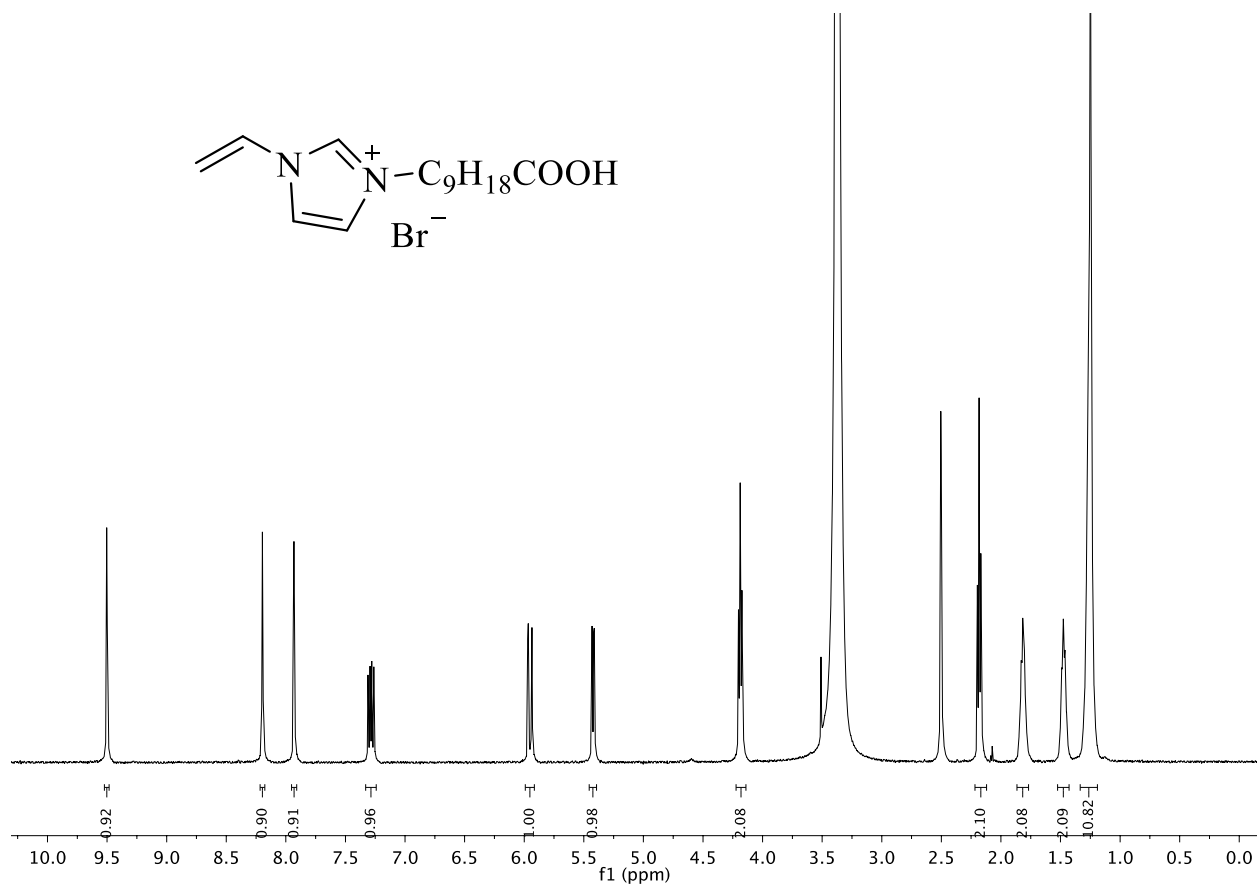


Figure S3 ¹H NMR of IL monomer (Fiber 4) ¹H NMR (500 MHz, DMSO-*d*₆) δ 9.50 (s, 1H), 8.20 (s, 1H), 7.93 (s, 1H), 7.29 (dd, *J* = 15.6, 8.7 Hz, 1H), 5.95 (dd, *J* = 15.6, 2.4 Hz, 1H), 5.42 (dd, *J* = 8.6, 2.3 Hz, 1H), 4.19 (t, *J* = 7.3 Hz, 2H), 2.18 (t, *J* = 7.3 Hz, 2H), 1.82 (p, *J* = 7.3 Hz, 2H), 1.48 (p, *J* = 7.0 Hz, 2H), 1.26 (d, *J* = 14.0 Hz, 10H).

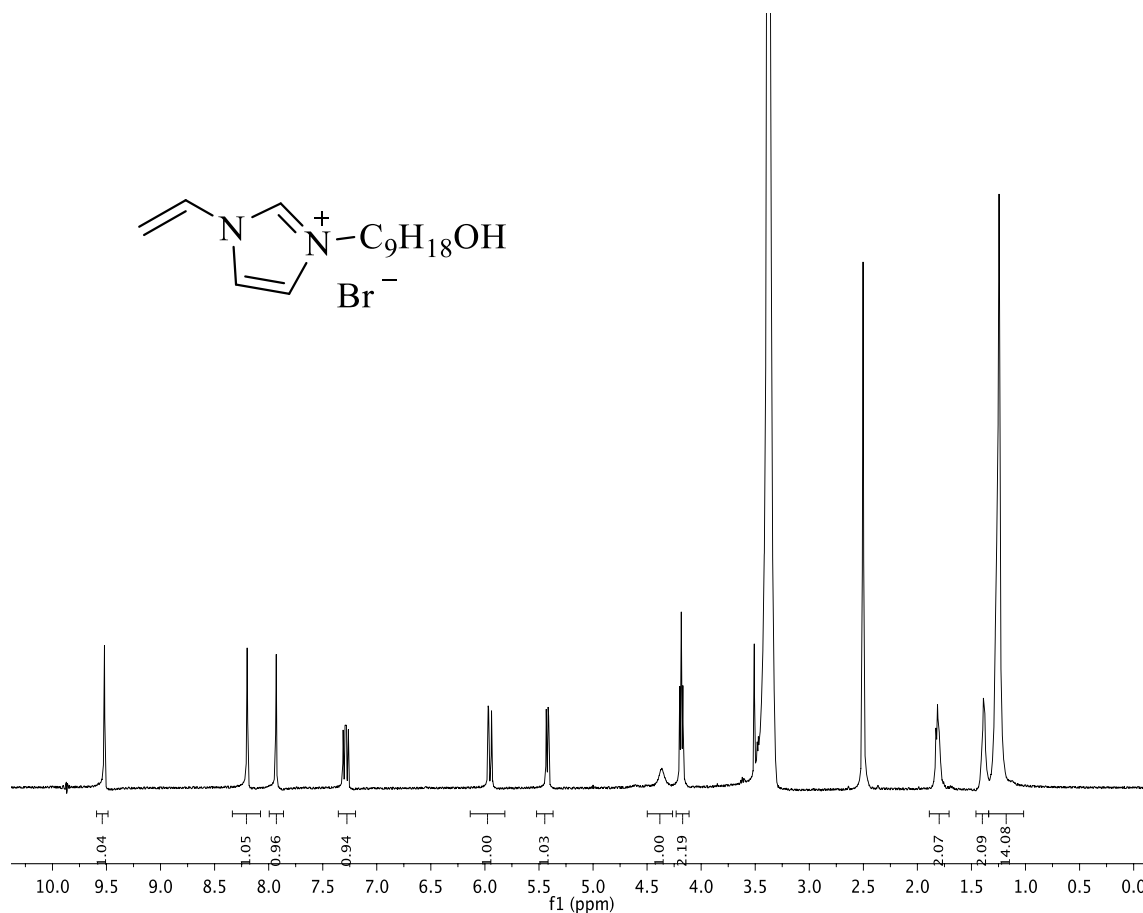


Figure S4 ^1H NMR of IL monomer (Fiber 7) ^1H NMR (500 MHz, DMSO- d_6) δ 9.52 (s, 1H), 8.20 (s, 1H), 7.93 (s, 1H), 7.29 (dd, $J = 15.6, 8.8$ Hz, 1H), 5.95 (dd, $J = 15.7, 2.4$ Hz, 1H), 5.42 (dd, $J = 8.7, 2.4$ Hz, 1H), 4.36 (s, 1H), 4.18 (t, $J = 7.3$ Hz, 2H), 1.89 – 1.71 (m, 2H), 1.46 – 1.34 (m, 2H), 1.26 (d, $J = 12.9$ Hz, 14H).

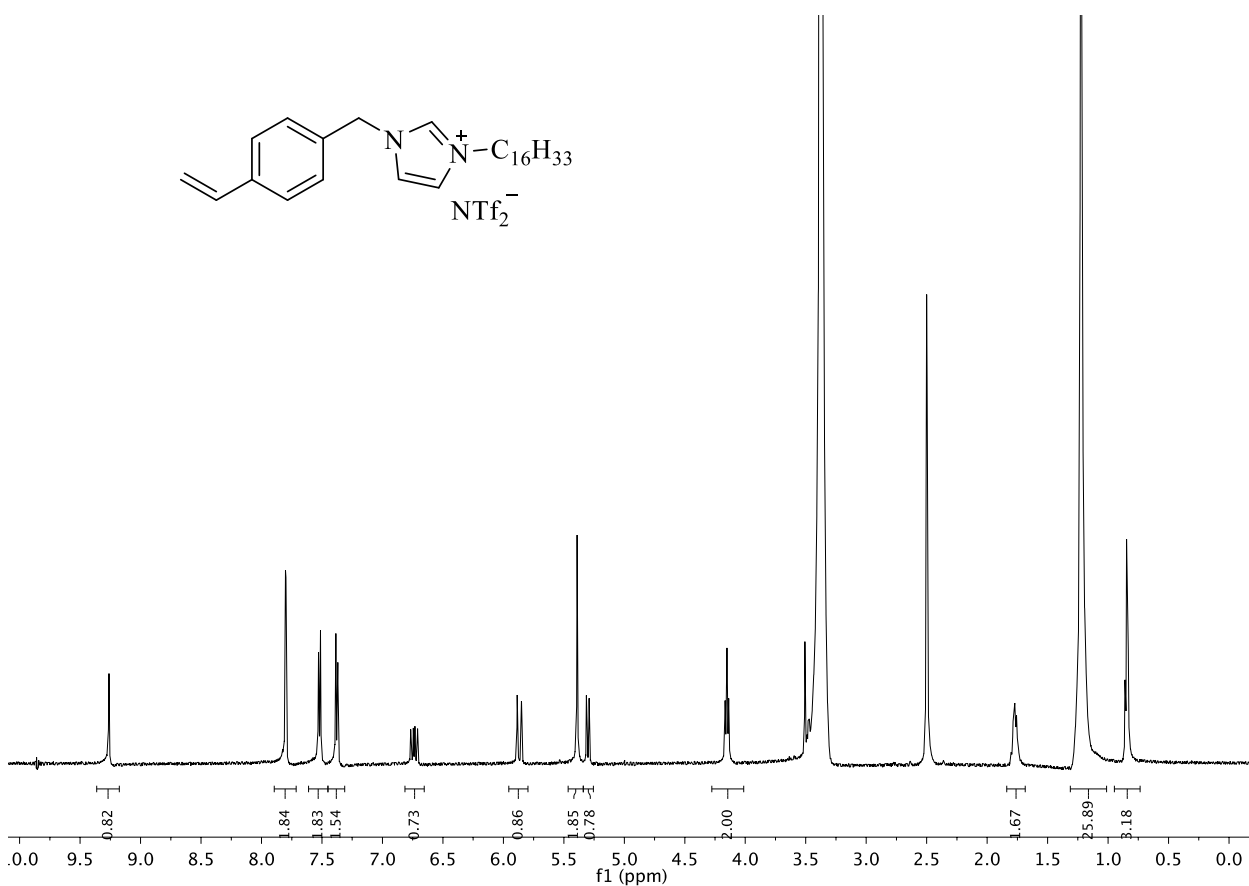


Figure S5 ¹H NMR of IL monomer (Fiber 3) ¹H NMR (500 MHz, DMSO-*d*₆) δ 9.26 (s, 1H), 7.80 (d, *J* = 1.6 Hz, 2H), 7.61 - 7.45 (m, 2H), 7.38 (d, *J* = 8.1 Hz, 2H), 6.74 (dd, *J* = 17.6, 10.9 Hz, 1H), 5.87 (dd, *J* = 17.7, 1.0 Hz, 1H), 5.39 (s, 2H), 5.30 (d, *J* = 11.0 Hz, 1H), 4.15 (t, *J* = 7.2 Hz, 2H), 1.84 - 1.68 (m, 2H), 1.22 (d, *J* = 4.2 Hz, 26H), 0.95 - 0.74 (m, 3H).

VImC9OH SS-_030816.1.fid
VImC9OH SS-_030816

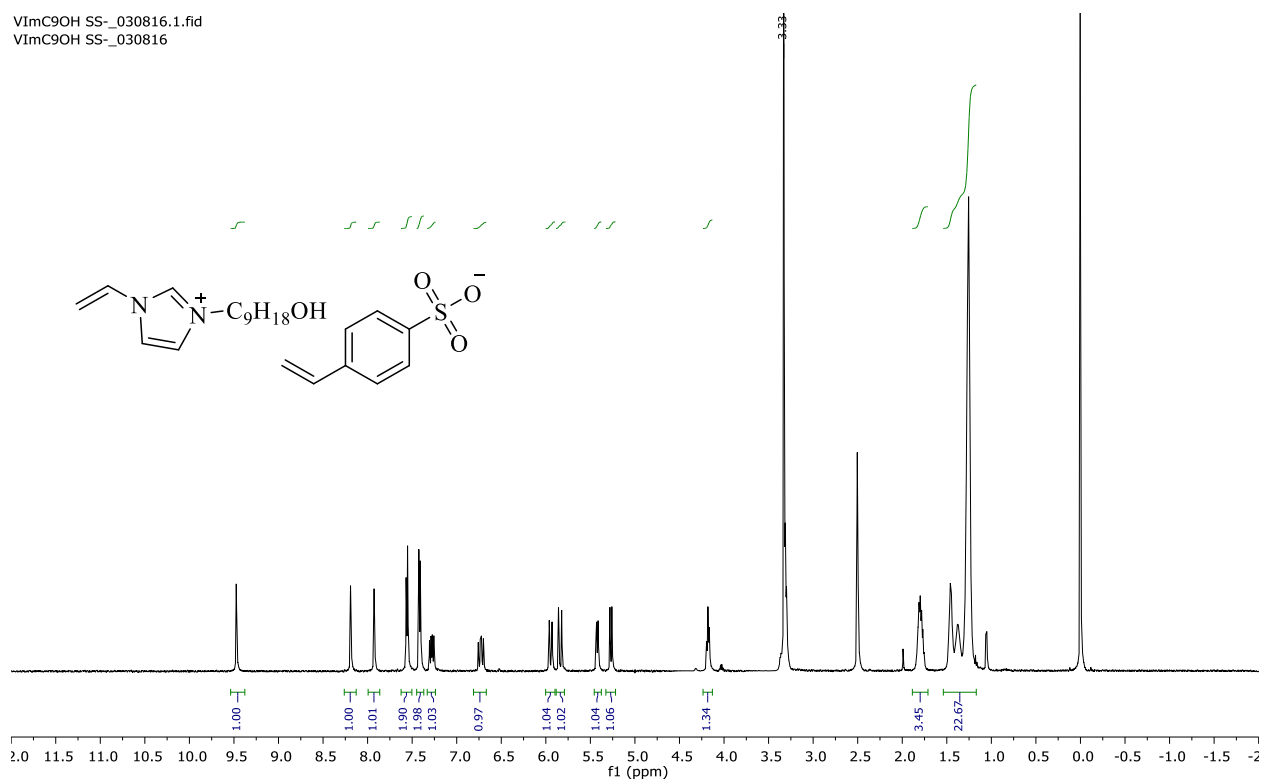


Figure S6 ^1H NMR of IL monomer (Fiber 8) ^1H NMR (500 MHz, DMSO) δ 9.47 (s, 1H), 8.19 (d, J = 2.0 Hz, 0H), 7.93 (s, 0H), 7.59 – 7.52 (m, 1H), 7.45 – 7.39 (m, 1H), 7.28 (dd, J = 15.6, 8.7 Hz, 0H), 5.95 (dd, J = 15.6, 2.5 Hz, 0H), 5.84 (d, J = 17.7 Hz, 0H), 5.42 (dd, J = 8.7, 2.4 Hz, 0H), 5.27 (d, J = 10.9 Hz, 0H), 4.18 (t, J = 7.2 Hz, 1H), 3.52 (td, J = 6.7, 2.2 Hz, 1H), 3.41 – 3.28 (m, 2H), 1.79 (dd, J = 14.4, 7.1 Hz, 1H), 1.45 (d, J = 7.2 Hz, 1H), 1.29 – 1.23 (m, 8H).

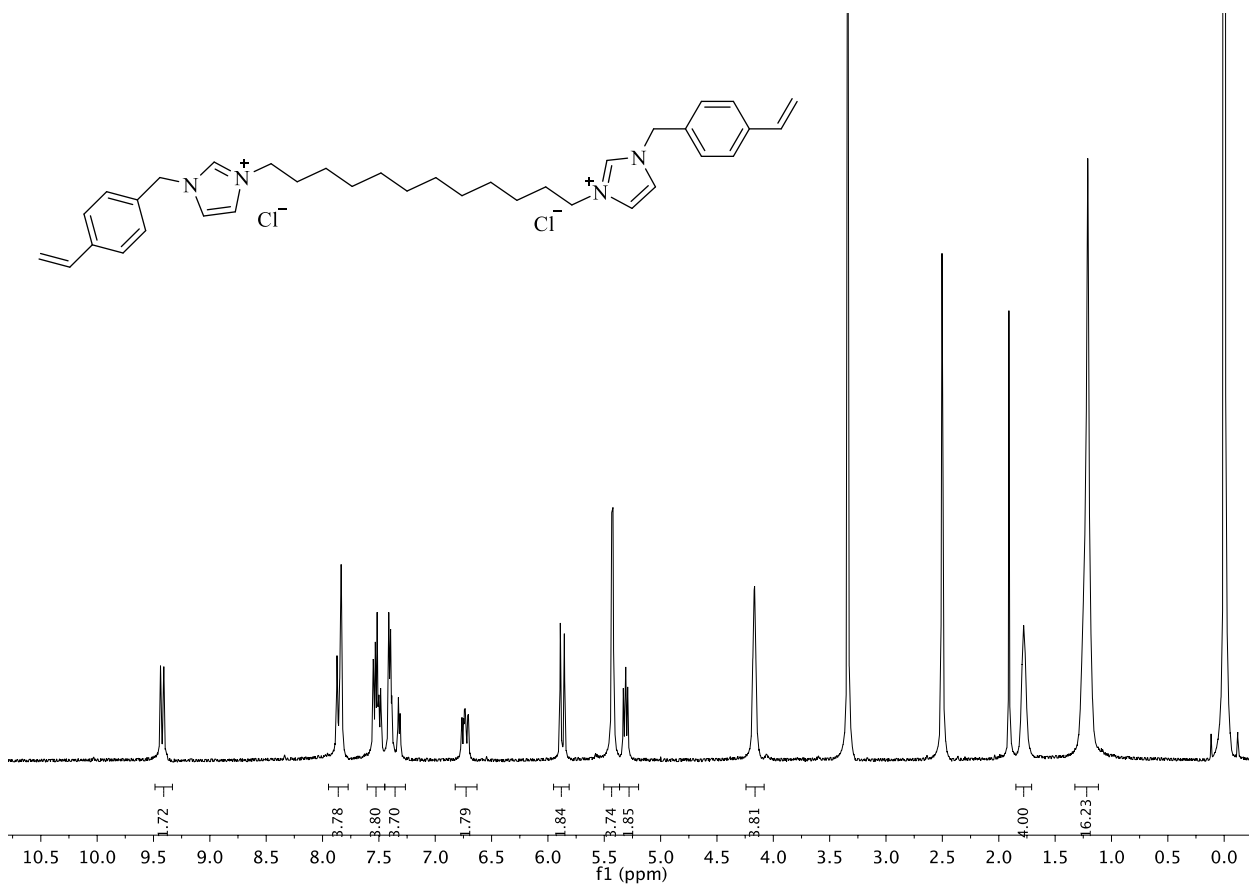


Figure S7 ¹H NMR of crosslinker (Fiber 2) ¹H NMR (500 MHz, DMSO-*d*₆) δ 9.42 (d, *J* = 14.7 Hz, 2H), 7.95 – 7.77 (m, 4H), 7.60 – 7.45 (m, 4H), 7.40 (dt, *J* = 7.6, 3.6 Hz, 4H), 6.74 (ddd, *J* = 17.8, 10.9, 3.4 Hz, 2H), 5.87 (d, *J* = 17.6 Hz, 2H), 5.43 (d, *J* = 5.8 Hz, 4H), 5.31 (dd, *J* = 10.9, 8.5 Hz, 2H), 4.17 (td, *J* = 7.8, 7.3, 3.1 Hz, 4H), 1.78 (s, 4H), 1.21 (s, 16H).

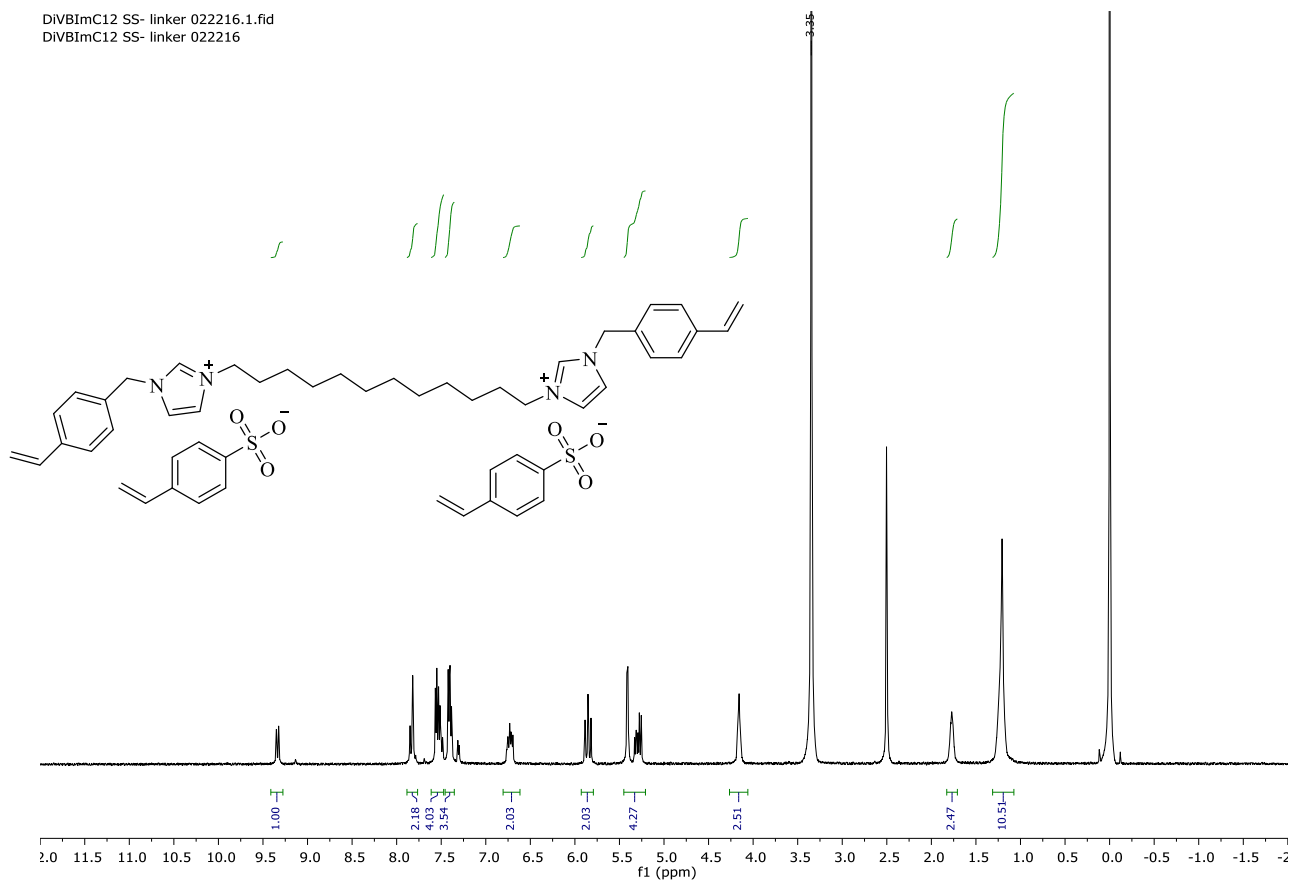


Figure S8 $^1\text{H NMR}$ of crosslinker (Fiber 8) $^1\text{H NMR}$ (500 MHz, $\text{DMSO-}d_6$) δ 7.88 – 7.77 (m, 2H), 7.61 – 7.47 (m, 4H), 7.40 (dd, $J = 11.2, 7.8$ Hz, 4H), 6.73 (dt, $J = 18.0, 9.4$ Hz, 2H), 5.93 – 5.79 (m, 2H), 5.45 – 5.21 (m, 4H), 4.16 (s, 3H), 1.77 (s, 2H), 1.21 (s, 11H).

blue_ntf2.1.fid

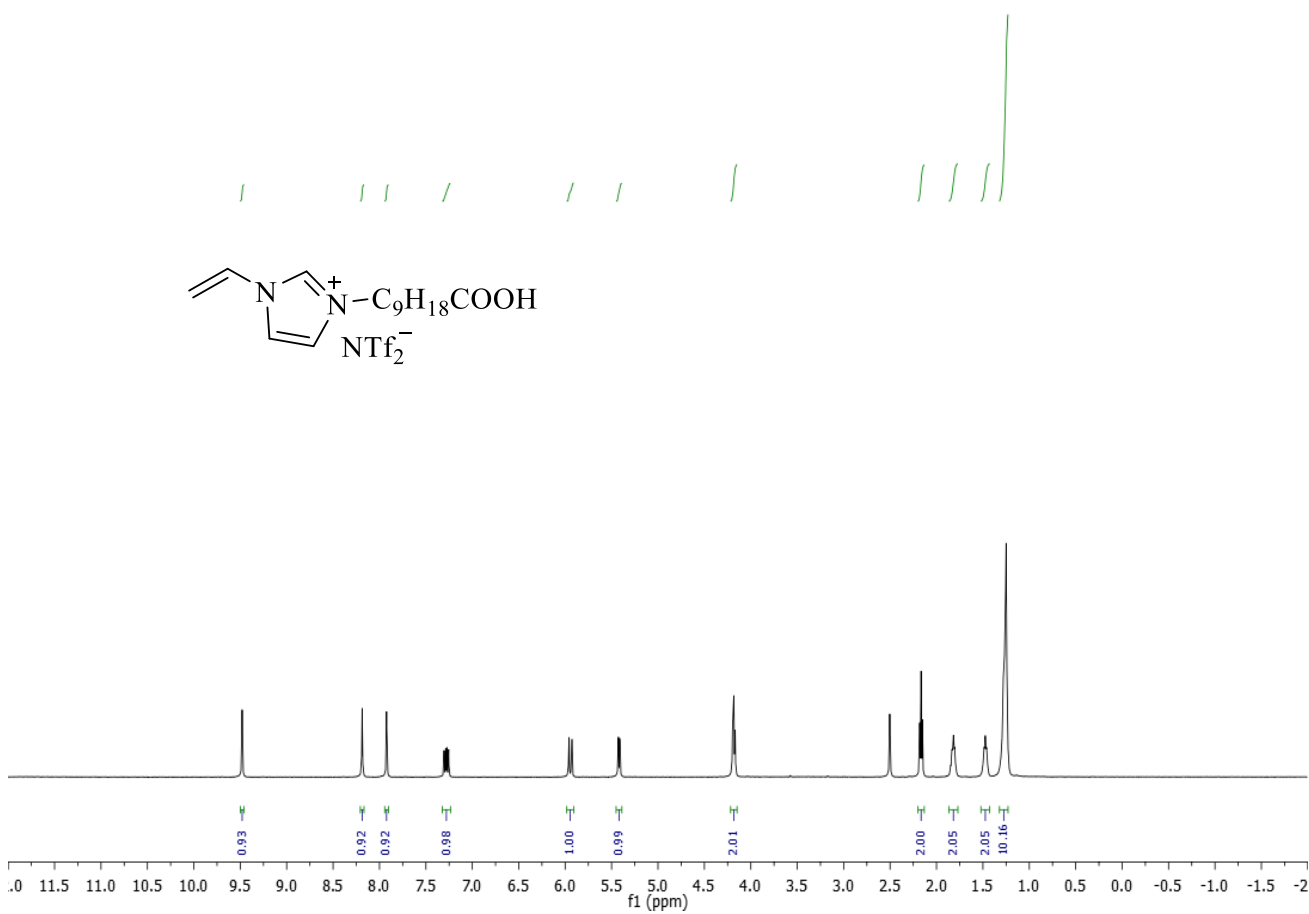


Figure S9 ^1H NMR of IL monomer (Fiber 6) ^1H NMR (500 MHz, $\text{DMSO-}d_6$) δ 9.48 (s, 1H), 8.19 (s, 1H), 7.92 (s, 1H), 7.28 (dd, $J = 15.6, 8.7$ Hz, 1H), 5.94 (dd, $J = 15.6, 2.4$ Hz, 1H), 5.42 (dd, $J = 8.7, 2.4$ Hz, 1H), 4.18 (t, $J = 7.3$ Hz, 2H), 2.17 (t, $J = 7.4$ Hz, 2H), 1.82 (p, $J = 7.1$ Hz, 2H), 1.47 (t, $J = 7.1$ Hz, 2H), 1.32 – 1.23 (m, 10H).

maron_ntf2.1.fid

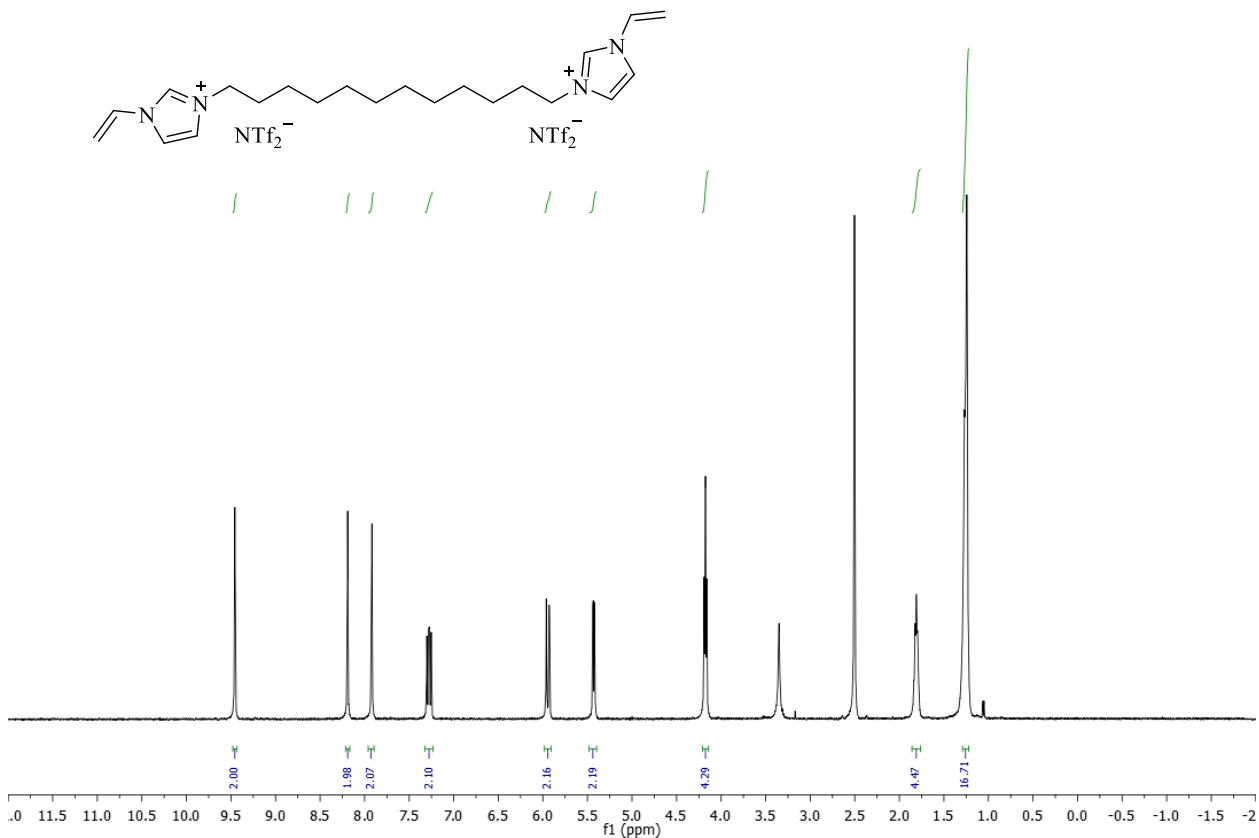


Figure S10 ^1H NMR of crosslinker (Fiber 3) ^1H NMR (500 MHz, $\text{DMSO-}d_6$) δ 9.46 (d, $J = 1.8$ Hz, 2H), 8.19 (t, $J = 1.9$ Hz, 2H), 7.92 (t, $J = 1.9$ Hz, 2H), 7.28 (dd, $J = 15.6, 8.8$ Hz, 2H), 5.94 (dd, $J = 15.6, 2.4$ Hz, 2H), 5.43 (dd, $J = 8.7, 2.4$ Hz, 2H), 4.18 (t, $J = 7.3$ Hz, 4H), 1.81 (p, $J = 7.2$ Hz, 4H), 1.26 (d, $J = 14.2$ Hz, 17H).

green_divinylbromide1.1.fid

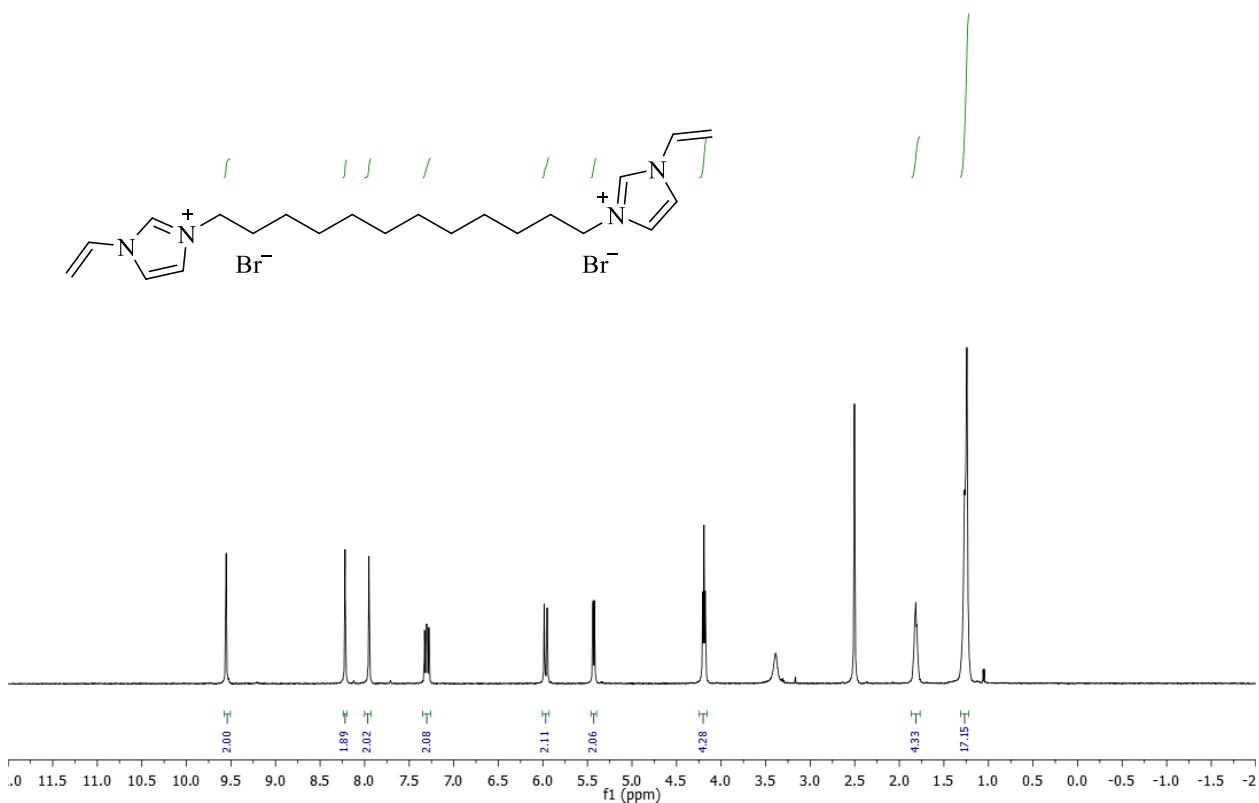


Figure S11 ^1H NMR of crosslinker (Fiber 1) ^1H NMR (500 MHz, $\text{DMSO-}d_6$) δ 9.56 (d, $J = 1.7$ Hz, 2H), 8.22 (s, 2H), 7.95 (t, $J = 1.9$ Hz, 2H), 7.35 - 7.26 (m, 2H), 5.97 (dd, $J = 15.6, 2.4$ Hz, 2H), 5.43 (dd, $J = 8.7, 2.4$ Hz, 2H), 4.19 (t, $J = 7.3$ Hz, 4H), 1.82 (p, $J = 7.1$ Hz, 4H), 1.31 - 1.22 (m, 17H).

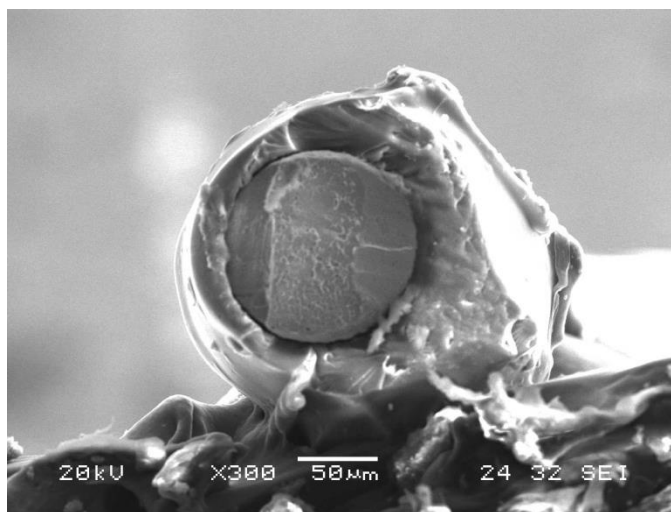


Figure S12. A representative SEM micrograph of a PIL-based sorbent coating (Fiber 4)

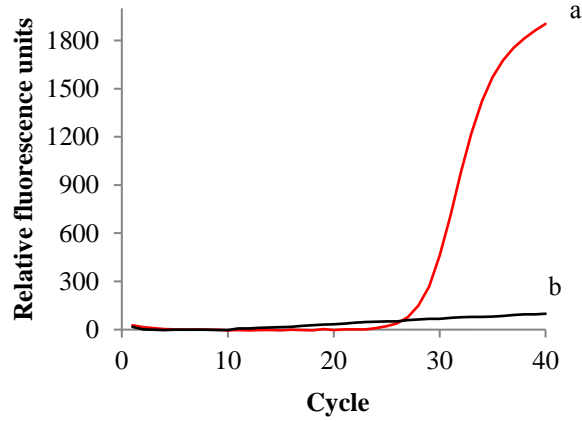


Figure S13. qPCR amplification plots (a) desorption following PIL-based SPME using Fiber 4; (b) washing prior to subsequent extraction. Concentration of 137 bp template DNA: 10 pg mL^{-1} ; sample solution: 1X TE buffer (pH: 8.0); desorption time: 30 min; desorption solvent: 1 M NaCl; desorption solvent volume: $50 \text{ }\mu\text{L}$.

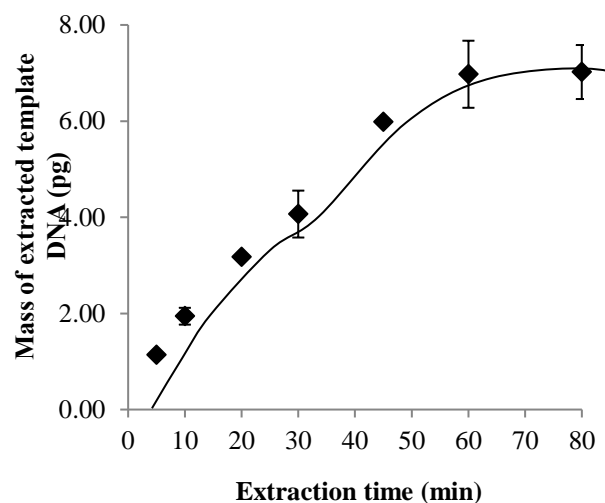


Figure S14. Sorption-time profile obtained using Fiber **4**. Concentration of 137 bp template DNA: 10 pg mL^{-1} ; triplicate extractions ($n = 3$) were performed at 10, 30, 60, and 90 mins; sample solution: 1X TE buffer (pH: 8.0); desorption time: 30 min; desorption solvent: 1 M NaCl; desorption solvent volume: $50 \text{ }\mu\text{L}$.

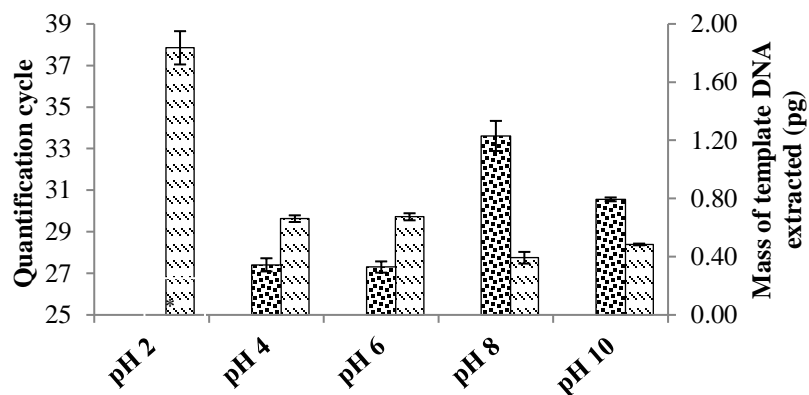


Figure S15. Effect of aqueous solution pH on extraction efficiency of 135 bp DNA using PIL Fiber 4. All experiments were performed in triplicate ($n = 3$); concentration of 135 bp DNA: 10 pg mL^{-1} ; desorption time 30 min; desorption solvent: 1 M NaCl; desorption solvent volume: $50 \text{ }\mu\text{L}$; (▨) quantification cycles; (▤) mass of extracted template DNA. *Mass of template DNA extracted by the fiber was not determined as the obtained Cq value was beyond the calibration range.

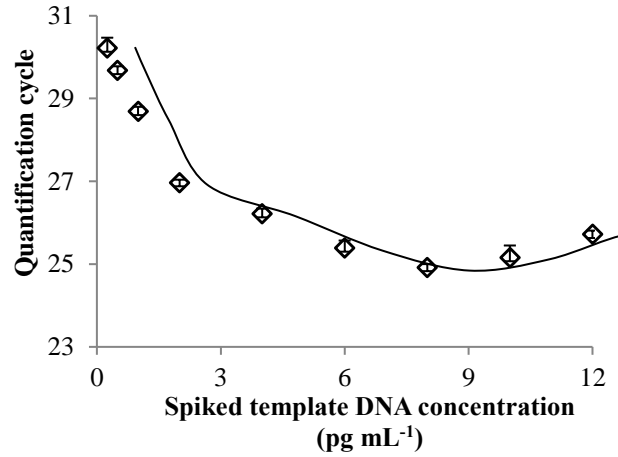


Figure S16. Evaluation of template DNA binding capacity of Fiber **4** in 1X TE buffer. Sample volume: 1.5 mL; extraction time: 30 min; desorption time: 30 min; desorption solvent: 1 M NaCl; desorption solvent volume: 50 μ L. A lower Cq value indicates a greater quantity of extracted template DNA. A difference in one Cq value corresponds to a two-fold difference in the amount of extracted DNA when the amplification efficiency is 100%.

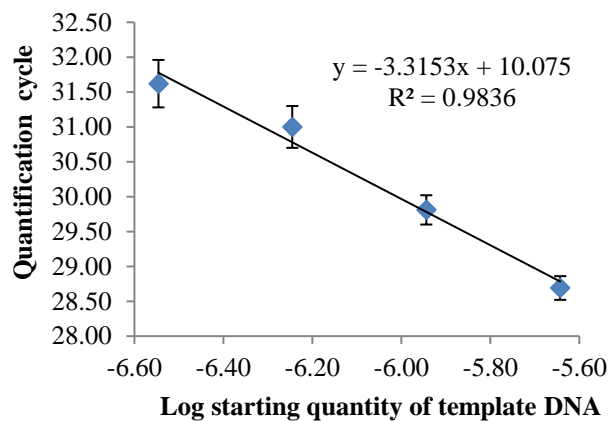


Figure S17. Four point calibration curve with a twofold dilution series was developed to evaluate the presence of potential qPCR inhibitors in extracted template DNA following PIL-based SPME (Fiber 4) on dilute cell lysate sample.

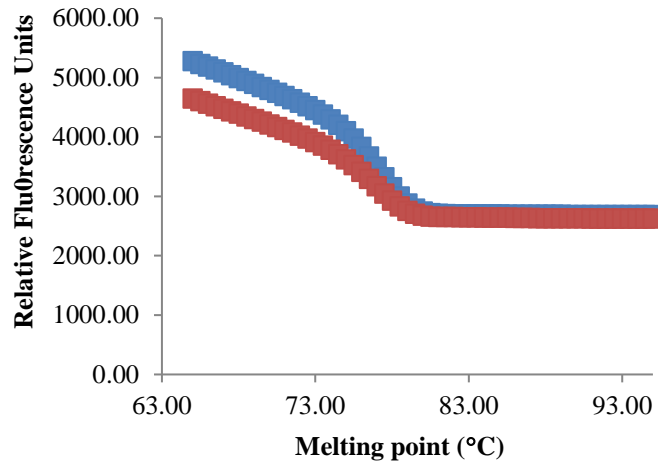


Figure S18. Melting point analysis on qPCR amplified products. (■) 1 pg of template DNA from 1X TE buffer as a starting quantity for qPCR amplification; (■) template DNA extracted from dilute cell lysate sample using Fiber 4 as a starting quantity for qPCR amplification.

Materials and Reagents Employed in the Preparation of PIL-based SPME fibers.

Acrylonitrile (99%), 1-bromohexadecane (95%), 1,12-dibromododecane (98%), 4-vinylbenzyl chloride (90%), 10-bromodecanoic acid (95%), 10-chloro-1-decanol (90%), 1-vinylimidazole ($\geq 99\%$), imidazole ($\geq 99\%$), vinyltrimethoxysilane (VTMS) (98%), and 2-hydroxyl-2-methylpropiophenone (DAROCUR 1173) ($>96\%$) were purchased from Sigma–Aldrich (St. Louis, MO, USA). Acetonitrile, methanol, and isopropanol were also purchased from Sigma–Aldrich with purities equal to or higher than 99%. Hydrogen peroxide (30%, w/w), glacial acetic acid, calcium chloride dehydrate, iron chloride hexhydrate, hydrochloric acid, sodium chloride, ethylenediaminetetraacetic acid (EDTA), and sodium hydroxide were purchased from Fisher Scientific (Fair Lawn, NJ, USA). Tris(hydroxymethyl)aminomethane (Tris) was obtained from P212121 (Ypsilanti, MI, USA). Lithium bis[(trifluoromethyl)sulfonyl]imide (LiNTf₂) was purchased from SynQuest Laboratories (Alachua, FL, USA). Sodium p-styrenesulfonate ($>93\%$) was purchased from TCI America (Portland, OR, USA). Deuterated dimethyl sulfoxide was purchased from Cambridge Isotope Laboratories (Andover, MA, USA). Nitinol wire with a diameter of 128 μm was purchased from Nitinol Devices & Components (Fremont, CA, USA).

Fabrication of PIL-based SPME fibers. The fabrication of PIL-based SPME fibers was performed according to methods from a previously published study. A super elastic nitinol wire was chosen as a support for the immobilization of the PIL-based sorbent coating using an “on-fiber” UV initiated polymerization technique.⁸⁹ Briefly, the nitinol wire was first polished using sand paper and cleaned with acetone and methanol. In order to generate free hydroxyl groups on the surface of the substrate, the nitinol support was immersed in boiling hydrogen peroxide at 70-75 °C for 2 h. The derivatized support was then reacted with neat VTMS at 85 °C for 2 h. The nitinol supports were ready for coating after being washed with methanol and dried at 150 °C for 5 min. A coating mixture consisting of IL monomer, crosslinker (50% by weight with respect to the monomer), and DAROCUR 1173 photoinitiator (3% by weight with respect to mass of IL monomer and crosslinker) was evenly coated on the surface of the previously cut 1 cm derivatized nitinol support. The coated support was then exposed to either 254 or 360 nm UV light for 2 h.⁹⁰ Following UV initiated polymerization, the fabricated PIL-based SPME fibers were immersed in 100 µL of methanol for 15 min and then washed with 10 mL of 1X TE buffer (1 mM Tris base; 0.1 mM EDTA; pH 8) for 30 min.

Table S1 Comparison of Cq values obtained from qPCR amplification plots following PIL-based SPME using Fiber 4 from three different sample matrices at varying spiked template DNA concentrations

Entry	Sample matrix type	Spiked template DNA concentration (pg mL ⁻¹)	^a Cq ± STD
1	Crude cell lysate	8	30.94 ± 0.09
		4	31.38 ± 0.33
		1	32.83 ± 0.17
2	Dilute cell lysate	8 ^b	28.17 ± 0.13
		4	29.69 ± 0.14
		1	31.83 ± 0.17
3	1X TE buffer	8	25.39 ± 0.08
		4	26.22 ± 0.12
		1	28.69 ± 0.11

^aAll experiments were carried out in triplicate (n = 3); ^bRSD of Cq values for inter-day experiments was found to be 2.9% (n = 6). Sample volume 1.5 mL; extraction time: 30 min; desorption time: 30 min; desorption solvent: 1 M NaCl; desorption solvent volume: 50 µL.

Conditions for *E. coli* Cell Transformation and Cell Cultures. Competent *E. coli* cells were transformed with a modified plasmid (pDNA) containing 135 bp DNA insert. Briefly, approximately 25 ng of purified pDNA were added to a microcentrifuge tube containing 10 μ L of NEB 5-alpha Competent *E. coli* cells and gently mixed. The solution was placed on ice for 30 min. The microcentrifuge tube was set in a water bath at 42 °C for 42 s, removed from heat, and immediately chilled on ice for 5 min. Then, 950 μ L of Luria Bertani (LB) media was added to the solution. The mixture was incubated at 37 °C for 1 h and subsequently transferred into 120 mL of LB media with 100 μ g mL⁻¹ ampicillin at 37 °C for 24 h.

Preparation of Bacterial Crude Cell Lysate. An aliquot of *E. coli* cell culture was centrifuged at 1,380g for 8 minutes and resuspended in of 1X TE buffer (to reach predetermined number of cells). A 250 μ L volume of 0.2 N NaOH, 1% (w/v) SDS was then added to the sample. After gently mixing the solution, 350 μ L of 3 M potassium acetate (pH 4.8) was added and the solution diluted to a final volume of 2 mL. A 1.5 mL aliquot of bacterial crude cell lysate was spiked with a predetermined concentration of template DNA and subsequently subjected to the PIL-based SPME approach. In the case of pDNA extraction, *E. coli* cells transformed with pDNA were isolated and subsequently subjected to same cell lysis conditions as described above.

APPENDIX G
SUPPORTING INFORMATION ACCOMPANYING
CHAPTER 8

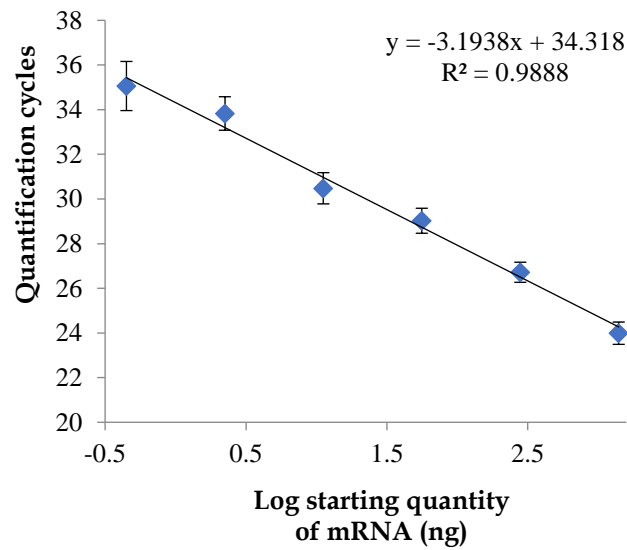


Figure S1. Six-point calibration curve with a five-fold dilution was developed to evaluate the reverse transcription efficiency and subsequently used for mRNA quantification

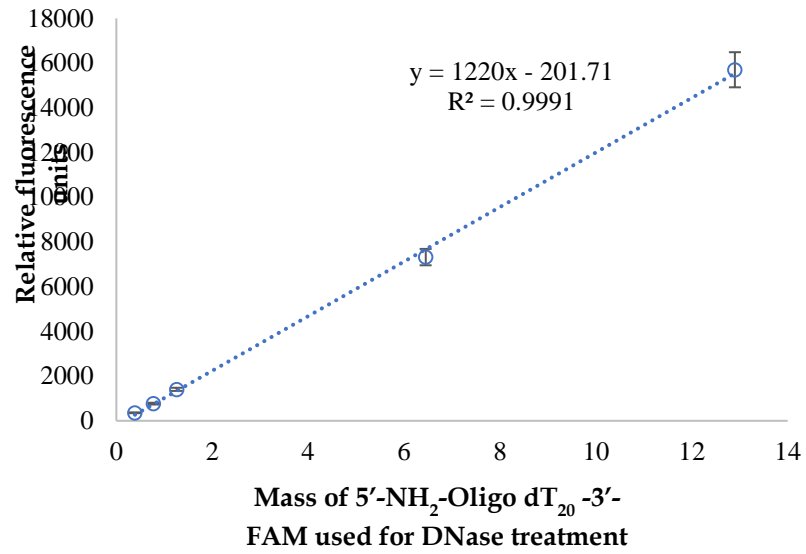


Figure S3. Five-point calibration curve used to quantify the amount of 5'-NH₂-oligo dT₂₀-FAM-3' immobilized on PA sorbent coating

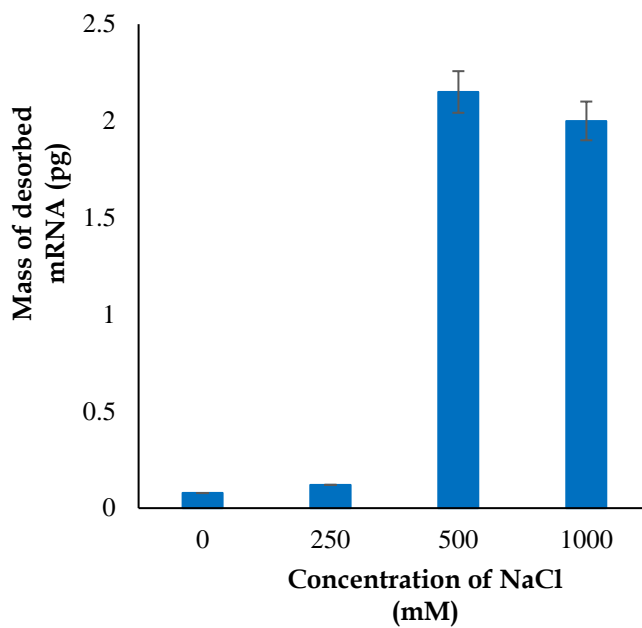


Figure S4. Effect of NaCl concentration on desorption of mRNA from PIL-based sorbent coating. Concentration of mRNA: $0.1 \text{ ng } \mu\text{L}^{-1}$; extraction time: 10 min; triplicate extractions ($n = 3$) were performed at 500 and 1000 mM NaCl concentrations; sample solution: deionized water ($100 \text{ } \mu\text{L}$); extraction time: 10 min; desorption time: 30 min; desorption solvent volume: $50 \text{ } \mu\text{L}$.

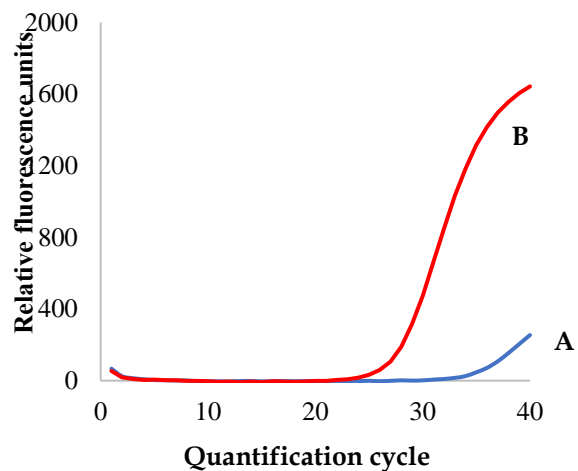


Figure S5. Representative RT-qPCR amplification plots for (A) carry-over fraction prior to next extraction; (B) desorption fraction following PIL-based SPME (Fiber 2) using regenerated sorbent coating.

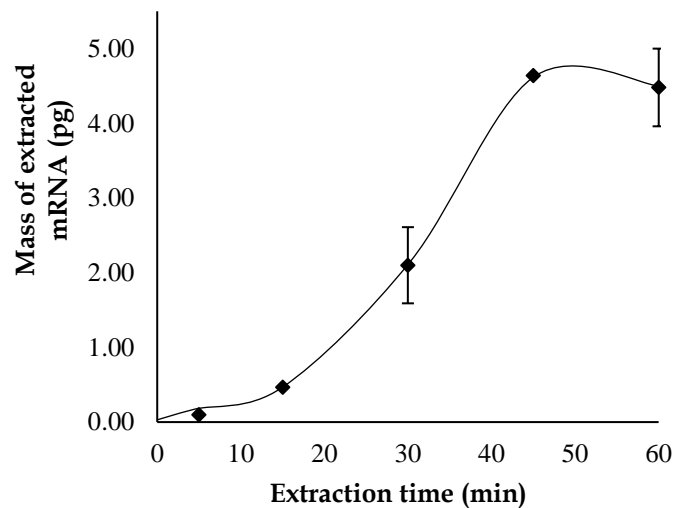


Figure S6. Sorption-time profile for Fiber 2. Concentration of mRNA: $0.1 \text{ ng } \mu\text{L}^{-1}$; triplicate extractions ($n = 3$) were performed at 30 and 60 mins; sample solution: deionized water ($100 \mu\text{L}$); desorption time: 30 min; desorption solvent: 500 mM NaCl; desorption solvent volume: $50 \mu\text{L}$.

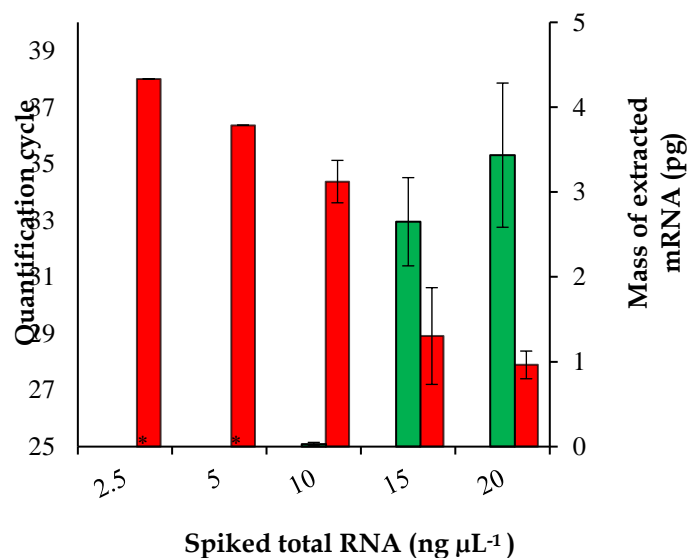


Figure S7. Extraction of mRNA from total RNA samples using Fiber **2**. Triplicate extractions ($n = 3$) were performed at 10, 15, and 20 $\text{ng } \mu\text{L}^{-1}$ of spiked total RNA samples; sample solution: deionized water (100 μL); desorption time: 30 min; desorption solvent: 500 mM NaCl; desorption solvent volume: 50 μL ; (■) represents quantification cycles; (■) denotes mass of extracted mRNA. *Mass of mRNA extracted by Fiber **2** at 2.5 and 5.0 $\text{ng } \mu\text{L}^{-1}$ was not determined as the Cq values obtained were out of the calibration range.

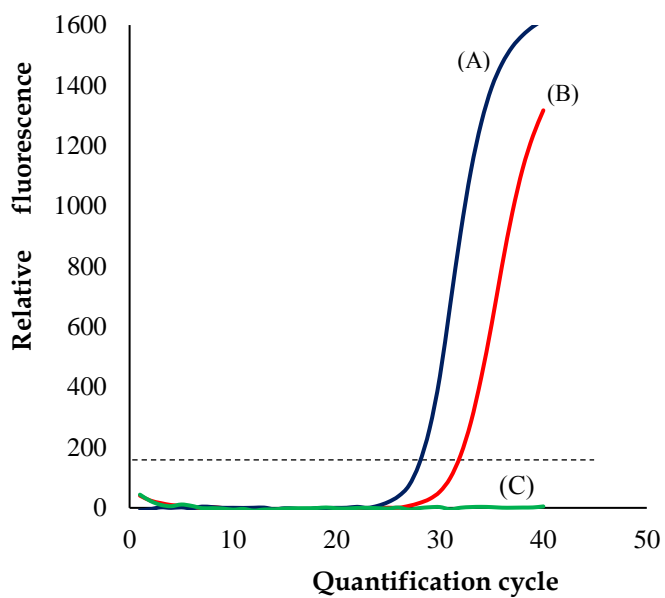


Figure S8. Selective mRNA extraction from total RNA samples using (A) commercial SPE kit (B) oligo dT₂₀-modified PA fiber. Triplicate extraction were performed using oligo dT₂₀-modified PA fiber; spiked total RNA concentration: 5 ng μL^{-1} ; sample solution: 100 μL . (C) NRT: no reverse transcriptase control (ensuring no genomic DNA contamination).

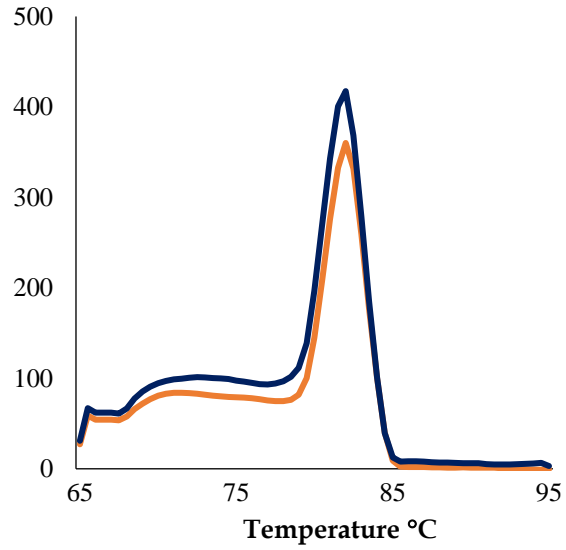


Figure S9. High resolution melting point analysis on RT-qPCR amplification product following mRNA extraction from yeast cell lysate using oligo dT₂₀ modified PA fiber (orange trace) and 0.5 ng of mRNA (standard; blue trace).

Materials and Measurements. Yeast Synthetic Drop-out Medium was obtained from Sigma-Aldrich (St. Louis, MO, USA). Difco Yeast Nitrogen Base w/o Amino Acids was purchased from Becton, Dickinson, and Company (Sparks Glencoe, MD, USA). Glass beads (acid-washed), liquified phenol (>89.0%), isoamyl alcohol ($\geq 98.0\%$), and chloroform ($\geq 99.8\%$) were obtained from Sigma-Aldrich (St. Louis, MO, USA). RQ1 RNase-Free DNase and 10X Reaction Buffer were obtained from Promega (Madison, WI, USA). SuperScript III Reverse Transcriptase (200 U/ μL) used in reverse transcription reactions was obtained from Invitrogen (Carlsbad, CA, USA). Deoxynucleoside triphosphate (dNTP) mix was obtained from Thermo Fisher Scientific (Waltham, MA, USA). Deionized water (18.2 M Ω cm) obtained from a Milli-Q water purification system was used for the preparation of all solutions (Millipore, Bedford, MA, USA). SsoAdvanced Universal SYBR Green supermix for real-time PCR assays was obtained from Bio-Rad Laboratories (Hercules, CA, USA). Forward primers (5'-GAA ATG CAA ACC GCT GCT CA-3'), reverse primers (5'-TAC CGG CAG ATT CCA AAC CC-3'), amine terminal oligo dT₂₀ (5'-/5A mMC12/TTT TTT TTT TTT TTT TTT TT-3'), and fluorescein (FAM) labelled oligo dT₂₀ (5'-/5A mMC12/TTT TTT TTT TTT TTT TTT TT-36-FAM/-3') were purchased from Integrated DNA Technologies (Coralville, IA, USA). 1-ethyl-3-(3-dimethylaminopropyl) carbodiimide hydrochloride (EDC.HCl, >97.0%), and N-hydroxysuccinimide (NHS, +98%) were purchased from Thermo Fisher Scientific (Waltham, MA, USA). DNA LoBind polypropylene microcentrifuge tubes and dextrose (anhydrous) were purchased from Fisher Scientific. The 85 μm polyacrylate (PA) SPME fibers were obtained from Supelco (Bellefonte, PA, USA).

Preparation of Total RNA and Messenger RNA Samples. Total RNA was isolated from BY4735 yeast cells that were cultured at 30 °C in synthetic dropout medium (without uracil) containing 2% glucose until the culture reached an OD₆₀₀ of 1.0. Yeast cells were centrifuged at 2985g for 6 min at 4 °C, washed with nuclease-free water, and resuspended in 0.6 mL of 50 mM Tris-HCl, 10 mM EDTA, 0.1 M NaCl, pH 7.5 with 5% sodium dodecyl sulfate (SDS). One volume (0.6 mL) of phenol (pH 4) chloroform:isoamyl alcohol (49.5:49.5:1) was then added and the mixture was incubated for 6 min at room temperature. Approximately 0.2 g of acid-washed glass beads were loaded into the sample tube which was then vortexed for 2 min in order to disrupt the yeast cell wall. After centrifuging at 17,000g for 5 min, the upper aqueous phase was transferred to a clean microcentrifuge tube and another volume of phenol:chloroform:isoamyl alcohol was added. The sample was vortexed for 2 min and centrifuged at 17,000g for 5 min to induce phase separation of the aqueous and organic layers. The aqueous layer was extracted with another volume of phenol:chloroform:isoamyl alcohol, centrifuged, and the upper layer transferred to a clean tube. Residual phenol was then removed by adding 0.6 mL of chloroform:isoamyl alcohol (24:1) and vortexing for 2 min. The sample was centrifuged to isolate the aqueous phase, to which 60 µL of 3 M sodium acetate (pH 5.2) and 1.8 mL of 100% ethanol were added. The sample was then stored at -20 °C for 1 h, centrifuged at 17,000g for 15 min, and washed with 70% ethanol. Following a final centrifugation step, the RNA pellet was dried at ambient temperature and resuspended in nuclease-free water. The total RNA was then treated with 1 U of DNase I in 1X Reaction Buffer for 1 h at 37 °C to degrade genomic DNA. The DNase I was inactivated using 2 mM EGTA at 65 °C for 15 min. mRNA was purified from 20-25 µg of total RNA using the Oligotex

RNA Mini Kit according to the manufacturer's instructions. The isolated mRNA was analyzed by a Nanodrop spectrophotometer and resulted in an A_{260}/A_{280} ratio of approximately 2.0.

Preconcentration of mRNA Using Oligo dT₂₀ Modified-PA Fibers. The mRNA (0.1 ng/ μ L) containing 100 mM aqueous solution was exposed to modified PA fiber for 3 min at 70 °C. Then, temperature of sample solution was decreased to 4 °C using ice-bath and held for 7 min. Subsequently, extracted mRNA was recovered by exposing the PA fiber to 30 μ L deionized water at 70 °C for 5 min. To determine the amount of mRNA extracted by PA sorbent coating, an aliquot of aqueous desorption solution was employed for RT-qPCR analysis. For selective mRNA analysis from total RNA, a 5.0 ng/ μ L of total RNA containing aqueous solution (sample volume: 100 μ L; 100 mM NaCl) was subjected to PA-based SPME. For yeast cell lysate experiments, 200 μ L of the crude cell lysate suspension (preparation using acid wash glass bead and vortexing method) was added to 200 μ L of deionized water and subjected to modified PA-based SPME. Following DNase I treatment, an aliquot of desorption solution was subjected to RT-qPCR analysis.